The kinetics of the dissociation of the dihydroxyacetone dimer in aprotic media

A thesis submitted in partial fulfilment

of the requirements for the degree

of

Masters of Science

in Chemistry

at

The University of Waikato

by

Adrian Owens

The University of Waikato

2016

THE UNIVERSITY OF
WAIKATO
Te Whare Wānanga o Waikato

Abstract

The dissociation of the dihydroxyacetone (DHA) dimer in mānuka honey has previously been proposed to be the rate determining step in the overall conversion of DHA to methylglyoxal, the agent reported to be responsible for the non-peroxide anti-bacterial activity displayed by mānuka honey.

The ^{1}H and ^{13}C NMR spectra for the DHA dimer and the DHA monomer in DMSO-*d6* were assigned using 1D and 2D NMR spectroscopy.

^{1}H and ^{13}C NMR spectroscopy were utilised to investigate the kinetics of the dissociation of the DHA dimer in DMSO-*d6,* an anhydrous solvent chosen to mimic the dehydrating conditions present in the honey matrix.

Four series of kinetic experiments were conducted, one without catalysis, one with D_2O catalysis, one with CD_3COOD catalysis and one with CD_3COOD/CD_3COOD catalysis. Each of these experiments obtained the equilibrium constant, K and the rate constants k, k_1 and k_{-1} for the dissociation of the DHA dimer under different conditions that may be present in the honey matrix, with the exclusion of the CD_3COOD/CD_3COOD catalysed experiments which were conducted as part of the investigation to determine a proposed reaction mechanism.

Two reaction intermediates were observed in the CD_3COOD catalysed experiments, they were characterised and provided supporting evidence for a proposed acid-catalysed reaction mechanism for the DHA dimer dissociation. The absence of reaction intermediates in the D_2O catalysed experiments provided supporting evidence for a proposed base-catalysed reaction mechanism for the DHA dimer dissociation.

Reaction mechanisms for the DHA dimer dissociation in DMSO-*d6* and mānuka honey were proposed based on the findings of previous studies and the findings associated with the kinetic experiments conducted in this study.

Acknowledgements

I would like to thank my supervisor, Associate Professor Merilyn Manley-Harris, for her great support and insightful observations and suggestions for the direction of this project.

I would like to thank Dr Joseph Lane for our discussions and his guidance with regards to the kinetics associated with this project.

I would like to thank Dr Woei Chet Lim for our discussions and his assistance with the treatment of the complicated mathematical integrals implicit with a kinetics project.

I would like to thank Emeritus Professor Richard Field for our discussions and his suggestions with regards to the kinetic treatment of experimental results.

I would like to thank Cheryl Ward (The School of Science librarian) for her continued assistance with research and document formatting.

I would also like to thank Associate Professor Graham Saunders for his help with questions relating to experiment, NMR spectroscopy and also a few organic chemistry related questions. Thanks needs to go the Associate Professor Michael Mucalo for his availability to answer questions relating to NMR spectroscopy and experiment and a big thank you must also go to Emeritus Professor Alistair Wilkins for his discussions, suggestions and enthusiasm related to NMR spectroscopy.

I would like to thank the University of Waikato for the University of Waikato Masters Research Scholarship which provided much needed support for me to continue my studies and research.

Last but not least, I would like to thank my family for their support throughout my time spent studying at the University of Waikato. My parents, Jan and Brian with their relentless encouragement and my sons Caleb, Oliver, Holden and Maxx and daughter Hayley (BSc student at the University of Waikato) who displayed

patience and understanding and have provided light relief when things were starting to heat up with regards to exams and impending deadlines.

Table of Contents

List of Figures

List of Tables

1 Introduction and literature review

1.1 Mānuka honey

Mānuka honey is produced by bees from the nectar obtained from mānuka (*Leptospermum scoparium* J.R. Forst & G. Forst (Myrtaceae)), a species of tree native to New Zealand and Australia. Mānuka honey has been found to be an effective topical agent for the healing of both acute wounds, including burns and lacerations, and chronic wounds, including diabetic ulcers and infected surgical wounds.[1,2] An important healing property of mānuka honey is its antibacterial action, especially towards methicillin-resistant staphylococcus (MRSA) and vancomycin-resistant enterococcus (VRE) infections,[3,4] which are wide spread bacterial strains that are of considerable concern to the medical community due to their resistance to antibiotics. Honey in general has wound healing properties resulting from its low pH (~pH 4),[5] high osmolarity[6] that restricts the amount of water available to bacteria, and the slow release of antibacterial hydrogen peroxide produced by the enzyme glucose oxidase as it catalyses the oxidation of glucose to D-glucono-δ-lactone.[7] Mānuka honey, however, exhibits antibacterial activity that is substantially higher than that for other honeys.[8,9] The increased antibacterial activity results from non-peroxide antibacterial activity attributed to methylglyoxal[9,10] (MGO) that is found in mānuka honey.

1.2 [10]Identification of methylglyoxal as the non-peroxide antibacterial agent

Methylglyoxal, IUPAC name: 2-oxopropanal, Figure 1.1, has been identified as the compound mainly responsible for the non-peroxide antibacterial activity in mānuka honey.[9,10]

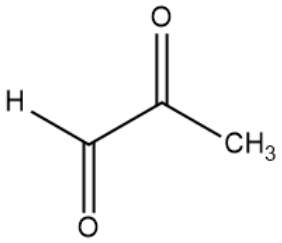

Figure 1.1: The molecular structure of MGO

Identification was achieved by isolating and characterising the bioactive HPLC fraction obtained from mānuka honey.[10] Standard variety honey samples did not contain this HPLC fraction and had undetectable non-peroxide antibacterial activity. The MGO concentration of mānuka[9] was recorded to be as high as 725 mg kg^{-1}. MGO was added to standard variety honey samples at equivalent concentrations of mānuka honey and these samples displayed similar non-peroxide antibacterial activity to mānuka honey.[10] These results strongly indicated that MGO was responsible for the non-peroxide activity observed in mānuka honey.

1.3 Methylglyoxal

Methylglyoxal is a reactive 1,2-dicarbonyl compound that exists as a yellow pungent liquid under standard conditions. MGO may be produced from triose starting material. In acidic conditions glyceraldehyde and DHA undergo irreversible dehydration to form MGO while in basic conditions, Figure 1.2, a mutual Lobry de Bruyn-van Ekenstein isomerisation[11] between glyceraldehyde and DHA occurs as well as an irreversible dehydration that leads to the formation of MGO.[12]

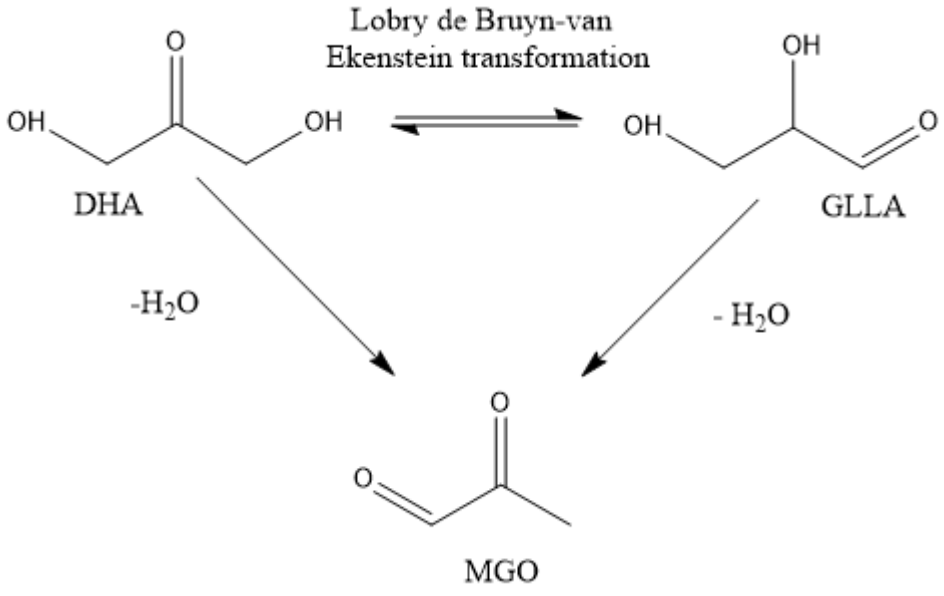

Figure 1.2: The proposed base catalysed reaction scheme

MGO is produced in all living cells during the metabolism of glucose, triglycerides and proteins. In glycolysis, MGO is formed from the dissociation of glyceraldehyde 3-phosphate and dihydroxyacetone phosphate.[13-15] MGO has been shown to modify lysine, arginine and cysteine residues in proteins to produce

advanced glycation end products (AGE's) and to react with guanine residues in DNA causing DNA-DNA polymerase crosslinks and the degradation of DNA. These pathophysiological processes have linked MGO to diabetes, aging and neurodegeneration.[16,17]

1.4 Identification of dihydroxyacetone as the precursor to methylglyoxal in mānuka honey

Beekeepers store mānuka honey to increase its non-peroxide antibacterial activity.[18] Fresh mānuka honey, obtained before any maturation had occurred, was analysed and it displayed relatively low levels of MGO but high levels of DHA. Over time the stored honey showed a decrease in DHA levels that was inversely proportional to an increase in MGO levels. DHA was added to clover honey, stored and showed a decrease in concentration inversely proportional to the formation of MGO similar to that observed in mānuka honey.[19] This strongly indicated that the MGO present in the matured mānuka honey was the product of the conversion of the DHA present in the nectar of mānuka flowers. To determine whether the conversion process was enzymic or non-enzymic, an artificial honey containing no enzymes was developed to which DHA was added. It was observed that conversion of DHA to MGO had occurred, albeit at a reduced rate, strongly indicating that the conversion of DHA to MGO in mānuka honey occurs via a non-enzymic process.[19]

1.5 Dihydroxyacetone

Dihydroxyacetone is a ketotriose; one of the three possible triose monosaccharides along with its structural isomers L- and D-glyceraldehyde but, unlike its glyceraldehyde structural isomers, DHA is achiral. DHA was first prepared in 1897[20] and in 1900 Wohl and Neuberg[21] proposed the 1,4-dioxane hemiketal structure for the DHA dimer. The dissociation kinetics of the DHA dimer were shown to be first order in DHA and catalysed by acid, base and water.[22] It was proposed that the mechanism for the dissociation would be similar to the mechanism for the mutarotation of glucopyranose.[22]

In the solid state, DHA takes the dimeric hemiketal form with a cyclic dioxane structure.[20,22-25] Upon heating or dissolution in aqueous media, the DHA dimer dissociates to give the DHA monomer. When solid DHA is dissolved in water it converts from the dimeric form to one of two monomeric forms, the free carbonyl

ketone form or the hydrate form with a 4 to 1 ratio.[23] This study proposes that the mechanism for the DHA dimer dissociation is analogous to the ring opening mechanism in the mutarotation reaction of pento- and hexopyranose rings. The observation that the DHA dimer dissociation displays first-order kinetics[22,23] offers a similarity comparison to the mutarotation, as it too displays first order kinetics.[26-30]

1.6 The structure of dihydroxyacetone

1.6.1 ^{1}H NMR assignment

A ^{1}H NMR study[23] observing the species present in the DHA dimer to monomer conversion in both D_2O and DMSO-d_6 obtained unique ^{1}H NMR signals for the DHA dimer and for the DHA monomer using a Varian A-60 (60 MHz) nuclear magnetic spectrometer.[1] Davis assigned the ^{1}H NMR spectrum for the DHA monomer and dimer in DMSO-*d6*, Table 1.1. This study described the DHA dimer structure as a centrosymmetric 1,4-dioxane ring in a chair conformation with two hydroxymethyl groups adopting equatorial positions and adjacent to these groups, endocyclic hydroxyl groups adopting axial positions, Figure 1.3. To obtain the spectra for the monomer, a sample was prepared in the solid state by lyophilising an aqueous solution of DHA.

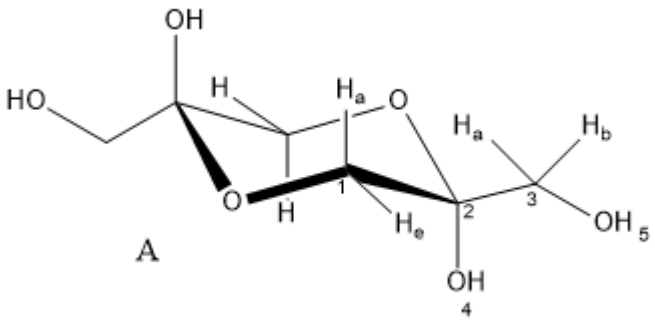

Figure 1.3: The DHA 1,3-dioxane dimer structure (A)

In assigning the spectrum for the two monomer signals: a triplet at 5.10 ppm (^{3}J 6 Hz) was assigned to the two hydroxyl protons and a doublet at 4.26 ppm was assigned to the four methylene protons. For assigning the dimer spectrum: a singlet at 5.90 ppm was assigned to the two axial ring hydroxyl protons (OH-4) and a triplet at 4.75 ppm (^{3} *J* 6 Hz) was assigned to the two exocyclic hydroxyl protons (OH5). A doublet at 4.05 ppm (^{2}*J* 12 Hz) was assigned to the two

[1] The Varian A-60 was an early model of NMR spectrometer that operated using the continuous wave signal acquisition method that gave very poor resolution.

equatorial protons (H1e) in the ring and the remaining methylene protons and the axial protons were assigned to a multiplet where their signals overlapped and could not be resolved.

Table 1.1: Davis's 1H NMR spectrum assignments[2] of DHA in DMSO-d6

Proton	δ (ppm)*	^2J (Hz)	^3J (Hz)
	Dimer		
H1e	4.05	12	-
OH4	5.9	-	-
OH5	4.75	-	6
	Monomer		
CH_2	4.26	-	6
OH	5.1	-	6

Kobayashi and Takahashi[25] assigned the spectra to the DHA monomer and multiple dimer forms using a 100 MHz spectrometer, Table 1.2. The monomer spectrum was assigned: a triplet at 4.99 ppm (^3J 6.0 Hz) was assigned to the two hydroxyl protons and a doublet at 4.15 ppm was assigned to the four methylene protons.

Table 1.2: Kobayashi's and Takahashi's ^{1}H NMR spectrum assignments of DHA in DMSO-*d6*. The structures A, C and D are represented in Figure 1.4.

Proton	δ (ppm)	^2J (Hz)	^3J (Hz)	^4J (Hz)
	Dimer A			
H-1a	3.94	11.3	-	1
H-1e	3.32	11.3	-	-
H-3a	3.20	11.5	6.5	-
H-3b	3.34	11.5	6.5	-
OH-4	5.62	-	-	1
OH-5	4.62	-	6.5	-
	Dimer C			
H-7a	3.16	11.2	6.4	-
H-7b	3.28	11.2	6.4	-
H-3e	3.49	12.0	-	-
H-3a	3.64	12.0	-	-
H-11	4.58	-	6.4	-

[2] converted from the tau (τ) scale using 10 - τ

H-9	5.77	-	-	-
		Dimer D		
H-8a	3.35	11.5	7.2	-
H-7	3.40	-	6.2	-
H-6	3.48	-	6.0	-
H-8b	3.51	11.5	5.2	-
H-5a	3.73	8.2	-	-
H-5e	4.00	8.2	-	-
H-11	4.64	-	6.2	-
H-10	4.80	-	6.0	-
H-12	4.86	-	5.2	-
H-9	6.15	-	-	-
		Monomer		
CH_2	4.62	-	6.0	-
OH	4.99	-	6.0	-

The dimer spectrum was assigned : a doublet (^4J 1.0 Hz) at 5.62 ppm was assigned to the OH-4 proton as the small *J*-coupling constant pointed to a long-range coupling which required a coplanar W geometry and for this to occur the hydroxyl group needed to be axial. The small J-coupling constant (^4J 1 Hz; ^2J 11.3 Hz) in the doublet of doublets at 3.94 ppm with the implied long-range coupling pointed to this proton being the axial ring proton signal as it needed to be in this position to have correct geometry to engage in long-range coupling with OH-4. The assignment of H-1a at 3.94 ppm and H-1e at 3.32 ppm is at odds with the assignments by Davis[23] which has the equatorial proton further downfield. Although an equatorial proton is generally further downfield than an axial proton in pyranose rings, the long-range coupling coplanar requirement rules out that arrangement in this case.

1.6.2 Infra-red assignment

An infrared and Raman spectroscopy study[24] focusing on the elucidation of the DHA dimer structure identified the presence of four DHA dimer polymorphs (α, ß, γ and δ) and one monomer crystal structure (ε) using powder X-ray diffraction. Four possible dimeric cyclic hemiketal molecular structures were originally conjectured, drawing from a previous study,[23] to be either confirmed or eliminated

based on the experimental evidence to be obtained, Figure 1.4. The five polymorphs, four dimer and one monomer, were originally differentiated by their X-ray diffraction powder patterns. The four dimer polymorphs were obtained from methanol at different temperatures and the monomer crystal structure was obtained by lyophilisation of an aqueous solution of DHA. The polymorphs α, ß and δ were stable at room temperature while the γ polymorph transforms to the α form within 24 hours. The IR and Raman spectra for the ε form showed carbonyl stretching bands at 1730 cm^{-1} indicating that the ε form is the carbonyl monomer. The α, ß, γ and δ forms showed no carbonyl stretching bands indicating that there were no carbonyl functional groups present in the molecular structures of these polymorphs.

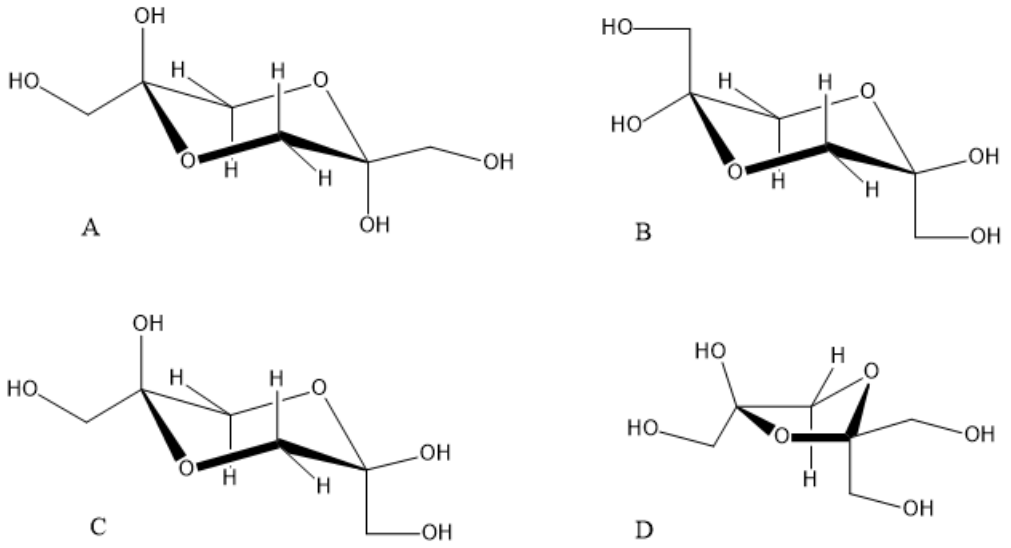

Figure 1.4: Four structures conjectured by Kobayashi et al.

The group theory rule of mutual exclusion states that centrosymmetric molecules cannot be both IR and Raman active.[31] Mutual exclusion was observed for the α, ß and γ forms indicating that they possessed the structure of either A or B, the centrosymmetric conjectured structures, Figure 1.4. Mutual correspondence was observed for the δ polymorph implying that either the molecular structure was non-centrosymmetric or the crystal structure was non-centrosymmetric. All four polymorphs gave the same IR spectra when dissolved in DMSO-*d6*, pointing to them all having the same molecular structure, thus the δ polymorph had a non-centrosymmetric crystal structure but a centrosymmetric molecular structure. Of the two conjectured centrosymmetric structures, it was determined that structure A was lower in energy due to the steric interactions of the hydroxymethyl and hydroxyl group and therefore the most likely structure for all four dimeric

polymorphs with different hydroxymethyl and hydroxyl substituent conformations for each polymorph. The double anomeric effect would be a major factor in increasing the stability of the dimer A[32], Figure 1.4.

1.6.3 Crystal structures

A study[33] focusing on the crystal structures of DHA identified three dioxane dimer crystal structures (α, β and γ), Figure 1.5, and one monomer crystal structure. The α polymorph was obtained by recrystallization from aqueous solution and the β polymorph was obtained by recrystallization from 2-propanol, both processes performed in ambient conditions. The γ polymorph was obtained by slow lyophilization from aqueous solution while the monomer polymorph was obtained by lyophilization from aqueous solution at a faster rate. All three dimer polymorphs adopted chair conformations and were present as *trans* isomers with the hydroxymethyl groups equatorial and the ring hydroxyl groups axial due to the anomeric effect.

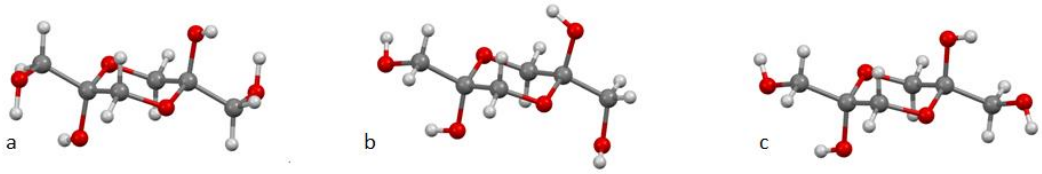

Figure 1.5: The ball and stick structures of the α, ß and γ dimer polymorphs

The conformation of the hydroxymethyl groups differed with each polymorph. Taking the Newman projection of the exocyclic oxygen, the exocyclic carbon, the quaternary carbon and either the adjacent ring oxygen (for the first assignment) or adjacent ring carbon (for the second assignment) different conformations were assigned to each of the dimer polymorphs with the α dimer: *gauche-anti*, the ß dimer: *gauche-gauche,* and the γ dimer: *anti-gauche*. The axial ring hydroxyls were all *gauche* to the hydroxymethyl groups except for one of the ß-polymorphs hydroxymethyl groups which adopted the *anti* conformation. The ß polymorph molecular structure was not centrosymmetric (point group P-1) while the α and γ polymorph molecular structures were centrosymmetric (point group P21/c).

The different polymorphs resulted from different hydrogen bonding conformations within the unit cell. These crystal structures elucidate the molecular conformation in the solid-state but in solution we would expect the hydroxymethyl groups to be freely rotating to some degree.

1.7 The proposed kinetics of the dihydroxyacetone dimer dissociation by various experimental procedures

1.7.1 Dilatometry

In 1937 Bell and Baughan performed a series of dilatometric kinetics experiments which followed the change in volume of various aqueous solutions of DHA.[22] The kinetics of the dimer to monomer conversion of DHA in water and various aqueous solutions containing carboxylic acids and carboxylate ions were observed using a dilatometer, an instrument that measures changes in volume as a chemical reaction or physical process progresses with time. The conversion of the DHA dimer to monomer in aqueous solution at 25 ^{o}C (± 0.005 ^{o}C) resulted in a molar volume increase (as one molar dimer dissociated to give two molar monomer) that was shown to be 36 mm^3 g^{-1}, a value that is very temperature dependent.[22] The dissolution process was exothermic and required a data acquisition delay of approximately 5 minutes to allow the solution temperature to drop back down to 25 ^{o}C. The reaction progress was monitored every 4 min by reading the change in volume on a capillary with an accuracy of ± 0.05 mm. The dimer to monomer conversion in triple distilled water was shown to be pseudo-first order in DHA with a rate constant of 1.72 min^{-1} which was determined using the Guggenheim Method.[34] A linear relationship was observed between the rate constants and acid concentrations suggesting that the dimer to monomer conversion is catalysed by acid and base.

1.7.2 UV spectroscopy

An ultraviolet spectroscopy kinetics experiment investigating the dissociation of the DHA dimer followed the formation of the DHA monomer carbonyl absorption band in aqueous D_2O solution (25°C)[23]. With the progression of time an absorption band appeared in the spectrum at 275 nm which was attributed to the n-π* transition of the ketone monomer[23]. This kinetics experiment determined that the conversion of the DHA dimer to monomer in D_2O has a first order rate constant of 0.034 min^{-1} which contrasts strongly with the value reported by Bell and Baughan of 1.72 min^{-1}.

1.7.3 Infra-red spectroscopy

Davis performed a somewhat impromptu qualitative infrared spectroscopy study that was able to monitor the dissociation of the DHA dimer whilst carrying out the previously mentioned NMR and UV experiments[23]. The DHA dimer dissociation was observed by following the formation of the DHA monomer carbonyl band with the evolution of time. DHA solid (dimer) was dissolved in D_2O (25°C). At T (0) there was no carbonyl band as the dimeric 1,4-dioxane ring had yet to dissociate to the free carbonyl ketone monomer. With the progression of time, a strong absorption band appeared at 1730 cm^{-1} indicating the formation of the ketone monomer[23]. Although this was a qualitative experiment to provide supporting data for an NMR experiment, tracking the appearance of this band as a function of time would be a possible method for obtaining kinetic information for the dissociation of the DHA dimer if, for example, it was shown that the NMR timescale was to slow to observe the DHA dimer dissociation in DMSO-*d6*.

A study[35] focusing on the effects of temperature, pH and solvent on the dissociation of the diose glycolaldehyde (GLLA) dimer, Figure 1.6, was performed using infrared spectroscopy in D_2O, acetone and DMSO.

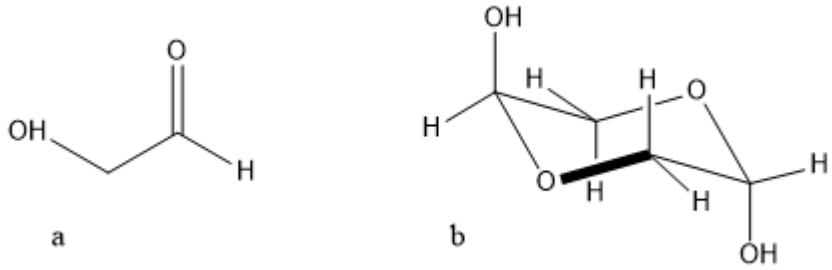

Figure 1.6: The molecular structures of GLLA (a) monomer (b) dimer

GLLA, like DHA, exists as a dimer in the solid state with a cyclic 1,4-dioxane structure and upon heating or in solution phase it has been shown that the GLLA dimer converts to the monomer via a mutarotation-like mechanism similar to the proposed mechanism for the dissociation of the DHA dimer[35]. The IR spectra of GLLA obtained in D_2O displayed absorption bands in the carbonyl region (1700 – 1750 cm^{-1}) and a band in the enediol region (1630 – 1700 cm^{-1}); these bands were observed to intensify with time[35] and upon equilibrium intensified with the application of heat and decreased in intensity when cooled. It was conjectured that a band at 1728 cm^{-1} resulted from the formation of the acyclic dimer, and that bands at 1744 cm^{-1} and 1703 cm^{-1} resulted respectively from the carbonyl monomer and the enediol monomer that were in equilibrium. Kinetic analysis of

the data allowed for a two-step process to be conjectured that incorporated a mutarotation like mechanism opening the ring to give the acyclic dimer intermediate which goes on to dissociate via the same mutarotation like mechanism to give monomeric GLLA which is in thermodynamic equilibrium with dimeric GLLA and two other conjectured species, one of which was an unlikely five membered ring. It was pointed out that the time scale for these interconversion were too fast for the NMR time scale[35]. This was a qualitative kinetics experiment that was done to determine what species were present during and after the dissociation of the dimer and to provide supporting evidence for a possible mechanism. Unfortunately no rate constants were obtained and recorded. This technique might be used to obtain the kinetic information for the DHA dimer dissociation by observing the increase in intensity of the carbonyl band as a function of time especially in instances where the NMR timescale is to slow.

1.7.4 ^{1}H NMR spectroscopy

A cursory ^{1}H NMR spectroscopy study of the DHA dimer dissociation in DMSO-*d6* at 25 °C provided kinetic data in the form a first order half-life of 64 hours.[23] This corresponded[3] to a rate constant of 1.81 x 10^{-4} min^{-1} a result which allowed the comparison between the DHA dimer dissociation rate constants obtained in water (3.4 x 10^{-2} min^{-1}) and obtained in DMSO-*d6*. The comparison suggested that the amphiprotic solvent water was catalysing the reaction at a faster rate than the aprotic DMSO-*d6*.

A kinetics study observing the dimer to monomer conversion of glycolaldehyde (GLLA) in deuterated methanol, acetone and DMSO was monitored using ^{1}H NMR spectroscopy.[36] The rate of conversion was determined using a Varian A-60-A (60 MHz) NMR spectrometer to monitor the disappearance of the dioxane ring, the appearance and subsequent disappearance of the intermediate and the appearance of the monomeric aldehyde, Figure 1.7.

[3] The value for the DHA dissociation in DMSO-*d6* had to be determined rearranging the first order half-life equation… $t_{1/2} = \frac{\ln[2]}{k}$… to give the expression in terms of $k = \frac{\ln[2]}{t_{1/2}}$, as the only kinetic information provided in the journal article consisted of the statement, "the conversion to monomer is only 50 % complete after 64h". Therefore the rate constant was determined… $k = \frac{\ln[2]}{t_{1/2}} = \frac{0.6931}{(64 \times 60) minutes}$ = 1.81 x 10^{-4} min^{-1}.

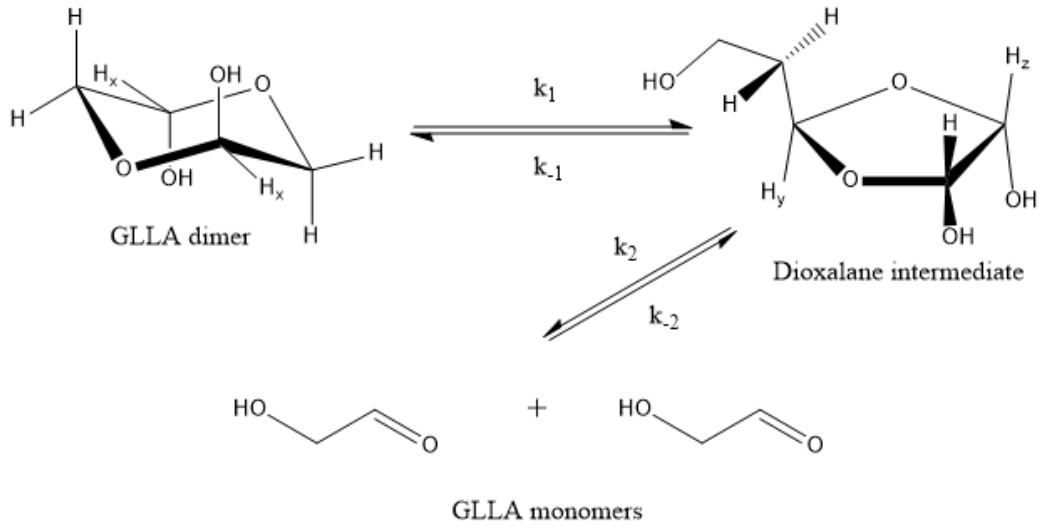

Figure 1.7: The originally proposed reaction scheme

The conjectured intermediate was a five-membered dioxolane ring, Figure 1.7. The monitoring of these species was achieved by assigning a unique proton signal(s) to each of the three species and integrating each of these signals to give response factor values. The thus obtained response factor values were proportional to the concentration of the species from which these signals emanated. For the disappearance of the dioxane ring in DMSO-*d6*, the H_x proton signal (4.67δ) was followed, Figure 1.7. For the appearance of the proposed dioxolane intermediate and the monomer, the H_z (5.45 δ) and H_y (5.00 δ) signals were followed for the dioxolane ring and both the hydroxyl (4.11 δ) and aldehyde (9.43 δ) proton signals were followed for the monomer.

The change in response factor value for each of these signals as a function of time was used to show an approximated first order two-step sequential process requiring two rate constants (k_1 and k_2) and involving an intermediate, Figure 1.8, with A: representing the dioxane ring, B: the intermediate and C: the monomer.

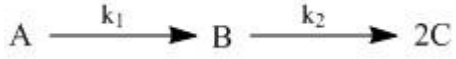

Figure 1.8: The sequential equation approximation

The rate constant determination was achieved by developing a set of differential rate equations that used the initial concentrations of the two cyclic species. These equations were integrated to give the rate equations in terms of concentration:

$$[A] = [A]_0 e^{-k_1 t} ,$$

$$[B] = [A]_0 \frac{k_1}{k_2 - k_1} (e^{-k_1 t} - e^{-k_2 t}) + [B]_0 e^{-k_2 t} ,$$

$$[C] = 2[A]_0\left(1 - \frac{k_2 e^{-k_A t} - k_1 e^{-k_B t}}{k_2 - k_1}\right) + [B]_0(1 - e^{-k_2 t})$$

When these integrated rate equations were plotted with the appropriate initial concentrations, the resulting graphs showed a reasonable correlation with the graphs for the experimentally obtained data points. The rate constants at different initial concentrations of GLLA in methanol-*d6* are given in Table 1.3.

Table 1.3: The rate constants for the dissociation of GCLA in methanol-*d6*

$[A]_0$ (mol L^{-1})	k_1 min^{-1}	k_2 min^{-1}	$\kappa = k_2 / k_1$
1.46	5.8×10^{-2}	3.9×10^{-2}	0.68
0.88	4.2×10^{-2}	2.8×10^{-2}	0.66
0.47	3.4×10^{-2}	2.2×10^{-2}	0.64

Unfortunately, as no error has been assigned to the data in Table 1.3, it was not possible to make any inferences about the relationship between concentration and the rate constants. The k_2 values in deuterated acetone and DMSO were not determined because without an acid catalyst, this final step proceeded at a very slow rate.

1.8 The anomeric effect

The anomeric effect[7,37-40] is a stereoelectronic effect that was first named in carbohydrate chemistry to describe an effect observed in pyranose rings containing electronegative substituents at the *anomeric* carbon (C-1). The term refers to the tendency of an electronegative substituent on the anomeric carbon of a pyranose ring to adopt the sterically unfavourable axial conformation. Were steric interactions alone taken into account, the bulkier substituents in a pyranose ring would preferentially adopt the equatorial position, as is the case for the cyclohexane analogues. Edward was the first to describe the high abundance of the α anomer of tetrahydro-2-methoxypyran, Figure 1.9, in terms of the geometrical arrangement of the lone pair of electrons on the ring oxygen relative to the position of the electronegative substituent in 1955.[37] In 1958 Lemieux coined the term "anomeric effect" to refer to this observation while studying the anomerisation of a selection of acetylated aldohexopyranoses.[37]

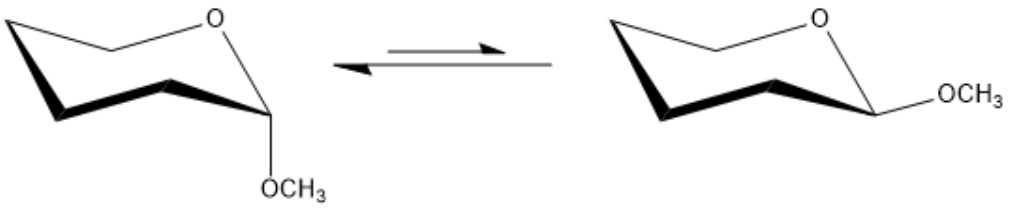

Figure 1.9: The tetrahydro-2-methoxypyran anomer equilibrium

Although the anomeric effect was first named in carbohydrate chemistry it is a general effect that can be observed in the system R-X-A-Y, Figure 1.10, with the preference of the sterically less favoured gauche-conformation over the anti-conformation. The higher the electronegativity of Y, the greater the anomeric effect.[39] The more established model for the anomeric effect is the "Antiperiplanar Lone Pair Hypothesis" (ALPH) which states that hyperconjugation resonance stabilises the axial configuration by distributing electron density from the HOMO non-bonding electrons (lone pair) of the X atom to the LUMO anti-bonding σ* orbital of the A atom[39], Figure 1.10.

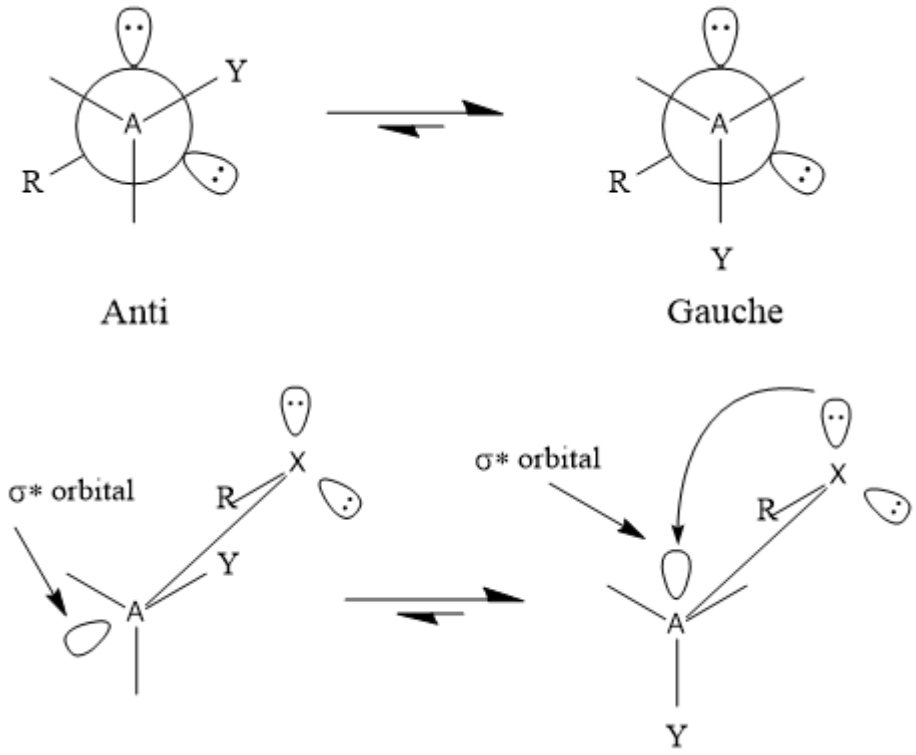

Figure 1.10: The conformational tendencies of the R-X-A-Y system. R represents hydrogen or carbon, X is an atom with a lone pair (s), A is usually carbon and Y is an electronegative atom.

Using the ALPH model, Figure 1.11, it can be shown that the high stability of the DHA dimer in the solid state results from a double anomeric effect afforded by the positions of the axial hydroxyl groups being anti-periplanar to the lone pair of electrons on the adjacent ring oxygens. The anti-periplanar geometry results in hyperconjugation between one of each of the ring oxygens lone pairs and the empty σ* antibonding orbitals extending from the carbon-hydroxyl carbon σ-bonds. The delocalization of electron density on both sides of the ring lowers the energy of the system thus increasing the stability of the ring.

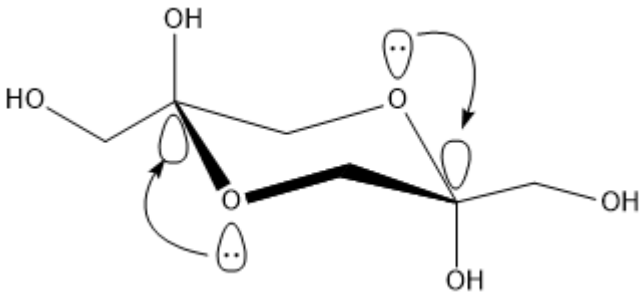

Figure 1.11: Stabilisation of the DHA dimer using the ALPH model

This effect is somewhat trivial in the case of the DHA dimer as the hydroxymethyl groups would be expected to be equatorial due to steric effects. A more demonstrable 1,4-dioxane example for the anomeric effect is the crystal structure for the glycolaldehyde dimer.[32] Although the glycolaldehyde dimer, Figure 1.12, has no hydroxymethyl groups occupying the equatorial positions, the relatively bulky hydroxyl groups still occupy the sterically unfavourable axial positions as a result of the anomeric effect.

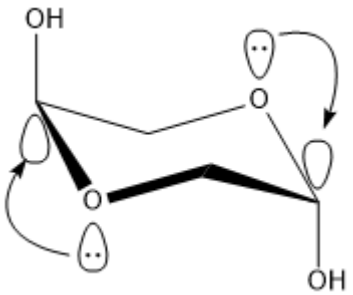

Figure 1.12: Stabilisation of the GLLA dimer using the ALPH model

1.9 Mutarotation

Mutarotation in carbohydrate chemistry is the change in optical rotation resulting from the anomerization of reducing sugars. In 1846 Dubrunfaut[41] observed that an aqueous solution of glucose experienced a change in optical rotation from ~110°

to ~52°. It has since been shown that this change in the optical rotation of D-glucose is a result of the equilibrium reached between α-D-glucopyranose[42] with an optical rotation of 112.2° and β-D-glucopyranose[42] with an optical rotation of +18.7°, via the mutarotation reaction to give an optical rotation of 52.5° at equilibrium for the racemic mixture.

Mutarotation has been shown to be catalysed by both acid and base with the proposed mechanisms,[28,43,44]Figure 1.13 and Figure 1.14. The rate determining step in both acid catalysis and base catalysis is the opening of the ring. Due to the very low concentration of any acyclic aldose intermediate it has been proposed that the pyranose or furanose ring opens to give a "pseudo-acyclic" intermediate before promptly closing again.[44,45] The conformation of the pseudo-acyclic intermediate is very close to that of the closed ring and free rotation around the anomeric and adjacent ring carbon allows for the anomerisation to proceed driven by opposing thermodynamic and anomeric effect contributions.

1.9.1 The acid catalysed mutarotation mechanism

The acid-catalysed mechanism, Figure 1.13, begins with a rapid and reversible proton exchange between the acid catalyst and the ring oxygen which is the fast 1st step. This is followed by the slow rate determining step that involves the abstraction of the anomeric hydroxyl proton with the transfer of electrons from the hydroxyl bond to form a carbonyl bond which initiates an electron transfer from the anomeric carbon to the ring oxygen to open the ring. Free rotation around the C-1 and C-2 bond (in this example) allows for a change in the anomeric hydroxyl orientation. The ring promptly closes with electrons being transferred back from the ring oxygen to the anomeric carbon and from the carbonyl bond to an available proton to give the anomeric hydroxyl group with a possible α orientation (36% for glucopyranose) or a possible β orientation (64% for glucopyranose). This step is followed by the abstraction of the ring oxygen proton to give the product.[28]

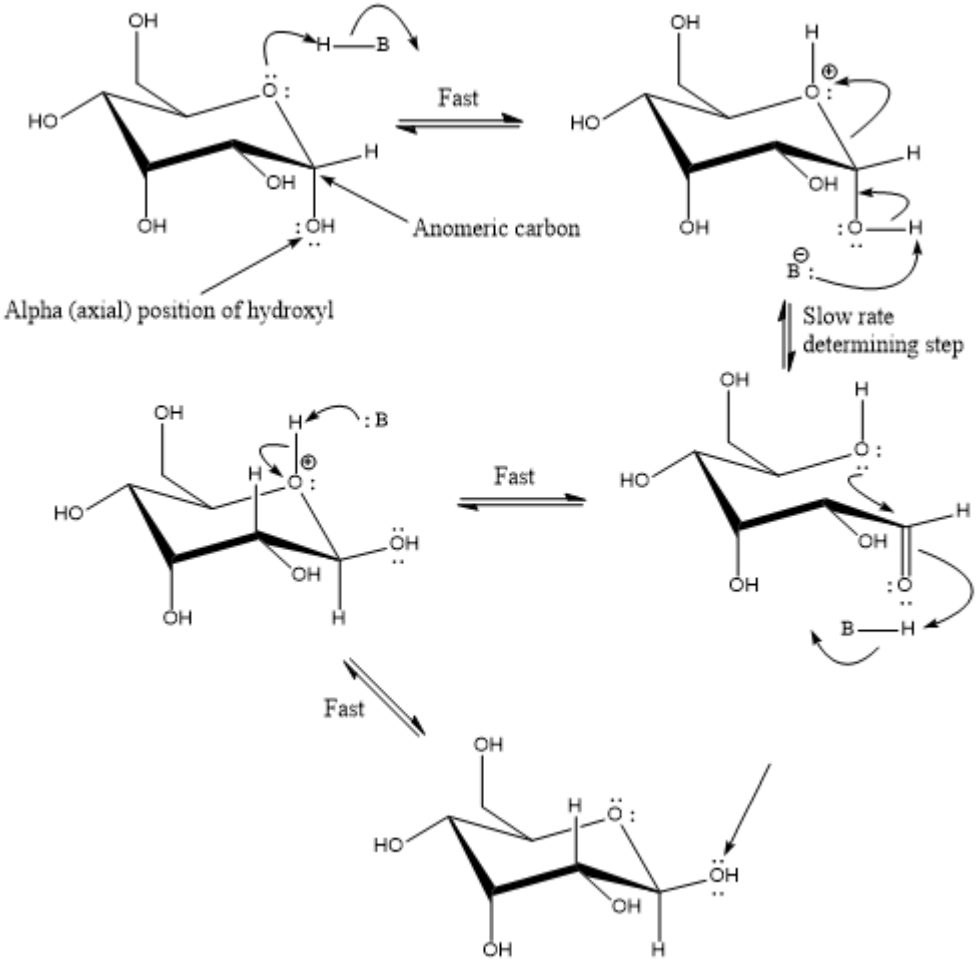

Figure 1.13: The acid catalysed mutarotation mechanism

1.9.2 The base catalysed mutarotation mechanism

The base catalysed mechanism, Figure 1.14, is initiated by the anomeric hydroxyl proton being abstracted with the transfer of electrons from the hydroxyl bond to form a carbonyl bond which initiates an electron transfer from the anomeric carbon to the ring oxygen to open the ring. Rotation of the anomeric carbon allows for a change in the anomeric hydroxyl orientation. The ring promptly closes again with electrons being transferred back from the ring oxygen to the anomeric carbon and from the carbonyl bond to an available proton and finally with the abstraction of the proton bonded to the ring oxygen to give the product.[28]

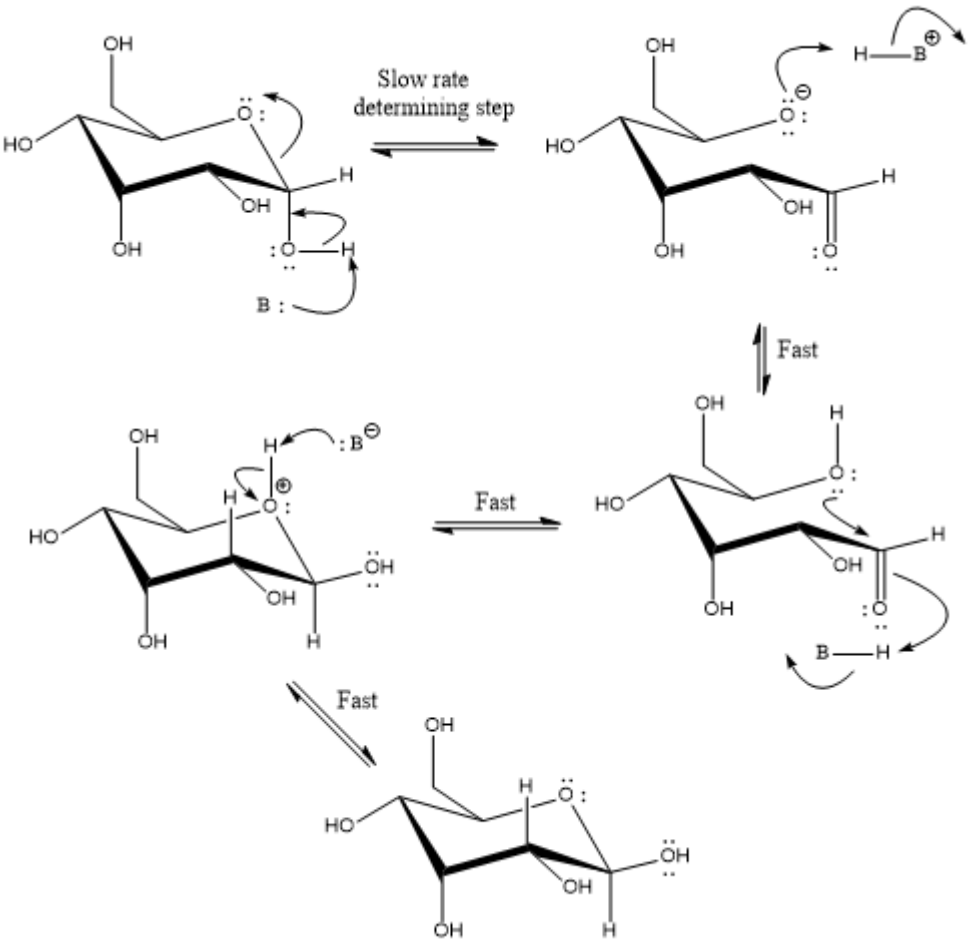

Figure 1.14: The base catalysed mutarotation mechanism

1.9.3 The effect of the solvent

Both acid catalysis and base catalysis each involve acid and base catalytic steps in their reaction mechanisms with classification depending on whether originally a proton was accepted by or abstracted from the cyclic sugar. Theoretical calculations[46] focusing on a series of monosaccharides showed that the hydroxyl oxygens contain almost twice the electron density as the ring oxygen and it would therefore be expected, under the acidic conditions of acid catalysis, that the hydroxyl protons would be protonated rather than the ring oxygen. In aqueous/dipolar solvent however, hydrogen bonding of the solvent to the anomeric hydroxyl proton transfers electron density to the ring oxygen making it more basic and a more likely proton acceptor. Theoretical calculations[46] indicate that the anomeric hydroxyl proton is the most acidic proton which corresponds to its preference for extraction in the mechanism.

Glucose is mainly present in its pyranose form in aqueous solution with insignificant traces of its furanose and aldehyde forms resulting in the mutarotation reaction exhibiting first order kinetics of the form α-D-glucopyranose ⇌ β-D-glucopyranose.

1.10 Dimethyl sulfoxide solvent

All NMR kinetic experiments in this study of the dissociation of the DHA dimer were performed in anhydrous DMSO-*d6* to simulate the dehydrating nature of the honey matrix. DMSO is a dipolar protophylic aprotic solvent that contains a trigonal pyramidal structure with a central sulphur atom and loan pair of electrons at the apex, Figure 1.15.

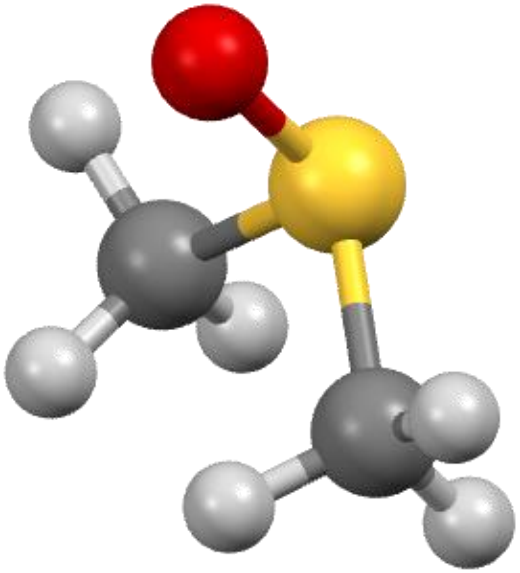

Figure 1.15: The ball and stick model of DMSO

DMSO is a relatively viscous liquid with a viscosity of 1.99 cP.[47,48] For comparison, water has a viscosity of 0.89 cP[47] and acetic acid has a viscosity of 1.06 cP.[47] DMSO is an effective hydrogen bond acceptor with the DMSO-water hydrogen bond being 1.33 times stronger than the water-water hydrogen bond,[49] a result that is related to DMSO being 1.5 times more basic than water.[50]

A permanent dipole results from the large difference in electronegativity between the electronegative oxygen atom (3.50 on the Pauling Scale)[47,51] and the relatively electropositive sulphur atom (2.44 on the Pauling Scale).[47,51] The methyl groups serve to shield the electropositive sulphur atom from engaging in intermolecular interactions thus effectively burying the positive component of the permanent dipole within the molecule. The buried positive component of the DMSO dipole

results in DMSO being able to stabilise and solvate cations via the electronegative oxygen atom but unable to stabilise or solvate anions. Anions are particularly reactive in DMSO as oxygen-cation solvation eliminates ion-pairing between the cation and anion resulting in the sulphur atom being unable to effectively solvate the anion and thus leaving the anion free to engage in reactions relatively unimpeded.[52]

1.11 Aim of this thesis

As the honey matrix is relatively dehydrating with the majority of its water content bound up in hydrogen bonding, it is reasonable to assume that the DHA in mānuka may exist, at least partially, in the dimeric form. The conversion of DHA in mānuka honey occurs in several steps over a period of approximately three months at a temperature of ~37 °C.[19] A kinetics study of the formation of MGO in mānuka honey identified the dissociation of the DHA dimer as the rate determining step.[53]

The aim of this study was to investigate the kinetics for the dissociation of DHA in mānuka honey by using DMSO-*d6* as a honey matrix anhydrous analogue and tracing the dissociation reaction using ^{1}H NMR spectroscopy.

2 Experimental

2.1 Materials

Dihydroxyacetone dimer (assay 97%), anhydrous sodium hydroxide (assay 97%), anhydrous dimethyl sulfoxide-*d6* (99.9 atom % D, <50 ppm water, d. 1.19g mL^{-1}), deuterium oxide (D_2O) standard grade (99.98 atom %±0.01atom % D, d. 1.12 g mL^{-1}), anhydrous acetic acid-*d4* (99.5 atom % D), hydrochloric acid (HCl) (36 % w/w: d. 1.18 g mL^{-1}) were all purchased from Sigma-Aldrich and used as supplied.

2.2 Nuclear Magnetic Resonance (NMR) Experiments[4]

2.2.1 Specifications[5]

All NMR experiments were performed on the University of Waikato School of Sciences Bruker AVIII (400) NMR spectrometer running Topspin 3.0 software. The spectrometer was fitted with a 5mm ATMA BBI probe operating at 400.13 MHz for ^{1}H and 100.62 MHz for ^{13}C spectrometry with all experiments being performed at 300.0 K (± 0.1).

2.2.2 NMR kinetic experiments

2.2.2.1 ^{1}H NMR

^{1}H NMR spectra were calibrated using the DMSO-d6 solvent peak at 2.50 ppm (relative to TMS). The ^{1}H NMR spectra that were acquired for standard kinetic data used 8 scans with a spectral width of 18.02 ppm. The kinetic experiments were performed with a fixed delay using the multi_zgvd Topspin 3.0 au program. For the standard ^{1}H NMR kinetic experiments a fixed inter-experiment delay of 70 seconds was used with the 8 scan experiment taking 50 seconds to give an overall inter-experiment acquisition cycle of 2 minutes. For experiments with half-lives less than 15 minutes no delay was used to give an overall acquisition cycle of 54 seconds.

---

[4] All processed ^{1}H NMR spectroscopic data obtained from the kinetic experiments is held in a DVD that is attached to the appendices.

[5] The parameters for all 1D and 2D NMR experiments are in the appendix: 10.2.1 – 10.2.9

2.2.2.2 ^{13}C NMR

^{13}C NMR spectra were calibrated using the DMSO-d6 solvent peak at 39.52 ppm (relative to TMS). The ^{13}C NMR spectra that were acquired to obtain kinetic data used 128 scans with a spectral width of 238.89 ppm. The kinetic experiments were performed with a fixed delay using the multi_zgvd Topspin 3.0 au program. For the standard kinetic experiments a fixed delay of 10 seconds was used with the 128 scan experiment taking 296 seconds to give an overall acquisition cycle of 5 minutes 6 seconds. Unfortunately this time could not be reduced for rapid experiments as the number of scans would need to be reduced which would greatly increase the noise in an already noisy baseline.

2.2.2.3 Data acquisition and treatment

On completion of the kinetic run the multicmd command in Topspin was used to automatically Fourier transform, phase and normalise the base line for all the spectra obtained. This was a very useful time saving device as the number of obtained spectra usually ran into the hundreds and sometimes into the thousands thus reducing a task that would have taken hours to complete to an automatic process that took 5 to 10 minutes to complete.

The first spectrum of the experiment set had all the non-overlapping signals integrated, making sure that all the as yet unseen signal chemical shifts ranges were also integrated. This first spectrum was saved and written as a misc file (wmisc). The multi_integ3 au program, using the saved wmisc file, integrated all the spectra using the integration ranges obtained in the first spectrum. The integration data for all spectra, including chemical shift ranges, were saved as a text file which was imported into Excel where the kinetic data was able to be analytically processed and graphed.

2.2.3 Sample preparation

2.2.3.1 Assignment of spectra

DHA dimer was weighed (~0.0200 g) in a vial and DMSO-*d6* (0.550 mL) was transferred into this vial. The solution was mixed using a vortex mixer and transferred into a 5 mm NMR tube.

2.2.3.2 Mutarotation experiments

2.2.3.2.1 D_2O mutarotation experiments

Glucose was weighed (~0.0050 g) in a vial and the required volume of D_2O was determined using the equation:

$$v(D_2O{:}mL) = 1000 \times \frac{m(glucose{:}\,g)}{conc.\,(glucose{:}\frac{mol}{L}) \times Mr(glucose{:}\frac{g}{mol})}$$

2.2.3.2.2 DMSO-d6 mutarotation experiments

Glucose was weighed (~0.0050 g) in a vial and the required volume of DMSO-*d6* was determined using the equation:

$$v(\mathrm{DMSO}d6 : mL) = 1000 \times \frac{m(glucose{:}\,g)}{conc.\,(glucose{:}\frac{mol}{L}) \times Mr(glucose{:}\frac{g}{mol})}$$

2.2.3.2.3 D_2O catalysed with HCl mutarotation experiments

A solution of appropriate concentration of HCl in D_2O was prepared

The concentration of HCl in the supplied aqueous solution was converted from 36 % w/w to 11.65 mol L^{-1} utilising the provided specific density of 1.18 g mL^{-1} using the following equation:

$$c\left(HCl{:}\frac{mol}{L}\right) = \frac{0.36 \times 1180\frac{g}{L}}{Mr(HCl{:}\,36.46\frac{g}{mol})} = 11.64\frac{mol}{L}$$

To obtain the appropriate concentration of HCl in D_2O using 0.100 mol L^{-1} as an example, 11.65 mol L^{-1} is converted to 0.1000 mol L^{-1} by…

$$c_i x = c_f \;\therefore\; 11.65\left(\frac{mol}{L}\right)x = 0.1000\left(\frac{mol}{L}\right)$$

$$x = \frac{c_f}{c_i} \;\therefore x = \frac{0.1000\left(\frac{mol}{L}\right)}{11.65\left(\frac{mol}{L}\right)} \;\therefore x = 8.583 \times 10^{-3}$$

The obtained value of x was utilised in solving the following equation to obtain the required volume of $HCl_{(aq)}$from a chosen volume of D_2O.

$$x = \frac{v(HCl)}{v(HCl) + v(D_2O)}$$

This relationship was derived from the previous relationship $x = \frac{c_f}{c_i}$ as follows…

$$x = \frac{c_f}{c_i} = \frac{\frac{n_f}{v_f}}{\frac{n_i}{v_i}} = \frac{v_i}{v_f}$$

See footnote[6] for symbol definitions.

n_i and n_f cancel out because $n_i = n_f$.

$$x = \frac{v_i}{v_f} = \frac{v(HCl)}{v(HCl) + v(D_2O)}$$

$$x = \frac{v(HCl)}{v(HCl) + v(D_2O)} \therefore\ v(HCl) = x.v(HCl) + x.v(D_2O)$$

$$\therefore\ v(HCl)(1-x) = x.v(D_2O) \therefore\ v(HCl) = \frac{x.v(D_2O)}{(1-x)}$$

The reaction mixture was prepared

Glucose was weighed (~0.0050 g) in a vial and the required volume of the D-$_2$O/HCl solution was determined using the equation:

$$v(D_2O/HCl{:}\,mL) = 1000 \times \frac{m(glucose{:}\,g)}{conc.\,(glucose{:}\frac{mol}{L}) \times Mr(glucose{:}\frac{g}{mol})}$$

An example calculation

This example used for a required HCl concentration of 0.100 mol L^{-1}, a volume of 2.00 mL of D_2O, a volume of 0.58 mL of the D_2O/HCl mixture, a required glucose concentration of 0.500 molL^{-1} and a glucose mass of 0.0540 g.

The required volume of $HCl_{(aq)}$ was determined…

$$v(HCl) = \frac{x.v(D_2O)}{(1-x)} = \frac{8.583 \times 10^{-3} \times 2.00\ mL}{(1 - 8.583 \times 10^{-3})} = 1.731 \times 10^{-2}\ mL$$

This volume of HCl_{aq} was added to the volume of D_2O and mixed in a vortex mixer. The volume of the required D_2O/HCl was determined…

$$v(D_2O/HCl{:}\,mL) = 1000 \times \frac{0.0540g)}{0.500\frac{mol}{L} \times 180.16\ \frac{g}{mol}} = 0.599\ mL$$

This volume of the D_2O/HCl mixture was transferred into the vial containing the weighed glucose and prepared for analysis on the NMR spectrometer.

2.2.3.3 Uncatalysed DHA dimer dissociation kinetic experiments

DHA dimer was weighed (~0.0050 g) in a vial and the required volume of DMSO-*d6* was determined using the equation:

---

[6] c_i = initial concentration (mol L^{-1}), c_f = final concentration (mol L^{-1}), n_i = initial amount (mol), n_f = final amount (mol), v_i = initial volume (mL), v_f = final volume (mL)

$$v(DMSOd6{:}mL) = 1000 \times \frac{m(DHA{:}\,g)}{conc.(DHA{:}\frac{mol}{L}) \times Mr(DHA{:}\frac{g}{mol})}$$

This volume of the DMSO-*d6* was transferred into the vial containing the weighed DHA dimer and a timer was immediately set to provide t(0) for the kinetic analysis. The reaction solution was mixed on the vortex mixer and transferred into an NMR tube and inserted into the NMR spectrometer

2.2.3.4 D_2O catalysed DHA dimer dissociation kinetic experiments

The concentration of D_2O in the solution of DMSO-*d6* was represented as a mass percentage (m%) for comparison with the concentration of water in honey (~18 m%) and as two liquids were being added together, the final volume was ambiguous thus this information was unavailable to determine a concentration in moles per litre.

A solution of appropriate concentration of D_2O in DMSO-d6 was prepared

The mass of the predetermined volume of DMSO-*d6* was calculated using the specific density of DMSO-*d6* at 20°C (d. 1.19 g mL^{-1})…

$$m(DMSOd6{:}\,g) = v(DMSOd6{:}mL) \times d(1.19\ g\ mL^{-1})$$

Using this determined mass of DMSO-*d6* and the required m% to determine the required volume of D_2O…

$$m\% = 100 \times \frac{m(D_2O)}{m(D_2O) + m(DMSOd6)}$$

$$100 \times m(D_2O) = m\% \times m(D_2O) + m\% \times m(DMSOd6)$$

$$100 \times m(D_2O) - m\% \times m(D_2O) = m\% \times m(DMSOd6)$$

$$m(D_2O)(100 - m\%) = m\% \times m(DMSOd6)$$

$$m(D_2O) = \frac{m\% \times m(DMSOd6)}{(100 - m\%)}$$

$$v(D_2O\ mL) = \frac{m(D_2O\ g)}{d(D_2O\ g\ mL^{-1})}$$

Preparation for the addition of the DHA dimer to the mixture is as reported in the preceding subsection 2.2.3.3.

An example calculation

This example used a required m% of 10m%, a 0.600 mL volume of DMSO-*d6*, a mass of 0.0048 g of DHA dimer, a concentration of 0.25 mol L^{-1} for the DHA

dimer, a relative molecular mass (Mr) for the DHA of 180.16 $gmol^{-1}$ and the specific densities of DMSO-*d6* (d. 1.19 g mL^{-1}) and D_2O (d. 1.12 g mL^{-1}).

$$m(DMSOd6{:}g) = 0.600\ mL \times 1.19\ g\ mL^{-1} = 0.714\ g$$

$$m(D_2O\ g) = \frac{10 \times 0.714\ g}{100 - 10} = 7.93 \times 10^{-2}\ g$$

$$v(D_2O\ mL) = \frac{7.93 \times 10^{-2}\ g}{1.12\ gmL^{-1}} = 7.08 \times 10^{-2}\ mL$$

This calculated volume of D_2O was added to the predetermined volume of DMSO-*d6* in a vial and mixed on the vortex mixer.

DHA dimer was weighed in a vial to give a mass 0.0248 g and the required volume of the DMSO-*d6*/D_2O was determined…

$$v(DMSOd6/D_2O{:}mL) = 1000 \times \frac{0.0248\ g}{0.25\ molL^{-1} \times 180.16\ gmol^{-1}} \cong 0.551\ mL$$

This volume of the DMSO-*d6*/D_2O mixture was transferred into the vial containing the weighed DHA dimer and prepared for analysis on the NMR spectrometer.

2.2.3.5 CD_3COOD catalysed DHA dimer dissociation kinetic experiments

The concentration of CD_3COOD in the solution of DMSO-*d6* was represented as a molar percentage (mol%) as this gave an intuitive appreciation on the relative amount of acid molecules present in a given reaction. The mol% was also used as two liquids were being added together with an ambiguous final volume thus this volume information was unavailable to determine a concentration in moles per litre.

A solution of appropriate concentration of CD_3COOD in DMSO-d6 was prepared

The number of moles of the predetermined volume of DMSO-*d6* was calculated using the specific density of DMSO-*d6*…

$$n(DMSOd6{:}mol) = \frac{v(DMSOd6{:}mL) \times d(1.19\ g\ mL^{-1})}{Mr(DMSOd6{:}gmoL^{-1})}$$

Using this determined number of moles of DMSO-*d6* and the required mol%, the required volume of CD_3COOD was determined …

$$n\% = 100 \times \frac{n(CD_3COOD)}{n(D_2O) + n(DMSOd6)}$$

$$100 \times n(CD_3COOD) = n\% \times m(CD_3COOD) + n\% \times n(DMSOd6)$$

$$100 \times n(CD_3COOD) - n\% \times m(CD_3COOD) = n\% \times n(DMSOd6)$$

$$n(CD_3COOD)(100 - n\%) = n\% \times n(DMSOd6)$$

$$n(CD_3COOD) = \frac{n\% \times n(DMSOd6)}{(100 - n\%)}$$

$$v(CD_3COOD\ mL) = \frac{n(CD_3COOD\ mol) \times Mr(CD_3COOD gmol^{-1})}{d(CD_3COOD\ g\ mL^{-1})}$$

Preparation for the addition of the DHA dimer to the mixture is as reported in the previous subsection 2.2.3.3.

An example calculation

This example used a required mol% of 65 mol%, a 1.200 mL stock solution volume of DMSO-*d6*, a mass of 0.00254 g of DHA dimer, a concentration of 0.25 mol L^{-1} for the DHA dimer, a relative molecular mass for the DHA of 180.16 $gmol^{-1}$ and for CD_3COOD of 64.08 $gmol^{-1}$ and the specific densities of DMSO-*d6* (d. 1.19 g mL^{-1}) and CD_3COOD (d. 1.12 g mL^{-1}).

$$n(DMSOd6{:}g) = \frac{1.200\ mL \times 1.12\ g\ mL^{-1}}{180.16\ gmol^{-1}} = 7.46 \times 10^{-3} mol$$

$$n(CD_3COOD{:}mol) = \frac{65 \times 7.46 \times 10^{-3} mol}{(100 - 65)} = 1.39 \times 10^{-2} mol$$

$$v(CD_3COOD\ mL) = \frac{1.39 \times 10^{-2} mol \times 64.08\ gmol^{-1}}{1.12\ g\ mL^{-1}} = 0.793\ mL$$

This calculated volume of CD_3COOD was added to the predetermined volume of DMSO-*d6* in a vial and mixed on the vortex mixer.

DHA dimer was weighed in a vial to give the mass 0.0254 g and the required volume of the DMSO-*d6*/ CD_3COOD mixture was determined…

$$v(DMSOd6/CD_3COOD{:}mL) = 1000 \times \frac{0.0254\ g}{0.25\ molL^{-1} \times 180.16\ gmol^{-1}} \cong 0.564\ mL$$

This volume of the DMSO-*d6*/D_2O mixture was transferred into the vial containing the weighed DHA dimer and prepared for analysis on the NMR spectrometer.

2.2.3.6 CD_3COOD/CD3COO- catalysed DHA dimer dissociation kinetic experiments

The concentrations of DHA (0.25 M) and CD_3COOD (10 mol%) were kept constant as the concentration of CD_3COO^- was incrementally increased. The concentration of CD_3COO^- was represented as a molar percentage (mol%) relative to the amount of CD_3COOD present in the DMSO-*d6* solution as these series of experiments were intended to examine the effect on the reaction rate constant as the concentration of CD_3COO^- was increased against a constant concentration of CD_3COOD. CD_3COO^- was produced *in situ* by the addition of sodium hydroxide (NaOH) which, as a strong base, deprotonated an equimolar amount of CD_3COOD thus producing an equimolar amount of CD_3COO^-. The molar amount of added NaOH was subtracted from the original amount of CD_3COOD added when calculating the amount of DMSO-*d6* to add to the CD_3COOD/ CD_3COO^- mixture. This was performed in order to maintain a constant concentration of CD_3COOD.

A stock solution of specified mol% of CD_3COO^- to CD_3COOH was prepared

A weighed mass value of NaOH, that had been transferred to a vial, was converted to moles and together with the required mol% inputted into the equation…

$$n(CD_3COOD) = \frac{n(OH^-) \times n(100 - mol(OH^-)\%)}{mol(OH^-)\%}$$

This molar value was converted to the volume value, by converting it to a mass value and dividing this by the specific gravity of CD_3COOD (d. 1.12 g mL^{-1}), and transferred to the vial containing the weighed NaOH and mixed with a vortex mixer for five minutes to give the stock solution of CD_3COOD/CD_3COO^-.

A mixture of CD_3COOD/CD_3COO^- of specified concentration was prepared from the stock solution

A volume of stock was transferred to a vial. The molar amount of OH^- used, i.e. the molar amount of CD_3COO^- present was determined by converting the volume value of the CD_3COOD to the mass value using the specific gravity of CD_3COOD and converting the mass value to the molar value. The determined molar value for CD_3COOD and molar percentage of the stock were used in the equation…

$$n(CD_3COO^-) = \frac{n(CD_3COOD)mol(CD_3COO^-)\%}{100 - mol(CD_3COO^-)\%}$$

to determine the amount of CD_3COO^- present in the diminished volume of stock. This molar value of CD_3COO^- and the required mol(x)% for the mixture were used to calculate what the total amount of CD_3COOD in the CD_3COOD/ CD_3COO^- mixture would be…

$$n(CD_3COOD) = \frac{n(CD_3COO^-) \times n(100 - mol(x)\%)}{mol(x)\%}$$

The original amount of moles of CD_3COOD in the reduced volume of stock was subtracted from the calculated total amount of moles of CD_3COOD that would be required to give the required mol%. This value for the difference in moles was the amount of moles of CD_3COOD that needed to be added to the stock volume. This value was converted to the mass value that was divided by the specific gravity of CD_3COOD to give the volume of CD_3COOD that was to be added to the stock solution in the vial to give a CD_3COOD/CD_3COO^- of required mol%.

Adding DMSO-d6 to the CD_3COOD/CD_3COO^- mixture

The molar amount of DMSO-*d6* to add to the CD_3COOD/CD_3COO^- mixture to produce the required mol% of CD_3COOD in DMSO-*d6* was determined using the equation…

$$n(DMSOd6) = \frac{[n(CD_3COOD) - n(OH^-)] \times n(100 - mol(x)\%)}{mol(x)\%}$$

The molar amount of OH^- added to produce the CD_3COOD/CD_3COO^- mixture was subtracted from the molar amount of CD_3COOD originally used in the production of the CD_3COOD/CD_3COO^- mixture as it was assumed that this had all been converted to CD_3COO^-. The calculated molar value of the required DMSO-*d6* was converted to the mass value and then to the volume value of DMSO-*d6* to be transferred into the vial containing the CD_3COOD/CD_3COO^- mixture to give the DMSO-d6/CD_3COOD/CD_3COO^- mixture.

Adding DHA to the DMSO-d6/CD_3COOD/CD_3COO^- mixture

The volume of DMSO-d6/CD_3COOD/CD_3COO^- mixture to be added to a weighed amount of DHA was calculated using the equation…

$$v(DMSOd6; CD_3COOD; CD_3COO^-) = 1000 \times \frac{m(DHA_{dimer})}{conc.(DHA_{dimer}) \times Mr(DHA_{dimer})}$$

This volume of DMSO-d6/CD_3COOD/CD_3COO^- mixture was added to a weighed amount of DHA in a vial and prepared for analysis.

An example calculation

A reaction mixture of DHA (0.25 M) in DMSO-*d6* with CD_3COOD (10 mol% relative to DMSO-*d6*) and CD_3COO^- (4 mol% relative to CD_3COOD) was prepared from a stock solution of CD_3COO^- (8 mol% relative to CD_3COOD)

1. *A stock solution of 8.00* mol% *of CD_3COO^- relative to CD_3COOH was prepared*

The amount of NaOH was transferred to a vial and weighed (0.0371 g). This value was converted to moles…

$$n(NaOH) = \frac{m(NaOH)}{Mr(NaOH)} = \frac{0.0371\ g}{40.00\ g\ mol^{-1}} = 9.28 \times 10^{-4}\ mol$$

This value and the value for the mol% was used to determine the number of moles of CD_3COOD needed…

$$n(CD_3COOD) = \frac{9.28 \times 10^{-4}\ mol \times (100 - 8)}{8} = 1.08 \times 10^{-2}\ mol$$

This molar value was converted to the mass value…

$$m(CD_3COOD) = n(CD_3COOD) \times Mr(CD_3COOD) = 0.684\ g$$

This mass value was converted to the volume value…

$$v(CD_3COOD) = \frac{m(CD_3COOD)}{d(CD_3COOD)} = \frac{0.684\ g}{1.12\ g\ mL^{-1}} = 0.610\ mL$$

This volume of CD_3COOD was transferred to the vial containing NaOH and mixed on the vortex mixer to produce the stock solution (actual 8.07 mol%) to be used for the series of CD_3COOD/CD_3COO^- catalysed experiments.

A mixture of CD_3COOD/CD_3COO^- (4 mol%) was prepared from the stock solution

An amount of CD_3COOD (0.0700 mL) of stock solution was transferred to a vial and the molar amount of CD_3COOD in the vial was calculated…

$$m(CD_3COOD) = v(CD_3COOD) \times d(CD_3COOD) = 0.0784\ g$$

$$n(CD_3COOD) = \frac{m(CD_3COOD)}{Mr(CD_3COOD)} = \frac{0.0784\ g}{64.1\ g\ mol^{-1}} = 1.22 \times 10^{-3}\ mol$$

This molar value was used to calculate the amount of CD_3COO^- in the 0.0700 mL volume of stock solution…

$$n(CD_3COO^-) = \frac{1.22 \times 10^{-3}\ mol \times 8.07}{100 - 8.07} = 1.07 \times 10^{-4}\ mol$$

This molar value was used to calculate the total amount of CD_3COOD required to produce a solution of concentration 4.00 mol%...

$$n(CD_3COOD)_{total} = \frac{1.07 \times 10^{-4}\ mol \times (100 - 8.07)}{8.07} = 2.58 \times 10^{-2}\ mol$$

The amount of moles in the reduced stock solution was subtracted from the total amount of moles required for the 4.00 mol% and converted to a volume value to give the volume of CD_3COOD to be added to the stock solution to give a solution of 4.00 mol% CD_3COO^- relative to CD_3COOD…

$$2.58 \times 10^{-2}\ mol - 1.07 \times 10^{-4}\ mol = 1.35 \times 10^{-3}\ mol$$

$$m(CD_3COOD) = 1.35 \times 10^{-3}\ mol \times 64.1\ g\ mol^{-1} = 8.68 \times 10^{-2}\ g$$

$$v(CD_3COOD) = \frac{8.68 \times 10^{-2}\ g}{1.12\ g\ mL^{-1}} = 7.75 \times 10^{-2}\ mL$$

This volume of CD_3COOD was transferred to the vial containing the 0.0700 mL volume of stock solution and mixed on the vortex mixer to produce a mixture of CD_3COOD/CD_3COO^- of concentration 4.00 mol%.

Adding DMSO-d6 to the CD_3COOD/CD_3COO^- 4.00 mol% mixture to produce a mol% concentration of CD_3COOD to DMSO-d6 of 10%

A volume of the CD_3COOD/CD_3COO^- (0.0553 mL) mixture was transferred to a vial. The amount of moles of CD_3COOD in this volume was calculated…

$$m(CD_3COOD) = 5.53 \times 10^{-2} mL \times 1.12\ g\ mL^{-1} = 6.19 \times 10^{-2}\ g$$

$$n(CD_3COOD) = \frac{6.19 \times 10^{-2}\ g}{64.1\ g\ mol^{-1}} = 9.67 \times 10^{-4}\ mol$$

This molar value and the mol% of 4 % were used to calculate the amount of CD_3COO^- present…

$$n(CD_3COO^-) = \frac{9.67 \times 10^{-4}\ mol\ \times 4.00}{100 - 4.00} = 4.03 \times 10^{-5}\ mol$$

These molar values for CD_3COOD and CD_3COO^- with the required mol% of 8 % were used to calculate the amount of moles of DMSO-*d6* required to produce a mixture of concentration CD_3COOD to DMSO-*d6* of 8 mol%...

$$n(DMSOd6) = \frac{[9.67 \times 10^{-4}\ - 4.03 \times 10^{-5}\ ]mol \times (100 - 10)}{10} = 8.34 \times 10^{-3}\ mol$$

This molar value of DMSO-*d6* was converted to a volume value…

$$m(DMSOd6) = 8.34 \times 10^{-3}\ mol \times 84.2\ g\ mol^{-1} = 7.02 \times 10^{-1}\ g$$

$$v(CD_3COOD) = \frac{7.02 \times 10^{-1}\ g}{1.19\ g\ mL^{-1}} = 5.90 \times 10^{-1}\ mL$$

Therefore 5.90 x 10^{-1} mL of DMSO-d6 was transferred to the vial containing 5.53 x 10^{-2} mL of CD_3COOD/CD_3COO^- mixture to produce a DMSO-d6/CD_3COOD/CD_3COO^- mixture with a CD_3COOD concentration to DMSO-d6 of 10.0 mol% and a CD_3COO^- concentration to CD_3COOD of 4.00 mol%.

Adding DHA to the DMSO-d6/CD_3COOD/CD_3COO^- mixture

An amount of DHA was transferred to a vial and weighed (0.0245 g). The volume of the DMSO-d6/CD_3COOD/CD_3COO^- mixture to be added to the weighed amount of DHA was calculated…

$$v(DMSOd6; CD_3COOD; CD_3COO^-) = 1000 \times \frac{0.0245\ g}{0.25\ mol\ L^{-1} \times 168.3\ g\ mol^{-1}} = 0.590\ mL$$

This volume of DMSO-d6/CD_3COOD/CD_3COO^- mixture was transferred to the weighed amount of DHA in the vial and hastily prepared for analysis on the NMR spectrometer.

3 Assignment of the ^{1}H NMR & ^{13}C NMR spectra of the dihydroxyacetone dimer and monomer in DMSO-*d6*

3.1 Introduction

1D and 2D NMR spectra of the freshly prepared DHA dimer sample, Figure 3.1, in DMSO-*d6* were obtained and the signals were assigned, Table 3.3, Table 3.6 and Table 3.7, to elucidate which ^{1}H and ^{13}C signals could be traced in the kinetic experiments that follow the disappearance of the DHA dimer. The ^{1}H and ^{13}C NMR spectra for the DHA monomer were assigned, Table 3.7, to allow for the kinetic data for the formation of the DHA monomer to be obtained. The chemical shifts and signal assignments were compared to the results of two earlier studies carried out in the 1970s on low resolution instruments.[23,25]

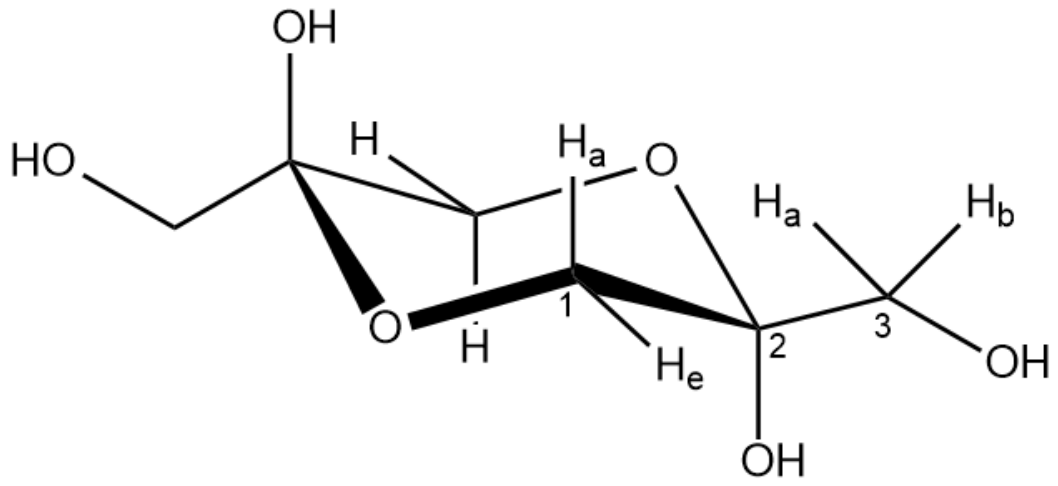

Figure 3.1: DHA 1,4-dioxane dimer structure showing labelling; due to symmetry there are only 2 carbon environments (C-1 and C-3 are equivalent and C-2) and 5 proton environments (H-1$_a$, H-1$_e$, C-2-O<u>H</u>, C-3-O<u>H</u> and the H-3$_a$ and H-3$_b$ environment)

3.2 Assignment of the ^{1}H NMR spectrum

The ^{1}H NMR spectrum for the DHA dimer, Figure 3.2, showed three discernible chemical environments at 5.62, 4.63 and 3.92 ppm and a multiplet in the 3.35 - 3.15 ppm region.

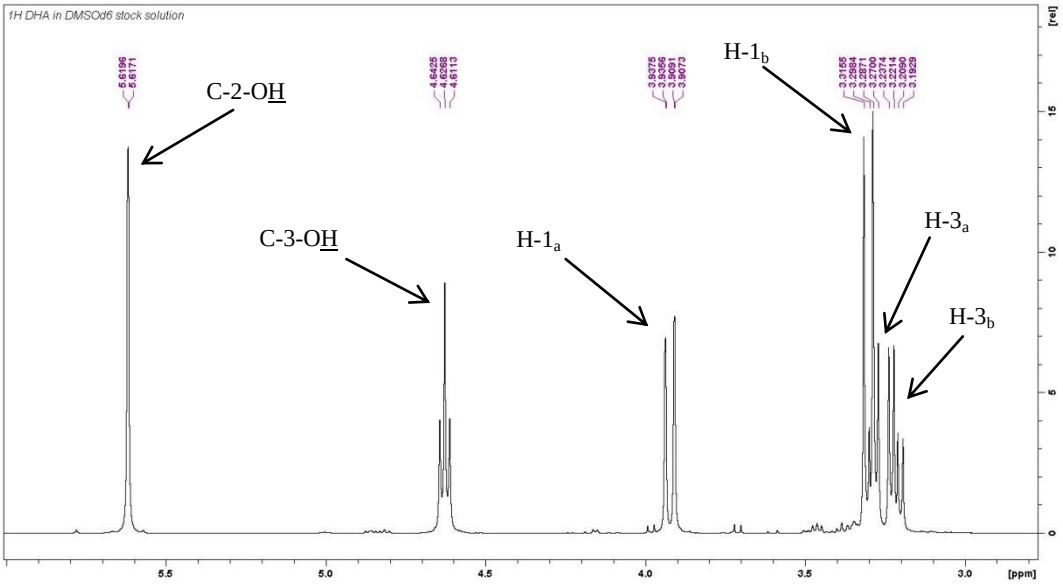

Figure 3.2: The assigned ^{1}H NMR spectrum of the DHA dimer in DMSO-d6

3.2.1 Integration:

Integration of the spectrum indicated that the three downfield signals resulted from single protons while the downfield portion of the multiplet contained two proton signals with the remainder of the multiplet containing one proton. This accounted for the six ^{1}H environments.

3.2.2 The signal at 5.62 ppm:

The doublet at 5.62 ppm was assigned to the axial hydroxyl proton C-2-O<u>H</u>. This signal was furthest down field due to deshielding as a result of being bonded to the anomeric carbon. The signal had a coupling constant of 1.00 Hz indicating that it was engaged in long-range coupling with the axial proton (H-1_a) as the two nuclei maintain a rigid planar W geometry.[54] This geometry allows for coupling to occur through the "tail ends" of the carbon and oxygen p-orbitals, thus circumventing the C – O bond.[54] If the C-2-O<u>H</u> group had been equatorial, there would have been no 1.00 Hz coupling constant as the rigid planar W geometry would not have been present.

3.2.3 The signal at 4.63 ppm:

The apparent triplet at 4.63 ppm was actually a doublet of doublets as the proton was coupling to a pair of non-equivalent protons. This signal was assigned to the hydroxymethyl hydroxyl proton (C-3-O<u>H</u>) which was coupled (^{3}J) to the methylene protons (H-3_a and H-3_b) with a coupling constant of ~6.24 Hz. The

chemical shift is in the range for hydroxyl protons (3.9 – 4.7 ppm)[55] in DMSO-*d6* and has the same shift as the hydroxyl proton in the primary alcohol ethanol.[55,56]

3.2.4 The signal at 3.92 ppm:

The doublet of doublets at 3.92 ppm was assigned to the axial proton (H-1_a) as its larger coupling constant (11.36 Hz) was indicative of diastereotopic geminal coupling[54,57] and its smaller coupling constant (0.74 Hz) was a indicative of long-range spin-spin coupling with the C-2-O<u>H</u> proton. H-1_a must be axial otherwise the W geometry would not be available to allow for long range coupling.

3.2.5 The signal at 3.30 ppm in the multiplet:

The peaks at 3.32 and 3.29 ppm in the multiplet were the doublet signal for the equatorial proton (H-1_e) with a diastereotopic geminal (^2J) coupling constant of 11.36 Hz to H-1_a. Unlike the axial proton, there was no long-range coupling with the axial hydroxyl proton as the geometry does not allow for p-orbital overlap.

3.2.6 The second-order splitting in the multiplet:

The remaining signals in the multiplet were assigned to the diastereotopic methylene protons (H-3_a, H-3_b) on the hydroxymethyl substituent. The complex splitting patterns of these two signals resulted from second-order (strong) coupling which alters the relative signal intensities and chemical shifts and therefore the true chemical shifts to be assigned to these protons needed to be calculated.

When the difference in chemical shifts ($\Delta\ \delta\nu$) and coupling constants (J) of a pair of coupling nuclei have the relationship:

$$\frac{\Delta\nu\delta}{J} > 10$$

Where $\delta\nu$ is over an order of magnitude greater than J, first-order (weak) coupling spectra are observed with simple splitting patterns where chemical shifts are at the centre of split lines and coupling constants are obtained directly from the spectrum. When the difference in chemical shifts and coupling constants approaches the same order of magnitude, the following relationship results:

$$\frac{\Delta\nu\delta}{J} < 10$$

Spectra start to exhibit complex second-order splitting effects where the signal intensities no longer follow Pascal's triangle and the true chemical shifts cannot be obtained directly from the spectrum.[58]

Second-order signals display characteristic splitting patterns often giving the "roofing" effect which can be useful in identifying coupling nuclei and the type of spin-system in simple systems. As the spin-system becomes more complex the second-order splitting patterns quickly become incomprehensible making manual interpretation of the spectrum impossible.

For complicated spin-systems there is software available (e.g. WinDNMR) that will solve simultaneously the quantum mechanical wave equations to untangle the multiplet and assign true chemical shift and coupling constant values to second-order splitting patterns.[54]

One of the advantages of having a spectrometer with higher field strength is that as the field strength increases the difference in chemical shift ($\Delta\ \delta\nu$) between two coupling nuclei (measured in Hertz) also increases whilst the coupling constant (J) remains the same. This results in the relationship $\Delta\ \delta\nu/J < 10$ for second-order splitting converting to $\Delta\ \delta\nu/J > 10$ for first-order splitting and thus simplifying the observed spectrum for manual inspection.

3.2.6.1 Spin-system notation:

The Pople notation incorporates letters of the alphabet to represent relative differences in chemical shift. The proton spin-system of the diastereotopic methylene and hydroxyl protons of the hydroxymethyl substituent is defined as ABX where A and B represent H-3_a and H-3_b that are of similar chemical shift and X representing C-2-O<u>H</u> that is of a relatively different chemical shift to both H-3_a and H-3_b. This simple spin-system is relatively common and has a characteristic splitting pattern that is easily recognisable. Before calculating the ABX chemical shifts an understanding of the simpler AB spin-system is required.

3.2.6.2 The AB spin-system:

The simplest second-order splitting pattern results from the AB spin-system that produces four lines in the spectrum and involves the spin-spin coupling of two nuclei with the relationship, Figure 1.3:

$$\frac{\Delta\nu\delta}{J} > 10$$

Second-order effects in this system result from the mixing of the four energy states predicted by quantum mechanics using the four spin-state combinations for the two coupling nuclei, Figure 1.4. This mixing alters the transition probabilities so that they can no longer be predicted by Pascal's triangle due to signal intensity being transferred from the outer lines to the inner lines[58] giving the characteristic "roofing" effect as can be seen in Figure 3.3.

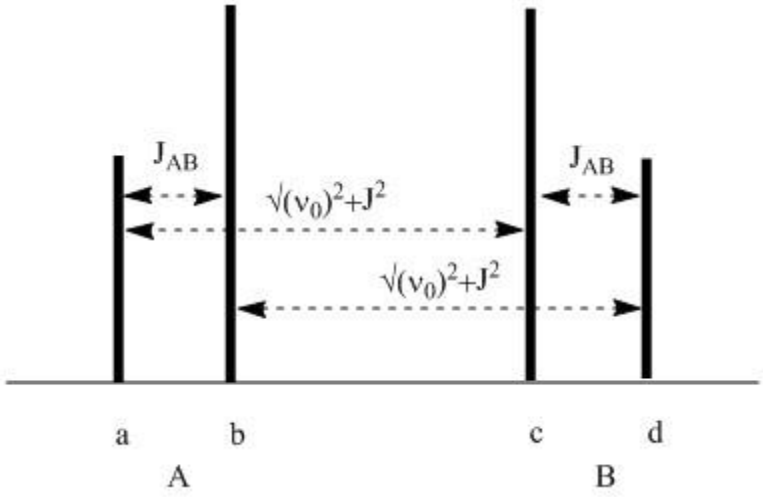

Figure 3.3: Second-order splitting for a AB spin-system with A arbitrarily further downfield

The AB spin-system can be defined by arbitrarily assigning nucleus A with a greater chemical shift relative to nucleus B, labelling the lower energy aligned spins α and the higher energy opposed spins ß, with the following spin-state combinations: αα, α ß, ß α and ß ß, Figure 3.4, and labelling the four lines a, b, c, d, from higher to lower chemical shifts.

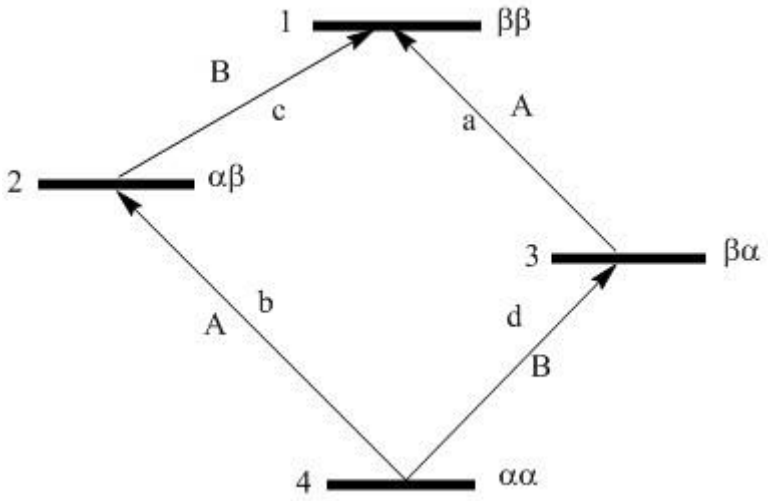

Figure 3.4: The spin-states and transitions (associated to each line) for the nuclei in the AB system

Labelling the true chemical shift separation (without second-order coupling effects) between nucleus A and nucleus B, $\nu_0\delta$, and the true chemical shifts for the nuclei ν_A and ν_B we get the equation:

$$\nu_0\delta = |\nu_A - \nu_B|$$

Table 3.1 shows the mathematical relationships between the transition energies and their relative intensities with the centre of the splitting pattern. The splitting pattern centre is obtained using the equation:

$$\nu_{Av} = \frac{\nu_A - \nu_B}{2}$$

Table 3.1: The transition energies and intensities relative to the centre of the splitting

Transition	Energy (Hz)	Relative intensity
$a \quad 3 \rightarrow 1$	$+\frac{1}{2}J + \frac{1}{2}\sqrt{(\nu_0\delta)^2 + J^2}$	$1 - \frac{J}{\sqrt{(\nu_0\delta)^2 + J^2}}$
$b \quad 4 \rightarrow 2$	$-\frac{1}{2}J + \frac{1}{2}\sqrt{(\nu_0\delta)^2 + J^2}$	$1 + \frac{J}{\sqrt{(\nu_0\delta)^2 + J^2}}$
$c \quad 2 \rightarrow 1$	$+\frac{1}{2}J - \frac{1}{2}\sqrt{(\nu_0\delta)^2 + J^2}$	$1 + \frac{J}{\sqrt{(\nu_0\delta)^2 + J^2}}$
$d \quad 4 \rightarrow 3$	$-\frac{1}{2}J - \frac{1}{2}\sqrt{(\nu_0\delta)^2 + J^2}$	$1 - \frac{J}{\sqrt{(\nu_0\delta)^2 + J^2}}$

From Figure 3.3 and Table 3.1, the relationship:

$$a - b = c - d = J$$

is derived. This relationship is constant for all ABX systems.

The true value, $\nu_0\delta$ can be derived from Figure 3.3and Table 3.1 as follows:

$$(a-d)(b-c) = (\sqrt{((\nu\_0\ \delta)\text{^}2 + J\text{^}2)} + J)(\sqrt{((\nu\_0\ \delta)\text{^}2 + J\text{^}2)} - J)$$

$$(a-d)(b-c) = (\nu_0\delta)^2 + J^2 - J^2$$

$$(a-d)(b-c) = (\nu_0\delta)^2$$

therefore:

$$\nu_0\delta = \sqrt{(a-d)(b-c)}$$

3.2.6.3 The ABX system

The differences in chemical shifts between the AB nuclei and the X nucleus have the relationship $\Delta\ \delta\nu/J > 10$, thus the X signal is not affected by second-order effects leaving only the A and B chemical shifts to each be calculated separately as simple AB systems. ν_A and ν_B will both be doublets as they are each coupled to X.

3.2.6.4 Calculating chemical shifts for the hydroxymethyl methylene protons

The eight peaks in the multiplet were labelled a to h moving from higher chemical shift to lower chemical shift (see figure 4). Lines a and c are a combination of the H-3_a and H-1_e signals which has distorted the chemical shift values for the two H-3_a lines. As the ABX system is centro-symmetric,[58] the lines f and h were reflected through the midpoint between lines d and e to give the undistorted frequency values for lines a and c, Table 3.2.

Table 3.2: The chemical shifts for the lines in the AB sub-system

Line	Chemical shift (ppm)	Chemical shift (Hz)
a	3.3145*	1326.23*
b	3.2984	1319.79
c	3.2860*	1314.83*
d	3.2700	1308.43
e	3.2374	1295.38
f	3.2214	1288.98
g	3.2090	1284.02
h	3.1929	1277.58

* Adjusted values

The eight lines constitute two AB sub-spectra with the bold lines in Figure 3.5 representing the H-3_a signal and the lighter lines representing the H-3_b signal. The true chemical shift for each AB sub-spectrum was calculated by reducing the four lines of each sub-spectrum to two lines using the method for solving AB systems as previously described. The remaining four lines are two doublets that can be paired depending on their coupling constants where the pairs that have coupling constants close to the coupling constants for the C-3-OH triplet.

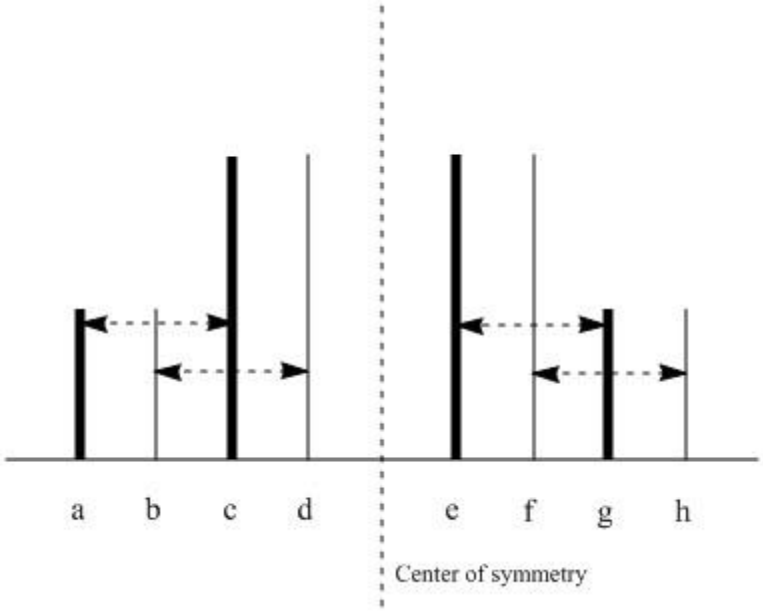

Figure 3.5: The graphical representation of the ABX splitting pattern of the hydroxymethyl methylene protons in the 1H NMR spectrum

The midpoints ν_{Av} and ν_{Bv} were first determined:

$$\nu_{Av} = \frac{a+c+e+g}{4} \quad \therefore \quad \nu_{Av} = 1305.11\ Hz$$

$$\nu_{Bv} = \frac{b+d+f+h}{4} \quad \therefore \quad \nu_{Bv} = 1298.69\ Hz$$

The true separations $\nu_0\delta_A$ and $\nu_0\delta_B$ were determined:

$$\nu_0\delta_A = \sqrt{(a-g)(c-e)} \quad \therefore \quad \nu_0\delta_A = 28.6514\ Hz$$

$$\nu_0\delta_A = \sqrt{(b-h)(d-f)} \quad \therefore \quad \nu_0\delta_A = 28.6514\ Hz$$

The determined separations were halved and added to and also subtracted from the midpoints for each sub-spectrum to give the calculated doublet lines for H-3_a and H-3_b.

$$1 - \nu_{Av} + \nu_0\delta = 1319.44\ Hz \quad or \quad 3.298\ ppm$$

$$2 - \nu_{Av} - \nu_0\delta = 1290.79\ Hz \quad or \quad 3.226\ ppm$$

$$3 - \nu_{Bv} + \nu_0\delta = 1313.02\ Hz \quad or \quad 3.281\ ppm$$

$$4 - \nu_{Bv} - \nu_0\delta = 1284.37\ Hz \quad or \quad 3.210\ ppm$$

The coupling constant for the calculated lines 1 and 3 is 6.42 Hz as is the coupling constant for lines 2 and 4. This value is relatively close to the coupling constant 6.24 Hz for the C-3-OH triplet therefore the H-3_a doublet was assigned the chemical shifts 3.298 (3.30) ppm and 3.281 (3.28) ppm and the H-3_b doublet was assigned the chemical shifts 3.226 (3.23) ppm and 3.210 (3.21) ppm.

3.2.7 H,H-COSY

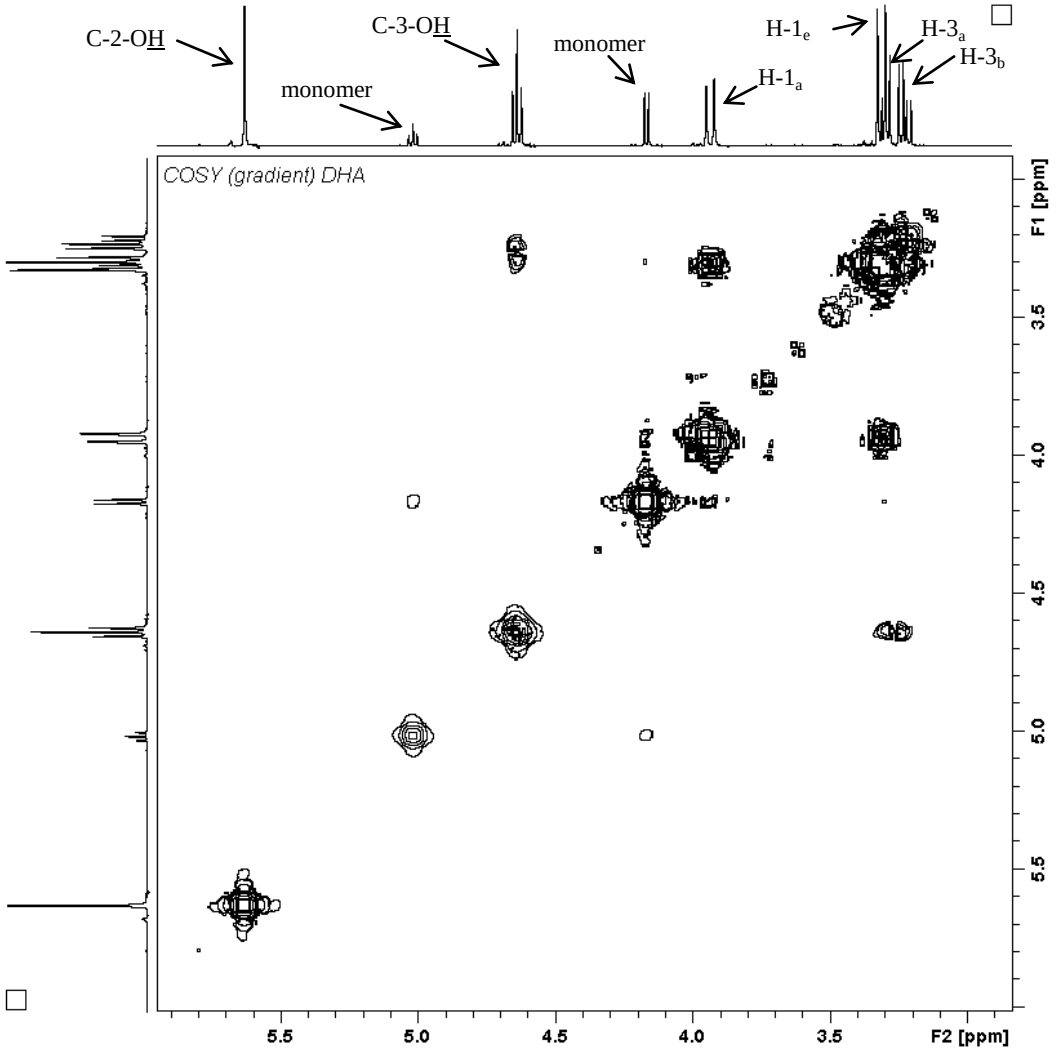

Figure 3.6: The COSY spectrum of the DHA dimer and DHA monomer in DMSO-d6

The COSY spectrum, Figure 3.6, and the expanded spectrum, Figure 3.7, showed ^3J correlations between the C-3-OH triplet at 4.63 ppm and the signals for H-3_b

(3.22 ppm) and H-3_a (3.29 ppm) in the multiplet which supported their assignment as hydroxymethyl protons in an ABX spin-system with A representing H-3_a, B representing H-3_b and X representing C-3-O<u>H</u>.

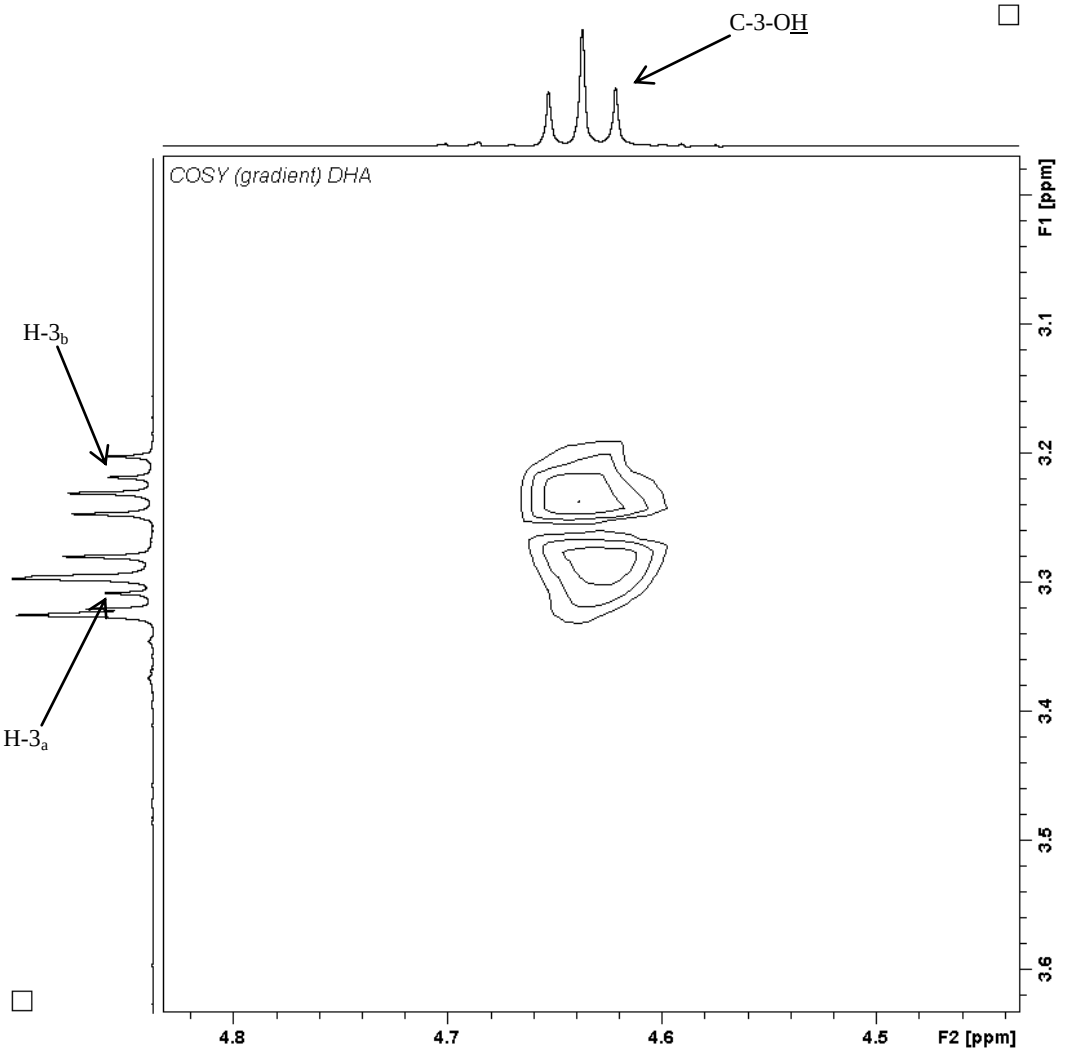

Figure 3.7: The expanded COSY spectrum of DHA is DMSO-*d6* showing the H-3_a/ C-2-OH and H-3_b/ C-2-OH correlations

There was a relatively strong ^2J correlation observed between the H-1_a doublet signal at 3.92 ppm and the H-1_e doublet signal at 3.30 ppm with coupling constants ^2J 11.4 Hz, Figure 3.8. This large coupling constant supported the assignment of these two signals to diastereotopic geminal protons, with one proton being axial and the other being equatorial in the dioxane ring.[59] The literature value range for diastereotopic geminal proton coupling in a 1,3-dioxane ring is 11-14 Hz.[57]

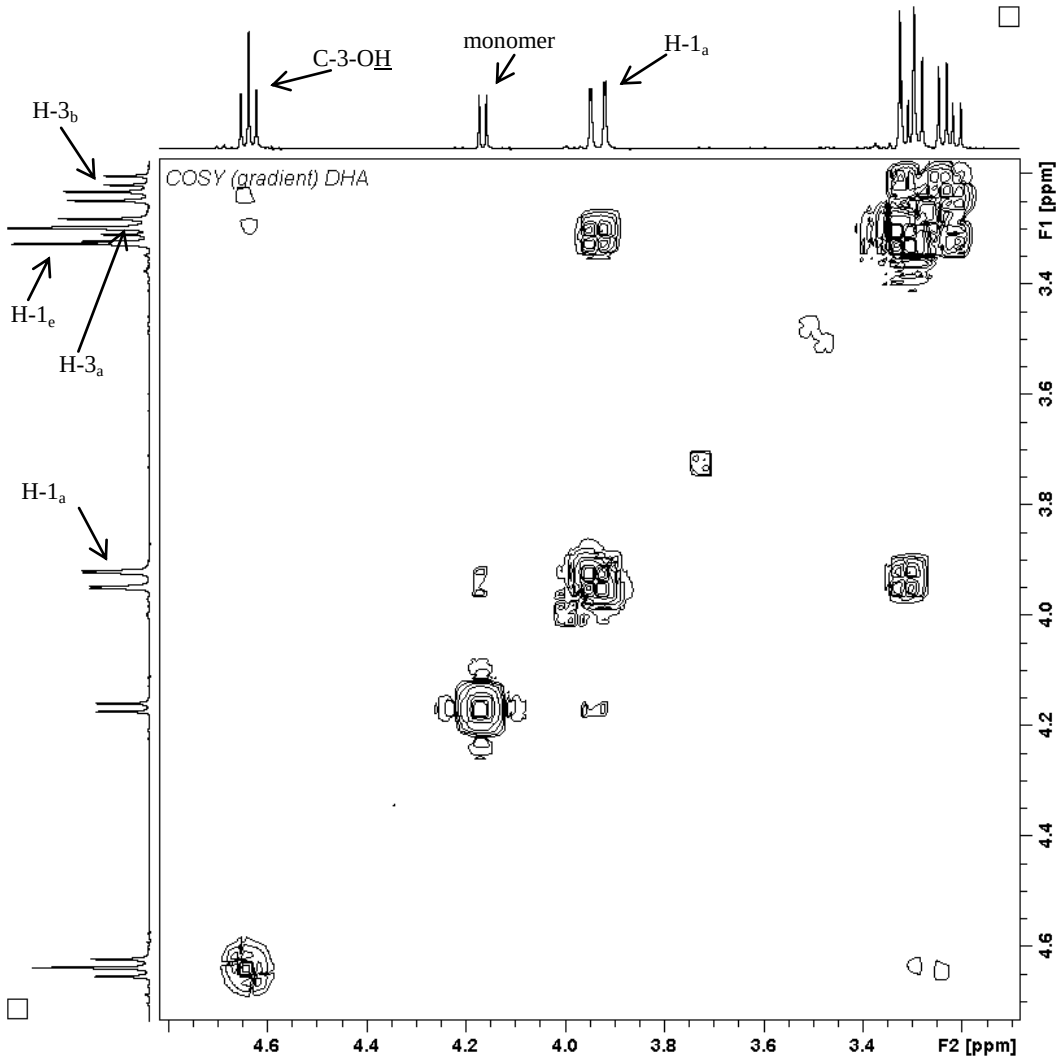

Figure 3.8: The expanded COSY spectrum of DHA is DMSO-*d6* showing the H-3_a/ C-2-OH and H-3_a /C-2-OH correlations and the H-2_e / H-2_a correlations. There is an inexplicable correlation between the monomer methylene signal and the H-1_a dimer signal.

On enlargement of the contour plot at 3.3 ppm, a ^2J correlation was observed, just off-diagonal, between the signals assigned to the H-3_a and H-3_b protons, Figure 3.9, with ^2J coupling constants of 11.4 Hz. This supported the assignment of as the two signals as the diastereotopic geminal methylene protons associated with the hydroxymethyl substituent.

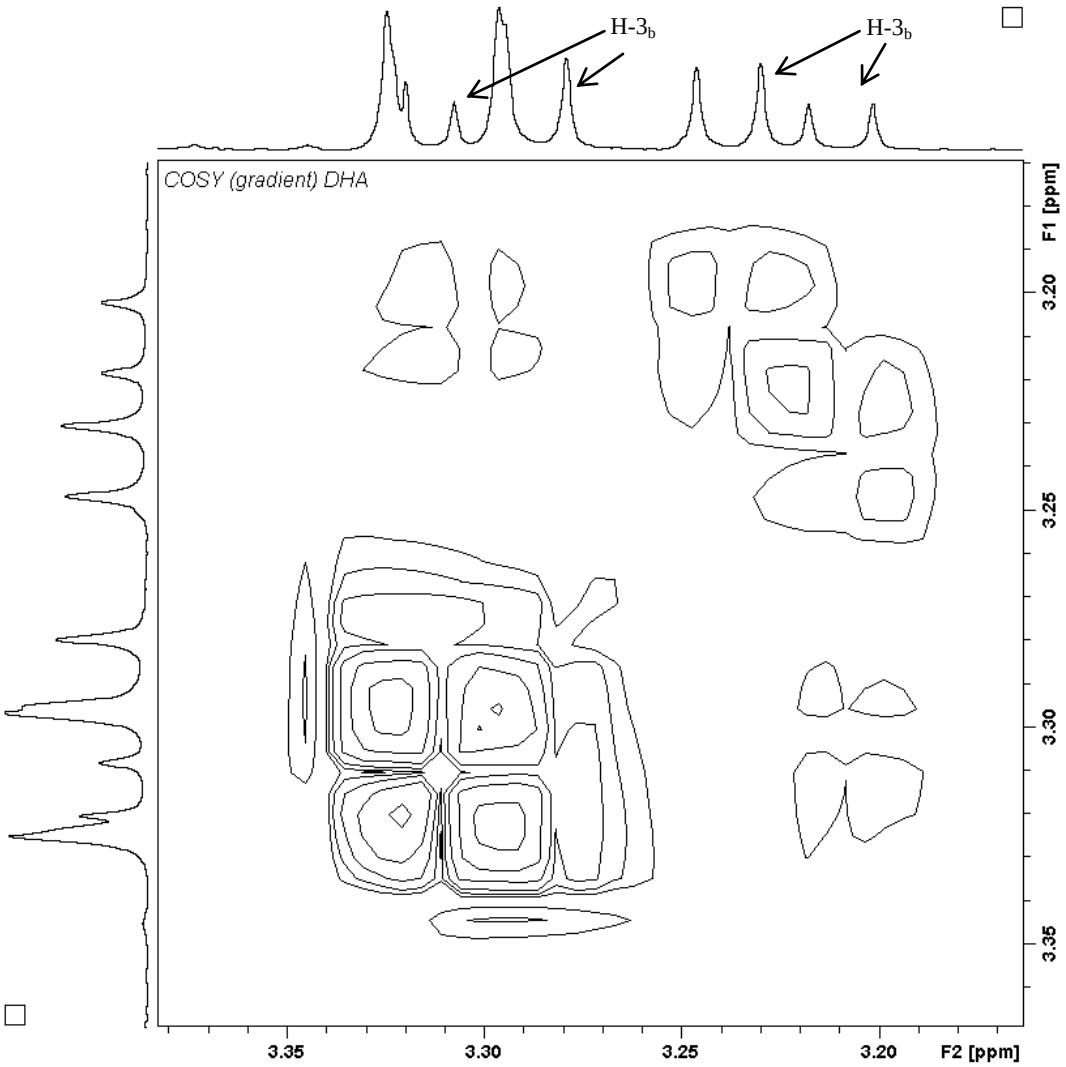

Figure 3.9: The expanded COSY spectrum of DHA is DMSO-*d6* showing the $H3_a$ and $H3_b$ correlations

The COSY spectrum shows no correlations for the signal at 5.62 ppm which supports the assignment of this signal to the axial hydroxyl proton in the ring as its closest couplings are ^4J which are out of the range (^2J - ^3J) for the COSY experiment.

In Figure 3.8 there is a weak correlation between the dimer H-1_a and monomer methylene proton. This apparent correlation is a result of coherence transfer between vicinal ring protons in the DHA dimer or the DHA monomer that maintain their magnetisation during the dissociation, which is in dynamic equilibrium, due to the long spin-lock acquisition times used in 2D spectroscopy.[60,61] During the long acquisition time the dimer has dissociated to form two monomer units and thus the monomer methylene protons, that had engaged in coherence transfer as dimer protons, appear to have coherence with the dimer. The same phenomena occurs in the reverse direction of the dynamic

equilibrium reaction. To verify that these correlations were artefacts of the COSY experiment the 1D SELCOSY experiment, with a shorter acquisition time, was performed to see if the dimer/monomer correlations would still be present.

3.2.8 SELCOSY

The SELCOSY experiment effectively takes slices from the F2 axis of the COSY experiment by exciting a selected signal and providing a 1D spectrum with correlating peaks to the excited signal being observed. To verify that the H-1_a was not engaging in coherence transfer with the monomer methylene protons in the COSY experiment, the H-1_a signal was excited in the SELCOSY experiment, Figure 3.10. The SELCOSY spectrum only showed a ^2J correlation between the H-1_a excited signal and the H-1_e signal with a very weak ^4J correlation between the H-1_a excited signal and the C-2-O<u>H</u> signal. There was no correlation between the H-1_a signal and the monomer methylene signal thus validating the assertion that the correlation observed in the COSY experiment was an artefact of that experiment.

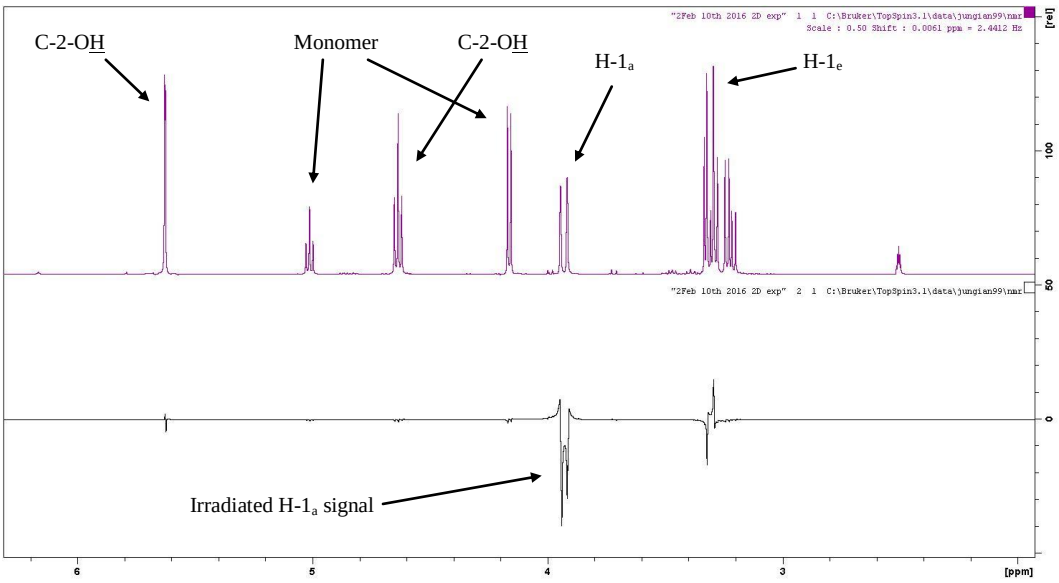

Figure 3.10: The H-1_a excited SELCOSY spectrum (bottom) stacked with the standard ^{1}H NMR spectrum.

The monomer methylene signal was excited to observe whether or not that it had a correlation with the H-1_a signal as was seen in the COSY experiment. The SELCOSY spectrum, Figure 3.11, only showed a correlation to the monomer hydroxyl proton with no correlation with the H-1_a as seen in the COSY

experiment. Thus providing further evidence that the correlation observed in the COSY experiment was an artefact.

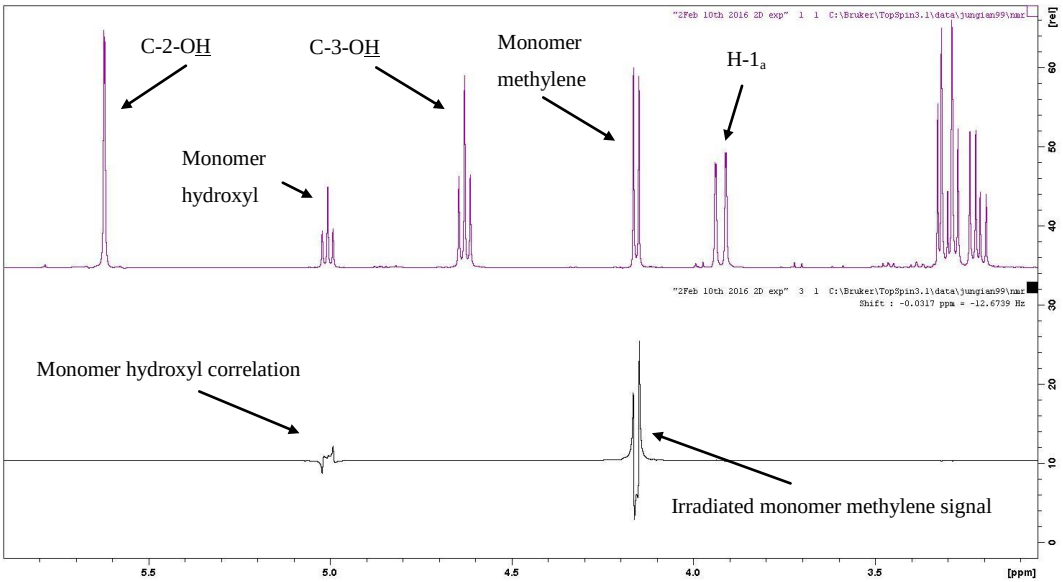

Figure 3.11: The monomer methylene excited SELCOSY spectrum (bottom) stacked with the standard 1H NMR spectrum.

3.2.9 HSQC

The HSQC experiment allowed differentiation between the two methylene carbons signals at 66.3 ppm and 63.2 ppm by the observation of their ^{1}J correlations with the attached protons, Figure 3.12 and Figure 3.13.

The ^{13}C signal at 66.3 ppm showed a ^{1}J correlation with the H-3_a and H-3_b signals in the multiplet thus allowing the ^{13}C signal at 66.3 ppm to be assigned to C-3.

The signal in the ^{13}C spectrum at 63.2 ppm showed ^{1}J correlations to the H-1_a signal at 3.92 ppm and the H-1_e signal in the multiplet at 3.3 ppm which allowed this ^{13}C signal to be assigned C-1, Figure 3.13.

The C-2 ^{13}C signal at 92.8 ppm showed no ^{1}J correlations as it was a quaternary carbon and therefore could not engage in ^{1}J coupling with any protons, Figure 3.12.

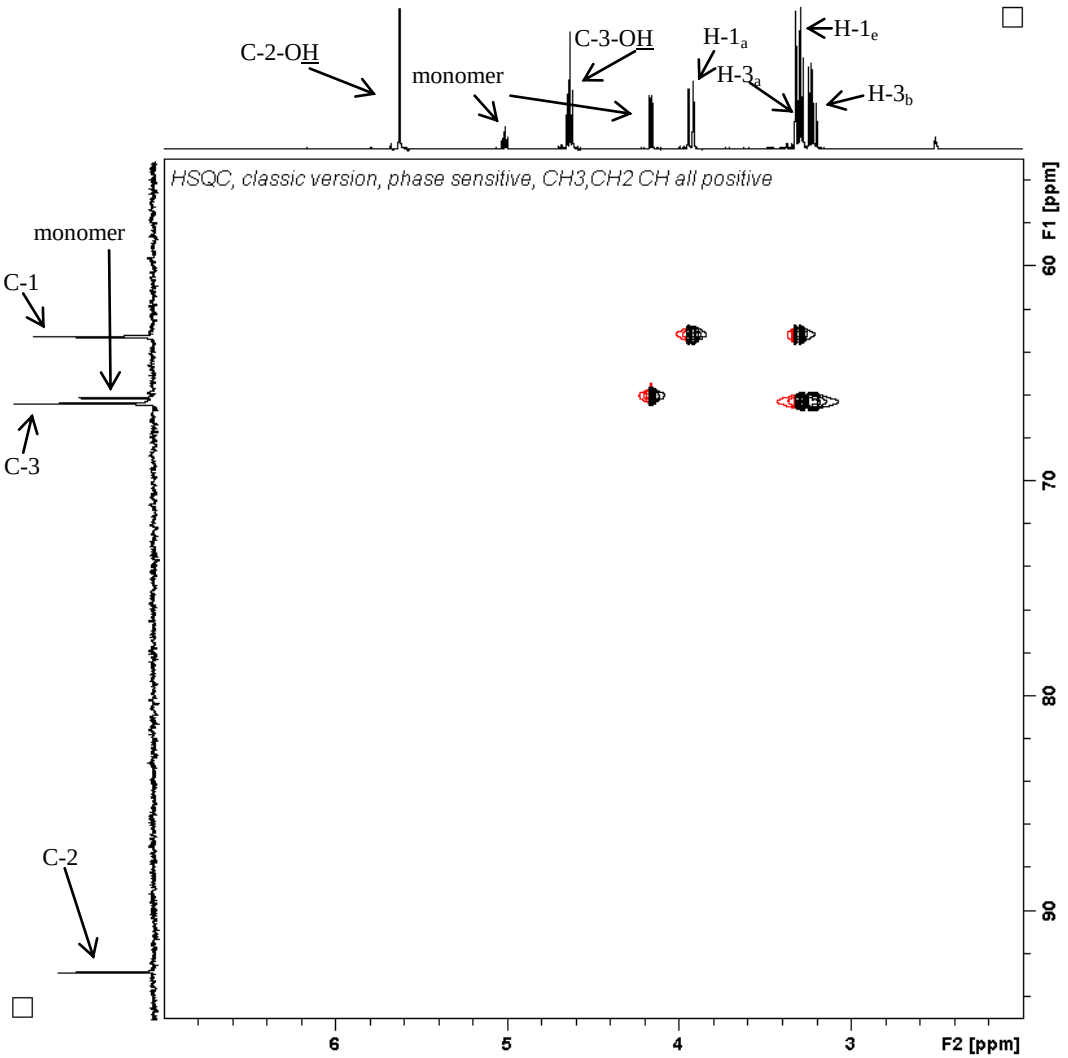

Figure 3.12: The HSQC spectrum of DHA dimer and DHA monomer in DMSO-*d6* showing correlations between carbon and proton signals.

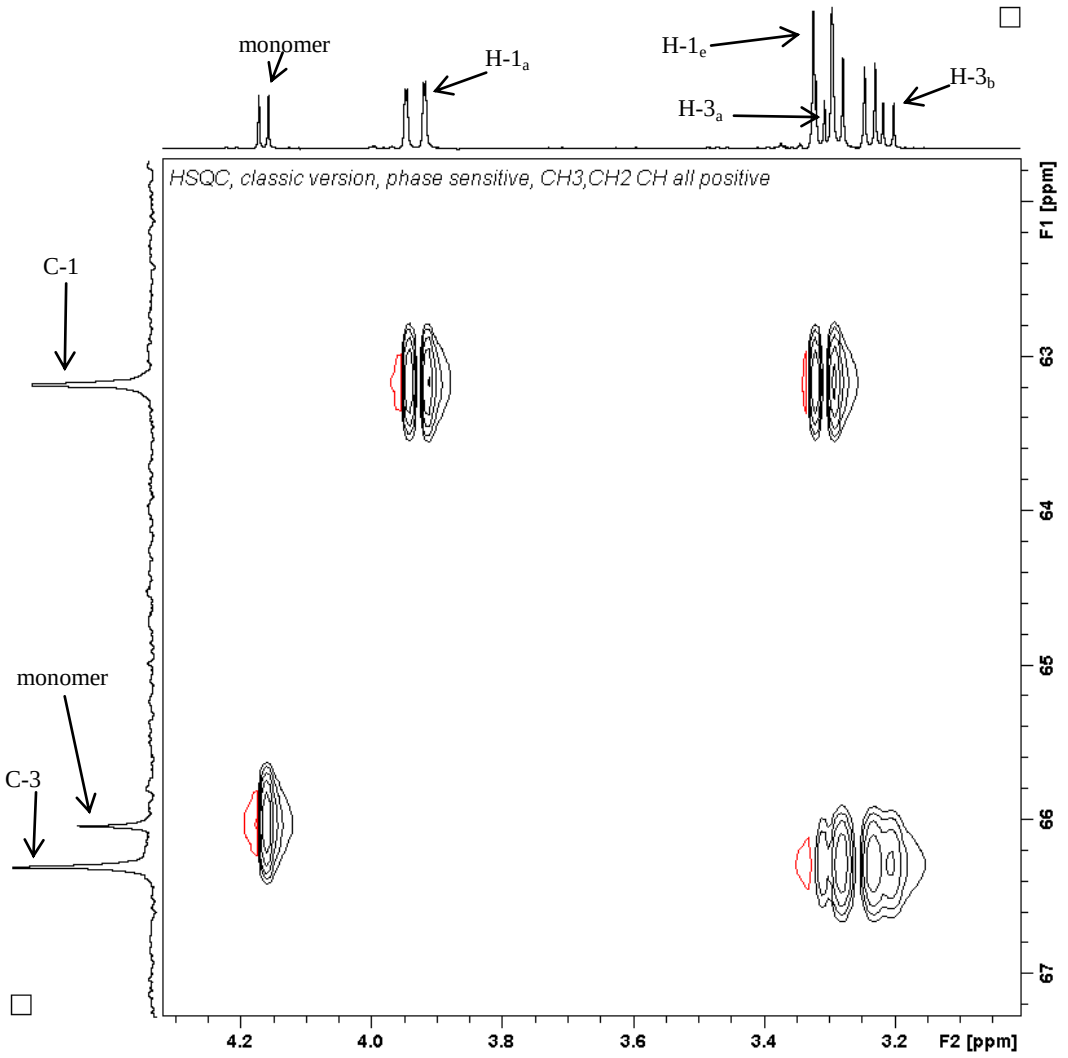

Figure 3.13: The expanded HSQC spectrum of DHA dimer and monomer in DMSO-*d6* showing correlations for C-1 with H-1a and H-1e and with correlations for C-3 with H-3a and H-3b. The monomer methylene signal shows correlation with monomer methylene carbon.

3.2.10 HMBC

The HMBC 2D experiment, Figure 3.14, detected ^{2}J and ^{3}J correlations between the proton and carbon signals. There was a ^{3}J correlation between the C-2-OH and the C-1 and C-3 signals and a ^{2}J correlation to the C-2 signal.

The HMBC spectrum showed that there was a ^{2}J correlation between the monomer hydroxyl proton and the methylene carbon and, as would be expected, there was no ^{1}J correlation between the methylene proton and methylene carbon as the ^{1}J correlations were suppressed. There was a ^{2}J correlation between the C-3-OH and C-3 and a ^{3}J correlation to C-2. There was no correlation to C-1 as this would have been a ^{4}J correlation which was out of range for this HMBC experiment.

There was a ^{3}J correlation between H-1_a and C-3 and a ^{2}J correlation to C-2. There were ^{2}J correlations between the H-3 protons in the multiplet and C-2 and ^{3}J correlations to C-1.

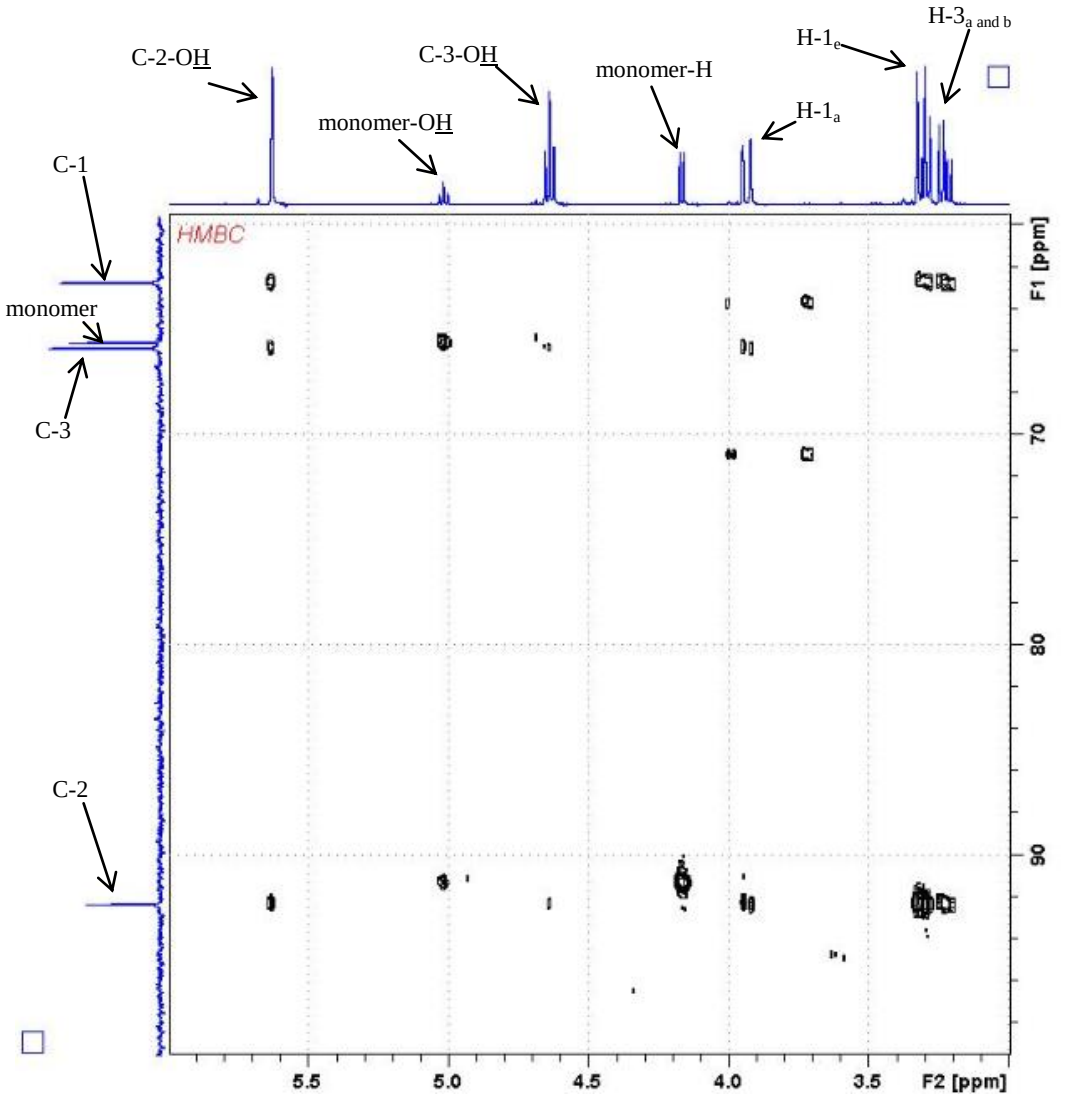

Figure 3.14: The HMBC spectrum showing ^{2}J and ^{3}J correlations between the proton and carbon signals

There were monomer hydroxyl and monomer methylene proton correlations about 1 ppm upfield from the C-2. This was a result of an artefact that can occur in 2D spectra in dynamic systems due to their extended acquisition times, see section 3.2.7.

3.2.11 ROESY

The NOESY and ROESY experiments observe through space correlations with the NOESY having phased peaks and the ROESY only having positive peaks.

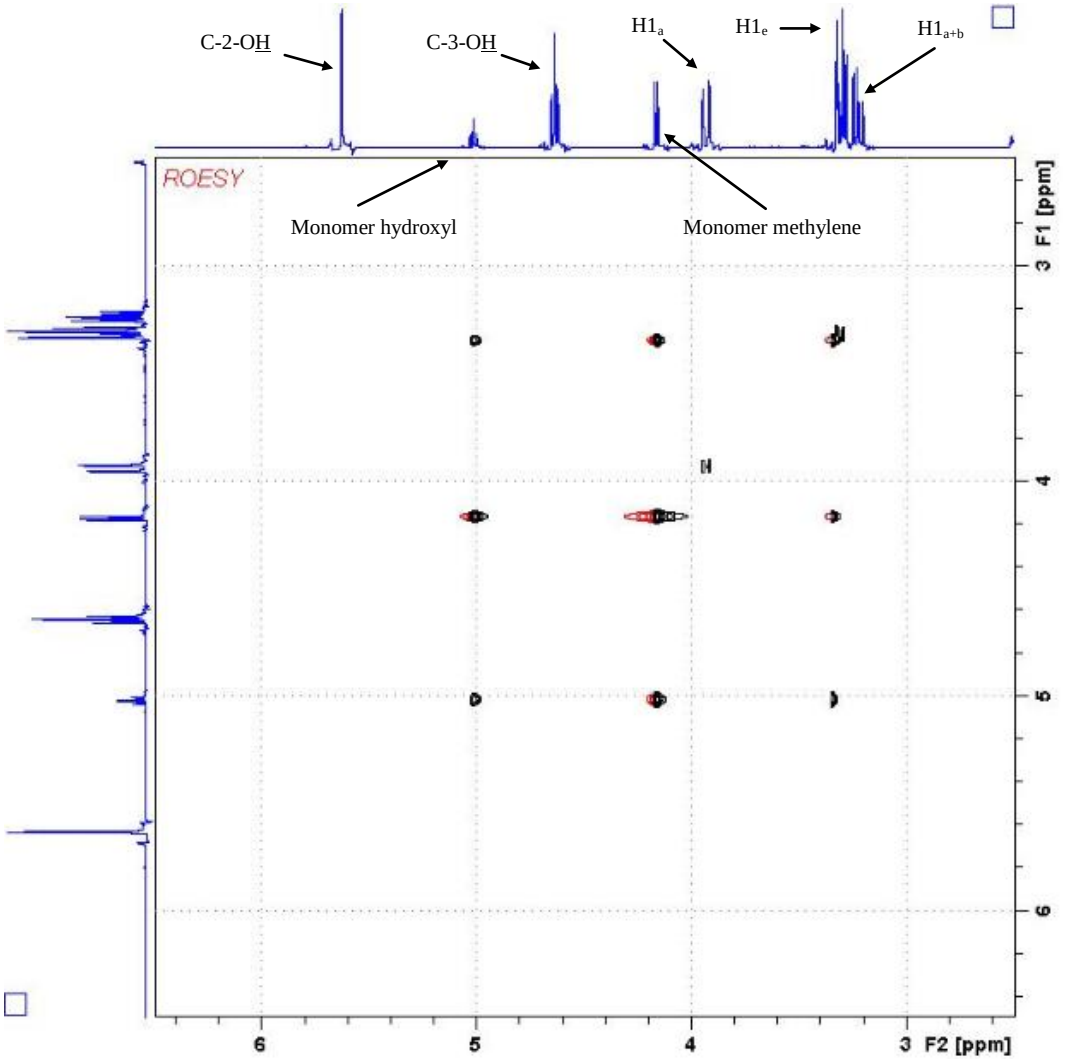

Figure 3.15: The ROESY spectrum of the DHA dimer and DHA monomer in DMSO-*d6*

The ROESY spectrum, Figure 3.15, did not show the expected correlations between the axial C-2-OH and $H1_a$ protons to assist in verifying their assignment. The ROESY spectrum displayed unexpected correlations between the monomer hydroxyl protons and the $H\text{-}1_e$ signal and the monomer methylene protons and the $H\text{-}1_e$ signal. Two artefacts associated with the NOESY/ROESY experiments may be involved with these anomalous correlations. Exchangeable protons can result in the transfer of NOE effects via hydrogen bonding of non-exchangeable protons[61] and in dynamic systems NOE effects from spatially close protons in one conformation/species can be transferred to a spatially distance protons in another

conformation/species,[61] an effect analogous to the artefact observed in through bond 2D NMR experiments, see section 3.2.7. The monomer hydroxyl correlation possibly resulted from the exchangeable proton NOE transfer mechanism to the non-exchangeable H-1_a and H-1_e protons while the monomer methylene correlation to the H-1_a and H-1_e protons would more likely to be a result of the NOE artefact present in dynamic systems as there is no apparent involvement of an exchangeable proton.

Verification of these two proposed NOE transference mechanisms was achieved by performing SELNOESY experiments on the two monomer signals. If the exchange mechanism is in effect, there will be exchange signals that are in the same phase as the excited signal.[61] If the dynamic system mechanism is in effect all correlations, if they exist, will be out of phase with the excited signal.[54,61,62]

3.2.12 SELNOESY

The SELNOESY spectrum was obtained for the excited monomer hydroxyl proton, Figure 3.16, to determine if the mechanism for the transfer of NOE effects between the monomer hydroxyl proton and the dimer H-1_e was via exchange. Subsequent correlations to the dimer hydroxyl protons and to the H-1_e confirm that NOE effects were being transferred through the dimer hydroxyl protons and thus the exchange mechanism is in effect in this case.

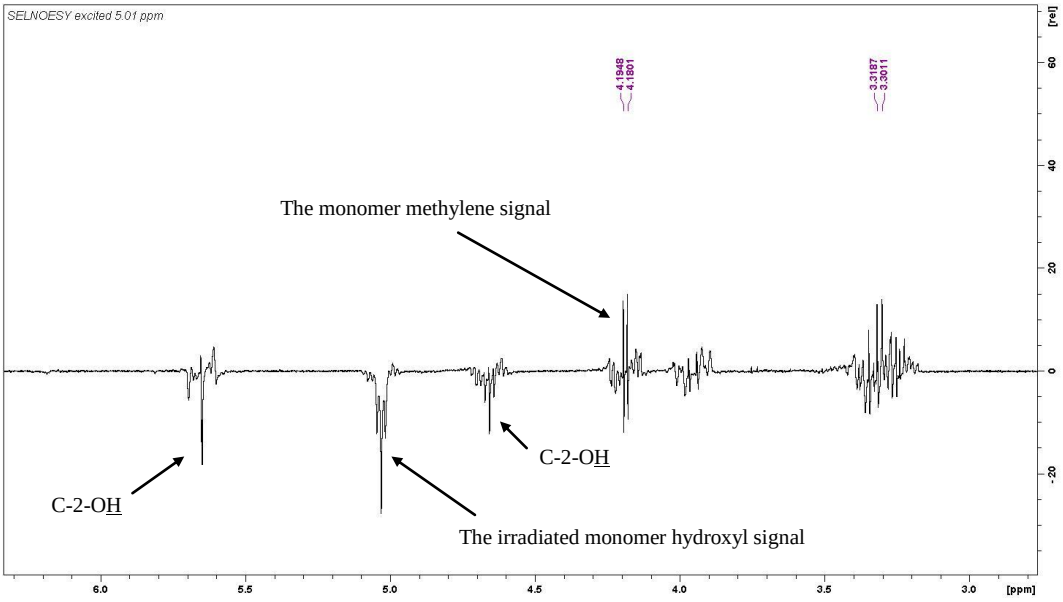

Figure 3.16: The SELNOESY experiment with the monomer hydroxyl proton excited (5.01 ppm) and correlations with the dimer hydroxyl protons, the monomer methylene proton and the dimer H-1_e. The orientation of the C-2-OH and C-3-OH signals relative to the irradiated signal indicates correlations resulting from exchange

The SELNOESY spectrum was obtained for the excited monomer methylene proton, Figure 3.17, to determine which NOE transfer mechanism was involved in the ROESY correlation between the monomer methylene proton and the dimer H-1_e. The lack of any correlations in the SELNOESY experiment confirms that the NOE transfer mechanism is not through exchange but as a result of NOE transfer occurring in one species being carried over to another species in the dynamic system.

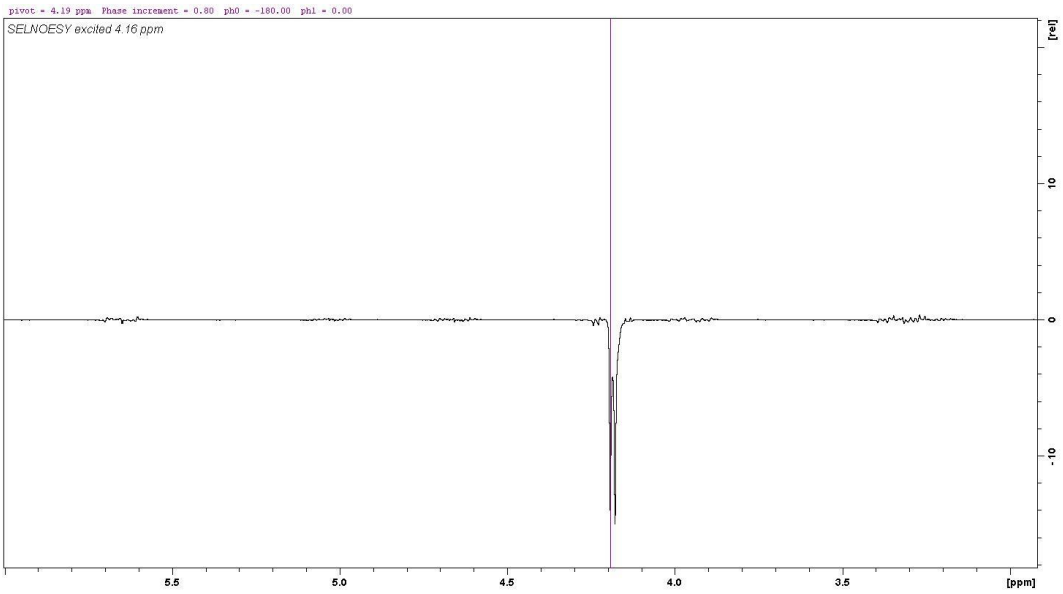

Figure 3.17: The SELNOESY experiment with the monomer methylene proton excited (4.16 ppm) and no correlations

3.2.13 DHA dimer 1H NMR spectrum assignment

The DHA dimer ^{1}H NMR spectrum was fully assigned, Table 3.3.

Table 3.3: Full assignment of the ^{1}H NMR spectrum of DHA in DMSO-*d6*

^{1}H	^{1}H δ (ppm)	Multiplicity	^2J (Hz)	^3J (Hz)	^4J (Hz)
H-1_a	3.92	d, d	11.36	-	0.74
H-1_e	3.30		11.36	-	-
H-3_a	3.29		d	6.42	-
H-3_b	3.22	d*	d*	6.42	-
C-2-O<u>H</u>	5.62	d	-	-	1.00
C-3-O<u>H</u>	4.63	t	-	6.24	-

**Second-order coupling requiring calculated shifts and coupling constants*

3.2.13.1 Comparison with the literature

Davis's ^{1}H NMR chemical shift values were shifted downfield by about 0.22 ppm, Table 3.4. One would not expect closely matching values between the Varian A60 60 MHz spectrometer used by Davis in 1973 and the Bruker AVIII 400 MHz NMR spectrometer used in the present study. The Varian A60 used an iron magnet and continuous wave acquisition, which took minutes to acquire one scan which resulted in a very low signal to noise ratio. Kobayashi and Takahashi's ^{1}H NMR chemical shift values and assignments, Table 3.5, on the other hand, were very close to those obtained in this study. Kobayashi and Takahashi used a JEOL PS-100 100 MHz spectrometer which became available after the Varian A60. The main advantage that the JEOL PS-100 held over the Varian A60, more so than it's increase in magnetic field strength, was its switch from the use of continuous wave acquisition to the use of Fourier Transform[63] acquisition. A Fourier Transform deconvoluted the free induction decay signal resulting from an excitation pulse of all signals within range of a carrier frequency. This resulted in one scan being acquired in a matter of seconds allowing for many scans to be added together *n* times with an increased signal to noise ratio proportional to $\sqrt{n}$ [62,64].

Table 3.4: ^{1}H NMR spectrum assignment of DHA dimer in DMSO-*d6* by Davis[23]

^{1}H	^{1}H δ* (ppm)	Multiplicity	^{2}J (Hz)	^{3}J (Hz)
H-1$_e$	3.95	doublet	12	-
C-2-O<u>H</u>	5.90	singlet	-	-
C-3-O<u>H</u>	4.75	triplet	-	6

The Davis study assigned H-1$_e$ the higher chemical shift relative to H-1$_a$, which he stated was unresolved up field in a multiplet, based on the argument that equatorial pyranose protons in most cases are further down field than the axial protons.[65] This differed in the case of the DHA dimer, as the W geometry was required to account for the long range coupling constant, the axial proton had to be assigned to the signal further down field than the equatorial proton. The Kobayashi and Takahashi study assigned H-1$_a$ further down field based on the long range coupling constant.

Kobayashi and Takahashi assigned the signals in the multiplet by inspection without applying the second-order coupling calculations.

Table 3.5: ^{1}H NMR spectrum assignment of DHA in DMSO-*d6* by Kobayashi and Takahashi[25]

^{1}H	^{1}H δ* (ppm)	Multiplicity	^{2}J (Hz)	^{3}J (Hz)	^{4}J (Hz)
H-1_a	3.94	doublet	11.5	-	-
H-1_e	3.32	doublet	11.3	-	-
H-3_a	3.20	doublet	-	6.5	-
H-3_b	3.34	doublet	-	6.5	-
C-2-O<u>H</u>	5.62	singlet	-	-	-
C-3-O<u>H</u>	4.62	triplet	-	-	1.0

Neither of the previous studies used ^{13}C or 2D NMR techniques to verify the results they obtained with ^{1}H NMR as these techniques were not available at the time.

3.3 Assignment of the ^{13}C NMR spectrum

3.3.1 Decoupled ^{13}C NMR

The decoupled ^{13}C NMR spectrum, Figure 3.18, showed three chemical environments for the DHA dimer carbons and the methylene signal for the DHA monomer. The signal at 92.3 ppm was assigned to the anomeric carbon (C-2) which is within the anomeric range of 90 ppm to 110 ppm and the HSQC spectrum, Figure 3.12, showed no correlations between this signal and any proton signals thus reinforcing the assignment of this signal as a quaternary carbon. The signals at 65.8 and 62.7 ppm are both in the range for methylene carbons bonded to an oxygen therefore the HSQC experiment, Figure 3.12 and Figure 3.13, was required to assign these signals. The signal at 66.3 ppm had correlations with the H-3_a and H-3_b signals in the multiplet so was assigned as C-3 and the signal at 63.2 ppm had correlations with the H-1_a signal at 3.92 ppm and the H-1_e signal overlapped by the multiplet so was assigned C-1.

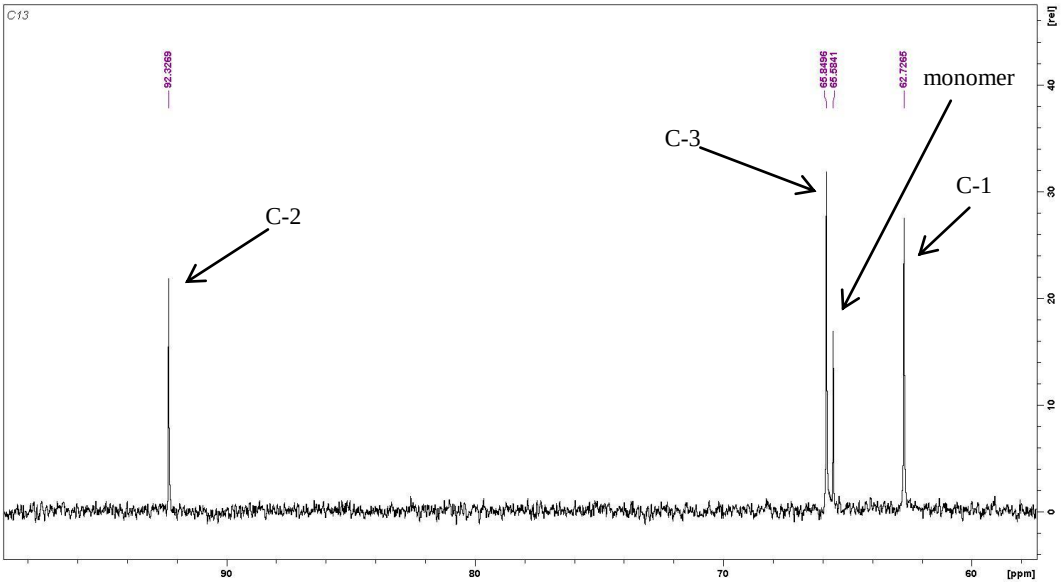

Figure 3.18: The ^{13}C NMR spectrum of the DHA dimer in DMSO-d6 with the methylene monomer signal present

3.3.2 Decoupled DEPT: Distortionless enhancement by polarisation transfer

The DEPT experiment uses a five pulse heteronuclear coherence transfer sequence to pass magnetisation from the abundant ^{1}H nucleus to the relatively rare ^{13}C and with decoupling applied during acquisition obtain multiplicity information. Magnetisation can be transferred in two ways:

1. By "z magnetisation" along the z-axis (i.e. parallel with applied field $\mathbf{B_0}$) in a through space process resulting in the Nuclear Overhauser Effect (NOE) which is used in the NOESY and ROESY experiments
2. By coherence transfer via the xy-plane after the RF pulse ($\mathbf{B_1}$) tips the net magnetisation vector from the z-axis into the transverse plane and transfers the magnetisation through bonds via *J*-coupling, as for the DEPT experiments.

By altering the tip angle θ of the last ^{1}H pulse for different DEPT experiments, different multicity information may be obtained.

- $DEPT\ 45 - \theta = {}^{\pi}/_{4}$ – all protonated carbons appear in the spectrum
- $DEPT\ 90 - \theta = {}^{\pi}/_{2}$ – only methine carbons appear in the spectrum

- $DEPT\ 135 - \theta = {}^{3\pi}/_{4}$ – methine and methyl carbons are phased positive and methylene carbons are phased negative (by convention) in the spectrum with quaternary carbons suppressed.
-

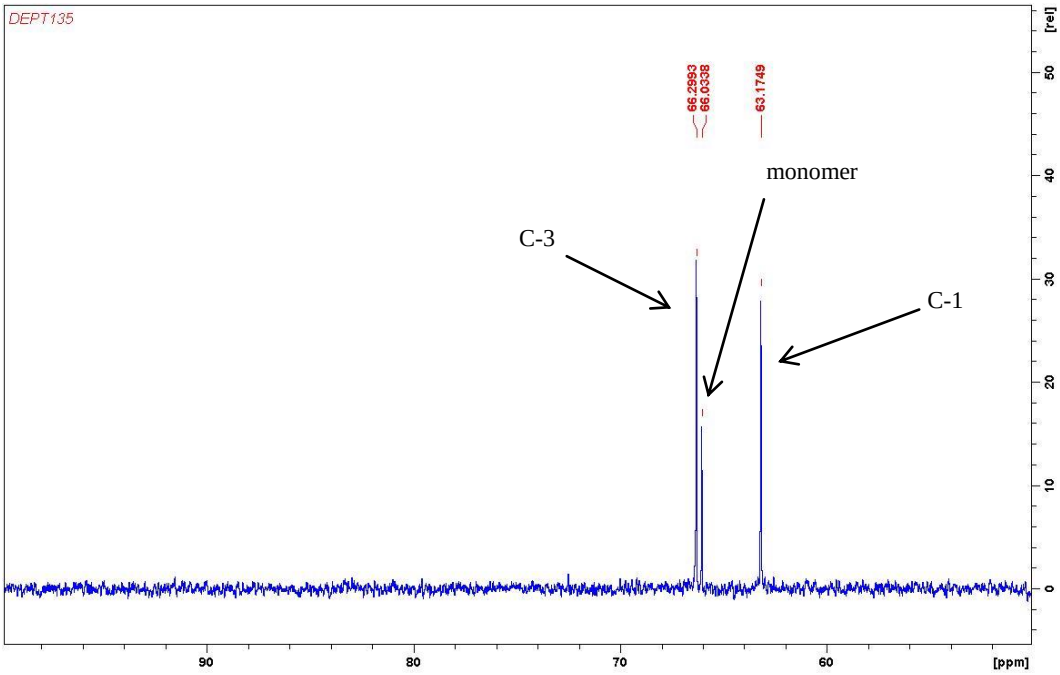

Figure 3.19: The DEPT135 spectrum of the DHA dimer in DMSO-d6 with absent C-2 signal (92.8 ppm) and monomer methylene signal present

A DEPT135 experiment was run on the DHA dimer in DMSO-*d6*, Figure 3.19, which allowed the assignment of C-2 to the signal at 92 ppm which is absent in the spectrum and therefore was produced by a quaternary carbon. Multiplicity of the two dimer carbon signals present in this spectrum was ambiguous as we could not know whether they were to be phased negative or positive as there was no unambiguous signal present to serve as a reference. That they both have the same phase supported the previous assignments to C-1 and C-3 as they had the same multiplicity and therefore it was expected that they would have the same phasing. The monomer methylene signal is present which supports the assignment of the dimer signals as methylene carbons.

3.3.3 DHA dimer ^{13}C NMR spectrum assignment

The DHA dimer ^{13}C NMR spectrum was fully assigned, Table 3.3. No studies could located that related to the ^{13}C chemical shifts for carbon in the DHA dimer and therefore no comparison could be made.

Table 3.6: The DHA dimer ^{13}C NMR spectrum assignment in DMSO-*d6*

^{13}C	^{13}C δ^7 (ppm)	Bonding
C-2	92.8	Quaternary
C-3	66.3	methylene
C-1	63.2	methylene

3.4 Monomer assignment

As the DHA monomer is a symmetric molecule, Figure 3.20, only two ^{1}H signals were observed, one that represented the four methylene ^{1}H signals and the other that represented the hydroxyl ^{1}H signals. Two ^{13}C signals were observed, one that represented the ketone ^{13}C signal and the other that represented the two chemically equivalent methylene ^{13}C signals.

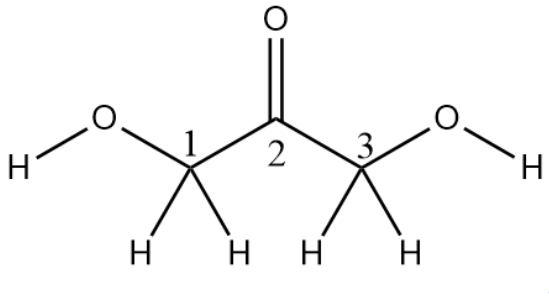

Figure 3.20: The DHA monomer structure

3.4.1 1H NMR assignment of the DHA monomer

The spectra of the DHA monomer in DMSO-*d6*, Figure 3.21 and Figure 3.22, were obtained by preparing solutions of the DHA dimer and allowing the dimer to dissociate over the period of a few days.

[7] All shifts relative to TMS

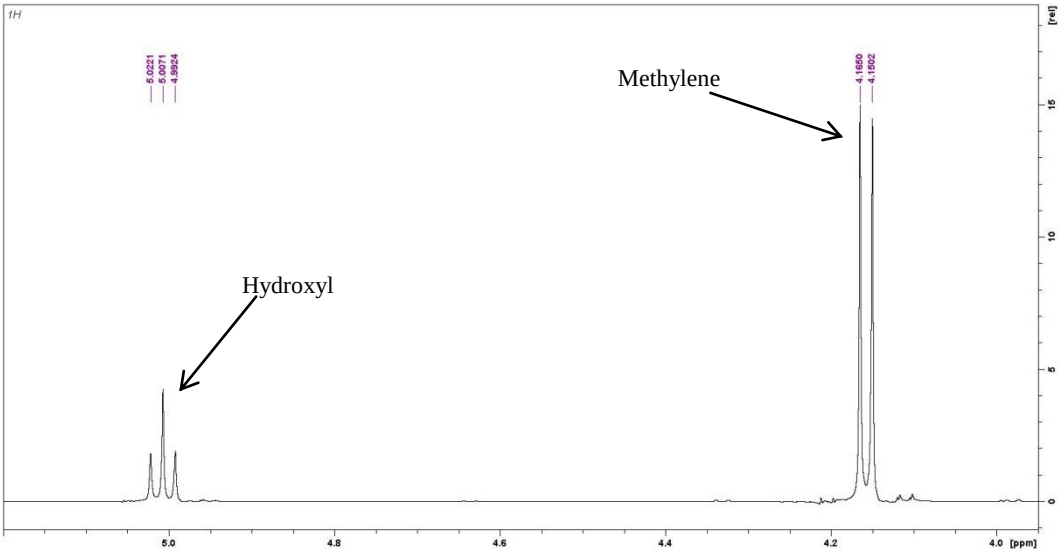

Figure 3.21: The ^{1}H NMR spectrum for the DHA monomer in DMSO-*d6*

The doublet signal at 4.16 ppm (^{3}J = 5.92 Hz), Figure 3.21, represented the two methylene protons that were engaged in spin-spin coupling with the hydroxyl protons to give the observed multiplicity. The triplet signal at 5.01 ppm (^{3}J = 5.94 Hz), Figure 3.21, represents the hydroxyl protons that were engaged in spin-spin coupling with the two methylene protons. These hydroxyl protons were not observed in D_2O as they engage in rapid exchange with the solvent.[23,66]

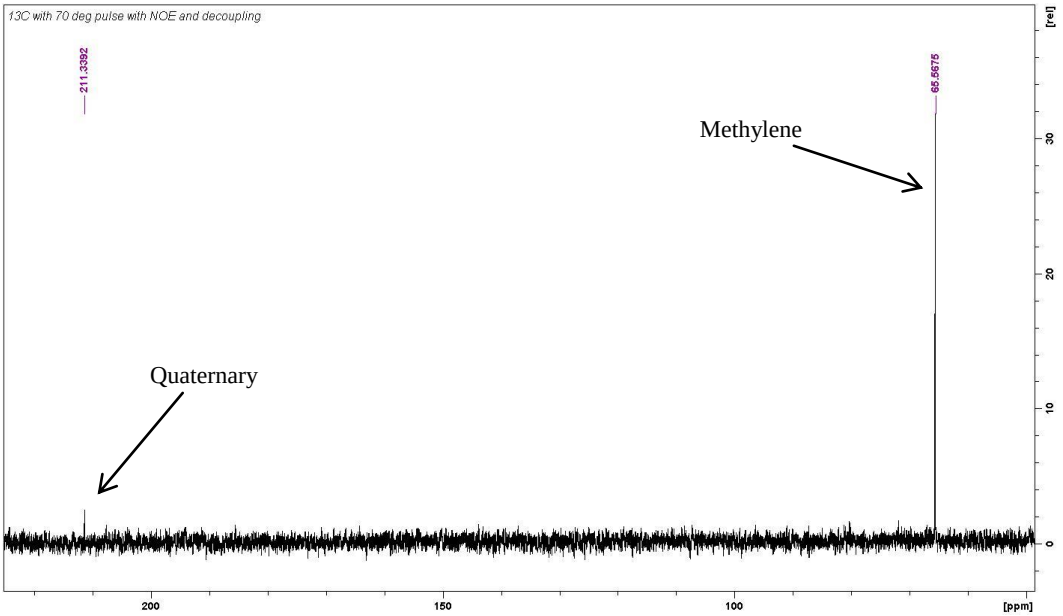

Figure 3.22: The ^{13}C NMR spectrum for the DHA monomer in DMSO-*d6*

There were two signals observed in the ^{13}C spectrum for the DHA monomer, Figure 3.22. The relatively diminished signal downfield at 211.7 ppm resulted

from the quaternary carbonyl carbon as this chemical shift value was within the range expected for a ketone (205-220 ppm).[31] The signal at 66.1 ppm was assigned to the two methylene carbons bonded to hydroxyl groups, the chemical shift value was within the range expected for a methylene carbon directly bonded to a hydroxyl group (50-90 ppm)[31] and the HSQC spectrum, Figure 3.12, shows a correlation between the ^{13}C signal at 66.1 ppm and the ^{1}H signal at 4.16 ppm.

Table 3.7: NMR spectrum assignments for the DHA monomer

^{1}H	^{1}H δ (ppm)	Multiplicity	^{3}J (Hz)
H-1 and H-3	4.16	doublet	5.92
OH	5.01	triplet	5.94
^{13}C	^{13}C δ (ppm)	Bonding	
C-1 and C-3	66.1	methylene	
C-2	211.7	Quaternary	

3.5 Conclusion

Assignment of the ^{1}H NMR spectrum verified the conformation of the substituted 1,4-dioxane dimer structure in Figure 3.1. To obtain the kinetic data for the dissociation of the DHA dimer this spectral assignment identified three appropriate signals that may be followed in the ^{1}H NMR spectrum, a doublet at 5.62 ppm, a triplet at 4.63 ppm and a doublet at 3.92 ppm. If significant overlap was to occur between these signals and the signals for another compound that may be present, ^{13}C NMR would be available by following the methylene signal at 63.2 ppm. The data obtained from ^{13}C NMR would contain a high level of scatter as the signal to noise ratio is relatively poor which would result in a high level of random variance with the integration values for these peaks. To obtain the kinetic data for the formation of the DHA monomer the ^{1}H NMR triplet signal at 5.01 ppm could be followed as could the doublet signal at 4.16 ppm. The ^{13}C NMR dimer signal at 66.3 ppm and monomer signal at 66.1 ppm could not be followed in kinetics experiments because they are engaged in overlap.

4 Method development

4.1 Introduction

Kinetic NMR spectroscopy in organic chemistry generally utilises the ^{1}H NMR or ^{13}C NMR spectroscopy techniques. Both NMR techniques have their pros and cons when it comes to their ability to acquire kinetic data and these needs to be worked through to decide which technique to utilise in this study. For kinetic data to be acquired using NMR spectroscopy, at least one unique signal emanating from one molecular species needs to be present and identified. For the NMR kinetic data to be useful, scatter in the integration values resulting from resolution and noise issued needs to be kept to a minimum. This could usually be achieved by increasing the number of scans and increasing the number of acquired data points for each scan but these measures had the effect of increasing the overall time for the spectrum to be obtained which resulted in less data points and increased scatter in the plotted graphs to determine the rate constants.

The ^{1}H NMR spectroscopy technique was tested with a preliminary study to determine the kinetics for the mutarotation of glucopyranose in D_2O and DMSO-*d6*. The mutarotation acid/base catalysed reaction mechanism of glucopyranose, see section 1.9, is analogous to the reaction mechanism proposed for the dissociation of the DHA dimer, see Chapter 6, therefore issues surrounding the acquisition of the mutarotation kinetic data and the analysis of this data can be assumed to be similar to those that one may encounter with the acquisition of the DHA dimer dissociation kinetic data and data analysis.

4.2 NMR kinetic method

4.2.1 ^{1}H NMR

An advantage to using the ^{1}H isotope is that it has a high natural abundance (99.99%)[67] and a relatively high gyromagnetic ratio (42.58 MHz T^{-1}),[67] conditions which allow for well resolved spectra to be obtained quickly with high resolution and a high signal to noise ratio.

A disadvantage to using the ^{1}H isotope is that ^{1}H NMR spectra possess a small spectral width (18 ppm) which can produce crowded spectra resulting in signal overlap that makes integration unreliable. For integration to be utilised, unique signals emanating from a single species need to be present.

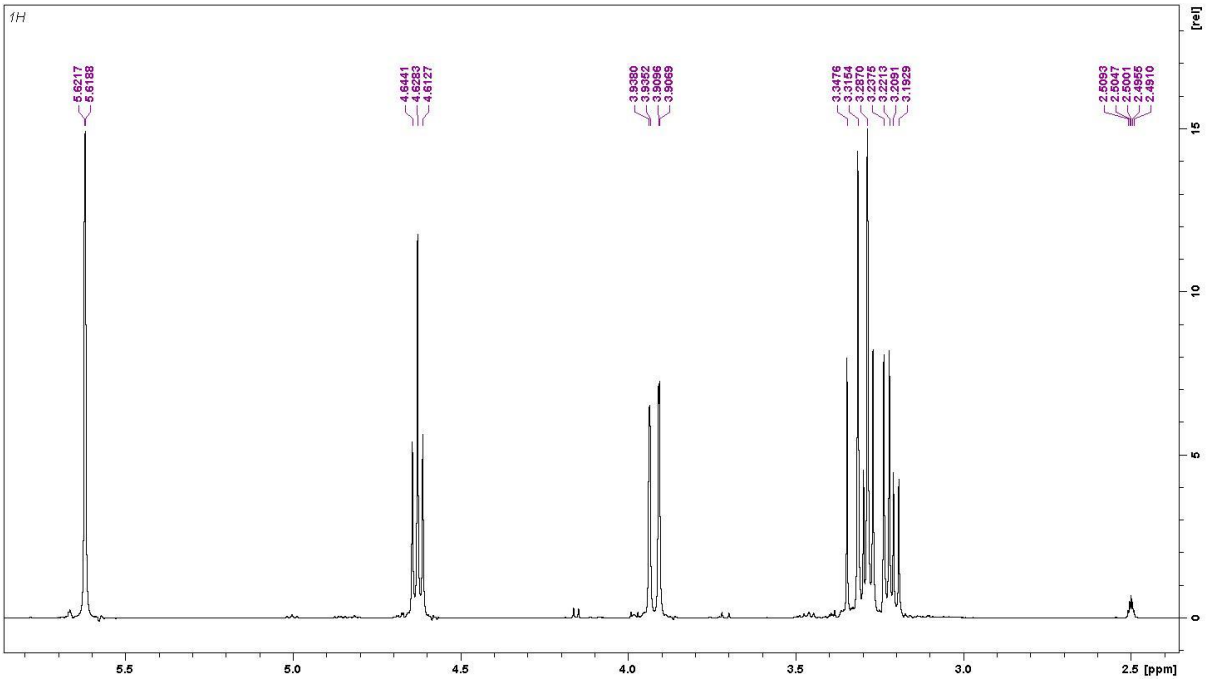

Figure 4.1: The 400 MHz ^{1}H NMR spectrum of the DHA dimer in DMSO-*d6*

The ^{1}H NMR spectrum for the DHA dimer in DMSO-d6 was obtained in 50 seconds, Figure 4.1, and three unique signals were identified at 5.62, 4.63 and 3.91 ppm. These three unique signals allow ^{1}H NMR spectroscopy to be used in the acquisition of kinetic data for the experiments in this study. As ^{1}H NMR has a low level of noise in the baseline compared with that of ^{13}C NMR, Figure 4.2, ^{1}H NMR is the technique of choice for the acquisition of kinetic data in the current study.

4.2.2 Decoupled ^{13}C NMR

An advantage to using decoupled ^{13}C NMR is that the spectra to be obtained contain a relatively large spectral width of 220 ppm which generally allows for excellent signal separation which results in a low level of signal overlap. This is a condition that needs to be met in kinetic NMR experiments as signals emanating from more than one species are unsafe to integrate.

A disadvantage to using decoupled ^{13}C NMR is that the spectra contain a large amount of baseline noise which results from ^{13}C having a low natural abundance (1.11%)[67] and a low gyromagnetic ratio (10.71 MHz T^{-1})[67]. When the signals with noisy baselines are integrated, the random spikes and troughs within the bounds of the integration range produce a high level of random scatter in the integration values resulting in unreliable rate constants being thus obtained.

Another disadvantage to using decoupled ^{13}C NMR results from the Nuclear Overhauser effect (NOE) generated by the decoupling process which uses a broadband pulse to irradiate all the proton signals. This gives the result of ^{13}C signals, emanating from carbons bonded to more protons, being more intense and thus having larger relative integration values than ^{13}C signals emanating from carbons bonded to less protons. The NOE will not affect the kinetic data emanating from one signal but could be an issue when absolute concentration values are required to determine the equilibrium constant.

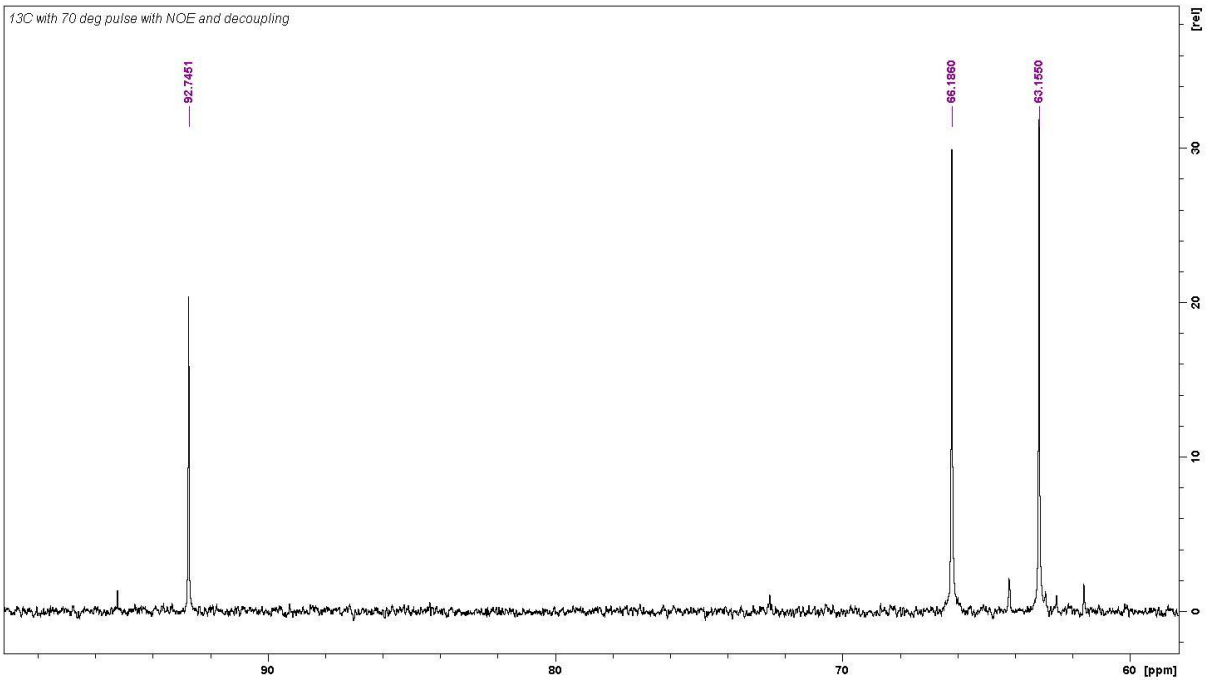

Figure 4.2: The 400 MHz ^{13}C NMR spectrum of the DHA dimer in DMSO-*d6*

The ^{13}C NMR spectrum for the DHA dimer in DMSO-d6 was obtained in 296 seconds, Figure 4.2, and three unique signals were identified at 92.7, 66.2 and 63.2 ppm. The high level of noise can be seen in the baseline when compared to the baseline for the ^{1}H NMR spectrum, Figure 4.1. It is noted that this comparatively noisy spectrum to approximately six time longer to acquire than the ^{1}H NMR spectrum that had very little noise. The three unique ^{13}C signals allow ^{13}C NMR spectroscopy to be used to acquire the kinetic data for the current study but the relatively noisy baseline makes ^{13}C NMR only a possible second choice option in the evident that signal overlap occurs in the ^{1}H NMR experiment.

4.2.3 The concentration of DHA

An investigation was carried out to ascertain the optimal DHA dimer

concentration to be used in this study. Preliminary experiments were performed (26.9 °C) at different DHA dimer concentrations and the rate constants for the dissociation of the DHA dimer in DMSO-d6 were obtained, Table 4.1. The data, Figure 4.3, showed a lot of scatter at lower DHA dimer concentration while at 0.25 M the rate constant values overlap in the graph. The scatter at low concentration may be a result of hidden variables, such a water contamination having a greater influence on the rate constant as the concentration of water, for example, is proportionally higher. It was decided that the DHA dimer concentration of 0.25 M would be used in this study as it had less scatter associated with its rate constants.

Table 4.1: The rate constants for the dissociation of the DHA dimer in DMSO-d6 at different concentrations with the mean value

Reaction number	Concentration (M)	k (min^{-1})
1	0.0125	6.75×10^{-2}
2	0.025	1.45×10^{-2}
3	0.05	3.86×10^{-2}
4	0.05	8.39×10^{-2}
5	0.15	3.34×10^{-2}
6	0.25	2.54×10^{-2}
7	0.25	2.44×10^{-2}
Mean k values with standard error	-	$4.11 \times 10^{-2} \pm 2.53 \times 10^{-2}$

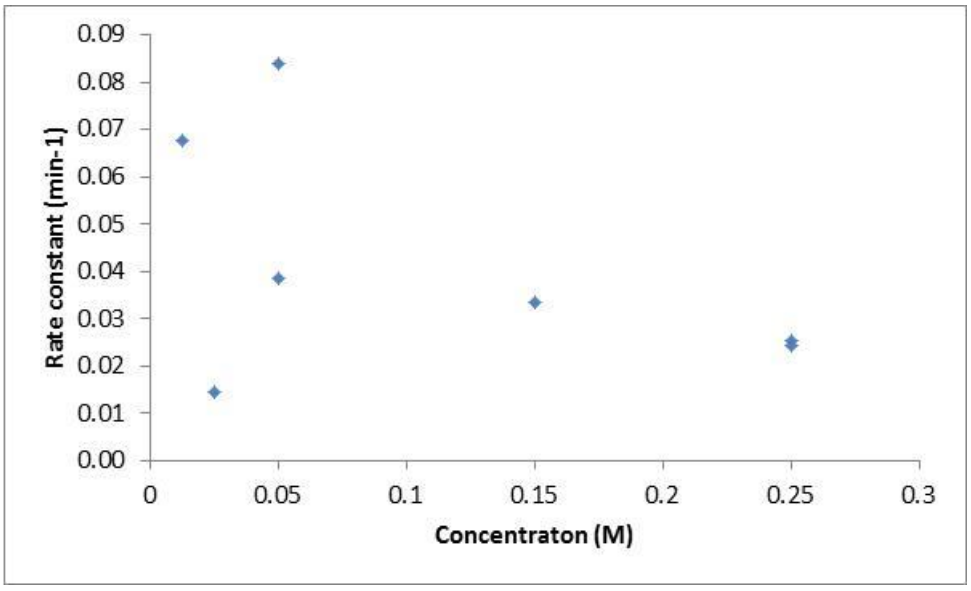

Figure 4.3: The graph for rate constant against concentration

4.2.4 Contamination of solvent

The original experiments, in section 4.2.3, were performed using DMSO-*d6* that had been sitting over 4Å molecular sieves to draw out any water that may have been present. When DMSO-*d6* obtained from sealed ampoules was used the thus obtained rate constant values were of an order of magnitude lower than those thus obtained using the DMSO-*d6* that had been sitting over molecular sieves. Referring to the literature associated with zeolites, one of the documented properties of zeolites is their ability to sorb organic molecules and catalyse proton exchange amongst a variety of other organic reactions.[68] As proton exchange is an integral process in the proposed DHA dimer dissociation mechanism, it is likely that molecular sieve held in suspension in the DMSO-*d6* was catalysing the dissociation of the DHA dimer thus giving elevated rate constant values. DMSO-*d6* obtained from sealed ampoules were used for all the following NMR spectroscopy experiments in this study.

4.3 A kinetic study of the mutarotation of d-glucopyranose to confirm experimental procedure

A series of kinetic experiments studying the mutarotation of D-glucose were performed using ^{1}H NMR to assist in the development of a method to determine the kinetics of the proposed mutarotation-like reaction of the dissociation of DHA. This preliminary study tested the validity of using ^{1}H NMR spectroscopy to obtain kinetic data for the investigation of the mutarotation reaction and therefore validated the use of ^{1}H NMR spectroscopy to obtain the kinetic data for the DHA dimer dissociation.

4.3.1 d-Glucose kinetic experiments

As the experiments for the mutarotation of D-glucose were followed by ^{1}H NMR spectroscopy, it was a requirement that they were carried out in a deuterated solvent. The reaction reaches equilibrium with a literature equilibrium constant (K) value of 1.76[27] in D_2O and 1.20[69] in DMSO-*d6*. The reaction is considered to be first order in D-glucopyranose as contributions from the less stable acyclic and furanose forms of glucose are negligible.[27,28,30,70]

4.3.2 Equilibrium and the determination of rate constants k, k_1 and k_2

Reversible reactions with elementary first-order forward and backward reactions can be represented by the equilibrium illustrated in Figure 4.4. The observed rate constant, k, is the sum of the forward, k_1 and reverse, k_{-1} rate constants.[67]

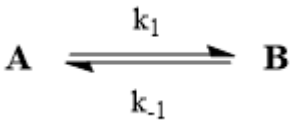

Figure 4.4: The elementary first order equilibrium reaction

The differential rate expression for A is written as:

$$\frac{d[A]}{dt} = -k_1[A] + k_{-1}[B] \tag{1}$$

Using the condition that at $[A]_0$, [B] = 0 we get:

$$[B] = [A]_0 - [A] \tag{2}$$

Rearranging equation (2) and inserting into equation (1) gives:

$$\frac{d[A]}{dt} = -[A](k_1 + k_{-1}) + k_{-1}[A]_0 \tag{3}$$

This rate expression, equation (3), is a separable 1st order ordinary differential equation (ODE) that can be rearranged to give the integrated expression:

$$\int_{[A]_0}^{[A]} \frac{d[A]}{[A](k_1 + k_{-1}) - k_{-1}[A]_0} = -\int_{t_0}^{t} dt \tag{4}$$

Equation (4) was evaluated using the standard integral $\int \frac{dx}{(a+bx)} = \frac{1}{b}\ln(a+bx)$ [67] and the initial conditions to give the expression in terms of [A]:

$$[A] = [A]_0 \frac{k_{-1} + k_1 e^{-(k_1+k_{-1})t}}{k_1 + k_{-1}} \tag{5}$$

At equilibrium the value for t approaches infinity with the $k_1 e^{-(k_1+k_{-1})t}$ term becoming $k_1 e^{-\infty}$ which approaches zero thus eliminating the term $k_1 e^{-(k_1+k_{-1})t}$ from equation (5) to give equation (6):

$$[A]_{eq} = [A]_0 \frac{k_{-1}}{k_1 + k_{-1}} \tag{6}$$

Rearranging equation (6) in terms of $[A]_0$ to give equation (7):

$$[A]_0 = [A]_{eq}\frac{k_1+k_{-1}}{k_{-1}} \quad (7)$$

Substitute equation (7) into equation (3) and rearrange to give:

$$\frac{d[A]}{dt} = -(k_1 + k_{-1})([A] - [A]_{eq}) \quad (8)$$

Equation (8) is a separable ODE which may be rearranged to give:

$$\int_{[A]_0}^{[A]} \frac{d[A]}{[A] - [A]_{eq}} = -(k_1 + k_{-1}) \int_{t_0}^{t} dt \quad (9)$$

This integral was solved using a u-substitution to give:

$$\ln \frac{[A] - [A]_{eq}}{[A]_0 - [A]_{eq}} = -(k_1 + k_{-1})t \quad (10)$$

The concentration and t values in this expression, equation (10), may be thus obtained experimentally and graphed as the log ratio expression against time to give $-(k_1 + k_{-1})$ which is solved using K to give the rate constants, k, k_1 and k_{-1}.

4.3.3 Assignment of the α-proton and ß-proton ^{1}H NMR signals

The anomeric proton signals for α-D-glucose and ß-D-glucose that were obtained experimentally in D_2O and DMSO-*d6* were assigned using the coupling constants and chemical shift values and comparing these to the literature values,[65,71,72] Table 4.2. The anomeric proton signals were integrated at equilibrium to determine the equilibrium constant (K) using the $\frac{[ß]_{eq}}{[\alpha]_{eq}}$ anomer ratio.

Table 4.2: Chemical shifts and coupling constants for the D-glucopyranose anomeric protons

Anomer	**Solvent D_2O**			
	δ Lit.[71]	**δ Exp.**	**$^3J_{HH}$ Lit.[71]**	**$^3J_{HH}$Exp**
α	5.21	5.14	3.80	3.76
ß	4.63	4.54	7.97	7.95
Anomer	**Solvent DMSO-*d6***			
	δ Lit.[72]	**δ Exp.**	**$^3J_{HH}$ Lit.[72]**	**$^3J_{HH}$ Exp.**
α	6.20	6.18	4.52	4.56
ß	6.56	6.55	6.47	6.52

The α-anomer has the hydroxyl substituents *cis* and the ß-anomer has the hydroxyl substituents *trans*, Figure 4.5. The ß-anomer is thermodynamically more stable than the α-anomer as the equatorial conformation of the anomeric hydroxyl group eliminates 1,3-diaxial interactions between the hydroxyl group and the axial protons. The relative prevalence of the α-anomer is a result of the anomeric effect, a stereoelectronic effect, that drives the tendency of substituent electronegative heteroatoms to adopt the more sterically hindered axial conformation.

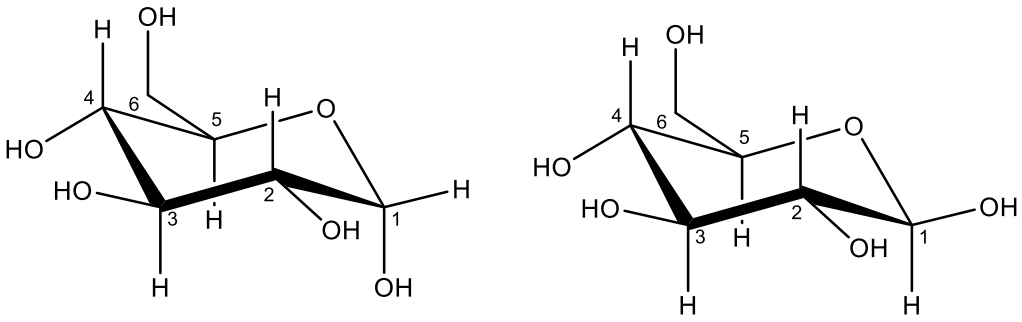

Figure 4.5: α-D-Glucopyranose (left) and ß-D-glucopyranose (right)

The differences in the $^3J_{HH}$ coupling constants are a function of the dihedral angle of the coupling vicinal protons. This relationship is mathematically expressed by the Karplus equation[59]:

$$^3J_{HH} = A\cos^2\varphi + B\cos\varphi + C$$

The original equation has A = 7.76, B = -1.10 and C = 1.40 and is graphically represented in Figure 4.6.

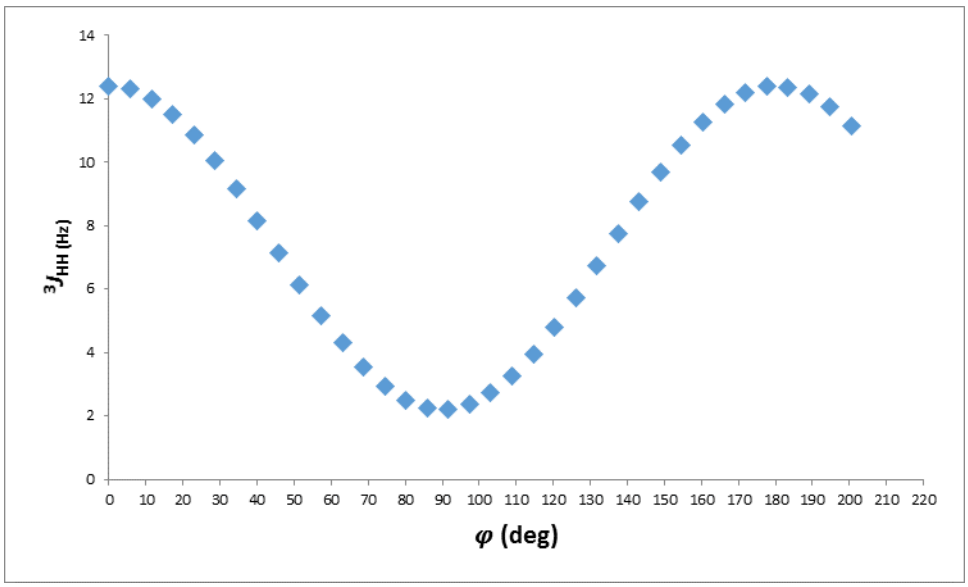

Figure 4.6: The Karplus equation graph

The α conformation has an approximate dihedral angle of approximately 60°, between H-1 and H-2, which gives a calculated $^3J_{HH}$ value of ~4.5 Hz and the ß conformation has an approximate dihedral angle of approximately 180° to give a calculated $^3J_{HH}$ value of ~12.4 Hz. Therefore the signal with $^3J_{HH}$ 3.76 Hz was assigned to the α-proton and the signal with $^3J_{HH}$ 7.95 Hz was assigned to the ß-proton.

Table 4.3: The literature and experimental values for the anomer ratios that were obtained at equilibrium

Anomer	Solvent D_2O			Solvent DMSO-*d6*		
	% Lit.[27]	% Exp.	Temp.(°C)	% Lit.[69]	% Exp.	Temp(°C)
α	36.2	36.4	26.9	45.4	43.3	26.9
ß	63.8	63.5	26.9	54.6	56.7	26.9

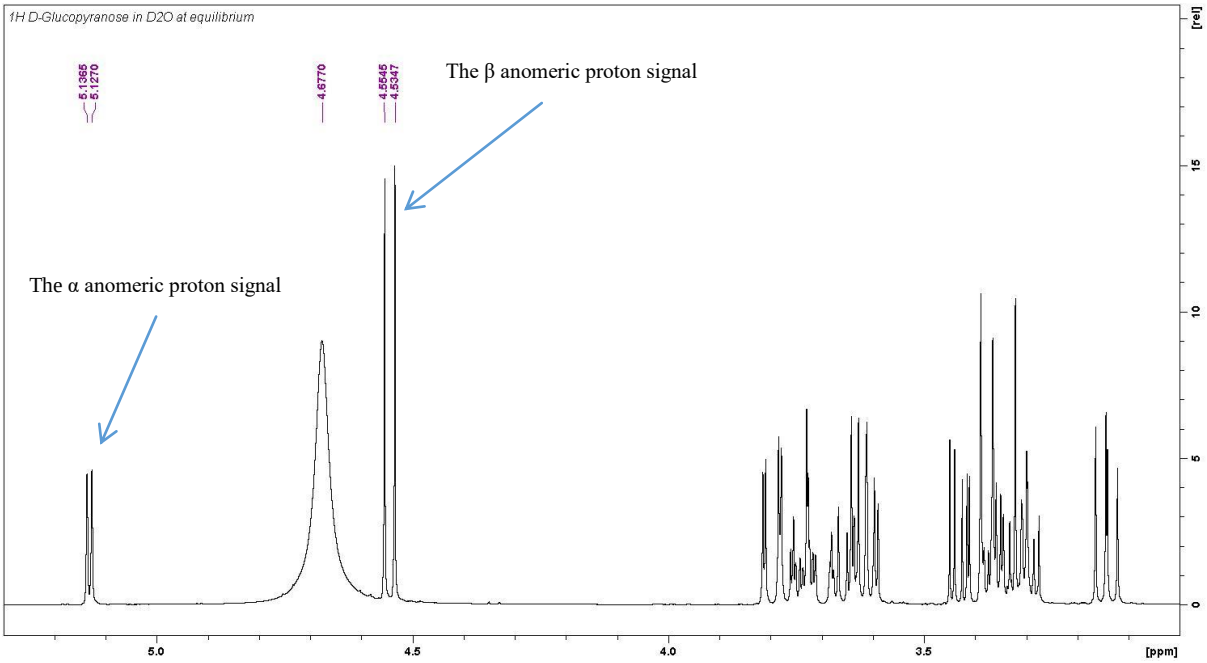

Figure 4.7: The ^{1}H NMR spectrum of D-glucopyranose in D_2O

To differentiate between the α and ß proton signals in DMSO-*d6*, the α and ß anomeric signal integration ratios at equilibrium were compared to the literature values, Table 4.3, and confirmed the assignments in Table 4.2. The coupling constants, point to the larger $^{3}J_{HH}$ 6.52 Hz at 6.55 δ being the ß-proton as the ß-anomer has a larger dihedral angle than the α-anomer which has $^{3}J_{HH}$ 4.56 Hz at 6.18 δ . The observation that the coupling constant values are closer in DMSO-*d6* than in D_2O suggests a closer dihedral angle for the α proton but, on inspection of the Karplus equation, Figure 4.6, a decrease in the coupling constant value for the ß proton could be the result of either an increase or a decrease in the dihedral angle. This solvent dependant variance in dihedral angles is likely to be a result of the different solvation characteristics of D_2O and DMSO-*d6* as they engage in hydrogen bonding with the hydroxyl groups and ring oxygen in glucopyranose. These differences may be rationalized by the observation that D_2O is both a hydrogen bond donor and accepter and relatively small whereas DMSO-*d6* is essentially only a hydrogen bond acceptor, though its methyl protons do engage in exchange to a lesser degree,[73,74] and is much larger DMSO-*d6* than D_2O.

An interesting result of the assignment of the anomeric protons in the different solvents is the observation that in D_2O the α-anomeric proton is downfield relative to the ß-anomeric proton while in DMSO-*d6* the ß-anomeric proton is downfield relative to the α-anomeric proton, i.e. the chemical shift values have switched

relative to one other. The axial ß-anomeric proton signal in DMSO-*d6* being further downfield than the equatorial α-anomeric proton signal goes against the literature which predicts that in a six-membered ring in the chair conformation the equatorial proton signal will be further downfield than an axial proton signal.[65,75] This observation could be a result of a convergence in the α and ß dihedral angles in DMSO-*d6*, due to the hydrogen bond accepting action of the bulkier DMSO-*d6* molecule, with the α-proton becoming more axial and the ß-proton becoming more equatorial as predicted by the Karplus equation, Figure 4.6.

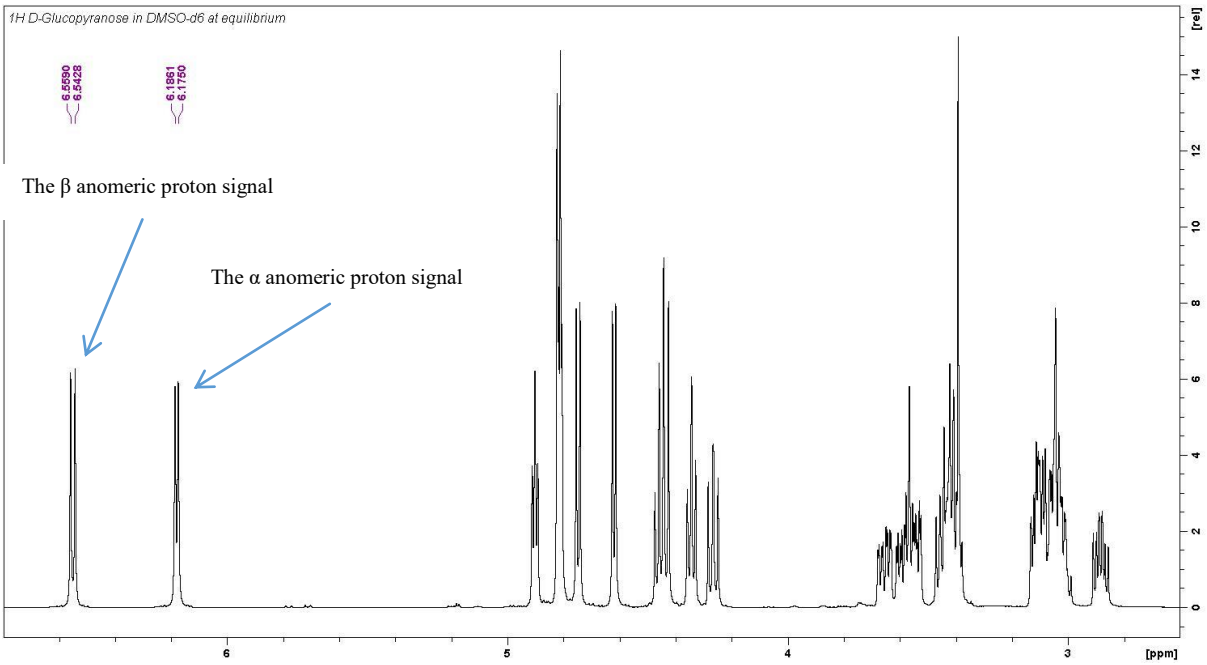

Figure 4.8: The ^{1}H NMR spectrum of D-glucopyranose in DMSO-*d6*

4.3.4 ^{1}H NMR kinetic experiments following the mutarotation of d-glucose

^{1}H NMR kinetic studies of the mutarotation equilibrium of D-glucose in D_2O and DMSO-*d6* were performed at various concentrations to verify the reaction order, to determine the mutarotation rate constants k, k_1 and k_{-1} and to compare these values with those in the available literature and to determine if ^{1}H NMR is an effective tool in the acquisition of kinetic data for mutarotation and therefore applicable to the acquisition of kinetic data for the mutarotation-like dissociation of the DHA dimer. All experiments were carried out at 300 K (~26.8°C).

4.3.4.1 Graphical data the determine reaction order

The kinetic data was graphed as zeroth order, first order and second order graphs for all experiments, Appendix A, to determine the reaction order. The front eighty

percent of the kinetic data was used for all kinetic analysis in this study as it represents approximately three first-order half-lives once the time lapse between the reaction starting and acquisition of the first spectrum is taken into account, which ranged from 5 to 15 minutes. The zeroth order graphs are presented with the full time frame of the experiments to give a sense of when and how equilibrium was reached. These graphs still allow inspection of the curvature of the graphs at 80% data acquisition. If the concentration against time graph, Figure 4.9, revealed a straight line, the reaction would be zeroth order.

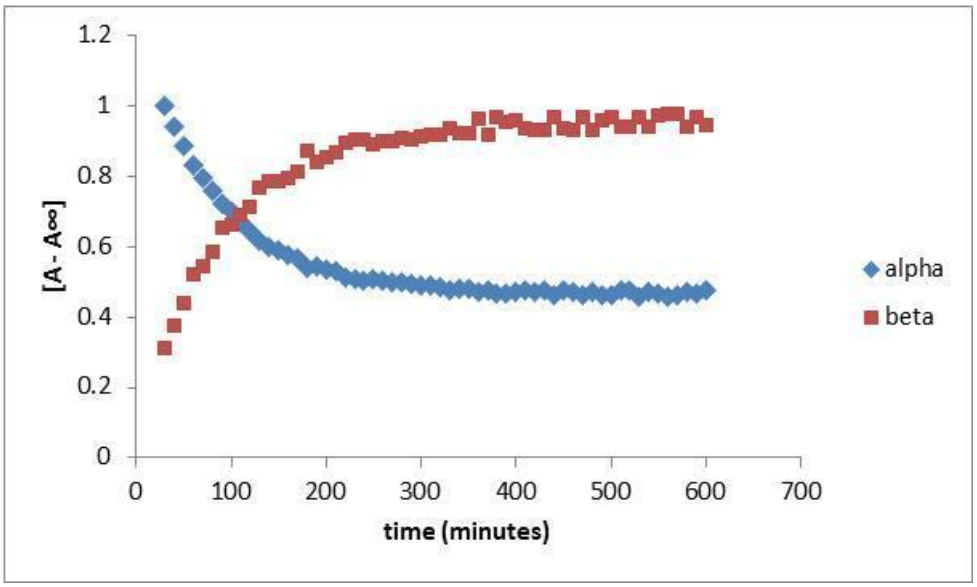

Figure 4.9: Relative concentration against time example, D-Glucopyranose (0.5 M) in D_2O.

If the log of concentration vs time, revealed a straight line, as it does in the example, Figure 4.10, the reaction would be first order.

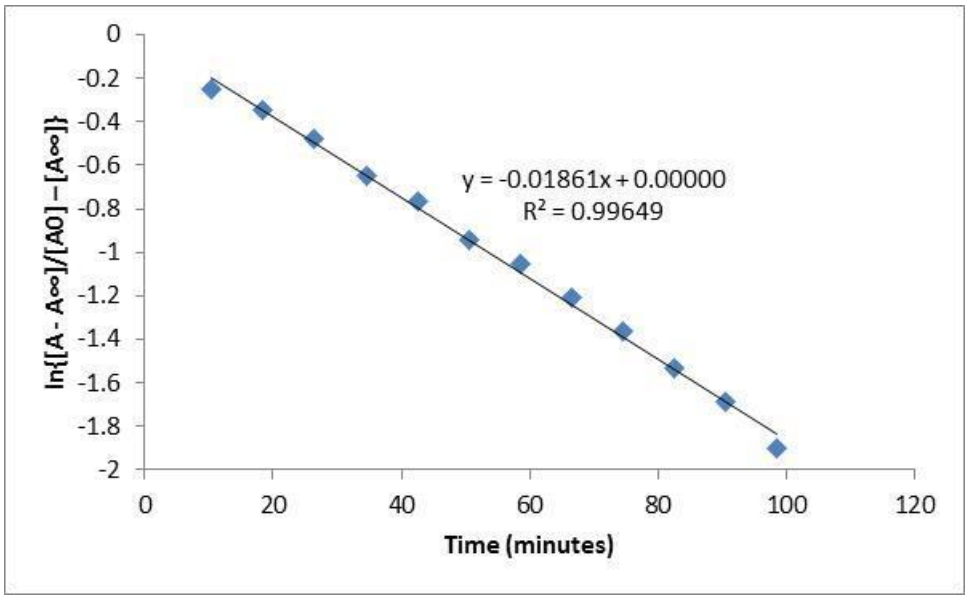

Figure 4.10: Log of concentration vs time example, D-Glucopyranose (0.5 M) in D2O

If the graph of inverse concentration against time, Figure 4.11, revealed a straight line, the reaction would be second order.

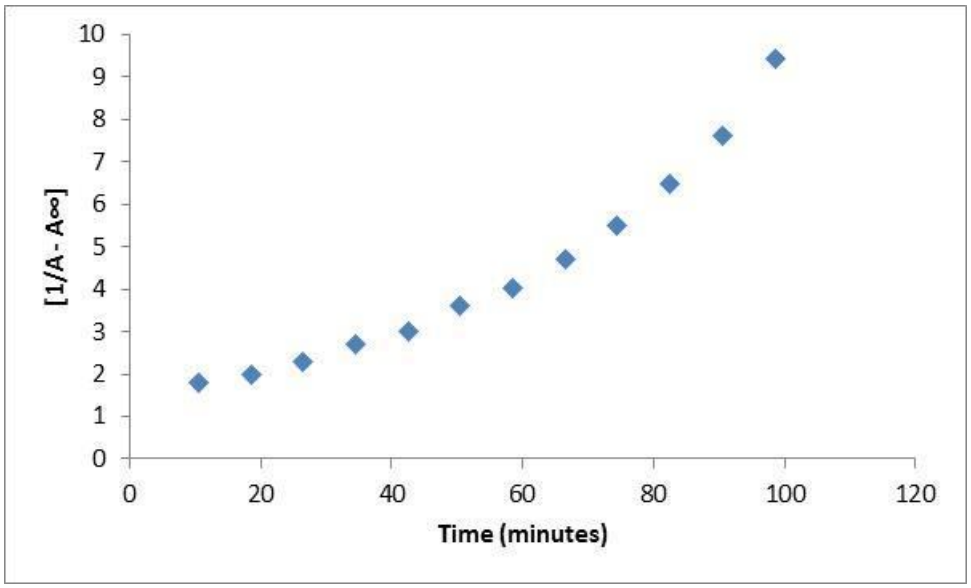

Figure 4.11: Inverse concentration against time example, D-Glucopyranose (0.5 M) in D2O.

4.3.4.2 $[A]_0$, k, k_1 and k_{-1} thus obtained by a graphical method

As the first order graph, Figure 4.10, was linear and the zeroth and second order graphs were curved, this reaction was regarded as occurring with first order kinetics.

Equation (10) was rearranged to give…

$$\ln([A] - [A]_{eq}) = -(k_1 + k_{-1})t + \ln([A]_0 - [A]_{eq}) \quad (11)$$

which was graphed to obtain the values for $[A]_0$ and $-(k_1 + k_{-1})$ which were used together with the value of K to determine the rate constants k_1 and k_{-1}. $[A]_{eq}$ was obtained by taking the mean concentration value from the set of data points starting from when equilibrium is reached to the last data point acquired. Where the equilibrium starts is decided by inspection of the graph of concentration versus time. $[A]_0$ was obtained by graphing $\ln([A] - [A]_{eq})$ vs time and substituting the graphical values into equation (11).

The experimentally determined value of $\ln([A]_0 - [A]_{eq})$ thus obtained from the graph, denoted as x, was used to solve for $[A]_0$…

$$\ln([A]_0 - [A]_{eq}) = x$$

$$[A]_0 - [A]_{eq} = e^x$$

$$[A]_0 = e^x + [A]_{eq} \quad (12)$$

The experimentally determined value of $(k_1 + k_{-1})_{exp}$ was obtained from the graph, and is the total rate constant k, i.e. the negative slope of the line. The rate constants in this expression are solved simultaneously using their relationship with the equilibrium constant K.

At equilibrium…

$$\frac{d[A]_{eq}}{dt} = \frac{d[B]_{eq}}{dt}$$

Therefore…

$$k_1[A]_{eq} = k_{-1}[B]_{eq}$$

$$\frac{[B]_{eq}}{[A]_{eq}} = K = \frac{k_1}{k_{-1}} \quad (13)$$

K can be determined experimentally with ^{1}H NMR by taking the ratio of the integrated signals for A and B at equilibrium. Solving for k_{-1} with $(k_1 + k_{-1})_{exp}$ and K_{exp}…

$$\frac{k_1}{k_{-1}} = K_{exp}$$

$$k_1 = K_{exp}k_{-1}$$

$$(k_1 + k_{-1})_{exp} = (k_{-1} + K_{exp}k_{-1})$$

$$k_{-1} = \frac{(k_1+k_{-1})_{exp}}{1+K_{exp}}$$

To solve for k_1 use…

$$k_1 = K_{exp}.k_{-1_{exp}}$$

4.3.4.3 Error

A source of error was arbitrarily choosing to use the first 80% of the acquired data. The proportional aspect of this range to the actual three half-lives for the reaction will vary depending on the delay between reaction start time and acquisition of the first spectrum. A proposed method to quantify some of this error related to the choice of using 80% of the first acquired data involved obtaining the rate constant using the first half of this selected data and obtaining the rate

constant using the second half of this selected data. The standard deviation fraction was obtained to calculate the standard error associated with the analytical method used in this study.

4.3.4.4 α-d-glucose (0.05 M) in D2O: example calculation

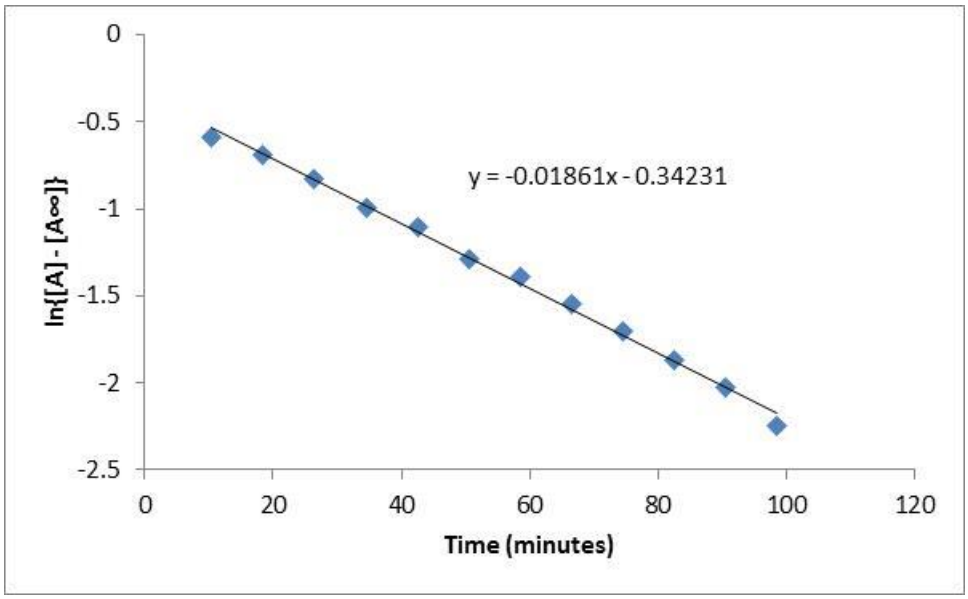

Figure 4.12: The graph to obtain $[A]_0$, k_1 and k_{-1}

The relative equilibrium concentration ($[\alpha]_{eq}$) was obtained by taking the mean of 109 ^{1}H NMR integrated signal data points from t(232 min) to t(1104 min) to give the value 0.5160. The length for each experiment is arbitrarily chosen to be well over the point that equilibrium is expected to be reached to ensure that equilibrium is reached. Excess data points after equilibrium is reached have minimal effect on the $[\alpha]_{eq}$ value as they contain random scatter around the mean.

The standard deviation fraction associated with the analytical method was determined by acquiring the rate constants for the first (1.757 x 10^{-2} min^{-1}) and second half (2.088 x 10^{-2} min^{-1}) of the selected data (first 80 %). The percentage standard deviation for 1.757 x 10^{-2} min^{-1} and 2.088 x 10^{-2} min^{-1} was calculated to be 0.1217. The thus obtained rate constants were multiplied by this value to give the absolute standard error associated with the analysis technique.

The value 0.5160, was input into equation 11 to give, Figure 4.12…

$$\ln([\alpha] - 0.5160) = -0.01861t - 0.3423$$

Substituting the value for $\ln([A]_0 - [A]_{eq})$ of -0.3423 into equation (12) gave…

$$[\alpha]_0 = e^{-0.3423} + 0.5160 \cong 1.23 \text{ moles}$$

The value for $(k_{-1} + Kk_{-1})$ is 0.01861 min^{-1}, Figure 4.12. This value, together with the value for K, was used to determine the rate constants k_1 and k_{-1}.

K was experimentally determined by taking the ratio $\frac{[ß]_{eq}}{[\alpha]_{eq}} = \frac{1.065}{0.5160}$ to obtain the value 2.064. Substituting this value into equation (13) to give $\frac{k_1}{k_{-1}} = 2.064$, and rearranging gave $k_1 = 2.064k_{-1}$. This term was substituted into the term, $(k_{-1} + k_1)$…

$$k = 1.861 \times 10^{-2} \pm 2.2 \times 10^{-3} \text{ min}^{-1}$$

$$(k_{-1} + 2.064k_{-1}) = 1.861 \times 10^{-2} \text{ min}^{-1}$$

$$k_{-1}(1 + 2.064) = 1.861 \times 10^{-2} \text{ min}^{-1}$$

$$k_{-1} = \frac{0.01861}{3.064} \text{ min}^{-1}$$

$$k_{-1} \cong 6.07 \times 10^{-3} \pm 7.3\times 10^{-4} \text{ min}^{-1}$$

k_1 is obtained by substituting the values of K and k_{-1} into…

$$k_1 = K_{exp}.k_{-1_{exp}}$$

$$k_1 = 2.064 \times 6.074 \times 10^{-3} \text{ min}^{-1}$$

$$k_1 \cong 1.25 \times 10^{-2} \pm 1.5 \text{ x } 10^{-3} \text{ min}^{-1}$$

Thus, the equilibrium constant and the three rates constants for the mutarotation of D-glucose were determined, Table 4.4, reaction 1.

4.3.4.5 Calculations under different conditions

The equilibrium constants and rate constants for seven mutarotation reactions, with varying conditions, were evaluated using the method described in section 4.3.4.2. As this mutarotation study was merely a comparison for work already reported in the literature, experiment duplication was not performed.

The rate constants for reactions **1** and **2**, Table 4.4, match each other relatively closely and fall within the standard error for the averaged literature values for experiments carried out at 25 °C, Table 4.5. The K values are a slightly higher (17%) than the literature value but still within an acceptable range and were likely result from the slightly elevated temperature of 26.9 °C versus 25 °C.

Reactions **3** and **4**, Table 4.4, were performed in DMSO-*d6* with glucose concentrations 0.05 M and 0.5 M respectively. All rate constants match very closely thus strongly supporting the assertion that the reaction is first order. The averaged K value for reactions **3** and **4** (1.18) matches very closely the literature K value (1.20).[27] These reactions had rate constants approximately 25 times smaller than the rate constants for reactions carried out in D_2O. Since the postulated acid/base catalysis mechanism for the mutarotation of glucopyranose requires the donation of a proton and the abstraction of a proton, Literature Review: section 1.9, and DMSO-*d6* is a relatively reluctant proton donor, one would expect the rate constant in DMSO-*d6* to be greatly reduced. It is important to note that although DMSO-*d6* does not have any obvious exchangeable protons, the methyl protons of DMSO-*d6* do undergo exchange[74,76,77] albeit at a much reduced rate when compared to D_2O. This would explain why mutarotation occurs at all in DMSO-*d6*. No previous studies could be found concerning the mutarotation of glucopyranose in DMSO-*d6* with which to compare the experimental results.

Reactions **5**, **6**, and **7** had HCl added to the reaction solution with incrementally increased concentrations. Reactions **5** and **6** had closely matching rate constants which also corresponded closely with the values for reactions **1** and **2** thus indicating that the added amount of HCl was too small to have any significant catalytic effect. Reaction **7** had an approximate 5 fold rate constant increase when compared to reactions **1**, **2**, **5** and **6** thus indicating that the mutarotation reaction had been catalysed by HCl. The k value that was obtained in reaction **7** is within the range of values that were obtained in a previous study of the acid catalysis of the mutarotation of glucopyranose.[70]

The kinetic data that were obtained in this preliminary mutarotation study reasonably corresponded to the kinetic data provided in the literature thus validating the use of the ^{1}H NMR method to obtain kinetic data for the mutarotation-like dissociation of the DHA dimer.

Table 4.4: The experimentally determined rate and equilibrium constants

Glc conc. (M)	Solvent	Acid conc. (M)	Temp.(°C)	K (no units)	k (min^{-1})	k_1 (min^{-1})	k_{-1} (min^{-1})
0.05	D_2O	n/a	26.9	2.064	$1.86 \times 10^{-2} \pm 2.2 \times 10^{-3}$	$1.25 \times 10^{-2} \pm 1.1 \times 10^{-3}$	$6.07 \times 10^{-3} \pm 7.3 \times 10^{-4}$
0.5	D_2O	n/a	26.9	2.048	1.21×10^{-2} *	8.19×10^{-3} *	4.00×10^{-4} *
0.05	DMSO-*d6*	n/a	26.9	1.318	$7.59 \times 10^{-4} \pm 3.0 \times 10^{-5}$	$4.31 \times 10^{-4} \pm 1.7 \times 10^{-5}$	$3.27 \times 10^{-4} \pm 1.3 \times 10^{-5}$
0.5	DMSO-*d6*	n/a	26.9	1.049	$7.91 \times 10^{-4} \pm 6.4 \times 10^{-5}$	$4.05 \times 10^{-4} \pm 3.3 \times 10^{-5}$	$3.86 \times 10^{-4} \pm 3.1 \times 10^{-5}$
0.5	D_2O	0.001	26.9	1.183	$1.31 \times 10^{-2} \pm 2.2 \times 10^{-3}$	$7.12 \times 10^{-3} \pm 1.2 \times 10^{-3}$	$6.01 \times 10^{-3} \pm 1.0 \times 10^{-3}$
0.5	D_2O	0.01	26.9	1.478	1.08×10^{-2} *	6.41×10^{-3} *	4.34×10^{-3} *
0.5	D_2O	0.1	26.9	1.931	$6.03 \times 10^{-2} \pm 1.6 \times 10^{-3}$	$3.97 \times 10^{-2} \pm 1.1 \times 10^{-3}$	2.06×10^{-2} *

** The error associated with the analytical method is below the order of magnitude for significant figures*

Table 4.5: A selection of literature values for mutarotation rate constants. The results for experiments carried out at 25 °C were averaged for comparison

No.	Method	Temp. (°C)	k (min^{-1})	k_1 (min^{-1})	k_{-1} (min^{-1})
1	^{1}H NMR[75]	34.2	1.20×10^{-2}		
2	Polarimetric[78]	22	4.60×10^{-3}	1.66×10^{-3}	2.95×10^{-3}
3	Dilatometric[30]	25	9.6×10^{-3}		
4	Polarimetric[79]	25	1.1×10^{-2}	7.0×10^{-3}	4.1×10^{-3}
5	G.L.C[79]	25	1.0×10^{-2}	6.3×10^{-3}	3.9×10^{-3}
6	Polarographic[80]	25	3.18×10^{-2}		
7	Polarimetric[80]	25	2.40×10^{-2}		
8	G.L.C[26]	30	3.51×10^{-2}	1.40×10^{-2}	2.11×10^{-2}
-	Averaged experiments 3-7	25	1.73×10^{-2}	6.65×10^{-3}	4.00×10^{-3}

All experiments were carried out in H_2O except the ^{1}H NMR experiment which was carried out in D_2O

4.4 Kinetic analysis

4.4.1 Reversible reactions

The DHA dimer dissociation is considered to be a reversible reaction that is pseudo-first order in DHA with H^+ or OH^- in excess. The reaction kinetics in the forward direction were first order in DHA dimer and in the reverse direction, second order in DHA monomer, Figure 4.13.

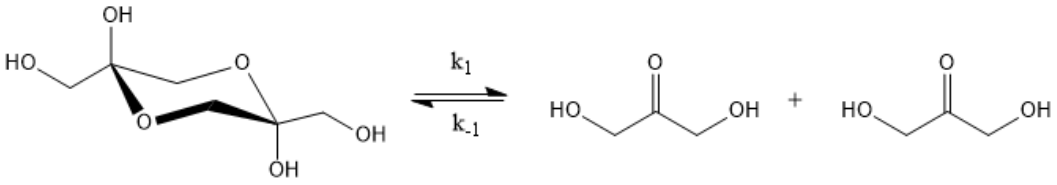

Figure 4.13: The reversible DHA dimer dissociation/dimer formation

which gave a second order term to define K

$$K = \frac{[products]^p_{eq}}{[reactants]^r_{eq}} = \frac{[DHA_{monomer}]^2_{eq}}{[DHA_{dimer}]_{eq}} \qquad (14)$$

4.4.2 Conversion of signal values to concentration values

Before K could be determined and therefore the forward and reverse rate constants k_1 and k_{-1}, the absolute concentration of the reactants and the products needed to be ascertained. As the product concentration is squared in the numerator of the equation associated with the determination of the equilibrium constant, the value of K becomes concentration dependent and therefore the absolute concentrations are required.

The ^{1}H signals utilised to trace the concentrations of the DHA dimer and monomer were the dimer doublet at 3.92 ppm, emanating from two axial methylene protons, and the monomer doublet at 4.16 ppm that emanates from eight methylene protons from the two monomer product molecules. The response of two protons was chosen to be Y, the standard response factor to define the concentration of all species identified in the kinetic experiments. As the monomer signal response emanated from four protons, this value was halved to convert the value to the standard response factor Y.

The slanting of the Int#1 doublet signal at 3.59 ppm indicated that this signal represented half of a second order splitting pattern that would emanate from the two pairs of diastereotopic protons, one pair on either side of the ring, according to the proposed structure of Int#1. If the signal was emanating from diastereotopic protons the full signal must represent two pairs as Int#2 is symmetric as characterised by only having three signals in the ^{13}C NMR spectrum. Therefore the Int#1 signal, emanating from two protons, is equivalent to Y, the standard response factor.

The Int#2 doublet at 3.71 ppm was determined to emanate from a single proton resulting from the proposed protonated ring structure for Int#2 having lost symmetry with each proton of the DHA dimer in a different chemical environment. To determine the concentration of Int#2, its signal response is doubled to get its Y value as it emanates from only one proton.

To determine the absolute concentrations for each species their values for [A], $[A]_o$, Y, Y_{eq}, and Y_o were determined experimentally and inputted into the following equations…

The DHA dimer data was inputted into…

$$[\mathrm{DHA}_{dimer}] = [\mathrm{DHA}_{dimer}]_0 \left(\frac{Y - Y_{eq}}{Y_0 - Y_{eq}} \right)$$

…to obtain the absolute concentration and the monomer and the intermediate signals were inputted into…

$$[\mathrm{A}] = [\mathrm{A}]_0 \left(\frac{Y - Y_{eq}}{Y_0 - Y_{eq}} \right)$$

4.5 Discussion

^{1}H NMR spectroscopy was chosen to be the NMR technique to be used to obtain kinetic data for this study incorporating a DHA dimer concentration of 0.25 M in DMSO-*d6* to be obtained from sealed ampoules. The mutarotation of glucopyranose, subsection 4.3, is a system similar to the dissociation of the DHA dimer,[12,20,22] consisting of a reversible acid or base catalysed reaction mechanism, therefore a similar method for the analytical treatment of the kinetic data used in subsection 4.3 will be employed in the treatment of the kinetics in this study of the dissociation of the DHA dimer in DMSO-*d6* with. The difference between the two systems is how the value of K is obtained. The molecularity of the products for the dissociation of the DHA dimer to form two DHA monomer units will have K in this study to be determined as…

$$K = \frac{[\mathrm{monomer}]^2}{[dimer]}$$

The NMR signal response values were converted to the standard Y form to be converted to absolute concentrations using the appropriate equation.

5 The kinetics of the dissociation of the DHA dimer in DMSO-*d6*

5.1 First order reversible reaction as the rate determining step

The kinetics for the dissociation of the DHA dimer to form two DHA monomer molecules in DMSO-*d6* were first order in the DHA dimer. It is proposed by this study that the unimolecular reversible break-up of the protonated DHA dimer to form the acyclic DHA dimer is the rate determining step, Figure 5.1, as the rupturing of the ring as the rate determining step is a common feature in reaction mechanisms for mutarotation in monosaccharides.[27,28,42,46,81] A relevant example is the acetic acid catalysed mutarotation of glucopyranose which utilizes the A1 (stepwise) mechanism with the rupturing of the protonated glucopyranose ring being the rate determining step.[28]

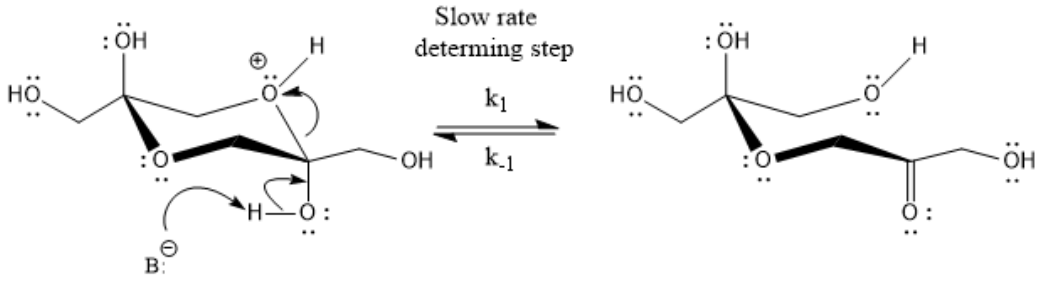

Figure 5.1: The rate determining step of the protonated DHA dimer breaking to form the acyclic DHA dimer

The proposed rate determining step is a first order reversible reaction represented by Figure 5.2.

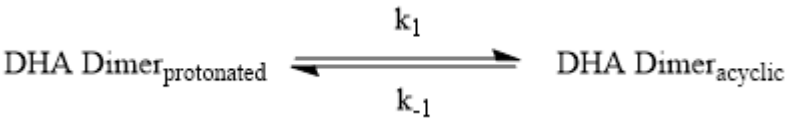

Figure 5.2: The elementary first order equilibrium reaction

The change in concentration of the DHA $dimer_{protonated}$ is described by the differential equation…

$$\frac{d[dimer_{protonated}]}{dt} = -k_1[\,dimer_{protonated}] + k_{-1}[DHA\ dimer_{acyclic}]$$

…using the integrated rate expression that was previously derived for the mutarotation reversible reaction, section 4.3.2, the following can be derived for this step…

$$\ln \frac{[dimer_{protonated}] - [dimer_{protonated}]_{eq}}{[dimer_{protonated}]_0 - [dimer_{protonated}]_{eq}} = -(k_1 + k_{-1})t$$

The kinetics for the DHA dimer to DHA monomer reversible reaction were first order in the DHA dimer as the equilibrium constant, K, was generally one to two orders of magnitude larger than one.

k_1 and k_{-1} were determined using the experimentally obtained equilibrium constant K value and the slope of the graph …

$$\ln([A] - [A]_{eq}) = -(k_1 + k_{-1})t + \ln([A]_0 - [A]_{eq})$$

… as described in section 4.3.2, for the mutarotation of glucopyranose. The slope of the graph represents the spontaneous reaction rate constant, k, defined as $k = (k_1 + k_{-1})$.

5.2 The second order reversible reaction

The overall reversible reaction for the dissociation of the DHA dimer to form two DHA monomer units, Figure 5.3, is a complex reaction consisting of multiple elementary reaction steps.

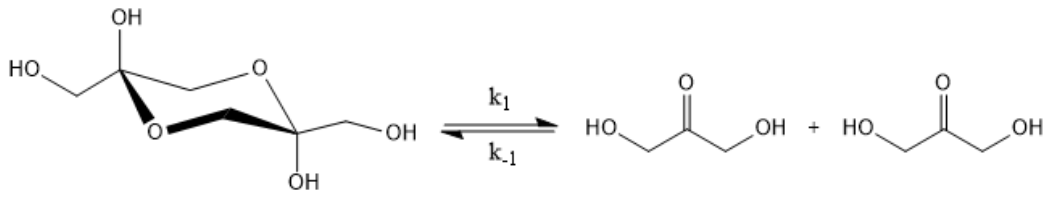

Figure 5.3: The overall dissociation of the DHA dimer to monomer

To determine the rate constants for the second order reversible reaction, that take into account the first order forward reaction kinetics and the second order

reversible reaction kinetics, the system of differential equations associated with both of these competing processes was solved.

The second order reversible reaction is represented in Figure 5.4, with D representing the DHA dimer and M representing the DHA monomer.

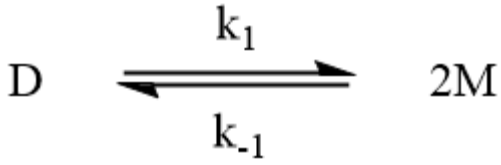

Figure 5.4: The second order equilibrium reaction

The rate of change in the concentration of the DHA dimer is represented with the differential equation for [D]…

$$\frac{d[\mathrm{D}]}{dt} = -k_1[\mathrm{D}] + k_{-1}[M]^2$$

A second order reversible reaction rate expression was derived from this equation using the MapleSoft[82] software program in terms of the concentration of the DHA dimer. A series of algebraic operations[8] were applied to the obtained derivation to get a rate expression in linear form so it could be applied to the kinetic data to determine the rate constants, k_1 and k_{-1}.

$$\ln\left(\frac{-8([\mathrm{D}]-[\mathrm{D}]_0)+K+\sqrt{K^2+16K[\mathrm{D}]_0}}{8([\mathrm{D}]-[\mathrm{D}]_0)-K+\sqrt{K^2+16K[\mathrm{D}]_0}}\right) = k_{-1}\sqrt{K^2+16K[\mathrm{D}]_0}.t$$

5.3 Discussion

This study investigated the DHA dimer dissociation equilibrium reaction that started with reactants and no products. This resulted in the first order forward reaction being the dominant component of the kinetics to describe the system.

Another feature of the DHA dimer dissociation reaction is that the equilibrium sits well to the right, favouring products, which by definition means that k_{-1} is small and K is large.

[8] The full derivation is in appendix: 10.5

It can be shown that when K gets large the first order and second order rate expressions approach equality and therefore provide for the first order reversible reaction rate expression to be utilised for the processing of the raw kinetic data to obtain the rate constants k, k_1 and k_{-1}.

The effect of K getting large on the equality between the two rate expressions can be investigated by making the right-hand sides of both expressions approximately equal.

$$-(k_1 + k_{-1})t \approx k_{-1}\sqrt{K^2 + 16K[\mathrm{D}]_0}.t$$

…allow t to cancel and the sign of the left hand side to be reversed in order to have both gradients positive…

$$(k_1 + k_{-1}) \approx k_1\sqrt{K^2 + 16K[\mathrm{D}]_0}$$

Substitute in $K.k_{-1} = k_1$ and pull k_{-1} out of the brackets…

$$k_{-1}(K + 1) \approx k_{-1}\sqrt{K^2 + 16K[\mathrm{D}]_0}$$

…allow k_{-1} to cancel…

$$K + 1 \approx \sqrt{K^2 + 16K[\mathrm{D}]_0}$$

On inspection of this equality approximation, with the left-hand side representing the first order expression and the right-hand side representing the second order expression, when K gets large the other terms lose weight and can be approximated to zero. Therefore, on the left-hand side 1 drops out and on the right-hand side $16K[\mathrm{D}]_o$ will become small relative to K^2 and therefore drops out.

These two approximations leave…

$$K \approx \sqrt{K^2}$$

$$K \approx K$$

…which implies that for large K the first order rate expression and the second order rate expression can be approximated as equivalent.

If the value for K is large, the expression will behave as a first order integrated rate expression to give similar opposite-signed rate constant values to the first order integrated rate expression derived for the mutarotation of glucopyranose. If the value of K gets close to or below the value of one, the first order reversible rate equation would no longer be applicable and the second order reversible rate expression would be utilised to obtain the kinetic data in this system.

One unhelpful consequence of using the second order rate expression is that the units for k obtained from the second order rate expression are in $L.mol^{-1}.min^{-1}$ while the units for k obtained from the first order rate expression are in min^{-1}. It would be inappropriate to assign second order reaction units to what is essentially a first order reaction.

Therefore, based on the reasons given above, the first order integrated rate expression approximation was used to obtain the kinetic parameters k, k_1 and k_{-1} for the DHA dimer dissociation reactions investigated in this study.

6 Proposed acid-catalysed and base catalysed reaction mechanisms

The glucopyranose and DHA carbohydrate molecules possess the same fundamental structural and chemical functional properties consisting of six membered rings with hemiketal/hemiacetal components incorporated into their rings that stabilise the ring structure via the anomeric effect, see section 1.8. With consideration of these parallels existing between the pyranose and DHA dimer systems, this study proposes that the DHA dimer dissociation reaction mechanism is analogous to the glucopyranose mutarotation reaction mechanism[28] with both acid catalysis and base catalysis pathways.

6.1 Acid catalysed dissociation of the DHA dimer in DMSO-*d6*

The proposed acid catalysis reaction mechanism, **Error! Reference source not found.**, begins with a rapid and reversible proton exchange between the acid catalyst and both ring oxygens. This process is presented as step 1 of the proposed reaction mechanism. Step 2, the slow rate determining step, involves a proton abstraction from the "anomeric" hydroxyl group of the protonated DHA dimer reaction intermediate with an electron transfer to form an oxygen-carbon carbonyl double bond and a concerted electron transfer to the cationic oxygen resulting in ring rupture.

This process is repeated with the other tertiary hydroxyl group, albeit at an accelerated rate as ring stability resulting from the double anomeric effect has been lost when the DHA dimer lost its rigid ring conformation and the anomeric stability offered by the first acetal moiety.

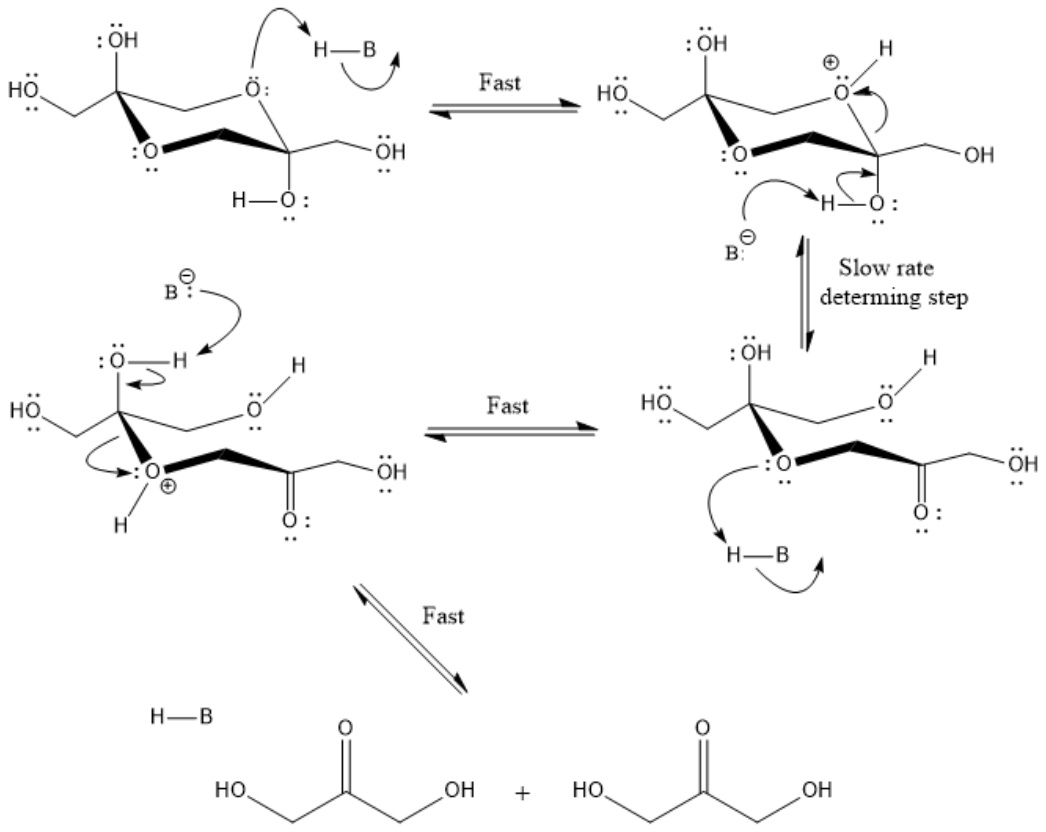

Figure 6.1: The proposed acid catalysed reaction mechanism for the dissociation of the DHA dimer in solution

6.2 The base catalysed dissociation of the DHA dimer in DMSO-*d6*

The proposed base-catalysed reaction mechanism, **Error! Reference source not found.**, begins with the abstraction of a ring hydroxyl proton, the slow rate determining step, followed by an electron transfer from the hydroxyl proton to the adjacent anomeric carbon to form a carbonyl bond, with a concerted electron transfer from the anomeric carbon to the ring oxygen resulting in ring rupture. This process is repeated at the other acetal group at a much increased rate resulting from the loss of stability associated with the original ring structure and double anomeric effect.

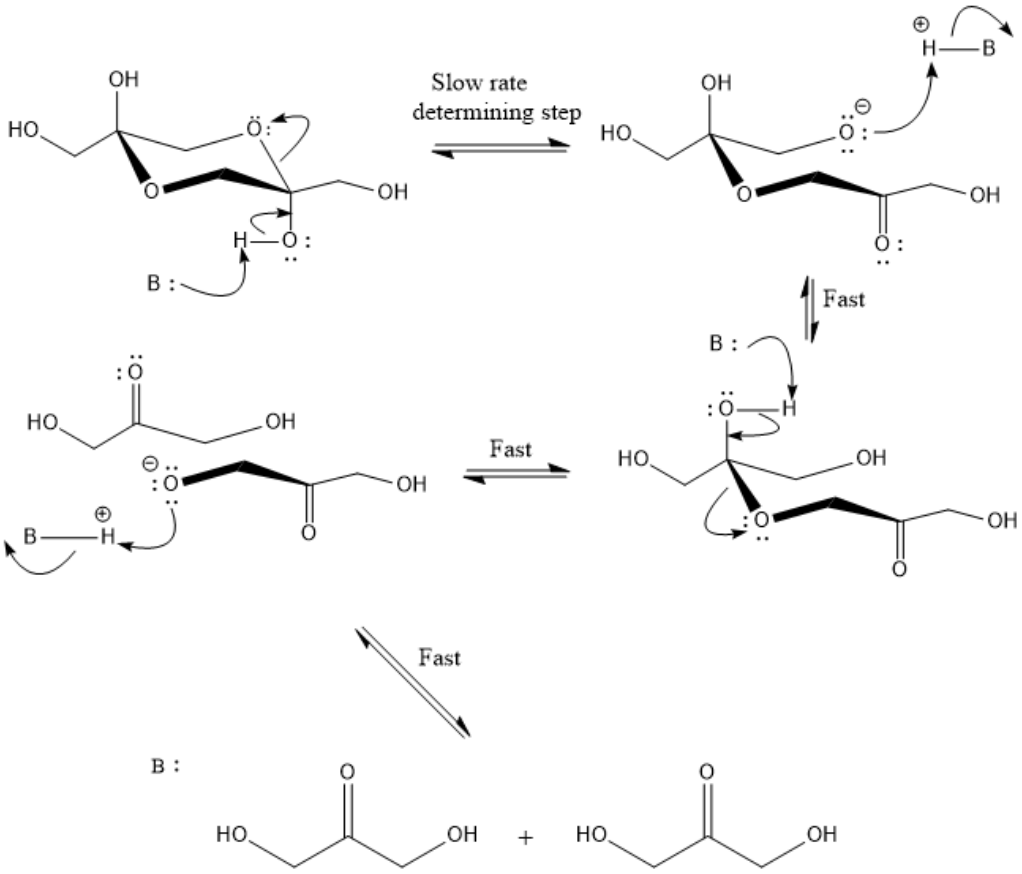

Figure 6.2: The proposed base catalysed reaction mechanism for the dissociation of the DHA dimer in solution

6.3 The kinetics

As the rate determining step of the proposed reversible break-up of the DHA dimer ring to form the acyclic DHA dimer is a unimolecular reversible reaction, in both the acid-catalysed and base-catalysed mechanisms, the system would fit a first order reversible reaction model, see section 5.1. The break-up of the acyclic DHA dimer intermediate to form two DHA monomer molecules, **Error! Reference source not found.**, is a mixed unimolecular bimolecular reversible reaction that would fit a mixed first order and second order reversible reaction model with the caveat that if the equilibrium was far enough to the right in favour of the products, the model would essentially become first order, see sections 5.2 and 5.3.

If the experimentally obtained kinetic data displayed second order kinetics, this would suggest that the equilibrium was closer to the centre and that the break-up of the acyclic intermediate to form two DHA monomer molecules was the rate determining step.

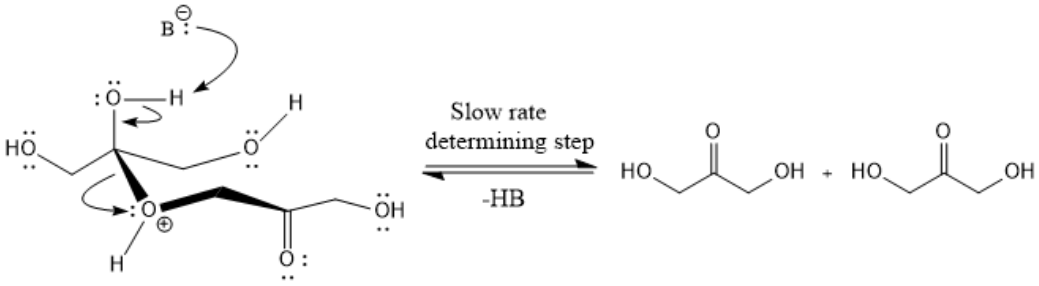

Figure 6.3: The second order bimolecular rate determining step

The proposed acid-catalysed reaction mechanism is an example of general acid-catalysis as the rate of reaction is dependent on the concentration of the buffer, i.e. the undissociated acid. Similarly, the proposed base-catalysed reaction mechanism is an example of general base-catalysis as the rate of reaction is dependent on the concentration of the buffer anion.

7 Results and Discussion

7.1 The DHA dimer dissociation in DMSO-*d6* without catalysis

7.1.1 Introduction

A set ^{1}H NMR spectroscopy experiments were performed in triplicate to determine the equilibrium constant K and the k, k_1 and k_{-1} rate constants for the proposed first order reversible acid/base catalysed reaction mechanism for the dissociation of the DHA dimer (0.25 M) to the DHA monomer in DMSO-*d6*. Both the first order and second order reversible reaction integrated rate expressions were used to determine the kinetics of the DHA dimer dissociation. This was performed to compare the results obtained by the two analytical methods.

7.1.2 Results

7.1.2.1 Reaction order determination[i]

The order of reaction was determined by inspection of the zeroth, first and second order graphs for the concentration of the DHA dimer and the change in time (minutes).

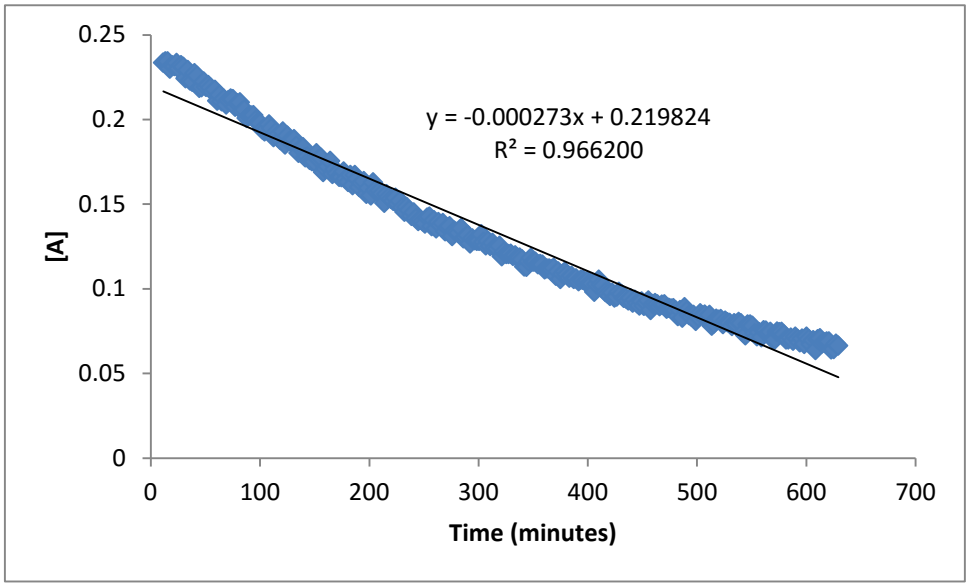

Figure 7.1: The experimental zeroth order graph example for the uncatalysed dissociation of the DHA dimer in DMSO-*d6*: Reaction #1

[i] The completed set of zeroth, first and second order graphs are contained in the appendix: A1 – A6

The zeroth-order graphs were all curved Figure 7.1, thus indicating that zeroth order kinetics were not operating in the dissociation of the DHA dimer in this system.

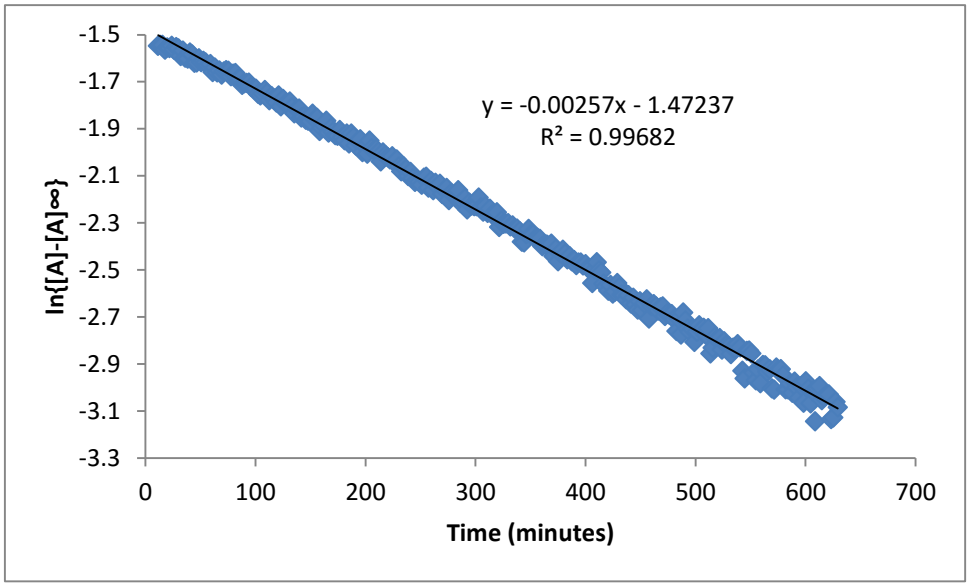

Figure 7.2: The experimental first order graph example for the uncatalysed dissociation of the DHA dimer in DMSO-d6: Reaction #1

The first-order plots produced straight lines with strong R^2 values, Figure 7.2. This indicated that first order kinetics were operating for the uncatalysed dissociation of the DHA dimer in DMSO-*d6*.

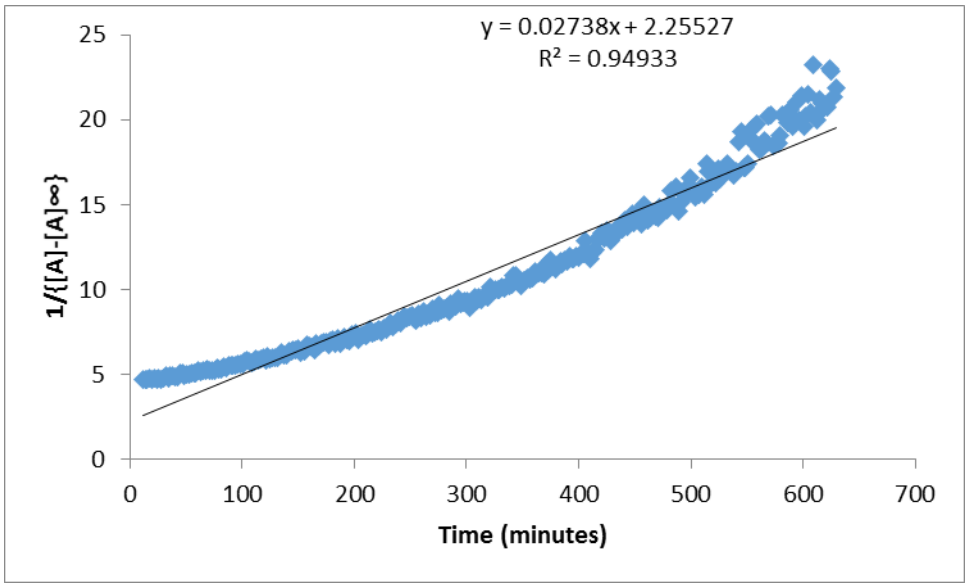

Figure 7.3: The standard second order graph example for the uncatalysed dissociation of the DHA dimer in DMSO-d6: Reaction #1

The standard second-order graphs were all curved, Figure 7.3, thus indicating that second order kinetics were not operating in the dissociation of the DHA dimer in this system.

7.1.2.2 Determination of rate constants using the second order reversible reaction integration expression[j]

The triplicate ^{1}H NMR experiments that traced the dissociation of the DHA dimer in DMSO-*d6* obtained kinetic data that was processed and graphed, Figure 7.4, using the second order reversible rate expression in order to determine the rate constants k, k_1 and k_{-1}, Table 7.1, associated with the reversible dissociation of the DHA dimer.

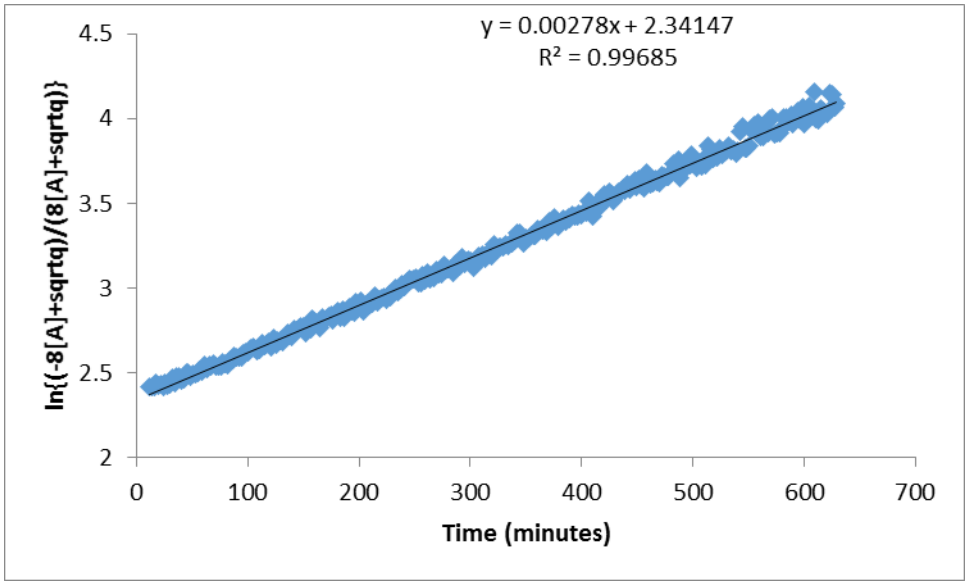

Figure 7.4: An example graph obtained from the second order reaction expression: Reaction #1

7.1.2.2.1 An example calculation

Using the equations…

$$\ln\left(\frac{-8([\mathrm{D}]-[\mathrm{D}]_0)+K+\sqrt{K^2+16K[\mathrm{D}]_0}}{8([\mathrm{D}]-[\mathrm{D}]_0)-K+\sqrt{K^2+16K[\mathrm{D}]_0}}\right)=k_{-1}\sqrt{K^2+16K[\mathrm{D}]_0}.t$$

$$K=\frac{[products]_0{}^2}{[reactants]_0}$$

[j] The completed set of the second order reversible reaction graphs are contained in the appendix: A7 and A8

$$k_{-1} = \frac{k}{\sqrt{K^2 + 16K[\mathrm{D}]_0}}$$

$$k_1 = K.k_{-1}$$

…that were derived in section 5.2, the equilibrium constant, K, and the rate constants k, k_1 and k_{-1} were determined.

The value for K was determined by taking the average of the K values obtained from each spectrum from time: 2000 minutes to time: 3150 minutes. Equilibrium was achieved by time: 2000 minutes. The obtained K value was 8.44 mol L^{-1}. The value for K and the initial concentration, 0.25 mol L^{-1}, were inputted into the logarithmic term that was graphed against time to obtain the slope provided by Excel with a trend-line. The values for K, k and $[D]_o$ were inputted into the derived k_{-1} expression...

$$k_{-1} = \frac{k}{\sqrt{K^2 + 16K[\mathrm{D}]_0}} = \frac{2.78 \times 10^{-3} mol}{\sqrt{8.44^2 (mol\ L^{-1})^2 + 16 \times 8.44\ mol\ L^{-1} \times 0.25\ mol\ L^{-1}}}$$

$$k_{-1} = 2.71 \times 10^{-4} L$$

This calculated value for k_{-1} was utilised to calculate k_1…

$$k_1 = K.k_{-1} = 8.44\ mol\ L^{-1} \times 3.92 \times 10^{-4} L = 2.40 \times 10^{-3} mol$$

This method was used to determine the values for K and the rate constants associated to the triplicate experiments that followed the dissociation of the DHA dimer in DMSO-*d6*, Table 7.2.

7.1.2.3 Determination of the first order rate constants

The triplicate ^{1}H NMR experiments that traced the dissociation of the DHA dimer in DMSO-*d6* obtained kinetic data to be used for the determination of the equilibrium and rate constants, Table 7.2, associated with the reversible dissociation of the DHA dimer.

Table 7.1: The tabulated values for K and the three rate constants for the uncatalysed DHA dimer dissociation reaction obtained using the second order reversible reaction rate expression

Reaction	K (No units)	k ($L.mol^{-1}.min^{-1}$)	k_1 ($L.mol^{-1}.min^{-1}$)	k_{-1} ($L.mol^{-1}.min^{-1}$)
1	8.44	2.78×10^{-3}	2.29×10^{-3}	2.71×10^{-4}
2	7.50	3.50×10^{-3}	2.56×10^{-3}	3.42×10^{-4}
3	6.74	5.07×10^{-3}	3.34×10^{-3}	4.95×10^{-4}
Average values	7.56 ± 0.85	$3.78 \times 10^{-3} \pm 1.17 \times 10^{-3}$	$2.73 \times 10^{-3} \pm 5.43 \times 10^{-4}$	$3.69 \times 10^{-4} \pm 1.14 \times 10^{-4}$

Table 7.2: The tabulated values for K and the three rate constants for the uncatalysed DHA dimer dissociation reaction obtained using the first order reversible reaction rate expression

Reaction	K (No units)	k (min^{-1})	k_1 (min^{-1})	k_{-1} (min^{-1})
1	8.44	2.57×10^{-3}	2.30×10^{-3}	2.72×10^{-4}
2	7.50	3.06×10^{-3}	2.68×10^{-3}	3.58×10^{-4}
3	6.74	4.33×10^{-3}	3.77×10^{-3}	5.59×10^{-4}
Average values	7.56 ± 0.85	$3.31 \times 10^{-3} \pm 9.1 \times 10^{-4}$	$2.92 \times 10^{-3} \pm 7.6 \times 10^{-4}$	$3.96 \times 10^{-4} \pm 1.47 \times 10^{-4}$

7.1.2.3.1 Example calculation

Using the equations…

$$\ln([A] - [A]_{eq}) = -(k_1 + k_{-1})t + \ln([A]_0 - [A]_{eq})$$

$$K = \frac{[products]_0{}^2}{[reactants]_0}$$

$$k_{-1} = \frac{k}{1 + K}$$

$$k_1 = K.k_{-1}$$

derived in section 4.3.2, the equilibrium constant and rate constants k_1 and k_2 were determined.

The value for K was determined from the kinetic data as describe in the previous section 7.1.2.2, to give...

$$K = \frac{[products]^2}{[reactants]} = 8.44$$

The value for K and the initial concentration, 0.25 mol L^{-1}, were inputted into the logarithmic term that was graphed against time to obtain the slope provided by Excel with a trend-line. The values for K, k and $[D]_o$ were inputted into the derived k_{-1} expression

k was obtained from the slope in the graph for $\ln[[A]-[A]_\infty]$ against time, in **Error! Reference source not found.**, to calculate k_{-1}…

$$k_{-1} = \frac{k}{1 + K} = \frac{2.57 \times 10^{-3} min^{-1}}{1 + 8.44} = 2.72 \times 10^{-4} min^{-1}$$

This calculated value for k_{-1} was utilised to calculate k_1…

$$k_1 = K_{exp}.k_{-1_{exp}} = 8.442 \times 2.72 \times 10^{-4} min^{-1} = 2.30 \times 10^{-3} min^{-1}$$

This method was used to determine the values for K and the rate constants associated to the triplicate experiments that followed the dissociation of the DHA dimer in DMSO-*d6*, Table 7.2.

7.1.3 Discussion

The uncatalysed DHA dimer dissociation in DMSO-*d6* at 26.9 °C was shown to exhibit the kinetics of a first order reversible reaction with an mean reaction rate constant k of 3.31 x 10^{-3} min^{-1}, a forward rate constant k_1 of 3.96 x 10^{-4} min^{-1}, a reverse rate constant k_{-1} of 3.96 x 10^{-4} min^{-1} and an equilibrium constant K of 7.56 mol L^{-1}. The uncatalysed DHA dimer dissociation also exhibited the kinetics of a second order reversible reaction, but as K was large, this was essentially another case of demonstrating first order kinetics. When the second order rate expression was used, the units for the kinetic terms were changed with the result that technically no comparison may be made between the values obtained from the different rate expressions. As the reaction exhibited first order kinetics with both rate expressions, the first order rate expression values will be used.

The experimentally determined value obtained for k, of 3.31 x 10^{-3} min^{-1}, was calculated to be 18.3 times greater than the literature value for the dissociation of the DHA dimer in DMSO-*d6* of 1.81 x 10^{-4} min^{-1} at 25 °C. the often cited k value for the dissociation of the DHA dimer in DMSO[23]. This previous study used ^1H NMR spectroscopy to determine the half-life for the dissociation of the DHA dimer in DMSO-*d6* in 1973. No indication of the reproducibility of this previously obtained rate constant value was provided within the paper[23] and it might therefore be regarded with a certain degree of suspicion.

7.2 The DHA dimer dissociation in DMSO-*d6* catalysed with D_2O

7.2.1 Introduction

A set of ten replicated ^1H NMR kinetic experiments (26.9 °C) were performed to determine the reaction order and the rate constants for the dissociation of the DHA dimer (0.25 M) to the DHA monomer in DMSO-*d6* as the concentration of D_2O was incrementally increased. The pKa value of H_2O in DMSO is 31.4[52,83] which, when compared to the pKa value of 15.6[52,83] for H_2O in H_2O, gives an acid dissociation constant that is reduced by 16 orders of magnitude. The ability of D_2O to donate a proton in the dissociation reaction is greatly reduced in the DMSO-*d6* reaction system. The concentration of D_2O was represented as a mass percentage to allow for comparison with the concentration of H_2O in honey which is commonly represented as a mass percentage. As the mutarotation of glucopyranose is catalysed by water[28,30,79], the expectation of adding D_2O to the dissociation reaction for the DHA dimer, which has a proposed reaction mechanism that is analogous to that for mutarotation, would be an increase in the forward rate constant values. For D_2O to be behaving as a pure catalyst, with the absence of any hidden variables, a constant value of K would be expected across the concentration range.

7.2.2 Results

7.2.2.1 Reaction order determination[k]

The order of reaction was determined by inspection of the zeroth, first and second order graphs for the concentration of the DHA dimer and the change in time (minutes).

[k] The completed set of first order graphs for the D_2O catalysed dissociation reactions are contained in the appendix: A9 – A27

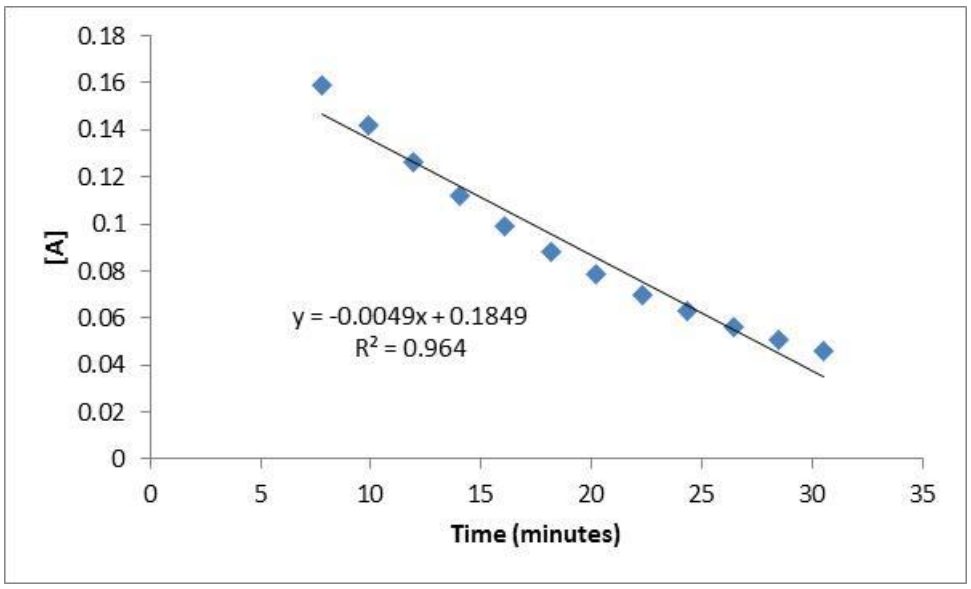

Figure 7.5: The experimental zeroth order graph example

The zeroth-order graphs were all curved, Figure 7.5, thus indicating that zeroth order kinetics were not operating in the dissociation of the DHA dimer in this system.

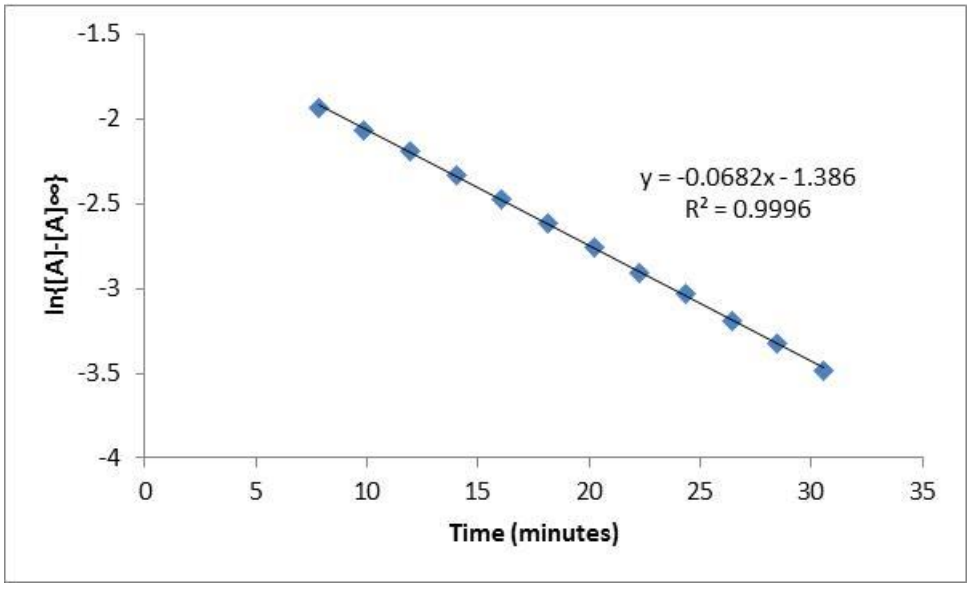

Figure 7.6: The experimental first order graph example

The first-order plots produced straight lines with strong R^2 values, Figure 7.6. This indicated that first order kinetics were operating for the D_2O catalysed dissociation of the DHA dimer in DMSO-*d6*.

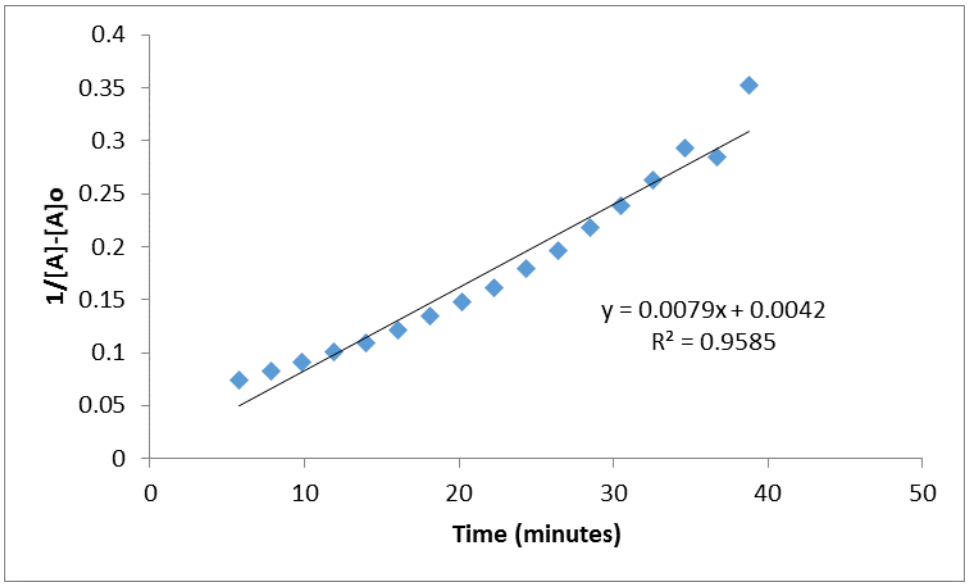

Figure 7.7: The experimental second order graph example

The standard second-order graphs were all curved, Figure 7.7, thus indicating that second order kinetics were not operating in the dissociation of the DHA dimer in this system.

7.2.2.2 Determination of rate constants[l]

The equilibrium and rate constant values for the $[D_2O]$ = 0 are the values determined in section 7.1.2 for the uncatalysed DHA dimer to monomer dissociation. The value for K and the rate constants were determined for ten duplicated ^{1}H NMR kinetic experiments, Table 7.3, that were performed while applying an incrementally increasing concentration of the D_2O catalyst for each successive experiment. The aim of this incremental D_2O concentration increase was to determine the effect that this increase would have on the rate constant values for the dissociation of the DHA dimer to the DHA monomer reaction.

The calculated results for K and the first order rate constants, Table 7.3, were graphed as rate constant against concentration of D_2O, Figure 7.8, Figure 7.9, Figure 7.10 and Figure 7.11, to illustrate what the effect of increasing the concentration of D_2O in the DHA dimer dissociation in DMSO-*d6* had on the values for K and the rate constants.

[l] The completed set of first order graphs for the D_2O catalysed dissociation reactions are contained in the appendix: A9 – A27

As all of the D_2O catalysed dissociation reaction displayed first order kinetics, the first order reversible reaction integrated rate expression was used to determine the rate constants in this series of kinetic experiments.

7.2.2.3 Graphs for rate constant against D_2O concentration

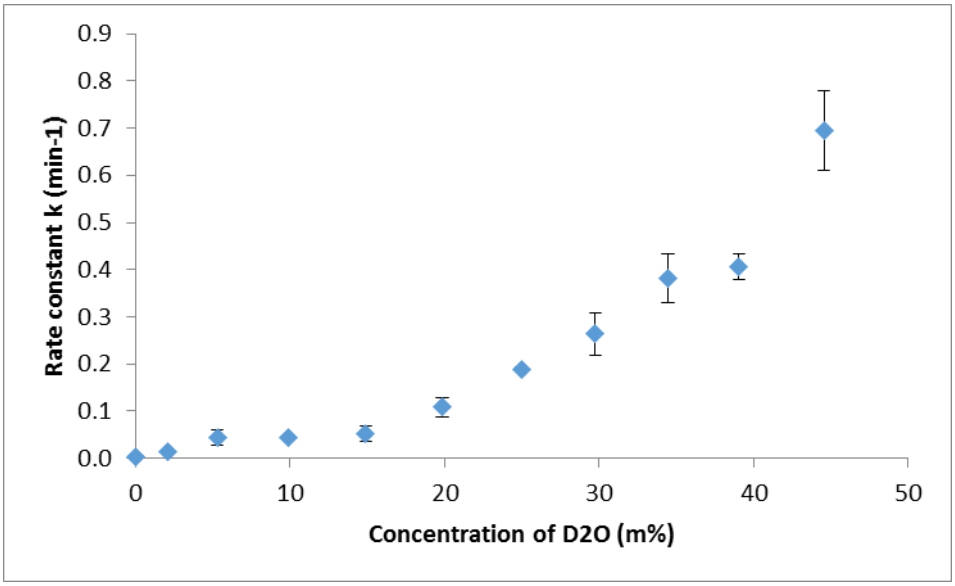

Figure 7.8: The graph for rate constant k against the concentration of D_2O for the dissociation of the DHA dimer in DMSO-*d6*

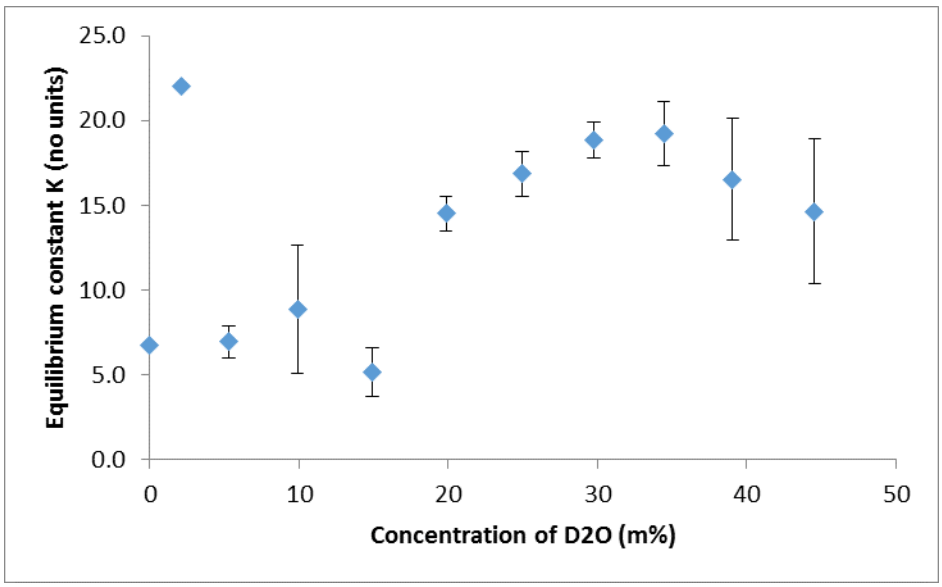

Figure 7.9: The graph for rate constant K against the concentration of D_2O for the dissociation of the DHA dimer in DMSO-*d6*

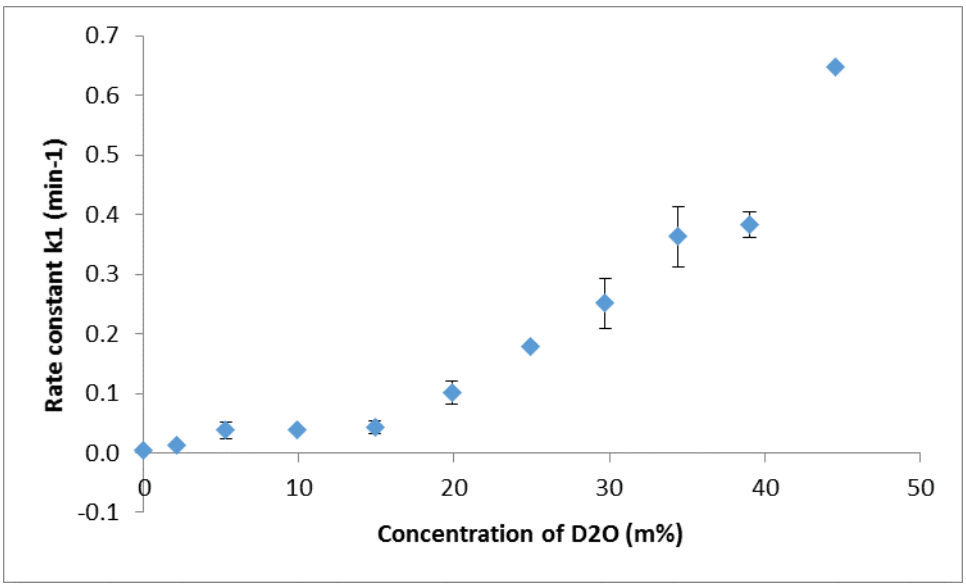

Figure 7.10: The graph for rate constant k_1 against the concentration of D_2O for the dissociation of the DHA dimer in DMSO-*d6*

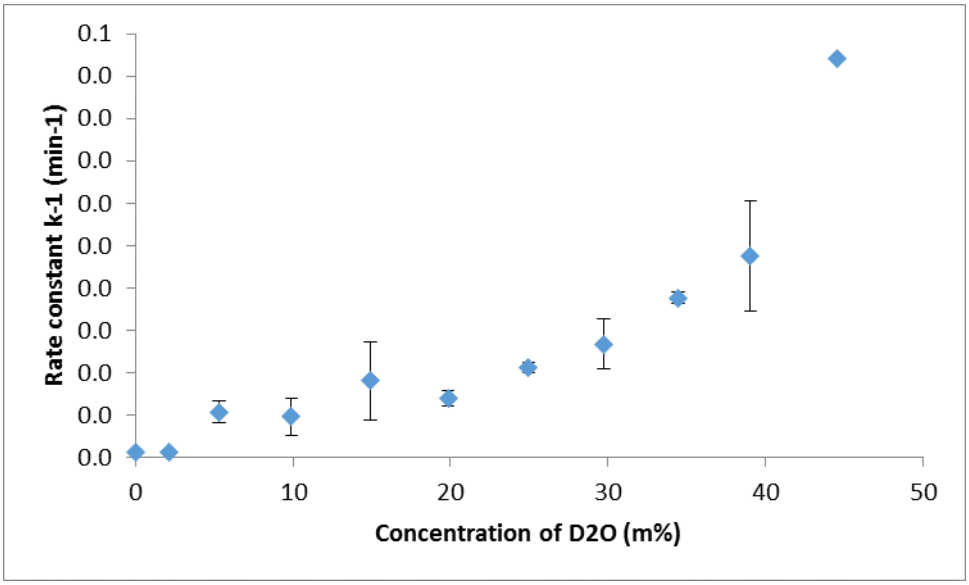

Figure 7.11: The graph for rate constant k_{-1} against the concentration of D_2O for the dissociation of the DHA dimer in DMSO-*d6*

Table 7.3: : The tabulated values for K and the three rate constants evaluated with the first order reversible rate expression

D_2O concentration (m%)	K (no units)	k (min^{-1})	k_1 (min^{-1})	k_{-1} (min^{-1})
0	7.56 ± 0.85	$3.31 \times 10^{-3} \pm 9.1 \times 10^{-4}$	$2.92 \times 10^{-3} \pm 7.6 \times 10^{-4}$	$3.96 \times 10^{-4} \pm 1.47 \times 10^{-4}$
2.1[m]	22.0	1.29×10^{-2}	1.23×10^{-2}	5.61×10^{-4}
5.3	6.94 ± 0.97	$4.34 \times 10^{-2} \pm 1.58 \times 10^{-2}$	$3.08 \times 10^{-2} \pm 1.44 \times 10^{-2}$	$5.38 \times 10^{-3} \pm 1.33 \times 10^{-3}$
9.9	8.86 ± 3.75	$4.37 \times 10^{-2} \pm 3.32 \times 10^{-3}$	$3.88 \times 10^{-2} \pm 1.1 \times 10^{-3}$	$4.84 \times 10^{-2} \pm 2.18 \times 10^{-3}$
14.9	5.14 ± 1.43	$5.24 \times 10^{-2} \pm 1.54 \times 10^{-2}$	$4.33 \times 10^{-2} \pm 1.08 \times 10^{-2}$	$9.07 \times 10^{-3} \pm 4.62 \times 10^{-2}$
19.9	14.5 ± 1.0	$1.08 \times 10^{-1} \pm 2.1 \times 10^{-2}$	$1.01 \times 10^{-1} \pm 2.0 \times 10^{-2}$	$6.94 \times 10^{-3} \pm 9.2 \times 10^{-4}$
25	16.9 ± 1.3	$1.89 \times 10^{-1} \pm 4 \times 10^{-3}$	$1.78 \times 10^{-1} \pm 5 \times 10^{-3}$	$1.06 \times 10^{-2} \pm 2 \times 10^{-4}$
29.8	18.9 ± 1.1	$2.64 \times 10^{-1} \pm 4.5 \times 10^{-2}$	$2.51 \times 10^{-1} \pm 4.2 \times 10^{-2}$	$1.34 \times 10^{-2} \pm 3.0 \times 10^{-3}$
34.5	19.2 ± 1.9	$3.82 \times 10^{-1} \pm 5.09 \times 10^{-2}$	$3.63 \times 10^{-1} \pm 5.0 \times 10^{-2}$	$1.88 \times 10^{-2} \pm 7 \times 10^{-4}$
39.0	16.5 ± 3.6	$4.06 \times 10^{-1} \pm 2.8 \times 10^{-2}$	$3.82 \times 10^{-1} \pm 2.2 \times 10^{-2}$	$2.38 \times 10^{-2} \pm 6.5 \times 10^{-3}$
44.6	14.6 ± 4.3	$6.96 \times 10^{-1} \pm 8.41 \times 10^{-2}$	$6.48 \times 10^{-1} \pm 6.6 \times 10^{-2}$	$4.70 \times 10^{-2} \pm 1.83 \times 10^{-2}$

[m] This reaction was not duplicated

7.2.3 Example calculation

Using the value for k obtained from the first order graph, Figure 7.5, and the equations…

$$K = \frac{[DHA_{monomer}]^2_{eq}}{[DHA_{dimer}]_{eq}}$$

$$k_{-1} = \frac{k_{exp}}{1 + K_{exp}}$$

$$k_1 = K_{exp}.k_{-1_{exp}}$$

derived in section 4.3.2, K, k_1 and k_2 were determined.

The values for $[DHA_{dimer}]_{eq}$ and $[DHA_{monomer}]_{eq}$ were obtained from the kinetic data to calculate K…

$$K = \frac{24.50^2}{5.631} = 106.6$$

$k_{}$ the experimental rate constant, was obtained from the slope in the graph for $\ln[[A]-[A]_\infty]$ against time, in Figure 7.5, to calculate k_{-1}…

$$k_{-1} = \frac{6.82 \times 10^{-2} min^{-1}}{1 + 106.6} = 6.34 \times 10^{-4} min^{-1}$$

This calculated value for k_{-1} was utilised to calculate k_1…

$$k_1 = 106.6 \times 6.34 \times 10^{-4} min^{-1} = 6.75 \times 10^{-2} min^{-1}$$

This method was used to determine the values for K and the rate constants associated with the ten replicate experiments that traced the D_2O catalysed reversible dissociation of the DHA dimer in DMSO-*d6*, Table 7.3.

7.2.4 Discussion

The graphs of k, k_1 (the forward rate constant) and k_{-1} (the reverse rate constant) against the concentration of D_2O in DMSO-*d6* illustrated a strong positive relationship between these rate constants and an increase in $[D_2O]$. When the $[D_2O]$ got higher than 45 m%, the reaction proceeded at too high a rate to obtain meaningful data. The observation that the rate of reaction increased with the addition of D_2O offered supporting evidence for the proposed mutarotation-like acid or base catalysed mechanisms, see sections 6.1 and 6.2, as D_2O, being amphoteric, would be able to donate a proton in one step and abstract a proton in another step. This capability of D_2O would be expected to produce an increase in

rate constant when added to the DMSO-d6/DHA dimer system where DMSO-*d6* can essentially only abstract a proton in the proposed reaction mechanism.

A lag phase was observed in the rate constant against [D_2O] graphs, Figure 7.8, Figure 7.9, Figure 7.10 and Figure 7.11 indicating that the D_2O was unavailable for catalysis at lower concentrations which is likely to be the result of the DMSO-*d6* solvent mopping up the D_2O with hydrogen bonding until a critical D_2O concentration of ~15 mass% was reached. At this stage in the proposed process, the DMSO-*d6* would have achieved D_2O saturation, resulting in any further D_2O added to the system being readily available to catalyse the DHA dimer dissociation in DMSO-*d6.*

The graph for K against [D_2O] displays a positive relationship with an increase in K as [D_2O] is increased. This would indicate that D_2O is not behaving strictly as a catalyst. If the D_2O was behaving as a pure catalyst, the value for K would remain constant across all concentrations.

7.3 The DHA dimer dissociation in DMSO-*d6* catalysed with CD_3COOD

7.3.1 Introduction

A series of experiments were performed to determine the kinetics for the acetic acid-*d4* (CD_3COOD) catalysed dissociation of the DHA dimer in DMSO-*d6* by incrementally increasing the concentration of CD_3COOD whilst maintaining a constant concentration of DHA dimer. The kinetic data was evaluated using the first order reversible reaction rate expression as all experiments contained large values for K and displayed first order kinetics therefore rendering use of the second order reversible reaction rate expression unnecessary, see section 5.3.

The concentration of CD_3COOD was represented as a molar percentage (mol%) to give an intuitive appreciation for the relative amount of acid molecules present in the DMSO-*d6*. The concentration term mol L^{-1} could not be used as two liquids were being combined to give an ambiguous final volume.

The pKa value for CH_3COOH in DMSO is 12.3[50,52,83] which is a relatively large value when compared to the pKa value of 4.45[52,83] for CH_3COOH in H_2O. This represents an acid dissociation constant for CH_3COOH in DMSO that is eight orders of magnitude lower than the acid dissociation constant for CH_3COOH in H_2O. CD_3COOD's ability to donate a proton is greatly reduced in the DMSO-*d6* reaction conditions.

Two intermediate species (Int#1 and Int#2) were identified in this series of kinetic experiments by the appearance of their associated ^{1}H signals, Figure 7.12, and ^{13}C signals, Figure 7.18, in the NMR spectra and by the behaviour of these signals when graphed as concentration against time, Figure 7.13. The two intermediates evolved at different rates which allowed for differentiation between the two species and provided an extra tool in their proposed characterisation, in addition to 1D and 2D NMR spectroscopy.

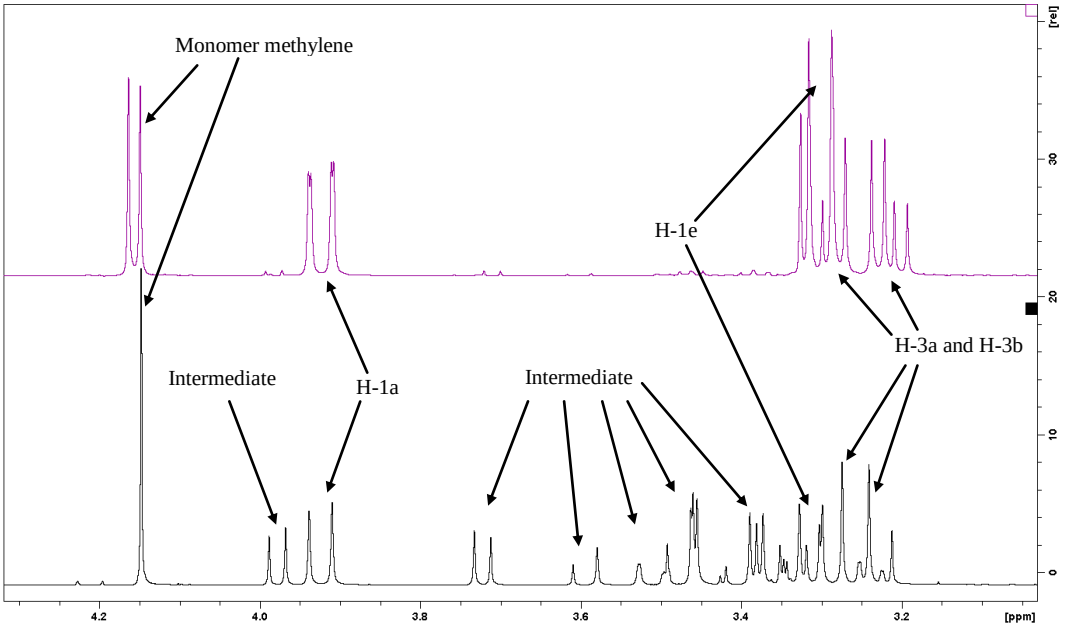

Figure 7.12: The 1H NMR spectra of a mixture of DHA monomer and dimer (top) and a mixture of dimer, monomer and the 2 intermediates (bottom)

To offer further evidence for the proposed acid catalysed mutarotation-like mechanism for the dissociation of the DHA dimer in solution, see section 1.9.1, sodium hydroxide was employed to ionise a portion of the CD_3COOD to form the CD_3COO^- anion. The proposed reaction mechanism predicts that an increase in anion available to abstract the axial hydroxyl proton would result in an increased rate constant. As CD_3COOD can only donate a proton (deuterium) the available anion able to abstract the hydroxyl proton becomes the limiting agent in the reaction. For CD_3COOD to be behaving as a pure catalyst, with the absence of any hidden variables, a constant value of K would be expected across the concentration range.

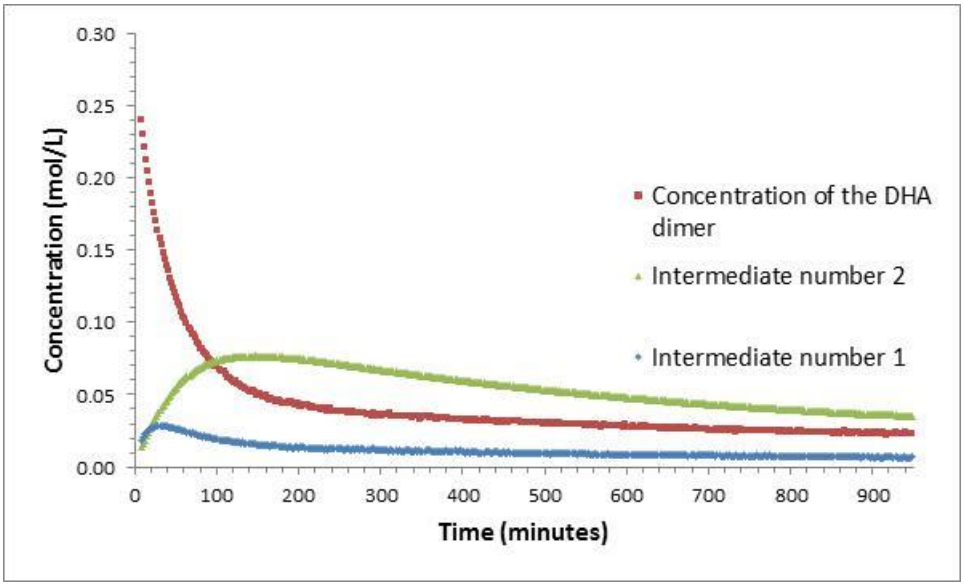

Figure 7.13: Graph of concentration vs time with the 2 intermediate species.

7.3.2 Identification of the two reaction intermediates

1D and 2D ^{1}H NMR and ^{13}C NMR techniques, predictive computational ^{13}C NMR spectra and rate constant comparison provided partial characterisation as evidence for the proposed structures of the two intermediate species.

7.3.2.1 ^{1}H NMR assignment

The previously assigned DHA dimer signals were eliminated from the list signals to be investigated. The DHA dimer H-3_a and H-3_b signals in the multiplet had reduced multiplicity as their associated protons no longer coupled to the C-3-O<u>H</u> as that proton was engaged in exchange with the CD_3COOD.

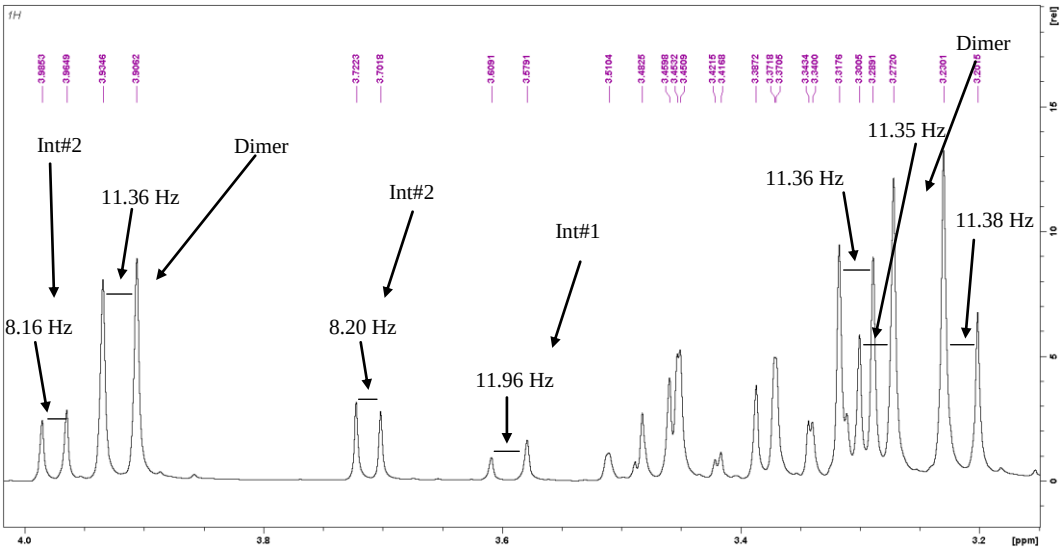

Figure 7.14: The ^{1}H NMR spectrum containing a mixture of the DHA dimer and the 2 intermediates

The doublet at 3.59 ppm had a coupling constant of 11.96 Hz which was characteristic of a geminal diastereotopic proton in a 1,3-dioxane ring[84] and closely matching the coupling constants for the geminal diastereotopic protons in the DHA dimer (11.36 Hz) . The signal emanating from this proton's geminal partner is likely to be hidden amongst the signals in the multiplet, ranging from 3.55 ppm to 3.20 ppm, as is the case for one of the geminal ring proton signals in the DHA dimer. The rate constant associated with this doublet at 3.59 ppm was 3.85 x 10^{-2} min^{-1} at 18 mol% of CD_3COOD, Figure 7.15, and was arbitrarily assigned as intermediate 1 (Int#1), the faster evolving intermediate.

The doublet signals at 3.98 and 3.71 ppm with coupling constants 8.16 Hz and 8.20 Hz respectively appeared to emanate from the same intermediate species due to these closely matching coupling constants. These two signals had very similar rate constants ([CD_3COOD] = 18 mol%) of 2.12 x 10^{-2}, Figure 7.16, and 2.10 x 10^{-2} min^{-1}, Figure 7.17, respectively which is further evidence that these two signals were emanating from the same intermediate species and were thus arbitrarily assigned as intermediate (Int#2). The roofing effect (slanting) that can be observed with this pair of doublets is a strong indicator that these signals emanate from diastereotopic protons although their relatively low coupling constant of 8.18 Hz is not within the usual range (10 – 14 ppm) expected for diastereotopic protons.

The region from 3.55 to 3.20 ppm contained signals engaged in overlap which rendered their associated rate constants unreliable.

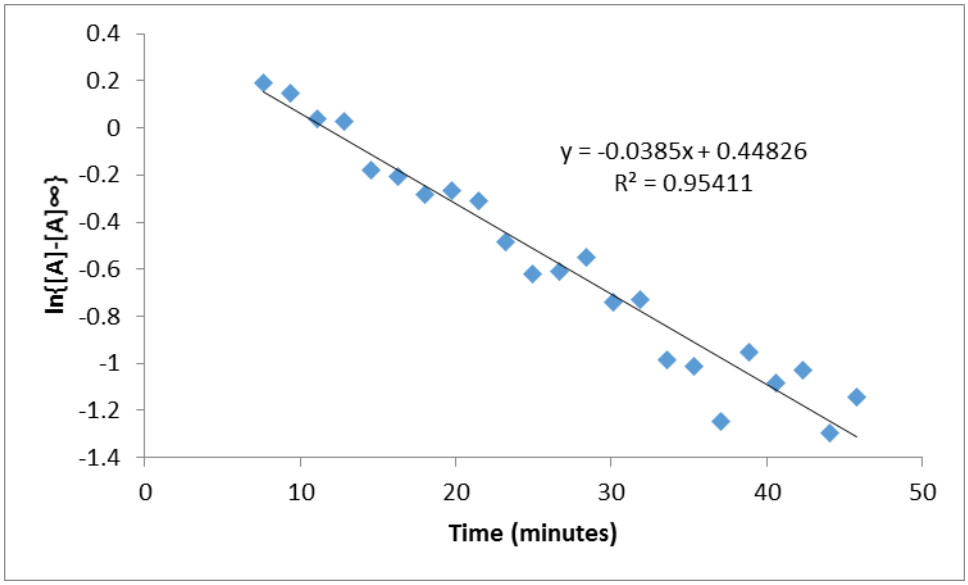

Figure 7.15: The first order graph for Int #1 participating in the dissociation of the DHA dimer in DMSO-d6 catalysed with 18 mass% CD3COOD.

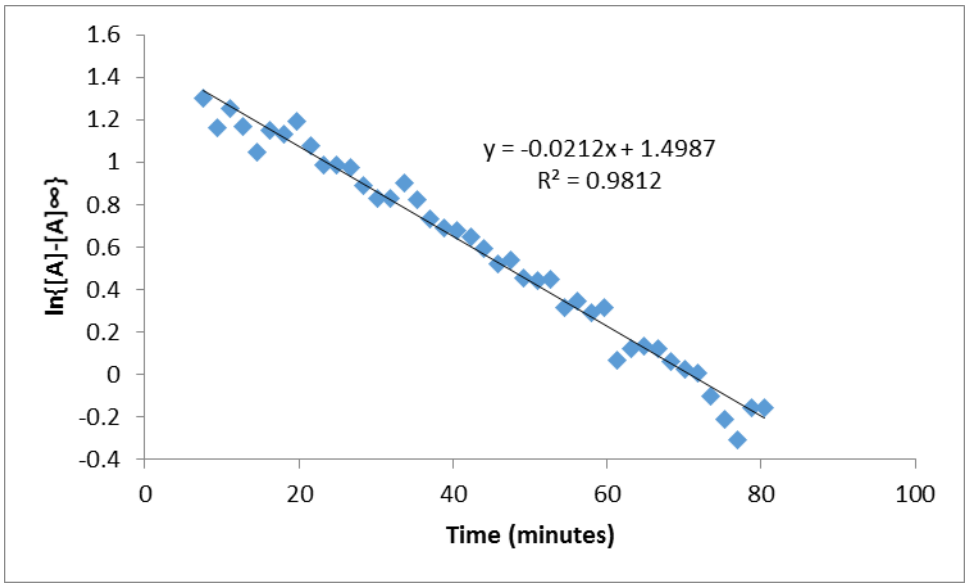

Figure 7.16: The first order graph for Int #2 participating in the dissociation of the DHA dimer in DMSO-d6 catalysed with 18 mass% CD_3COOD.

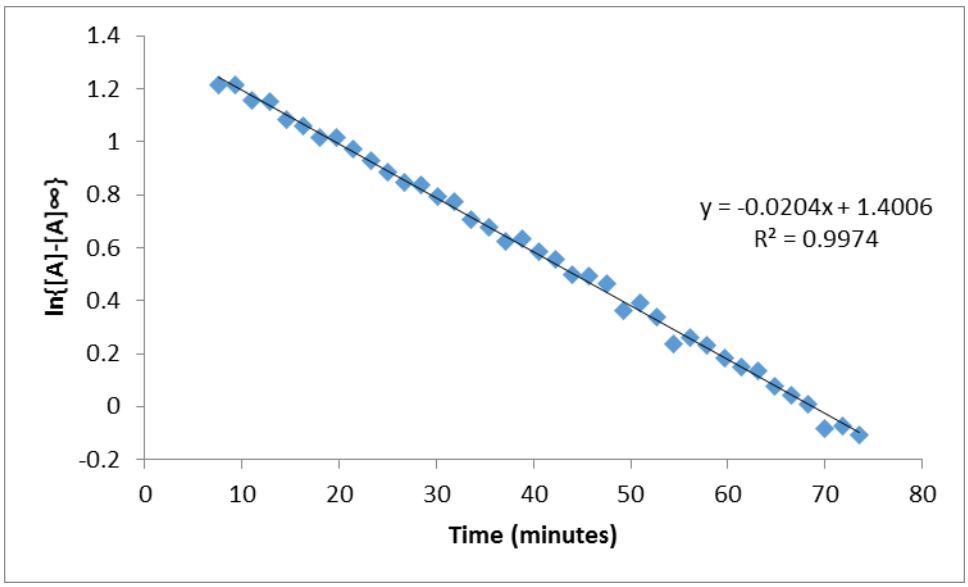

Figure 7.17: The first order graph for Int #2 participating in the dissociation of the DHA dimer in DMSO-d6 catalysed with 18 mass% CD3COOD.

7.3.2.2 ^{13}C NMR

^{13}C NMR experiments were performed to further assist in the identification of the two reaction intermediates. The ^{13}C NMR spectra, Figure 7.18 and Figure 7.19, showed nine signals that were unaccounted for, after the solvent and DHA dimer and monomer signals were eliminated and were therefore assumed to emanate from the two intermediate species. Nine signals provided two possible scenarios:

1. Three intermediates species were present and they all contained symmetry resulting in each intermediate species giving rise to three signals.
2. Two intermediates species were present with one intermediate containing symmetry to give rise to three signals and the other intermediate without symmetry giving rise to six signals.

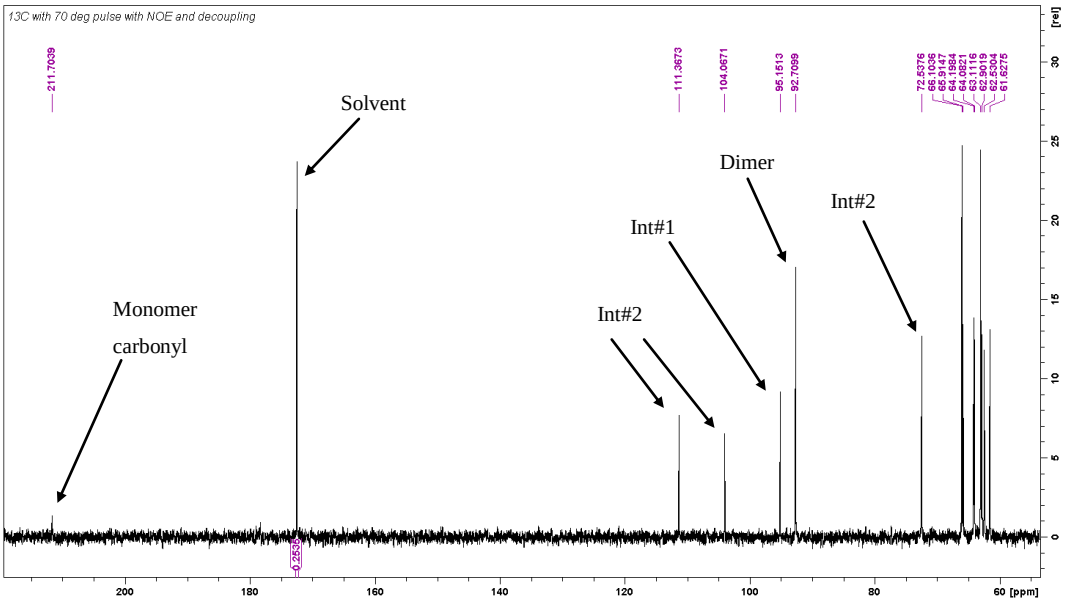

Figure 7.18: The full 13C NMR spectrum of the DHA dimer, the DHA monomer, Int#1 and Int#2 in DMSO-d6

^{13}C NMR kinetic experiments were performed on the dissociation of the DHA dimer in DMSO-*d6* catalysed with CD_3COOD (18 mol%) to help differentiate between the two intermediate signals by comparison of the rate constants associated with each signal. This data was further supported by a viewing of a sped up movie containing an ordered spectral set of images from experiments that were obtained once every five minutes. This method was employed because ^{13}C NMR spectra, obtained in the time frame required by the kinetic experiment, had an excessive amount of scatter resulting from a noisy baseline and thus rendered the kinetic data unreliable in some instances. By observing a movie of the ordered spectral set, the intermediate signals that were observed to rise and fall in unison could be denoted as signals emanating from the same intermediate species even though the base line contained too much noise for the integration/rate constant method to be effective.

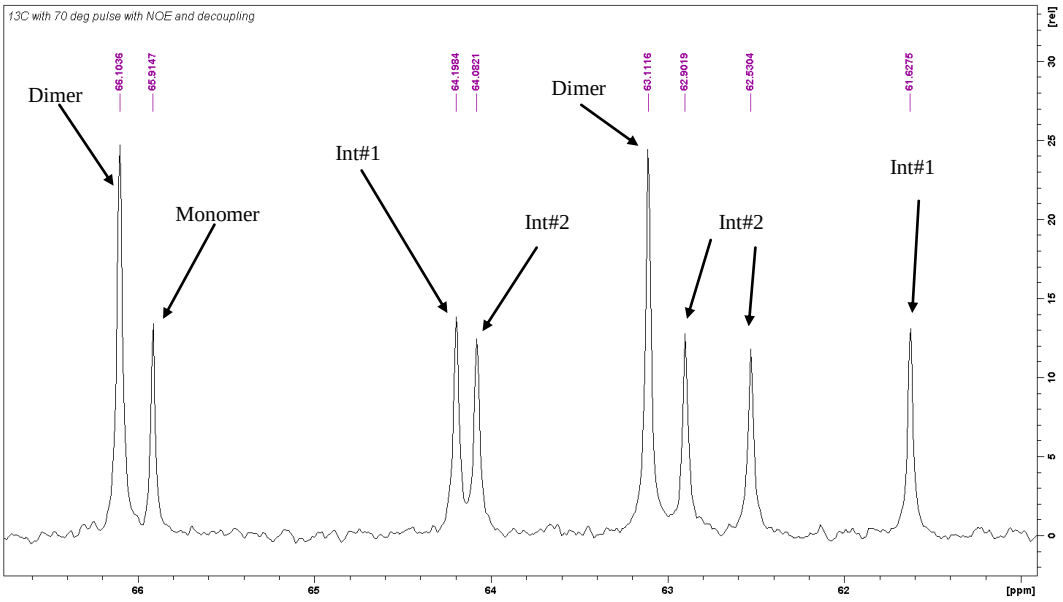

Figure 7.19: The enlarged ^{13}C NMR spectrum with the signals for the DHA dimer, the DHA monomer, Int#1 and Int#2

The rate constant data for Int#1, Table 7.4, was very scattered as this species evolved relatively quickly and was never present at large concentrations, therefore the absolute values could not be trusted although the relative values associated with the signals at 95.1 ppm and 64.2 ppm strongly indicated that these signals arose from the same species. These signals were observed to move in unison in a movie of the ordered spectral set thus supporting the assertion that these two ^{13}C signals emanated from the same species, Int#1.

The rate constant data for Int#2 was relatively unscattered with R^2 values ranging from 92 to 96. The average rate constant for Int#2 (1.82×10^{-2} min-1) matched closely to the rate constant value (1.98×10^{-2} min-1) obtained in the ^{1}H NMR experiments for the formation of Int#2 at the same concentration of CD_3COOD (18 mol%). This information connected the Int#2 ^{13}C signals to the Int#2 ^{1}H signals. Assignment of the Int#2 ^{13}C signals was achieved by comparison of rate constants and verified by observation of the spectra image movie. The intermediate signals at 64.2 ppm and 64.1 ppm overlapped and therefore no kinetic data could be obtained from these two signals. Therefore, to differentiate between these signals, observation of the spectral images moving in time was required resulting with the signal at 64.2 ppm being assigned to Int#1, as this signal was observed to move in unison with the signal at 61.6 ppm, and the signal at 64.1 ppm being assigned to Int#2 as it was observed to move in unison with the signals at 62.9 and 62.5 ppm.

Table 7.4: The ^{13}C NMR signals, rate constants and assignments of intermediates based on comparison of rate constants

Signal (ppm)	Rate constant (min-1)	Assignment
111.4	2.11×10^{-2}	Int#2
104.1	1.40×10^{-2}	Int#2
95.1	6.04×10^{-2}	Int#1
72.5	2.00×10^{-2}	Int#2
64.2	-	Int#1[n]
64.1	-	Int#2[o]
62.9	1.69×10^{-2}	Int#2
62.5	1.94×10^{-2}	Int#2
61.6	5.92×10^{-2}	Int#1

7.3.2.3 DEPT135

The full DEPT135 spectrum, Figure 7.20, indicates that the Int#2 signals at 111.4 and 104.1 ppm as well as the Int#1 signal at 92.7 ppm are associated with quaternary carbons while the Int#2 signal at 72.5 ppm is associated with a methylene carbon.

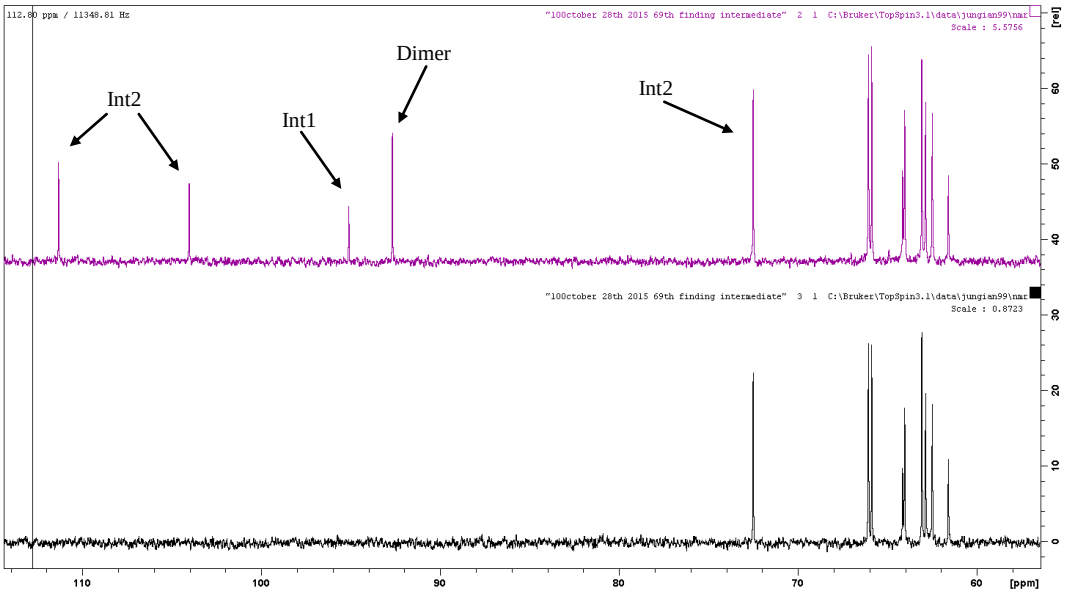

Figure 7.20: The full DEPT135 containing the DHA dimer and monomer and the 2 intermediated signals (bottom) stacked with the standard ^{13}C NMR spectrum (top)

[n] Assigned using observation of the ordered spectral set moving in time
[o] Assigned using observation of the ordered spectral set moving in time

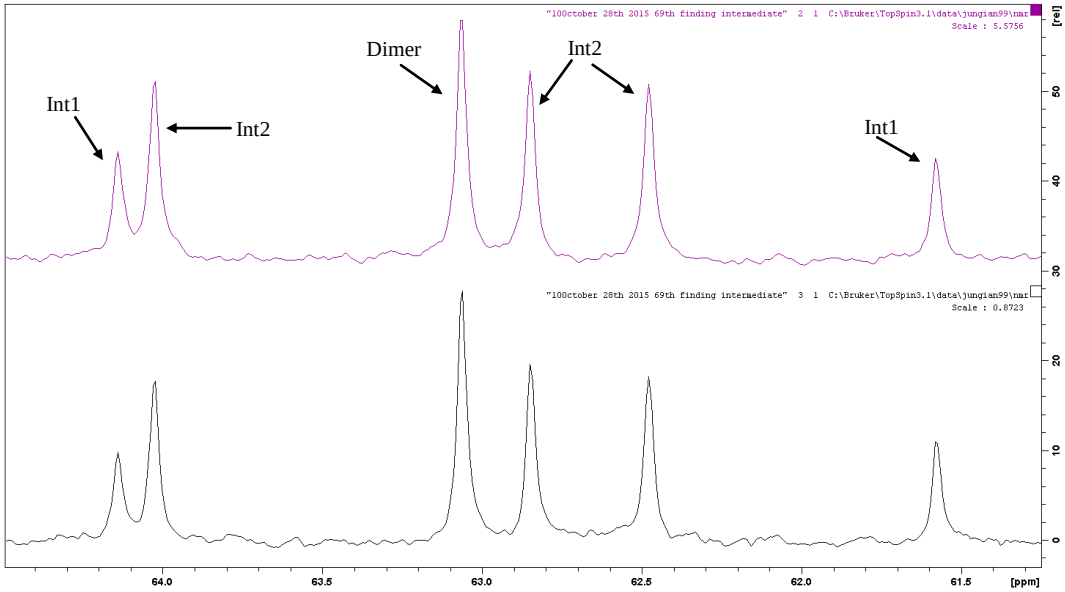

Figure 7.21: The expanded DEPT135 spectrum containing the DHA dimer and the 2 intermediated signals (bottom) stacked with the standard ^{13}C NMR spectrum (top)

The expanded DEPT135 spectrum, Figure 7.21, indicates that the Int#1 signals at 64.2 and 61.6 ppm and the Int#2 signals at 64.1, 62.9 and 62.5 ppm are all associated with methylene carbons as the dimer peak is known to emanate from a methylene carbon and the Int#1 and Int#2 peaks are present with the same phasing as the DHA dimer methylene peak.

7.3.2.4 HSQC

The HSQC spectrum, Figure 7.22, verified the results obtained from the DEPT135 spectrum that the Int#2 ^{13}C signals at 111.4 and 104.1 ppm and the Int#1 ^{13}C signal at 92.7 ppm were associated with quaternary carbons as they did not show coherence with any ^{1}H signals in the HSQC spectrum.

Figure 7.22 shows the methylene Int#2 carbon signal at 72.5 ppm has correlations with the Int#2 proton signals at 3.97 (^{2}J 8.16 Hz) and 3.71 ppm (^{2}J 8.16 Hz), indicating that these proton signals emanated from geminal diastereotopic methylene protons on a six membered ring[84] thus strongly indicating that Int#2 contains a six membered ring, though the ^{2}J. This result served to confirm the earlier suggestion that these signals emanated from the same intermediate species.

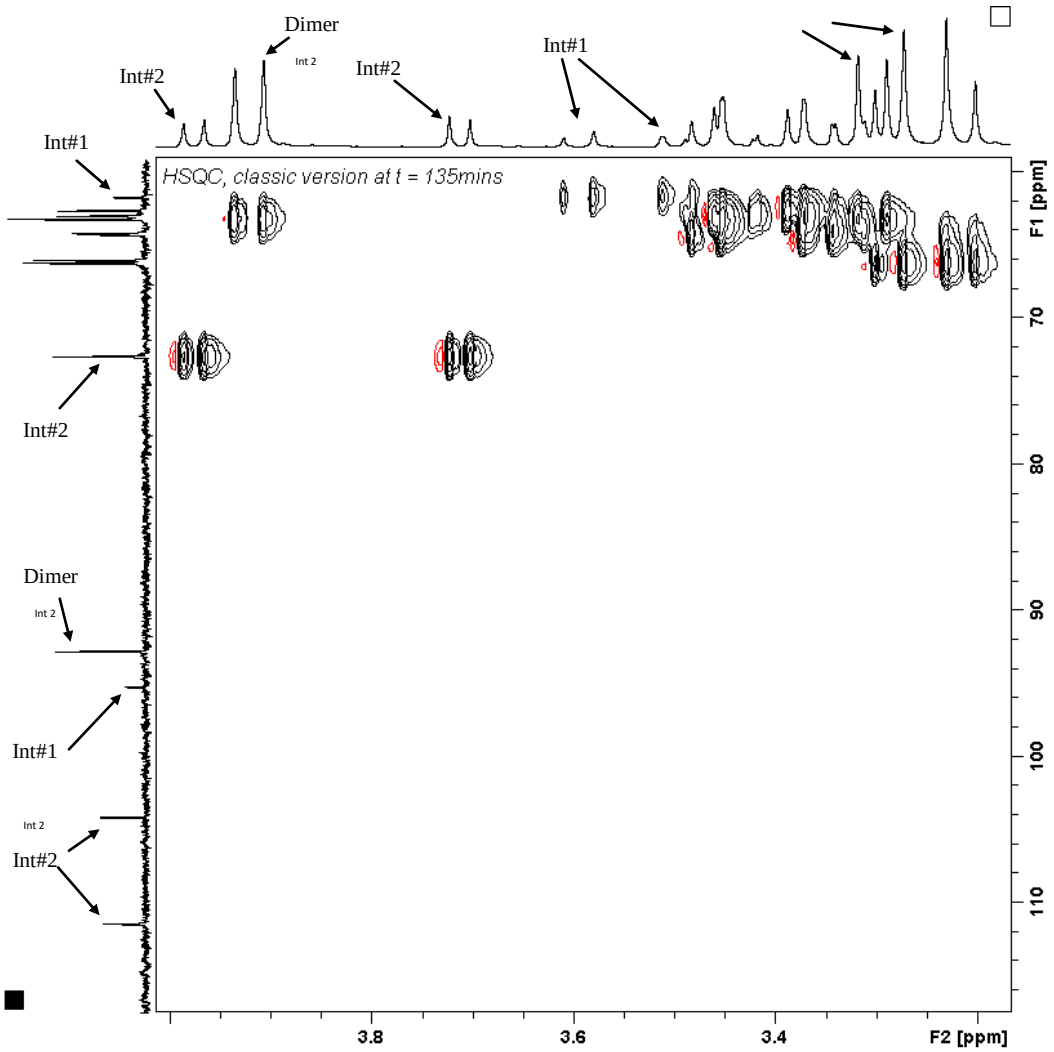

Figure 7.22: The HSQC spectrum containing signals for the DHA dimer, the DHA monomer and Int#1 and Int#2

The methylene Int#2 ^{13}C signal at 64.1 ppm had correlations with ^{1}H signals at 3.48 and 3.34 ppm in the region where there was a lot of signal overlap which resulted in coupling constants and multiplicity being unattainable. The methylene Int#2 ^{13}C signal at 62.5 had correlations with the ^{1}H signal at 3.39 ppm and the methylene Int#2 ^{13}C signal at 62.9 had correlations with the ^{1}H signal at 3.46 ppm. The ^{1}H correlations for both of these ^{13}C Int#2 signals were in the signal region with a lot of signal overlap so that it was not possible to obtain the ^{1}H coupling constants or multiplicity.

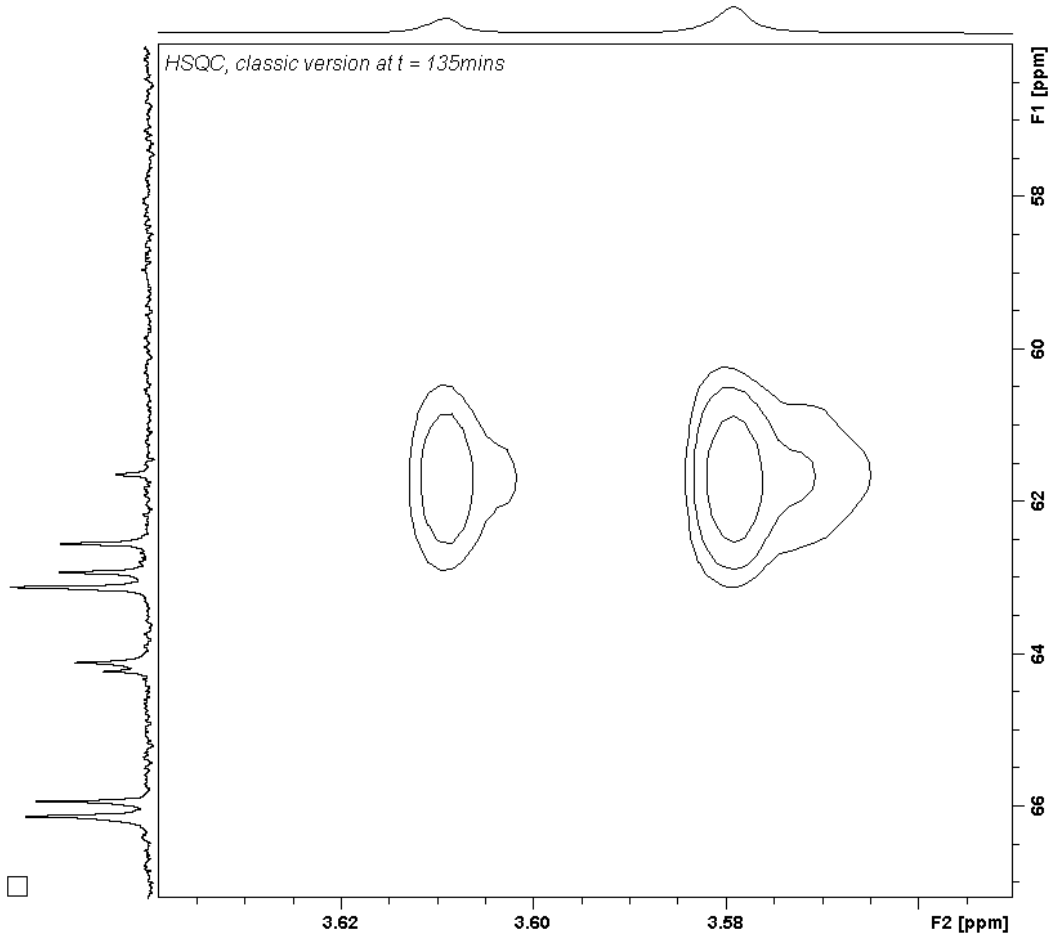

Figure 7.23: The HSQC spectrum showing correlations between Int#1 signals at 61.6 ppm and 3.70 ppm

Figure 7.22 and Figure 7.23 show correlations between the Int#1 carbon signal at 61.6 ppm and the two Int#1 proton doublets at 3.60 and 3.48 ppm with an associated coupling constant of ~11.96 Hz. This characteristic coupling constant[57] indicated that two diastereotopic methylene protons were in a 1,3-dioxane ring or at least an environment with restricted rotation. The Int#1 ^{13}C signal at 64.2 ppm had a correlation with the ^{1}H signal at 3.47 ppm in the region where there is a lot of signal overlap thus rendering multiplicity and coupling constants unobtainable. The results obtained using HSQC served to confirm the earlier suggestion that ^{1}H and ^{13}C NMR signals emanated from the same intermediate species with no conflicting results

7.3.2.5 The proposed intermediate structures

The ^{13}C assignments indicated that Int#1 contained three carbon signals and therefore contained symmetry similar to the DHA dimer. Int#1 and the DHA dimer had very similar ^{13}C chemical shifts, Table 7.5, implying that Int#1, like the DHA dimer, contains a 1,3-dioxane ring with hydroxymethyl group substituents. It was therefore proposed on these grounds that Int#1 was the DHA dimer involved in dynamic intermolecular interactions with the solvent and/or CD_3COOD, Figure 7.24, resulting in a subtle alteration of chemical shifts but maintaining symmetry.

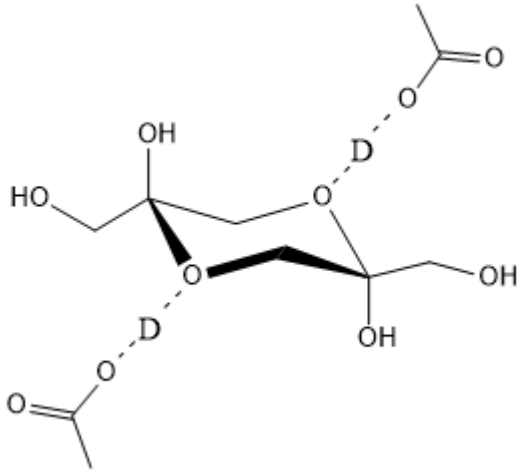

Figure 7.24: The proposed Int#1 species engaging in rapid proton exchange with undissociated CD_3COOD

Table 7.5: The DHA dimer and Int#1 ^{13}C signal comparison with multiplicity obtained in DMSO-d6 with CD_3COOD

DHA dimer ^{13}C signals	Int#1 ^{13}C signals	Multiplicity (see DEPT135)
92.8	95.2	Quaternary
66.3	64.2	Methylene
63.2	61.6	Methylene

The ^{13}C assignments for Int#2, Table 7.4, contained six carbon signals and therefore Int#2 had lost symmetry. The methylene carbon chemical shifts are still relatively close to those expected in a 1,3-dioxane ring in the literature[84], and indeed close to those found in the DHA dimer. The quaternary carbon chemical shifts have moved downfield by 16.2 and 8.9 ppm but still fall within/close to the range of 90-105 ppm expected for anomeric carbons.[71]

The possibility of Int#2 being the DHA acyclic intermediate species was investigated but quickly dispelled as all ^{13}C signals are accounted for with no ^{13}C signal downfield in the ketone range, 220-189 ppm.[84] This signal would be expected if this species was the opened 1,3-dioxane ring.

It was therefore proposed that Int#2 was the protonated cyclic DHA dimer that had lost symmetry and undergone alterations to its ^{13}C chemical shifts resulting from protonation occurring on only one of the ring oxygens, Figure 7.25.

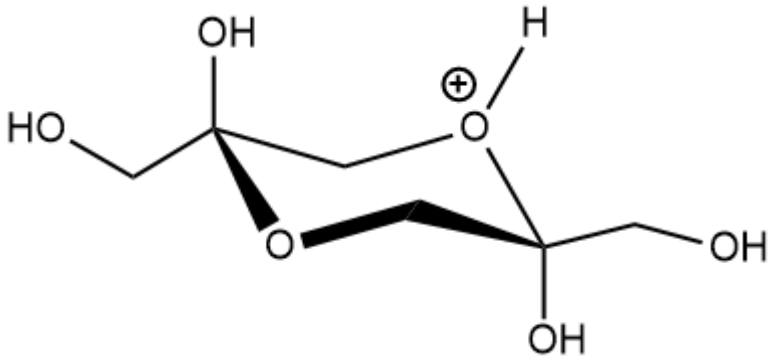

Figure 7.25: The proposed cationic cyclic Int#2 species

7.3.2.5.1 Computational ^{13}C NMR to investigate Int#2 protonation

Computational ^{13}C NMR data for the predicted spectra of the DHA dimer and the protonated DHA dimer were provided by Annesofie Jenson.[85] This data was obtained to investigate the possible ^{13}C chemical shift changes one may observe when the ring oxygen of the DHA dimer is protonated.

There was a difference in the predicted values and the experimentally obtained values for the DHA dimer with all ^{13}C spectra of the predicted chemical shifts being further downfield than the experimentally determined chemical shifts by approximately the same amount, 9.3 ±0.9 ppm, Table 7.6. This discrepancy was possibly a result of the predicted chemical shifts being obtained in the gas phase and thus not taking into account the solvation effects of DMSO-*d6*, which may be substantial as DMSO is a known hydrogen bond acceptor in systems containing hydroxyl groups.[49,84] Although there is a difference in the absolute chemical shift values between the predicted spectra and experimental spectra, both data sets are qualitatively similar with respect to the shifts relative to the carbon positions and therefore provide a valid comparison for the effects of the protonation of the DHA dimer.

Table 7.6: The predicted and experimental ^{13}C NMR chemical shifts for the DHA dimer with predicted shifts appearing downfield from experimental shifts

Atom	Predicted shifts (ppm)	Experimental shifts (ppm)	Difference
C-2	102.6	92.8	9.8
C-3	76.1	66.3	9.8
C-1	71.5	63.2	8.3

Table 7.7: The predicted and experimental ^{13}C NMR chemical shifts for the protonated DHA dimer with predicted shifts appearing downfield from experimental shifts[p]

Atom	Predicted shifts (ppm)	Experimental shifts (ppm)	Difference
C_2	110.9	111.4	-0.5
C_5	105.1	104.1	1.0
C_4	78.0	72.5	5.5
C_3	74.5	62.9	11.6
C_6	73.8	62.5	11.3
C_1	71.1	64.1	7.0

The change in chemical shifts on protonation of the DHA dimer predicated shifts are qualitatively similar to the change in chemical shifts obtained experimentally for Int#2, Figure 7.26 and Table 7.7, with the hemiketal carbon adjacent to the protonated ring oxygen engaging in a large shift downfield as a result of deshielding from the positively charged oxygen drawing electron density away from the neighbouring nuclei. Similar relative shifts for all nuclei were observed depending on their distance from the protonated ring oxygen.

[p] See carbon labelling in Figure 7.26

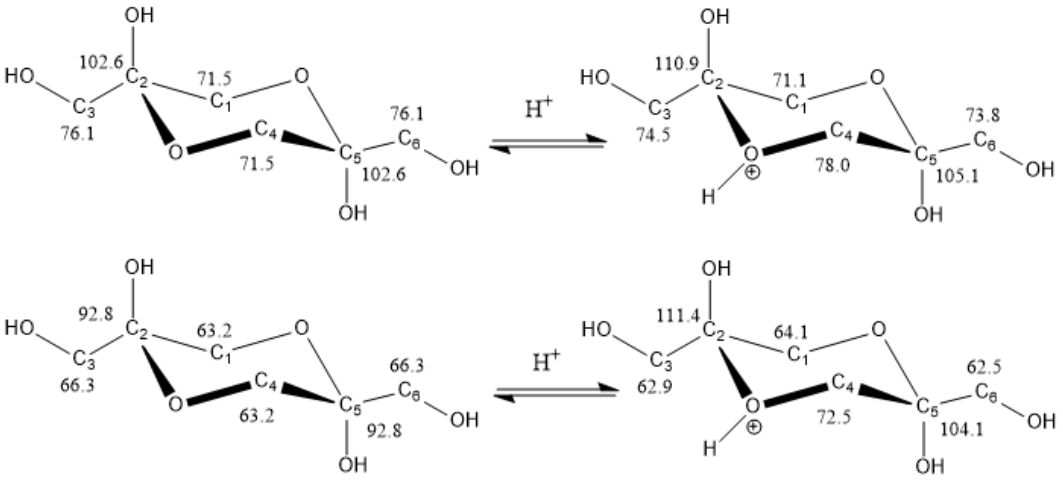

Figure 7.26: The 13C chemical shifts of labelled carbons for the protonation of the DHA dimer with predicted shifts (top) and the experimental shifts (bottom) for the proposed protonation of the DHA dimer

The spectra changes predicted by computational ^{13}C NMR for the protonation of the DHA dimer were qualitatively the same ^{13}C NMR spectra changes observed experimentally between the DHA dimer starting material and Int#2. This observation offered support to the proposal that Int#2 was the protonated DHA dimer.

7.3.3 Results

7.3.3.1 The DHA dimer dissociation in DMSO-*d6* catalysed with CD_3COOD

The doublet signal identified as emanating from the DHA dimer (3.92 ppm) was traced using ^1H NMR spectroscopy to determine the equilibrium constant K and the rate constants, k, k_1 and k_{-1} for the dissociation of the DHA dimer in DMSO-*d6* catalysed by CD_3COOD. An increase in rate constants with an associated increase in [CD_3COOD] would support the proposed acid-catalysed reaction mechanism for the DHA dimer dissociation as the amount of available protons able to engage in proton exchange with the DHA dimer ring would increase.

7.3.3.1.1 Reaction order determination

The zeroth, first and second order graphs, using the first 80 % of data to approximate three half-lives, were obtained for all the experiments to determine the order of the reaction.

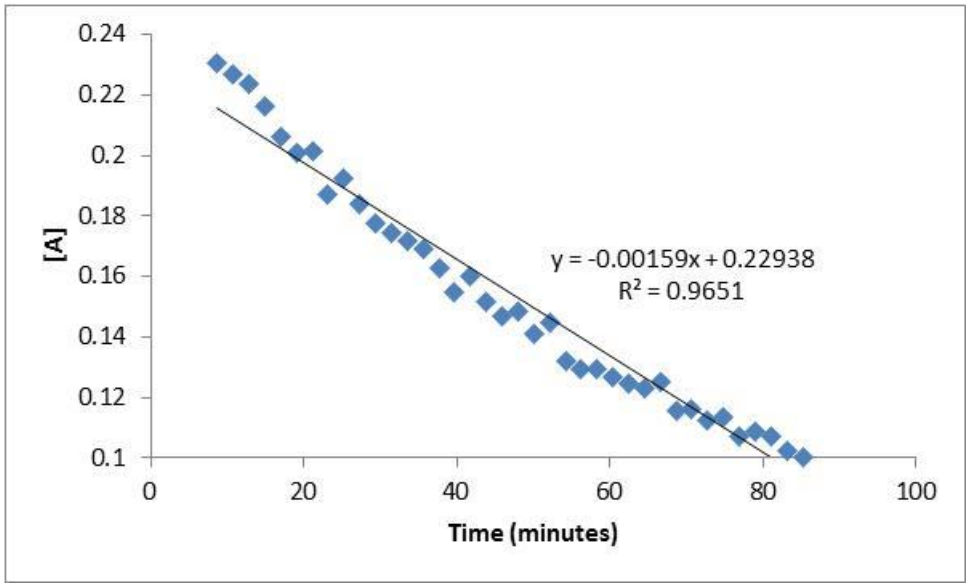

Figure 7.27: The zeroth order graph for the dissociation of the DHA dimer in DMSO-d6 catalysed with CD_3COOD

The zeroth order graphs were all curved, Figure 7.27, thus indicating that zeroth order kinetics were not operating in the dissociation of the DHA dimer in this system.

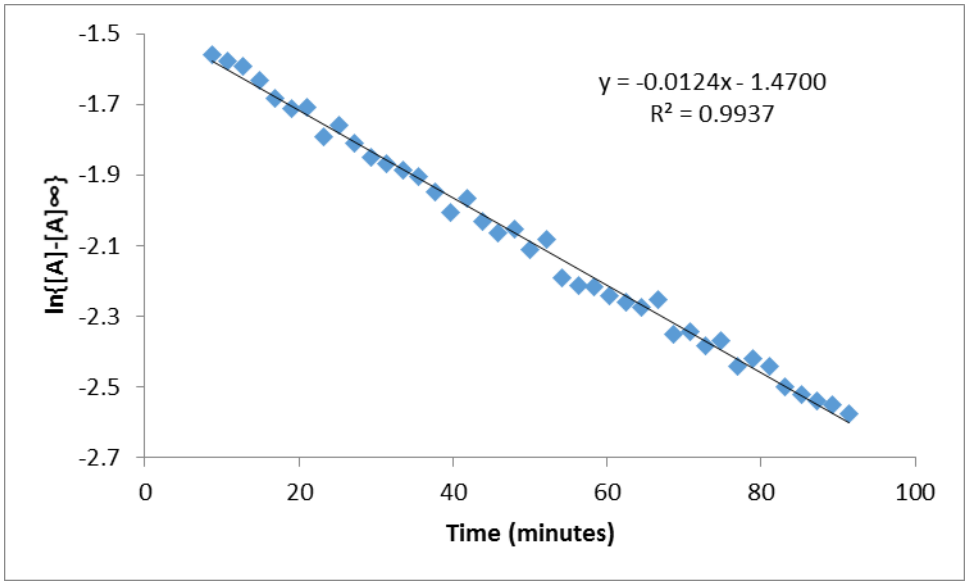

Figure 7.28: The first order graph for the dissociation of the DHA dimer in DMSO-*d6* catalysed with CD_3COOD

The first-order plots produced straight lines with strong R^2 values, Figure 7.28, This indicated that first order kinetics were operating for the CD_3COOD catalysed dissociation of the DHA dimer in DMSO-*d6*.

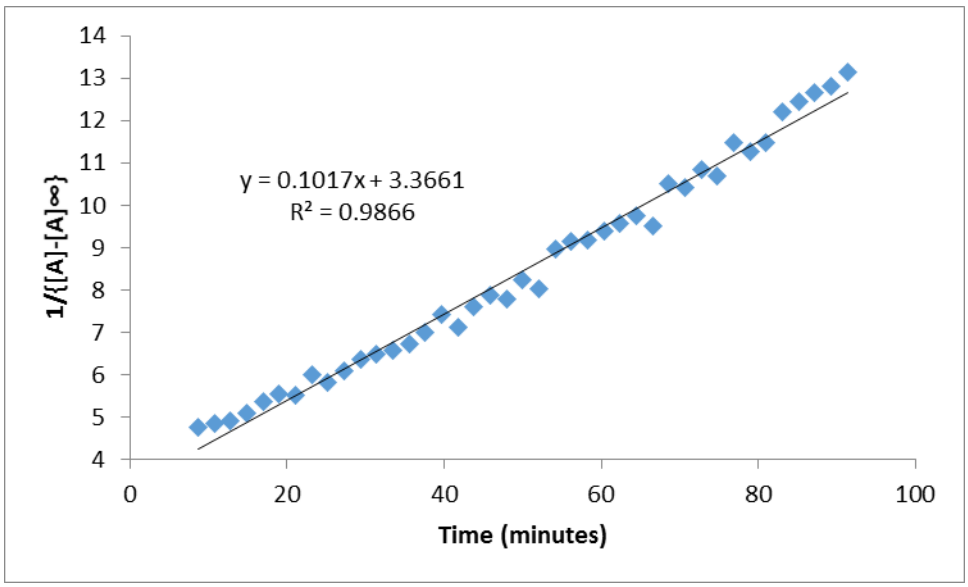

Figure 7.29: The second order graph for the dissociation of the DHA dimer in DMSO-*d6* catalysed with CD_3COOD

The standard second-order graphs were all curved, Figure 7.29, thus indicating that second order kinetics were not operating in the dissociation of the DHA dimer in this system

7.3.3.1.2 Effects of increasing CD_3COOD concentration on the DHA dimer dissociation[q]

The values for K and the rate constants for [CD_3COOD] = 0 were obtained from the results for the uncatalysed DHA dimer dissociation in section 7.1.2. Six duplicated experiments were performed that incrementally increased the concentration of CD_3COOD to determine if CD_3COOD catalysed the dissociation reaction of the DHA dimer in DMSO-*d6* as predicted by the proposed reaction mechanism.

The results in

Table 7.8 were graphed as rate constant against concentration, Figure 7.30, Figure 7.31, Figure 7.32 and Figure 7.33 to demonstrate the effect on the rate constant as the concentration of CD_3COOD was increased.

[q] The completed set of first order graphs for the CD_3COOD catalysed dissociation reaction are contained in the appendix: A28 – A37

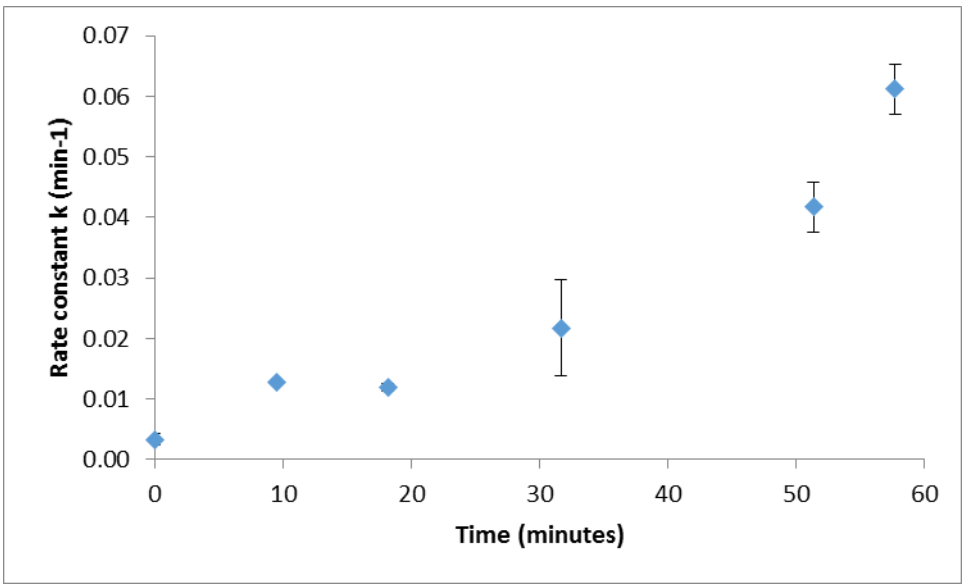

Figure 7.30: The graph for rate constant k against concentration of CD_3COOD for the DHA dimer dissociation in DMSO-*d6*

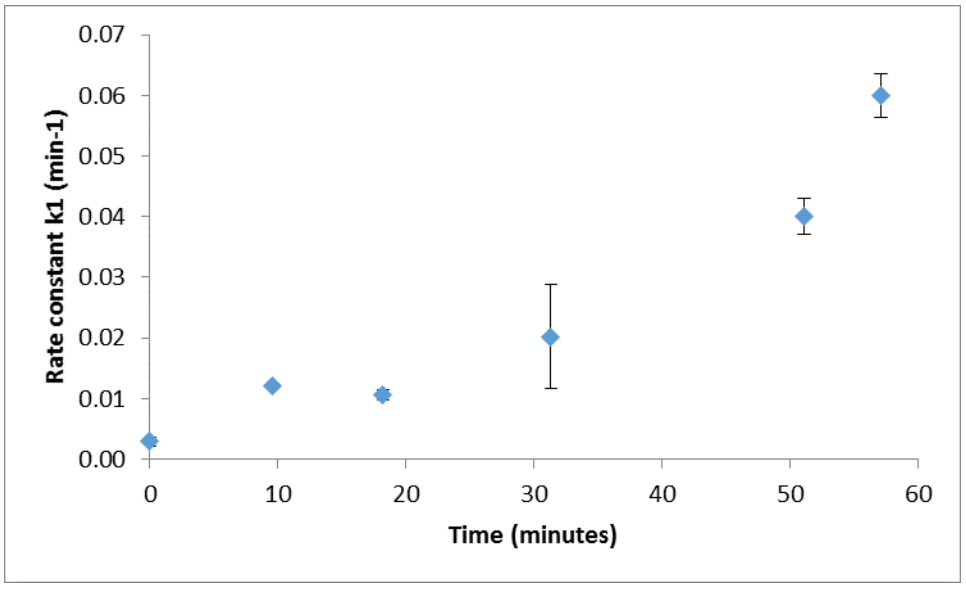

Figure 7.31: The graph for rate constant k_1 against concentration of CD_3COOD for the DHA dimer dissociation in DMSO-$_{d6}$

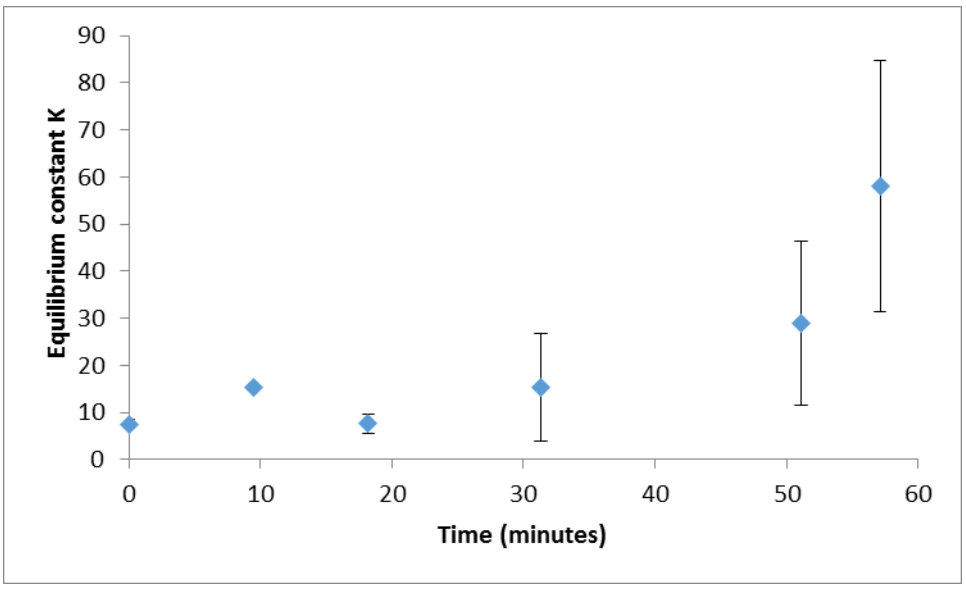

Figure 7.32: The graph for rate constant K against concentration of CD_3COOD for the DHA dimer dissociation in DMSO-*d6*

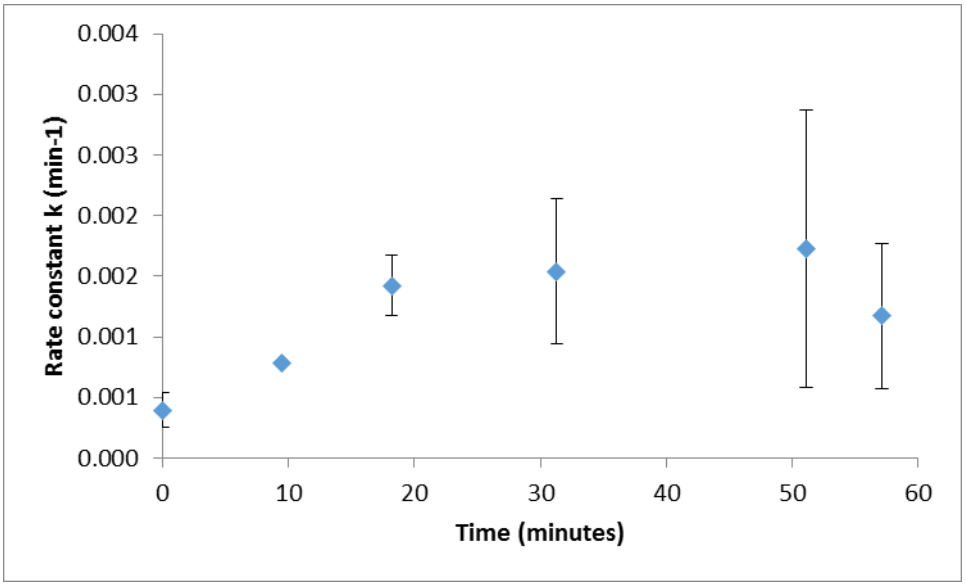

Figure 7.33: The graph for rate constant k_{-1} against concentration of CD_3COOD for the DHA dimer dissociation in DMSO-*d6*

7.3.3.1.3 Discussion

The graphs in Figure 7.30 and Figure 7.31, which portray the change in rate constants k and k_1 with the change in [CD_3COOD], show a lag phase at low concentration suggesting that a critical concentration level of CD_3COOD was required before any added amount of CD_3COOD would become available to catalyse the DHA dimer dissociation. The subsequent rate constant increase with the increase in [CD_3COOD] supports the proposed acid-catalysed reaction

mechanism, section 6.1, as more available CD_3COOD would increase the rate at which the DHA dimer ring would be protonated.

Table 7.8: The tabulated values for K and the three rate constants with the averaged values and standard error

CD_3COOD conc. (mass%)	K (no units)	k (min^{-1})	k_1 (min^{-1})	k_{-1} (min^{-1})
0	7.56 ± 0.85	$3.31 \times 10^{-3} \pm 9.1 \times 10^{-4}$	$2.92 \times 10^{-3} \pm 7.6 \times 10^{-4}$	$3.96 \times 10^{-4} \pm 1.47 \times 10^{-4}$
9.51[r]	15.4	1.28×10^{-2}	1.20×10^{-2}	7.80×10^{-4}
18.2	7.58 ± 1.94	$1.20 \times 10^{-2} \pm 6 \times 10^{-4}$	$1.05 \times 10^{-2} \pm 9 \times 10^{-4}$	$1.42 \times 10^{-3} \pm 2 \times 10^{-4}$
31.7	15.3 ± 11.5	$2.18 \times 10^{-2} \pm 7.9 \times 10^{-3}$	$2.02 \times 10^{-2} \pm 8.6 \times 10^{-3}$	$1.54 \times 10^{-3} \pm 6.0 \times 10^{-4}$
51.4	30.0 ± 17.5	$4.17 \times 10^{-2} \pm 4.1 \times 10^{-3}$	$4.00 \times 10^{-2} \pm 3.0 \times 10^{-3}$	$1.73 \times 10^{-3} \pm 1.14 \times 10^{-3}$
57.8	58.1 ± 26.8	$6.12 \times 10^{-2} \pm 4.1 \times 10^{-3}$	$6.00 \times 10^{-2} \pm 3.6 \times 10^{-3}$	$1.17 \times 10^{-3} \pm 6.0 \times 10^{-4}$

[r] This experiment was not duplicated

7.3.3.2 The effects on the rate constant k for Int#1 and Int#2 as the concentration of CD_3COOD was increased

The two doublet signals identified as emanating from Int#2 (3.98 ppm and 3.71 ppm) and single doublet signal identified as emanating from Int#1 (3.59 ppm) were traced by ^1H NMR spectroscopy to determine the experimental rate constants, k, for the formation of these species in the DHA dimer dissociation reaction in DMSO-*d6* catalysed by CD_3COOD with incrementally increasing concentration with each successive experiment.

7.3.3.2.1 Reaction order determination[s]

The zeroth, first and second order graphs were obtained for all the experiments to determine the order of the reaction. On inspection of the graphs all reactions were determined to be first order.

7.3.3.2.2 The effects on rate constant k for Int#1 as the concentration of CD_3COOD was increased[t]

Five kinetic experiments followed the Int#1 doublet signal. Of the five experiments only two of the experiments, at low concentration, provided viable data, Table 7.9. This was a result of the reactions proceeding at too high a rate when reaching concentrations of 51.4 mol% and upwards. At these concentrations the signals were only observed to diminish.

Table 7.9: The CD3COOD concentration and rate constants for the formation of Int#1

CD_3COOD conc. (mol%)	k (min^{-1})	Std Dev (min^{-1})
18.2	3.97×10^{-2}	6.8×10^{-3}
31.7	2.14×10^{-1}	1.00×10^{-1}

The two data points follow a positive relationship between the rate constant for the formation of Int#1 and an increased concentration CD_3COOD.

7.3.3.2.3 The effects on rate constant k for Int#2 as the concentration of CD_3COOD was increased[u]

[s] The zeroth, first and second order graphs tracing Int#1 in the CD_3COOD catalysed dissociation reaction are contained in the appendix: A38 – A40

[t] The first order graphs tracing Int#1 in the CD_3COOD catalysed dissociation reaction are contained in the appendix: A41 – A44

Six kinetic experiments followed the Int#2 doublet signal. The results of these ^{1}H NMR kinetic experiments were in Table 7.10, and graphed as rate constant versus concentration, Figure 7.34, to demonstrate the effect on the rate constant as the concentration of CD_3COOD was incrementally increased.

Table 7.10: The CD3COOD concentration and rate constants for the formation of Int#2

CD_3COOD conc. (mol%)	k (min^{-1})	Std Dev (min^{-1})
9.51[v]	1.96×10^{-2}	
18.2	2.00×10^{-2}	5×10^{-4}
31.7	3.50×10^{-2}	1.29×10^{-2}
51.4	1.41×10^{-1}	5.9×10^{-2}
57.8	2.47×10^{-1}	1.24×10^{-1}
65[w]	4.99×10^{-1}	-

7.3.3.2.4 Discussion

The graph in Figure 7.34, illustrating the relationship between k and the increase in [CD_3COOD] for the formation of Int#2, displays a lag phase at low concentration in the dissociation of the DHA dimer. This signifies that a critical concentration level of CD_3COOD was required to be reached before the rate for the formation of Int#2 starts to increase with an increase in [CD_3COOD].

[u] The zeroth, first and second order graphs for reaction order determination and the first order graphs tracing Int#2 in the CD_3COOD catalysed dissociation reaction are contained in the appendix: A45 – A57

[v] This experiment was not duplicated

[w] This experiment was not duplicated

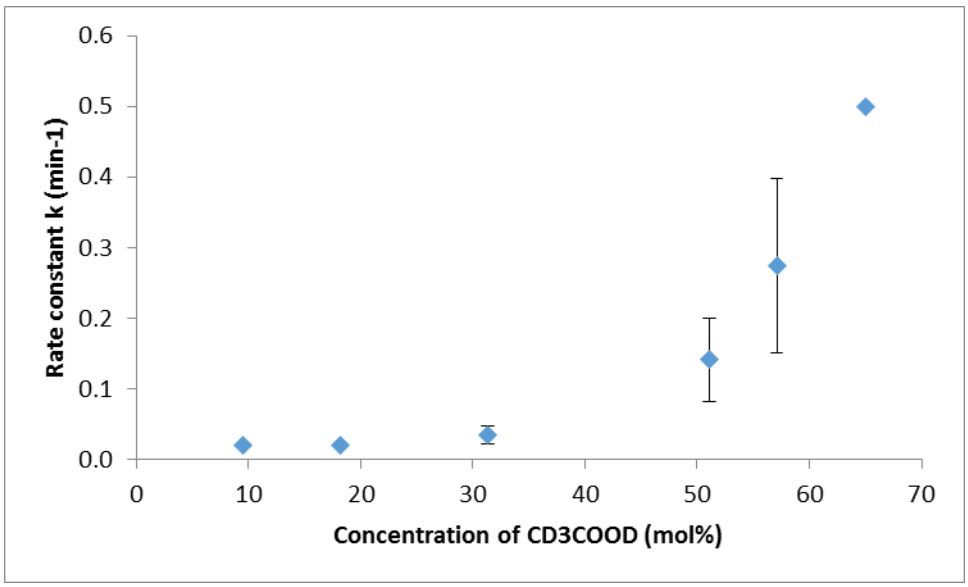

Figure 7.34: The graph for the rate constant k against concentration of CD3COOD for the formation of Int#2

7.3.3.3 The DHA dimer dissociation in DMSO-*d6* catalysed with CD_3COOD/CD_3COO^-

To offer supporting evidence for the proposed acid-catalysed reaction mechanism for the dissociation of the DHA dimer in solution in which base is also required, see section6.1, OH^- was added to the mixture of DMSO-*d6* and CD_3COOD to deprotonate CD_3COOD and thus produced CD_3COO^- *in situ.* In the DMSO-d6/CD_3COOD system the free acid is in great excess relative to its conjugate base (CD_3COO^-) resulting in the system's ability to abstract a proton abstraction being limited. If the proposed mechanism was operating, an increase in rate constant would be expected as a result of an increase in CD_3COO^- concentration as more anion would be available to abstract the hydroxyl ring proton in step 2 of the proposed acid catalysed reaction mechanism.

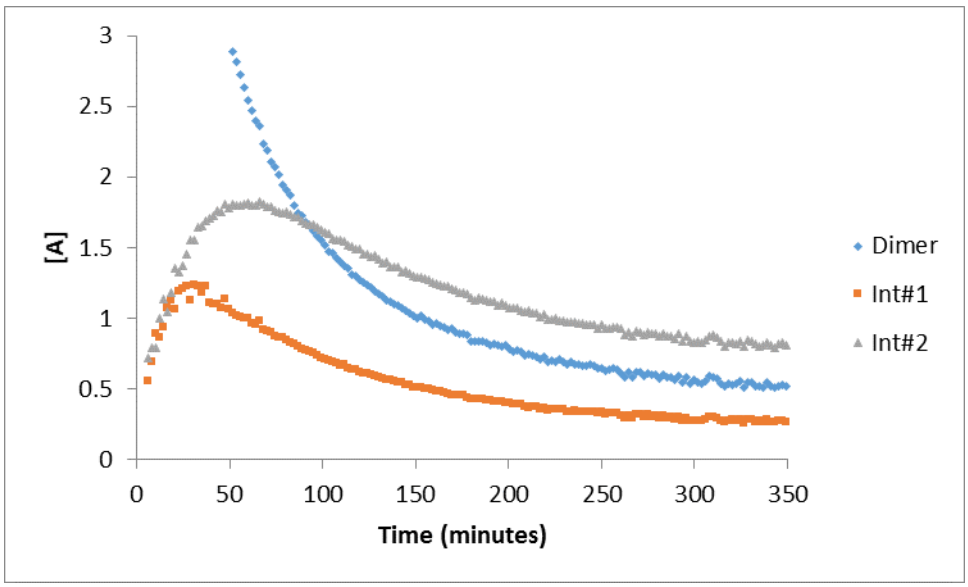

Figure 7.35: The graph for concentration against time for the disappearance of the DHA dimer and the formation and disappearance of Int#1 and Int#2 in the CD3COOD/CD3COO- catalysed dissociation reaction

The CD_3COOD/CD_3COO^- catalysed dissociation of the DHA dimer in DMSO-*d6* had Int#1 and Int#2 present, Figure 7.35.

7.3.3.3.1 Reaction order determination[x]

The zeroth, first and second order graphs were obtained for all the experiments to determine the order of the reaction. On inspection of the graphs all reactions were determined to be first order.

7.3.3.3.2 The effects of increasing the concentration of CD_3COO^- in the DMSO-d6/ CD_3COOD reaction system[y]

The concentrations of the DHA dimer (0.25M) and CD_3COOD (10 mol%) were held constant as the concentration of CD_3COO^- was incrementally increased.

The results, Table 7.11, were graphed as rate constant against the concentration of OH^- relative to the amount of CD_3COOD, Figure 7.36, Figure 7.37, Figure 7.38 and Figure 7.39 to demonstrate the effect on the rate constant as the concentration of CD_3COO^- was incrementally increased.

[x] The zeroth, first and second order graphs for the CD_3COO^- catalysed dissociation reaction are contained in the appendix: A58 – A60

[y] The completed set of first order graphs for the CD_3COO^- catalysed dissociation reaction are contained in the appendix: A61 – A74

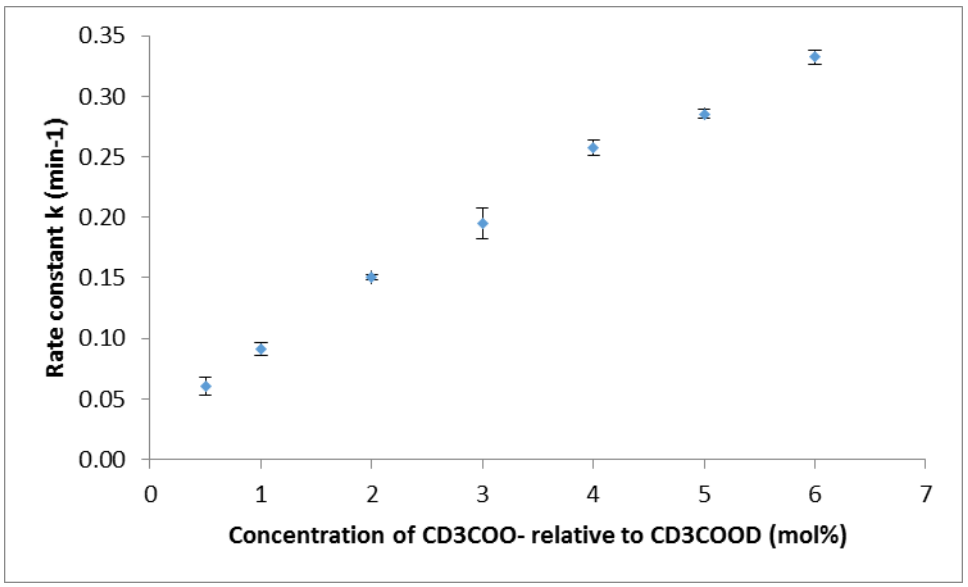

Figure 7.36: The graph for rate constant k against concentration of CD_3COO^- for the DHA dimer dissociation in DMSO-*d6*

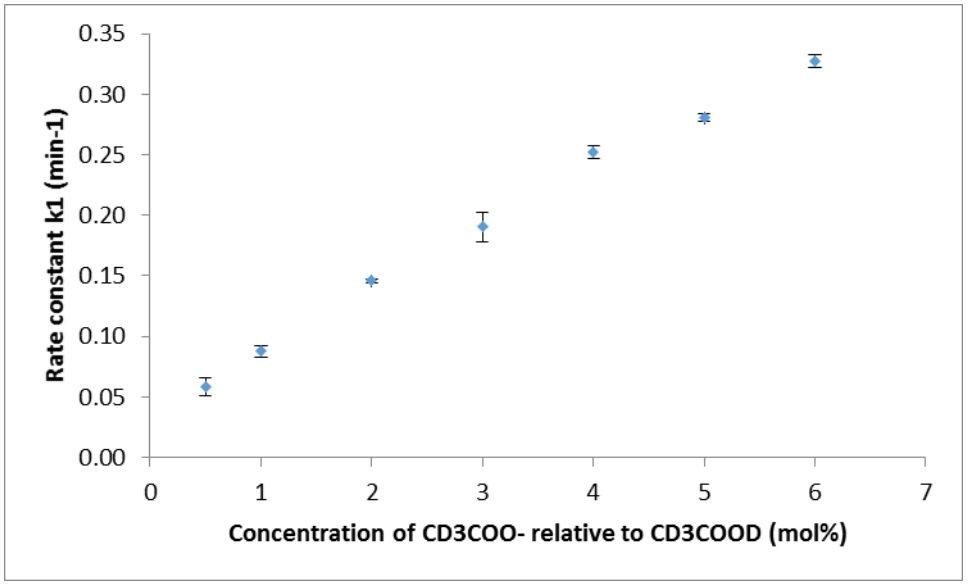

Figure 7.37: The graph for rate constant k_1 against concentration of CD_3COO^- for the DHA dimer dissociation in DMSO-*d6*

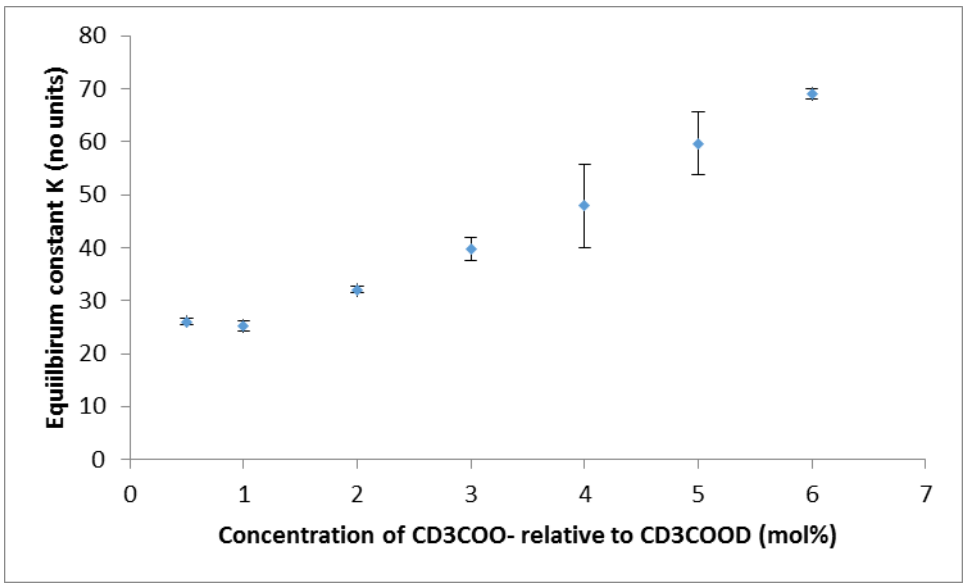

Figure 7.38: The graph for rate constant K against concentration of CD_3COO^- for the DHA dimer dissociation in DMSO-*d6*

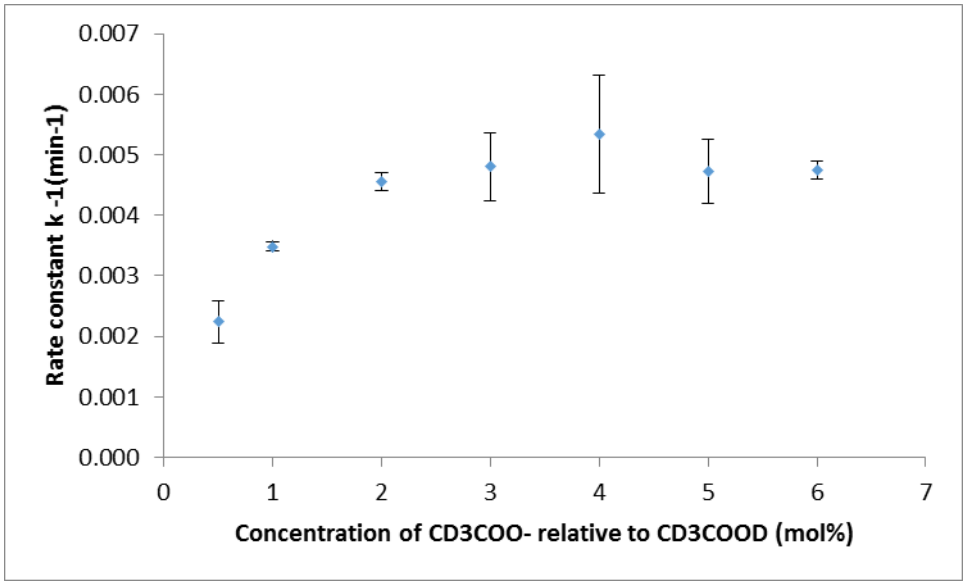

Figure 7.39: The graph for rate constant k_{-1} against concentration of CD_3COO^- for the DHA dimer dissociation in DMSO-*d6*

7.3.4 Discussion

The graphs for the forward rate constants, k and k_1, against the concentration of CD_3COO^- displayed a positive linear relationship. This result supported the proposed reaction mechanism as the incremented increase in $[CD_3COO^-]$ would be expected to increase the rate of proton abstraction. The lag phase that was observed in the D_2O and CD_3COOD catalysed experiments was not presents in these series of experiments

.

Table 7.11: The tabulated values for K and the three rate constants for the dissociation of the DHA dimer in DMSO-d6 catalysed with CD_3COOD/OH^-

$[OH^-]$ (mol%)	K(no units)	k (min^{-1})	k_1 (min^{-1})	k_{-1} (min^{-1})
0	7.56 ± 0.85	$3.31 \times 10^{-3} \pm 9.1 \times 10^{-4}$	$2.92 \times 10^{-3} \pm 7.6 \times 10^{-4}$	$3.96 \times 10^{-4} \pm 1.47 \times 10^{-4}$
0.500	26.0 ± 0.7	$6.04 \times 10^{-2} \pm 7.8 \times 10^{-3}$	$5.82 \times 10^{-2} \pm 7.4 \times 10^{-3}$	$2.24 \times 10^{-3} \pm 3.4 \times 10^{-4}$
1.00	25.2 ± 0.9	$9.13 \times 10^{-2} \pm 4.9 \times 10^{-3}$	$8.78 \times 10^{-2} \pm 4.8 \times 10^{-3}$	$3.49 \times 10^{-3} \pm 6x\ 10^{-5}$
2.00	32.0 ± 0.6	$1.50 \times 10^{-1} \pm 2 \times 10^{-3}$	$1.46 \times 10^{-1} \pm 2 \times 10^{-3}$	$4.56 \times 10^{-3} \pm 1.5 \times 10^{-4}$
3.00	39.7 ± 2.1	$1.95 \times 10^{-1} \pm 1.2 \times 10^{-2}$	$1.90 \times 10^{-1} \pm 1.2 \times 10^{-2}$	$4.81 \times 10^{-3} \pm 5.6 \times 10^{-4}$
4.00	47.9 ± 7.8	$2.58 \times 10^{-1} \pm 6 \times 10^{-3}$	$2.52 \times 10^{-1} \pm 5 \times 10^{-3}$	$5.34 \times 10^{-3} \pm 9.8 \times 10^{-4}$
5.00	59.7 ± 5.9	$2.85 \times 10^{-1} \pm 4 \times 10^{-3}$	$2.81 \times 10^{-1} \pm 3 \times 10^{-3}$	$4.73 \times 10^{-3} \pm 5.2 \times 10^{-4}$
6.00	69.0 ± 1.0	$3.32 \times 10^{-1} \pm 6 \times 10^{-3}$	$3.27 \times 10^{-1} \pm 6 \times 10^{-3}$	$4.75 \times 10^{-3} \pm 1.5 \times 10^{-4}$

7.4 Summary of result

7.4.1 Experiment analysis

All kinetic experiments displayed first order behaviour. Therefore the first order reversible reaction rate expression was used, without exception, to process the raw kinetic data to obtain the rate constants, k, k_1 and k_{-1}.

7.4.1.1 The uncatalysed experiments

The kinetics for the uncatalysed dissociation of the DHA dimer in DMSO-*d6* were shown to be first order in DHA dimer with a reaction rate constant of 3.96×10^{-4} min^{-1}. This value is approximately eighteen times greater than the literature value[23] that used a less precise method to obtain its value.

7.4.1.2 The D_2O catalysed experiments

The D_2O catalysed DHA dimer dissociation reaction experiments showed a strong positive relationship between an increase in [D_2O] and an increase in the value for the reaction rate constants. These observations supported both the acid-catalysed, Figure 7.41, and base-catalysed, Figure 7.40, proposed reaction mechanisms as D_2O is able to donate and abstract protons. Reaction mechanisms for the mutarotation of various pyranose analogues in H_2O, presented in the literature,[27,28,86] assign the base-catalysed reaction mechanism. The absence of the two intermediate species in the D_2O catalysed system suggests that the proposed base-catalysed mechanism is operating in this system as it is reported to do for the H_2O catalysed mutarotation reaction mechanism for glucopyranose.[27,28,45] In the base catalysed reaction mechanism proposed in this study, the first step is the slow rate determining step that is the deprotonation of an axial hydroxyl group on the DHA dimer ring with no lingering intermediate species as all successive steps are fast.

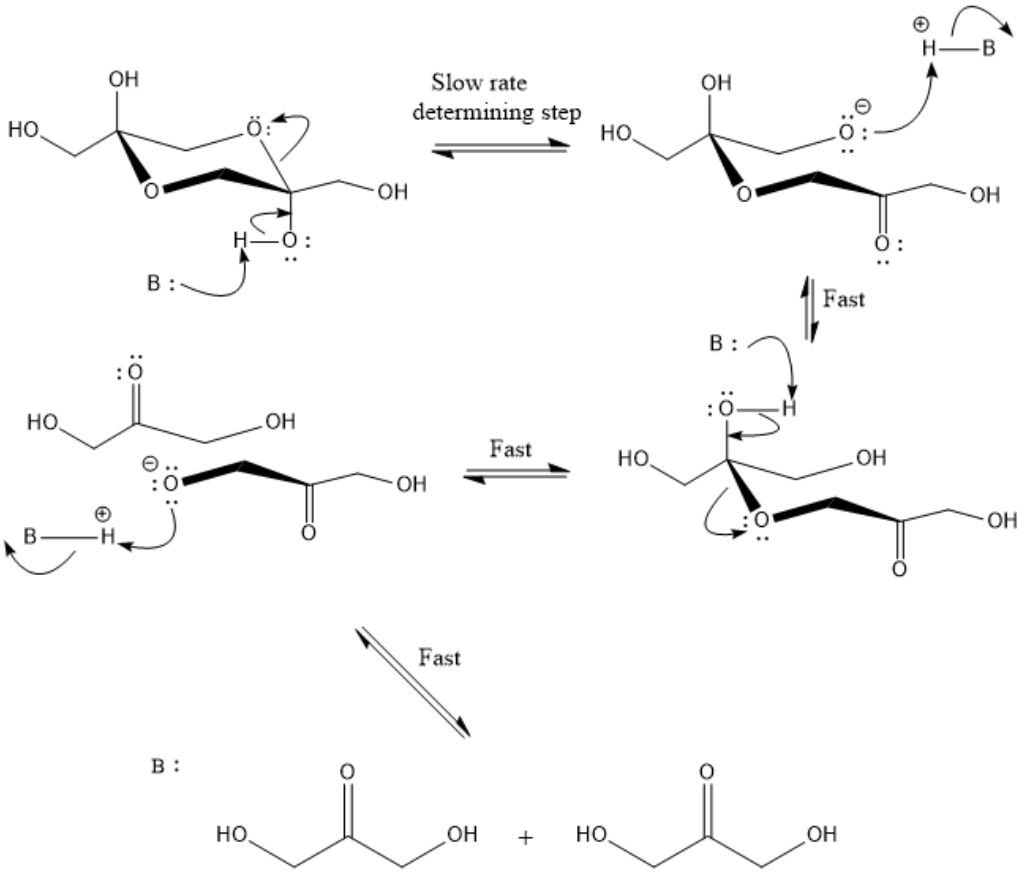

Figure 7.40: The proposed base catalysed reaction mechanism for the dissociation of the DHA dimer in solution

A lag phase in rate constant increase was observed as [D_2O] was increased at low concentration up to ~15 mass%, suggesting that the DMSO-*d6* solvent was utilising the D_2O with hydrogen bonding until the DMSO-*d6* reached a level of saturation through hydrogen bonding.

The concentration range of H_2O content in honey is 13 – 25 m%[5] but the low water activity of honey (~0.6 a_w)[5] would suggest that most of this H_2O is bound up in the honey matrix with hydrogen bonding and would be unavailable to catalyse the DHA dimer dissociation in mānuka honey. Without a H_2O catalyst, the ability of the DHA dimer to dissociate to form the DHA monomer in the honey matrix is greatly reduced resulting in a large proportion of the DHA present in mānuka honey being in its dimeric form. When there is sufficient H_2O, the DHA dissociation will utilise the proposed base-catalysed reaction mechanism.

There is a positive relationship between an increase in [D_2O] and an increase in K which indicates that not only does D_2O catalyse the DHA dimer dissociation, it also moves the equilibrium further to the right in favour of DHA monomer. This

may be a result of H_2O destabilising the DHA dimer ring with solvation that disrupts the electron delocalisation afforded by the anomeric effect.

7.4.1.3 The CD_3COOD catalysed experiments

As with the D_2O experiments, the CD_3COOD catalysed experiments show a lag phase at low concentration up to, in this case, a concentration of ~20 mol%. This indicates that the DMSO-*d6* solvent needs to reach a level of CD_3COOD saturation before any added CD_3COOD becomes available to catalyse the DHA dissociation reaction. The subsequent positive relationship between an increase in [CD_3COOD] and an increase in rate constant the supports the proposed acid-catalysed reaction mechanism, Figure 7.41.

There was an observed increase in K as [CD_3COOD] was increased indicating that the addition of CD_3COOD was moving the DHA dimer dissociation reaction equilibrium to the right.

7.4.1.4 The CD_3COOD/CD_3COO^- catalysed experiments

The CD_3COOD/CD_3COO^- catalysed experiments showed a positive relationship between an increase in [CD_3COO^-] and an increase in reaction rate constants which supported the proposed acid-catalysed reaction mechanism as an increase in CD_3COO^- anion would increase the rate at which the axial hydroxyl proton may be abstracted. There was no observed lag phase associated with low concentration and reaction rate constant increase suggesting that the level of solvation required for this process had already been achieved by the CD_3COOD present in the reaction system.

7.4.2 Identification of intermediates

The incorporation of CD_3COOD to catalyse the DHA dimer dissociation reaction resulted in the appearance of two reaction intermediate species participating in the DHA dimer dissociation in DMSO-*d6*. Symmetry, NMR spectroscopic kinetic data supported by visual inspection of the NMR spectral signals moving in time, ^1H and ^{13}C NMR chemical shifts and computationally predicated ^{13}C NMR spectral information provided evidence for the two intermediate structures (Int#1 and Int#2) to be characterised and to determine their mechanistic relevance to the proposed DHA dimer acid-catalysed dissociation reaction mechanism.

7.4.2.1 Int#1

It was proposed that the Int#1 NMR signals were emanating from the DHA dimer reaction adduct that was engaged in rapid proton/deuterium exchange via its ring oxygens and hydroxyl groups with the CD_3COOD catalyst, a dynamic process that produced symmetric and slightly altered ^{13}C NMR signals that were a statistical representation of the DHA dimer species in a dynamic environment.

7.4.2.2 Int#2

It was proposed that the Int#2 NMR signals were emanating from an asymmetric cationic DHA dimer intermediate species that had been protonated at a single ring oxygen, which was the result of the Int#1 reaction adduct having covalently bonded to an exchanging proton/deuterium after engaging in rapid proton/deuterium exchange.

7.4.3 The proposed acid-catalysed reaction mechanism

7.4.3.1 Step 1 of the proposed acid-catalysed reaction mechanism

This study proposes that Int#1 is a DHA dimer reaction adduct engaging in rapid proton exchange with the CD_3COOD catalyst. This process is presented as the first step in the proposed acid-catalysed reaction mechanism, Figure 7.41. After an undefined thresh-hold condition has been met, an exchanging proton covalently bonds to an Int#1 ring oxygen to form Int#2. This process is also the first step in the proposed reaction mechanism in a study that investigated the acetic acid catalysed mutarotation of glucopyranose using a method that tested whether a thermodynamically unstable intermediate would have to react faster than the diffusion-control limit.[28] The same study proposes that the first step in the H_2O catalysed mutarotation mechanism is not the fast acid catalysed process but the slow base catalysed process, as is proposed in this study for the D_2O catalysed DHA dimer dissociation to explain the absence of reaction intermediate signals in the NMR spectra.

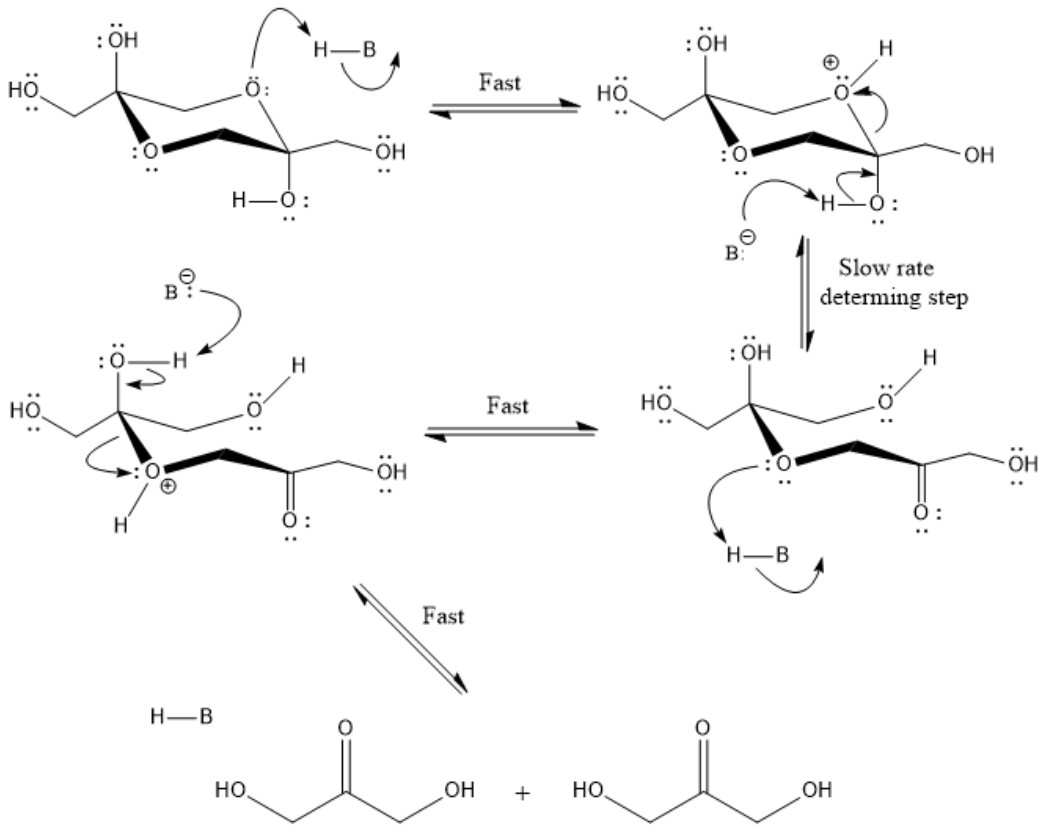

Figure 7.41: The proposed acid catalysed reaction mechanism for the dissociation of the DHA dimer in solution

7.4.3.2 Step 2 of the proposed acid-catalysed reaction mechanism

This study proposes that Int#2 is the cationic protonated DHA dimer represented in step 2 of the proposed acid-catalysed reaction mechanism. The formation of Int#2 is followed by the slow rate determining step that has CD_3COO^- abstracting a proton from the axial hydroxyl group adjacent to the protonated ring oxygen with an electron transfer from the hydroxyl oxygen to the adjacent anomeric carbon to form a carbonyl bond and an electron transfer from the anomeric carbon to the ring oxygen resulting in ring cleavage. The acyclic DHA dimer species is assumed to be unstable, as is the case for the pseudo-acyclic intermediate that has been proposed in the mutarotation reaction mechanism.[29,45,81,87] The pseudo-acyclic intermediate was proposed to account for the undetectably low concentration of the acyclic carbonyl species in the mutarotation reaction and to account for the relatively slow exchange of the 1-^{18}O in labelled glucopyranose with the ^{16}O in H_2O which indicates that the ring is rupturing then closing very rapidly, before the carbonyl is able to become hydrated. The pseudo-acyclic intermediate is the ruptured ring that maintains its ring conformation before it

rapidly closes again. It would be reasonable to assume that the same process may be operating in the DHA dimer dissociation system, with the protonated DHA dimer ring rupturing to form a pseudo-acyclic intermediate and then rapidly closing again with a percentage of ring ruptures continuing on to step 3 of the proposed mechanism in this study.

7.4.3.3 Step 3 of the proposed acid-catalysed reaction mechanism

Protonation of the ether oxygen on the ruptured ring restricts the rings ability to close again as this would result in a 2+ cationic cyclic dimer which is energetically very unfavourable. Therefore step 3 rapidly leads to step 4 of the proposed reaction mechanism.

7.4.3.4 Step 4 of the proposed acid-catalysed reaction mechanism

Proton abstraction from the tertiary hydroxyl group in step 4 is relatively rapid when compared to step 2, as there is no equilibrium associated with a rupturing ring forming a pseudo-acyclic intermediate that rapidly closes again, as is the case in step 2. When the acyclic intermediate is protonated, step 3, a proton is rapidly abstracted from the hydroxyl group with an electron transfer from the hydroxyl oxygen to its adjacent carbon to form a carbonyl and from the carbonyl carbon to the ether oxygen quickly results in the formation of two DHA monomer molecules. The energy barrier would be expected to be much larger for the reforming of the acyclic dimer from two DHA monomer molecules than the energy barrier for the pseudo-acyclic dimer closing to form the protonated cyclic DHA dimer.

7.4.3.5 Summary of the proposed acid-catalysed reaction mechanism

This proposed acid-catalysed reaction mechanism is analogous to the accepted acid-catalysed reaction mechanisms for the mutarotation[44] of reducing monosaccharides,[45,81] which describes a fast reversible proton exchange between the ring oxygen followed by a slow rate determining rupturing of the ring due to an equilibrium between the protonated ring and a pseudo-acyclic intermediate. In the case of the dissociation of the DHA dimer, this process is repeated on the other hemiketal group but without the slow rate determining equilibrium which results in a fast rupturing of the C-O bond and break-up of the DHA dimer to form two DHA monomer molecules.

8 Conclusions and suggestions for further work

8.1 Background

It has been shown in previous studies[9] that the unique non-peroxide bioactivity exhibited in matured mānuka honey was mainly a result of the MGO found to be present in mānuka honey in relatively high concentrations. DHA, present in mānuka flowers in high concentrations, was identified as the precursor to the MGO present in matured mānuka honey,[19] a reaction that had been studied previously with a proposed reaction mechanism that required DHA to be in its monomeric form. DHA exists in the solid state in its dimeric form[20,22,24,25,88,89], a form of DHA that is also stabilised in anhydrous environments. Due to the dehydrating nature of honey it is possible that the DHA in honey exists in dimeric form and it has been proposed that the conversion of the DHA dimer to the DHA monomer in mānuka honey is the rate determining step for the overall conversion of DHA to MGO.[53,90,91]

8.2 The current study

This studied utilised ^{1}H and ^{13}C NMR spectroscopy to perform a series of kinetic experiments that determined the kinetics of the DHA dimer dissociation in the anhydrous environment of DMSO-*d6*, to mimic to anhydrous conditions of mānuka honey.

8.3 Proposed reaction mechanisms

Reaction mechanisms were proposed for the acid-catalysed and a base-catalysed dissociation of the DHA dimer based on accepted reaction mechanisms for the mutarotation of glucopyranose[27,28,30,42,45,46,81,92] and the experimental results obtained in the current study.

8.4 Experimental results

8.4.1 Uncatalysed DHA dimer dissociation

First order kinetics for the DHA dimer dissociation reaction in DMSO-*d6* were identified, with an experimental rate constant of 3.78×10^{-3} min^{-1} for the uncatalysed reaction.

8.4.2 D_2O catalysed DHA dimer dissociation

A series of D_2O catalysed DHA dimer dissociation experiments identified an increase in the experimental rate constant with an increase in $[D_2O]$ offering evidence for the catalytic role of D_2O in the dissociation of the DHA dimer with the observation that before D_2O could catalyse the DHA dimer dissociation, the solvent was required to reach a level of saturation.

8.4.3 CD_3COOD catalysed DHA dimer dissociation

A series of CD_3COOD catalysed DHA dimer dissociation experiments identified an increase in the experimental rate constant with an increase in $[CD_3COOD]$ providing evidence for the catalytic role of CH_3COOH, and other organic acids present in the honey matrix[5], in the dissociation of the DHA dimer. A lag phase was observed at low concentration suggesting a pre-saturation requirement that can be assumed to be met in the relatively acidic environment contained within honey.

8.4.4 CD_3COO^- catalysed DHA dimer dissociation

A CD_3COO^- catalysed series of experiments offered further evidence supporting the proposed reaction mechanism as an increase in $[CD_3COO^-]$ resulted in an increase in experimental rate constants, which is predicted by the proposed reaction mechanism as an increase in available anion would increase the rate at which the axial hydroxyl group could be deprotonate in step 2.

8.4.5 Acid-catalysed reaction intermediates

The CD_3COOD catalysed experiments identified the two reaction intermediates that are predicated by the proposed acid-catalysed reaction mechanism, thus offering evidence for the proposed reaction mechanism.

8.5 Experimental evidence for the proposed acid-catalysed reaction mechanism

8.5.1 Int#1

The reaction intermediate in step 1 of the proposed reaction mechanism is engaged in rapid proton exchange, a condition that explains the retention of symmetry and similar ^{13}C NMR signals to the DHA dimer reactant of the NMR

observed reaction intermediate, Int#1, and therefore it is propose that Int#1 is the intermediate species in step 1.

8.5.2 Int#2

The second reaction intermediate identified by NMR spectroscopy (Int#2) is proposed to be the protonated DHA dimer predicated in step 2 of the proposed reaction mechanism which accounts for Int#2s observed ^{13}C NMR chemicals shifts and loss of symmetry. Theoretical investigation of the ^{13}C NMR chemical shifts of this species supported the characterisation of Int#2 as the protonated DHA dimer.

8.6 Proposed reaction mechanisms for the dissociation of the DHA dimer in DMSO-*d6*

This study proposes, based on accepted reactions mechanisms[27,28,30,81,93-95] proposed for the analogous hemiacetal and hemiketal hydration reactions conducted under different conditions and based on the experimental evidence obtained in this kinetic study, that the CD_3COOD catalysed DHA dimer dissociation reactions utilised the proposed acid-catalysed reaction mechanism and that the D_2O catalysed DHA dimer dissociation reactions utilised the proposed base-catalysed reaction mechanism.

8.7 Proposed reaction mechanisms for the dissociation of the DHA dimer in mānuka honey

This study proposes that if the amount of available organic acid present in the honey matrix was greater than the amount of available water the DHA dimer dissociation would utilise the proposed acid-catalysed reaction mechanism while if the amount of available water was greater than the amount of available organic acid, the proposed base-catalysed reaction mechanism would be utilised by the system.

8.8 Suggestions for further work

8.8.1 A variable temperature NMR study

The activation energies for the DHA dimer dissociation reaction intermediates might be determined using variable temperature NMR spectroscopy. This would allow fine tuning of storage temperatures for maturing mānuka honey.

8.8.2 Intermediate rate constants in the acid-catalysed reaction

A study investigating the effects on the rate constants of the acid-catalysed reaction intermediates as the concentrations of various catalysts known to be present in mānuka honey, for example proline, are increased may provide further evidence for the DHA dimer dissociation reaction mechanism in mānuka honey.

8.8.3 A numerical study

Application of the proposed reaction mechanism produces a reversible reaction system that will require numerical treatment,[96] Figure 8.1.

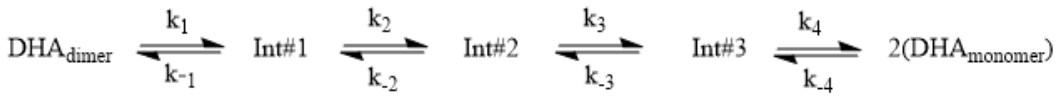

Figure 8.1: The overall reversible reaction system for the dissociation of the DHA dimer

Analysing this system, acquisition of the equilibrium constant, $K = \frac{[DHA_{monomer}]^2}{[DHA_{dimer}]}$,

becomes a non-trivial procedure with…

$$[DHA_{monomer}] = ([DHA_{dimer}]_0 - [DHA_{dimer}] - [Int\#1] - [Int\#2] - [Int\#3])$$

This will require numerical treatment using the equilibria and mass balance of all species present in the system with…

$$K_1 = \frac{Int\#1}{DHA_{dimer}}, K_1 = \frac{Int\#2}{Int\#1}, K_1 = \frac{Int\#3}{Int\#2}, K_1 = \frac{[DHA_{monomer}]^2}{Int\#3}$$

And mass balance…

$$[DHA_{dimer}]_0 = ([DHA_{dimer}] + [Int\#1] + [Int\#2] + [Int\#3] + 2[DHA_{monomer}]^2)$$

9 References

1. Al-Waili, N.; Salom, K.; Al-Ghamdi, A. A. Honey for wound healing, ulcers, and burns; data supporting its use in clinical practice. *ScientificWorldJournal* **2011**, *11*, 766-787.

2. Gethin, G. T.; Cowman, S.; Conroy, R. M. The impact of Manuka honey dressings on the surface pH of chronic wounds. *Int Wound J* **2008**, *5*, 185-194.

3. Molan, P. C. The evidence supporting the use of honey as a wound dressing. *Int J Low Extrem Wounds* **2006**, *5*, 40-54.

4. Gethin, G.; Cowman, S. Case series of use of Manuka honey in leg ulceration. *Int Wound J* **2005**, *2*, 10-15.

5. White, J. W.; Agriculture, U. S. D. o. *Composition of American Honeys*; U.S. Department of Agriculture, 1962.

6. Chirife, J.; Scarmato, G.; Herszage, L. Scientific basis for use of granulated sugar in treatment of infected wounds. *Lancet* **1982**, *1*, 560-561.

7. Sinnott, M. *Carbohydrate Chemistry and Biochemistry: Structure and Mechanism*; RSC Publishing, 2007.

8. Allen, K. L.; Molan, P. C.; Reid, G. M. A survey of the antibacterial activity of some New Zealand honeys. *J Pharm Pharmacol* **1991**, *43*, 817-822.

9. Mavric, E.; Wittmann, S.; Barth, G.; Henle, T. Identification and quantification of methylglyoxal as the dominant antibacterial constituent of Manuka (Leptospermum scoparium) honeys from New Zealand. *Mol. Nutr. Food Res.* **2008**, *52*, 483-489.

10. Adams, C. J.; Boult, C. H.; Deadman, B. J.; Farr, J. M.; Grainger, M. N. C.; Manley-Harris, M.; Snow, M. J. Isolation by HPLC and characterisation of the bioactive fraction of New Zealand manuka (Leptospermum scoparium) honey. *Carbohydr Res* **2008**, *343*, 651-659.

11. Angyal, S. J. The Lobry de Bruyn-Alberda van Ekenstein transformation and related reactions. *Top. Curr. Chem.* **2001**, *215*, 1-14.

12. Fedoronko, M.; Koenigstein, J. Kinetics of mutual isomerization of trioses and their dehydration to methyl glyoxal. *Collect. Czech. Chem. Commun.* **1969**, *34*, 3881-3894.

13. Allaman, I.; Belanger, M.; Magistretti, P. J. Methylglyoxal, the dark side of glycolysis. *Front Neurosci* **2015**, *9*, 23.

14. Kalapos, M. P. Methylglyoxal in living organisms: chemistry, biochemistry, toxicology and biological implications. *Toxicol Lett* **1999**, *110*, 145-175.

15. Kalapos, M. P. Methylglyoxal and glucose metabolism: a historical perspective and future avenues for research. *Drug Metab. Drug Interact.* **2008**, *23*, 69-91.

16. Matafome, P.; Sena, C.; Seica, R. Methylglyoxal, obesity, and diabetes. *Endocrine* **2013**, *43*, 472-484.

17. Murata-Kamiya, N.; Kamiya, H. Methylglyoxal, an endogenous aldehyde, crosslinks DNA polymerase and the substrate DNA. *Nucleic Acids Res.* **2001**, *29*, 3433-3438.

18. Molan, P. The explanation of why the level of UMF varies in manuka honey. *New Zealand BeeKeeper* **2008**, 17-21.

19. Adams, C. J.; Manley-Harris, M.; Molan, P. C. The origin of methylglyoxal in New Zealand manuka (Leptospermum scoparium) honey. *Carbohydr. Res.* **2009**, *344*, 1050-1053.

20. Levene, P. A.; Walti, A. Polymerization and condensation. III. Autocondensation of dihydroxyacetone. *J. Biol. Chem.* **1928**, *78*, 23-33.

21. Wohl, A.; Neuberg, C. Identification of glycerol aldehydes. *Ber. Dtsch. Chem. Ges.* **1900**, *33*, 3095-3110.

22. Bell, R. P.; Baughan, E. C. Acid-base catalysis in the depolymerization of dimeric dihydroxyacetone. *J. Chem. Soc.* **1937**, 1947-1953.

23. Davis, L. Structure of dihydroxyacetone in solution. *Bioorg. Chem.* **1973**, *2*, 197-201.

24. Kobayashi, Y.; Igarashi, T.; Takahashi, H.; Higasi, K. Infrared and Raman studies of the dimeric structures of 1,3-dihydroxyacetone, D-(+)- and DL-glyceraldehyde. *J. Mol. Struct.* **1976**, *35*, 85-99.

25. Kobayashi, Y.; Takahashi, H. Conformational studies of glycolaldehyde and 1,3-dihydroxyacetone in solution by proton NMR. *Spectrochim. Acta, Part A* **1979**, *35A*, 307-314.

26. Le Barc'H, N.; Grossel, J. M.; Looten, P.; Mathlouthi, M. Kinetic study of the mutarotation of D-glucose in concentrated aqueous solution by gas-liquid chromatography. *Food Chem.* **2001**, *74*, 119-124.

27. Capon, B. Mechanism in carbohydrate chemistry. *Chem. Rev.* **1969**, *69*, 407-498.

28. Capon, B.; Walker, R. B. Kinetics and mechanism of the mutarotation of aldoses. *J. Chem. Soc., Perkin Trans. 2* **1974**, 1600-1610.

29. Pigman, W. W. *THE CARBOHYDRATES 2E V1A: Chemistry and Biochemistry*; Elsevier Science, 2012.

30. Bronsted, J. N.; Guggenheim, E. A. Theory of acid and basic catalysis. The mutarotation of glucose. *J. Am. Chem. Soc.* **1927**, *49*, 2554-2584.

31. Sindhu, P. S. *Fundamentals of Molecular Spectroscopy*; New Age International (P) Limited, 2006.

32. Mohacek-Grosev, V.; Prugovecki, B.; Prugovecki, S.; Strukan, N. Glycolaldehyde dimer in the stable crystal phase has axial OH groups: Raman, infrared and X-ray data analysis. *J. Mol. Struct.* **2013**, *1047*, 209-215.

33. Slepokura, K.; Lis, T. Crystal structures of dihydroxyacetone and its derivatives. *Carbohydr. Res.* **2004**, *339*, 1995-2007.

34. Guggenheim, E. A. The determination of the velocity constant of a unimolecular reaction. *Philos. Mag. (1798-1977)* **1926**, *2*, 538-513.

35. Yaylayan, V. A.; Harty-Majors, S.; Ismail, A. A. Investigation of the mechanism of dissociation of glycolaldehyde dimer (2,5-dihydroxy-1,4-dioxane) by FTIR spectroscopy. *Carbohydr. Res.* **1998**, *309*, 31-38.

36. Stassinopoulou, C. I.; Zioudrou, C. Study of the dimeric structures of glycolaldehyde solutions by NMR. *Tetrahedron* **1972**, *28*, 1257-1263.

37. Edward, J. T. Stability of glycosides to acid hydrolysis. *Chem. Ind. (London, U. K.)* **1955**, 1102-1104.

38. Tvaroska, I.; Bleha, T. Anomeric and exo-anomeric effects in carbohydrate chemistry. *Adv. Carbohydr. Chem. Biochem.* **1989**, *47*, 45-123.

39. Juaristi, E.; Cuevas, G. Recent studies on the anomeric effect. *Tetrahedron* **1992**, *48*, 5019-5087.

40. Cumpstey, I. On a so-called "kinetic anomeric effect" in chemical glycosylation. *Org. Biomol. Chem.* **2012**, *10*, 2503-2508.

41. Hudson, C. S. A Review of Discoveries on the Mutarotation of the Sugars. *J. Am. Chem. Soc.* **1910**, *32*, 889-895.

42. Angyal, S. J. Composition and conformation of sugars in solution. *Angew. Chem., Int. Ed. Engl.* **1969**, *8*, 157-166.

43. Imamura, A.; Okajima, T.; Kanda, K. A molecular orbital approach to the effect of acid and base on mutarotation of D-glucose. *Bull. Chem. Soc. Jpn.* **1986**, *59*, 943-945.

44. Meurant, G. *ADV IN CARBOHYDRATE CHEM & BIOCHEM*; Elsevier Science, 1970.

45. Isbell, H. S.; Frush, H. L.; Wade, C. W. R.; Hunter, C. E. Transformations of sugars in alkaline solutions. *Carbohyd. Res.* **1969**, *9*, 163-175.

46. Zhdanov, Y. A.; Minkin, V. I.; Ostroumov, Y. A.; Dorofeenko, G. N. Quantum chemistry of carbohydrates. I. The electronic structure of some pentoses. *Carbohyd. Res.* **1968**, *7*, 156-160.

47. Haynes, W. M. *CRC Handbook of Chemistry and Physics, 93rd Edition*; Taylor & Francis, 2012.

48. Ciocirlan, O.; Iulian, O. Density, viscosity and refractive index of the dimethyl sulfoxide + o-xylene system. *J. Serb. Chem. Soc.* **2009**, *74*, 317-329.

49. MacGregor, W. S. The chemical and physical properties of DMSO. *Ann N Y Acad Sci* **1967**, *141*, 3-12.

50. Kolthoff, I. M.; Chantooni, M. K., Jr.; Bhowmik, S. Dissociation constants of uncharged and monovalent cation acids in dimethyl sulfoxide. *J. Am. Chem. Soc.* **1968**, *90*, 23-28.

51. Little, E. J., Jr.; Jones, M. M. Complete table of electronegativities. *J. Chem. Educ.* **1960**, *37*, 231-233.

52. Anslyn, E. V.; Dougherty, D. A. *Modern Physical Organic Chemistry*; University Science, 2006.

53. Grainger, M. N. C.; Manley-Harris, M.; Lane, J. R.; Field, R. J. Kinetics of conversion of dihydroxyacetone to methylglyoxal in New Zealand ma[n.773]nuka honey: Part III - A model to simulate the conversion. *Food Chem.* **2016**, Ahead of Print.

54. Macomber, R. S. *A Complete Introduction to Modern NMR Spectroscopy*; Wiley, 1998; 382 pp.

55. Abraham, R. J.; Byrne, J. J.; Griffiths, L.; Perez, M. 1H chemical shifts in NMR: part 23, the effect of dimethyl sulphoxide versus chloroform solvent on 1H chemical shifts. *Magn. Reson. Chem.* **2006**, *44*, 491-509.

56. Gottlieb, H. E.; Kotlyar, V.; Nudelman, A. NMR chemical shifts of common laboratory solvents as trace impurities. *J. Org. Chem.* **1997**, *62*, 7512-7515.

57. Jackman, L. M.; Sternhell, S.; Barton, D. H. R.; Doering, W. *Application of Nuclear Magnetic Resonance Spectroscopy in Organic Chemistry: International Series in Organic Chemistry*; Elsevier Science, 2013.

58. Akitt, J. W.; Mann, B. E. *NMR and Chemistry: An introduction to modern NMR spectroscopy, Fourth Edition*; Taylor & Francis, 2000.

59. Haasnoot, C. A. G.; De Leeuw, F. A. A. M.; Altona, C. The relation between proton-proton NMR coupling constants and substituent electronegativities. I. An empirical generalization of the Karplus equation. *Tetrahedron* **1980**, *36*, 2783-2792.

60. Claridge, T. D. W. *High-resolution NMR Techniques in Organic Chemistry*; Elsevier, 2009.

61. Croasmun, W. R.; Carlson, R. M. K. *Two-Dimensional NMR Spectroscopy: Applications for Chemists and Biochemists*; Wiley, 1994.

62. Jacobsen, N. E. *NMR Spectroscopy Explained: Simplified Theory, Applications and Examples for Organic Chemistry and Structural Biology*; Wiley, 2007.

63. Takeuchi, T. *Analytical Chemistry: Session Lectures Presented at the Twentysixth International Congress of Pure and Applied Chemistry, Tokyo, Japan, 4-10 September 1977*; Elsevier Science, 2013.

64. Lambert, J. B.; Mazzola, E. P. *Nuclear Magnetic Resonance Spectroscopy: An Introduction to Principles, Applications, and Experimental Methods*; Pearson Education, 2004.

65. Lemieux, R. U.; Kullnig, R. K.; Bernstein, H. J.; Schneider, W. G. Configuration effects on the proton magnetic resonance spectra of six-membered ring compounds. *J. Am. Chem. Soc.* **1958**, *80*, 6098-6105.

66. Bociek, S.; Franks, F. Proton exchange in aqueous solutions of glucose. Hydration of carbohydrates. *J. Chem. Soc., Faraday Trans. 1* **1979**, *75*, 262-270.

67. Engel, T.; Reid, P. J. *Physical Chemistry*; Prentice Hall, 2010.

68. Klinowski, J. Solid-state NMR studies of molecular sieve catalysts. *Chem. Rev.* **1991**, *91*, 1459-1479.

69. Bubb, W. A. NMR spectroscopy in the study of carbohydrates : characterizing the structural complexity. *Concepts Magn. Reson., Part A* **2003**, *19A*, 1-19.

70. Andrews, J. C.; Worley, F. P. Mutarotation. II. The relative velocities of mutarotation of α- and β-glucose: effect of acid and salt. *J. Phys. Chem.* **1927**, *31*, 882-885.

71. Roslund, M. U.; Taehtinen, P.; Niemitz, M.; Sjoeholm, R. Complete assignments of the 1H and 13C chemical shifts and JH,H coupling constants in NMR spectra of D-glucopyranose and all D-glucopyranosyl-D-glucopyranosides. *Carbohydr. Res.* **2008**, *343*, 101-112.

72. AIST:RIO-DB Spectral Database for Organic Compounds,SDBS. http://sdbs.db.aist.go.jp/sdbs/cgi-bin/direct_frame_top.cgi (accessed 17-6-2015 2015).

73. Dore, J. C.; Teixeira, J. *Hydrogen-Bonded Liquids*; Springer Netherlands, 2012.

74. Brauman, J. I.; Nelson, N. J. Rates of proton exchange between dimethyl sulfoxide and its conjugate base. *J. Am. Chem. Soc.* **1966**, *88*, 2332-2334.

75. Drake, E. N.; Brown, C. E. Application of NMR to biochemical kinetics. A laboratory experiment in physical biochemistry. *J. Chem. Educ.* **1977**, *54*, 124-127.

76. Bender, M. L. *Mechanisms of Homogeneous Catalysis from Protons to Proteins*; John Wiley & Sons, Inc., 1971.

77. Ritchie, C. D.; Uschold, R. Proton transfers in dipolar aprotic solvents. I. Transfer to fluorenyl and trityl anions in dimethyl sulfoxide solution. *J. Am. Chem. Soc.* **1964**, *86*, 4488-4489.

78. Lin, C.-E.; Yu, C.-J.; Chen, C.-L.; Chou, L.-D.; Chou, C. Kinetics of Glucose Mutarotation Assessed by an Equal-Amplitude Paired Polarized Heterodyne Polarimeter. *J. Phys. Chem. A* **2010**, *114*, 1665-1669.

79. Lee, C. Y.; Acree, T. E.; Shallenberger, R. S. Mutarotation of D-glucose and D-mannose in aqueous solution. *Carbohyd. Res.* **1969**, *9*, 356-360.

80. Ikeda, T.; Senda, M. Polarographic study of monosaccharides in unbuffered solution and its application to the determination of the mutarotation rate constants. *Bull. Chem. Soc. Jap.* **1973**, *46*, 2107-2111.

81. Meurant, G. *Advances in Carbohydrate Chemistry and Biochemistry*; Elsevier Science, 1970.

82. © Maplesoft [Computer software], a division of Waterloo Maple Inc. 2016., 2016.

83. Bordwell, F. G. Equilibrium acidities in dimethyl sulfoxide solution. *Acc. Chem. Res.* **1988**, *21*, 456-463.

84. Silverstein, R. M.; Webster, F. X.; Kiemie, D. *Spectrometric Identification of Organic Compounds, 7th Edition*; John Wiley & Sons Ltd, 2002; 490 pp.

85. Jensen, A. A Computational Study of the Dimerization Reaction of 1,3-dihydroxyacetoneThesis, 2016.

86. Wann, S. R.; Kreevoy, M. M. Acetal hydrolysis: the A1 mechanism. *J. Org. Chem.* **1981**, *46*, 419-423.

87. Khadem, H. E. *Carbohydrate Chemistry: Monosaccharides and Their Oligomers*; Elsevier Science, 2012.

88. Davis, D. G.; Bax, A. Separation of chemical exchange and cross-relaxation effects in two-dimensional NMR spectroscopy. *J. Magn. Reson.* **1985**, *64*, 533-535.

89. Slepokura, K.; Lis, T. Dihydroxyacetone phosphate, DHAP, in the crystalline state: monomeric and dimeric forms. *Carbohydr. Res.* **2010**, *345*, 512-529.

90. Grainger, M. N. C.; Manley-Harris, M.; Lane, J. R.; Field, R. J. Kinetics of conversion of dihydroxyacetone to methylglyoxal in New Zealand ma[n.773]nuka honey: Part I - Honey systems. *Food Chem.* **2016**, Ahead of Print.

91. Grainger, M. N. C.; Manley-Harris, M.; Lane, J. R.; Field, R. J. Kinetics of the conversion of dihydroxyacetone to methylglyoxal in New Zealand ma[n.773]nuka honey: Part II - Model systems. *Food Chem.* **2016**, Ahead of Print.

92. Meurant, G. *ADVANCES IN CARBOHYDRATE CHEMISTRY*; Elsevier Science, 1967.

93. Bell, R. P.; de B. Darwent, B. Kinetics of the hydration of acetaldehyde. *Trans. Faraday Soc.* **1950**, *46*, 34-41.

94. Bell, R. P.; Rand, M. H.; Wynne-Jones, K. M. A. Kinetics of the hydration of acetaldehyde. *Trans. Faraday Soc.* **1956**, *52*, 1093-1102.

95. Sorensen, P. E.; Jencks, W. P. Acid- and base-catalyzed decomposition of acetaldehyde hydrate and hemiacetals in aqueous solution. *J. Am. Chem. Soc.* **1987**, *109*, 4675-4690.

96. Field, R. J. Personal Communication, 2016.

10 Appendices

10.1 Introduction

10.2 Experimental

10.2.1 ^{1}H NMR

PULPROG	zg	Current pulse program
TD	65536	Size of FID
SW [ppm]	18.0229	Spectral width
AQ [sec]	4.5438795	Acquisition time
DW [μsec]	69.333	Dwell time
DE [μsec]	6.50	Pre-scan-delay
D1 [sec]	0.500	Relaxation delay
FIDRES [Hz]	0.110039	Fid resolution
FW [Hz]	125000	Filter width
DS	2	Number of dummy scans
NS	8	Number of scans
OP1 [ppm]	7.500	Transmitter frequency offset
SF01 [MHz]	400.1330010	Frequency of channel 1
P1 [μsec]	7.75	F1 ch. high power pulse

10.2.2 ^{13}C NMR

PULPROG	zgpg70	Current pulse program
TD	32768	Size of FID
SW [ppm]	238.894	Spectral width
AQ [sec]	0.6816244	Acquisition time
DW [μsec]	20.800	Dwell time
DE [μsec]	6.50	Pre-scan-delay
D1 [sec]	1.500	Relaxation delay
FIDRES [Hz]	0.733596	Fid resolution
FW [Hz]	125000	Filter width
DS	4	Number of dummy scans
NS	128	Number of scans

OP1 [ppm]	110.000	Transmitter frequency offset
SF01 [MHz]	100.6238364	Frequency of channel 1
P1 [μsec]	14.00	F1 ch. high power pulse

10.2.3 H,H-COSY

PULPROG	cosygpqf	Current pulse program
TD	1024	Size of FID
SW [ppm]	0.899	Spectral width
AQ [sec]	1.42218	Acquisition time
DW [μsec]	1388.800	Dwell time
DE [μsec]	6.50	Pre-scan-delay
D1 [sec]	1.500	Relaxation delay
D16 [sec]	0.00020000	Delay for gradient recovery
DS	4	Number of dummy scans
NS	128	Number of scans
OP1 [ppm]	3.600	Transmitter frequency offset
SF01 [MHz]	400.1314405	Frequency of channel 1
P1 [μsec]	14.00	F1 ch. high power pulse

10.2.4 HSQC

PULPROG	hsqcgpph	Current pulse program
TD	1024	Size of FID
SW [ppm]	1.2003	Spectral width (F2)
SW [ppm]	164.9975	Spectral width (F1)
AQ [sec]	1.06610	Acquisition time (F2)
AQ [sec]	0.0077097	Acquisition time (F1)
FIDRES[Hz]	0.4690	Fid resolution (F2)
FIDRES[Hz]	64.853424	Fid resolution (F1)
DW [μsec]	1041.067	Dwell time
DE [μsec]	6.50	Pre-scan-delay
CNST2	145.0000	=J(XH)
D1 [sec]	1.500	Relaxation delay

D16 [sec]	0.00020000	Delay for gradient recovery
DS	4	Number of dummy scans
NS	8	Number of scans

10.2.5 HMBC

PULPROG	hmbcgplpndqf	Current pulse program
TD	2048	Size of FID (F2)
TD	128	Size of FID (F1)
SW [ppm]	3.000	Spectral width (F2)
SW [ppm]	40.0014	Spectral width (F1)
AQ [sec]	0.8531103	Acquisition time (F2)
AQ [sec]	0.0159007	Acquisition time (F1)
FIDRES[Hz]	0.586125	Fid resolution (F2)
FIDRES[Hz]	31.445107	Fid resolution (F1)
DW [µsec]	416.533	Dwell time
CNST2	145.0000	=J(XH)
CNST13		=J(XH) long range
D1 [sec]	1.500	Relaxation delay
D16 [sec]	0.00020000	Delay for gradient recovery
DS	4	Number of dummy scans
NS	16	Number of scans

10.2.6 ROESY

PULPROG	roesyph	Current pulse program
TD	2048	Size of FID (F2)
TD	320	Size of FID (F1)
SW [ppm]	4.0000	Spectral width (F2) + (F1)
IN_F [µsec]	624.80	Increment for delay
AQ [sec]	0.6398452	Acquisition time (F2)
AQ [sec]	0.0999680	Acquisition time (F1)
FIDRES[Hz]	0.781500	Fid resolution (F2)
FIDRES[Hz]	5.001600	Fid resolution (F1)

DW [μsec]	312.4	Dwell time
DE [μsec]	6.50	Pre-scan-delay
D1 [sec]	1.500	Relaxation delay
D16 [sec]	0.00020000	Delay for gradient recovery
DS	4	Number of dummy scans
NS	8	Number of scans

10.2.7 SELCOSY

PULPROG	selco	Current pulse program
TD	32768	Size of FID
SW [ppm]	18.0229	Spectral width
AQ [sec]	2.2719646	Acquisition time
DW [μsec]	69.333	Dwell time
DE [μsec]	6.50	Pre-scan-delay
D1 [sec]	1.0000	Relaxation delay
D14 [sec]	0.0350000	Delay for evolution
FIDRES [Hz]	0.220079	Fid resolution
FW [Hz]	125000	Filter width
DS	4	Number of dummy scans
NS	96	Number of scans
OP1 [ppm]	3.460	Transmitter frequency offset
SF01 [MHz]	400.1330010	Frequency of channel 1
P1 [μsec]	7.75	F1 ch. high power pulse

10.2.8 SELTOCSY

PULPROG	selmlgp	Current pulse program
TD	32768	Size of FID
SW [ppm]	18.0229	Spectral width
AQ [sec]	2.2719646	Acquisition time
DW [μsec]	69.333	Dwell time
DE [μsec]	6.50	Pre-scan-delay
D1 [sec]	1.0000	Relaxation delay

D9 [sec]	0.01000	TOCSY mixing time
D16 [sec]	0.0002000	Delay for gradient recovery
FIDRES [Hz]	0.220079	Fid resolution
FW [Hz]	125000	Filter width
DS	4	Number of dummy scans
NS	32	Number of scans
OP1 [ppm]	3.923	Transmitter frequency offset
SF01 [MHz]	400.1330010	Frequency of channel 1
P1 [μsec]	15.00	F1 ch. high power pulse

10.2.9 SELNOESY

PULPROG	awselnogp4	Current pulse program
TD	32230	Size of FID
SW [ppm]	18.0229	Spectral width
AQ [sec]	2.2346632	Acquisition time
DW [μsec]	69.333	Dwell time
DE [μsec]	6.50	Pre-scan-delay
D1 [sec]	1.0000	Relaxation delay
D8 [sec]	0.50000	mixing time
D16 [sec]	0.0002000	Delay for gradient recovery
FIDRES [Hz]	0.220079	Fid resolution
FW [Hz]	125000	Filter width
DS	4	Number of dummy scans
NS	8	Number of scans
OP1 [ppm]	3.923	Transmitter frequency offset
SF01 [MHz]	400.1330010	Frequency of channel 1
P1 [μsec]	7.50	F1 ch. high power pulse

10.3 Assignment of DHA spectra

10.4 Method development

10.5 The kinetics of the DHA dissociation

The differential equation for [D] is…

$$\frac{d[\mathrm{D}]}{dt} = -k_1[\mathrm{D}] + k_{-1}[M]^2$$

Using the initial conditions…

$$[M] = 2([\mathrm{D}]_0 - [\mathrm{D}])$$

…and the relationship

$$k_1 = Kk_{-1}$$

[M] and k_1 were replaced and the equation was rearranged…

$$\frac{d[\mathrm{D}]}{dt} = -K.k_{-1}[\mathrm{D}] + 4k_{-1}\left[[\mathrm{D}]_0 - [\mathrm{D}]\right]^2$$

$$\frac{d[\mathrm{D}]}{dt} = -K.k_{-1}[\mathrm{D}] + 4k_{-1}([\mathrm{D}]_0{}^2 - 2[\mathrm{D}][\mathrm{D}]_0 + [\mathrm{D}]^2)$$

$$\frac{d[\mathrm{D}]}{dt} = -K.k_{-1}[\mathrm{D}] + 4k_{-1}[\mathrm{D}]^2 - 8k_{-1}[\mathrm{D}][\mathrm{D}]_0 + 4k_{-1}[\mathrm{D}]_0{}^2$$

$$\frac{d[\mathrm{D}]}{dt} = 4k_{-1}[\mathrm{D}]^2 + [\mathrm{D}](-K.k_{-1} - 8k_{-1}[\mathrm{D}]_0) + 4k_{-1}[\mathrm{D}]_0{}^2$$

$$\frac{d[\mathrm{D}]}{dt} = 4k_{-1}[\mathrm{D}]^2 + [\mathrm{D}]k_{-1}(-K - 8[\mathrm{D}]_0) + 4k_{-1}[\mathrm{D}]_0{}^2$$

The final expression is a quadratic equation that was rearranged to give the quadratic integral…

$$\int_{[\mathrm{D}]_0}^{[\mathrm{D}]} \frac{d[\mathrm{D}]}{4k_{-1}[\mathrm{D}]^2 + [\mathrm{D}]k_{-1}(-K - 8[\mathrm{D}]_0) + 4k_{-1}[\mathrm{D}]_0{}^2} = \int_{t_0}^{t} dt$$

The quadratic integral was evaluated using the Maplesoft computer program to obtain the integrated equation in terms of [D]…

$$[\mathrm{D}] = \frac{1}{8k_{-1}}\left[Kk_{-1} + 8k_{-1}[\mathrm{D}]_0 - k_{-1}\sqrt{K^2 + 16K[\mathrm{D}]_0}.\,tanh(\frac{k_{-1}\sqrt{K^2 + 16K[\mathrm{D}]_0}}{2}t)\right]$$

The integrated rate expression was required to be in terms of some expression containing [D] on the left hand side and some constant of proportionality of time containing k_{-1} on the right hand side. This condition is required in order to provide a linear equation of the form, $y = mx + c$, so that k_{-1} may be extracted from the constant of proportionality when the data is graphed using Excel. Therefore the expression needed to be manipulated.

The brackets were expanded and the k_{-1} terms outside the tanh term cancelled…

$$8([\mathrm{D}] - [\mathrm{D}]_0) - K = -\sqrt{K^2 + 16K[\mathrm{D}]_0}.\,tanh(\frac{\sqrt{K^2 + 16K[\mathrm{D}]_0}}{2}k_{-1}t)$$

The external root term was moved to the left-hand side…

$$\frac{8([\mathrm{D}]_0 - [\mathrm{D}]) + K}{\sqrt{K^2 + 16K[\mathrm{D}]_0}} = tanh(\frac{k_{-1}\sqrt{K^2 + 16K[\mathrm{D}]_0}}{2}k_{-1}t)$$

The arctanh operator was applied to the equation to extract k_{-1} and t from the tanh term and t was made the subject of the equation…

$$t = \frac{1}{k_{-1}}\frac{2}{\sqrt{K^2 + 16K[\mathrm{D}]_0}}arctanh(\frac{8([\mathrm{D}]_0 - [\mathrm{D}]) + K}{\sqrt{K^2 + 16K[\mathrm{D}]_0}})$$

The identity, $\mathrm{arctanh}(x) = \frac{1}{2}\ln(\frac{1+x}{1-x})$, was applied to the arctanh term…

$$t = \frac{1}{k_{-1}} \frac{2}{\sqrt{K^2 + 16K[\mathrm{D}]_0}} \ln\left(\frac{1 + \frac{8([\mathrm{D}]_0 - [\mathrm{D}]) + K}{\sqrt{K^2 + 16K[\mathrm{D}]_0}}}{1 - \frac{8([\mathrm{D}]_0 - [\mathrm{D}]) + K}{\sqrt{K^2 + 16K[\mathrm{D}]_0}}}\right)$$

The denominator and numerator of the logarithmic term were simplified…

$$t = \frac{1}{k_{-1}} \frac{2}{\sqrt{K^2 + 16K[\mathrm{D}]_0}} \ln\left(\frac{-8([\mathrm{D}] - [\mathrm{D}]_0) + K + \sqrt{K^2 + 16K[\mathrm{D}]_0}}{8([\mathrm{D}] - [\mathrm{D}]_0) - K + \sqrt{K^2 + 16K[\mathrm{D}]_0}}\right)$$

k_{-1} and the root term were carried over to t to be defined as the constant of proportionality…

$$\ln\left(\frac{-8([\mathrm{D}] - [\mathrm{D}]_0) + K + \sqrt{K^2 + 16K[\mathrm{D}]_0}}{8([\mathrm{D}] - [\mathrm{D}]_0) - K + \sqrt{K^2 + 16K[\mathrm{D}]_0}}\right) = k_{-1}\sqrt{K^2 + 16K[\mathrm{D}]_0}.t$$

This expression is a linear equation of the form, $y = mx + c$, and therefore if…

$$\ln\left(\frac{-8([\mathrm{D}] - [\mathrm{D}]_0) + K + \sqrt{K^2 + 16K[\mathrm{D}]_0}}{8([\mathrm{D}] - [\mathrm{D}]_0) - K + \sqrt{K^2 + 16K[\mathrm{D}]_0}}\right)$$

…is graphed against time, k_{-1} can be obtained using the value for m obtained from the linear equation, $y = mx + c$, provided with the trend-line in Excel, with m representing the experimental rate constant, k.

$$k_{-1}\sqrt{K^2 + 16K[\mathrm{D}]_0} = k \therefore\ k_{-1} = \frac{k}{\sqrt{K^2 + 16K[\mathrm{D}]_0}}$$

k_1 may be obtained using the k_{-1} value and the experimentally obtained K value…

$$k_1 = k_{-1}.K$$

10.6 The proposed acid- and base-catalysed reaction mechanisms

10.7 The DHA dimer dissociation without catalysis

10.7.1 Zeroth, first and second order graphs

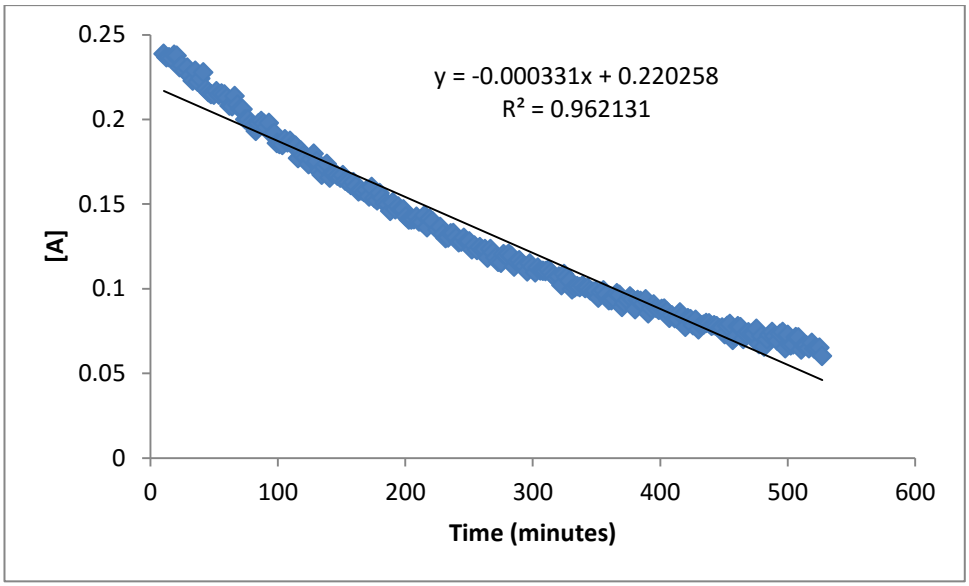

A1: Zeroth order plot for the uncatalysed DHA dimer dissociation in DMSO-*d6*: reaction # 2

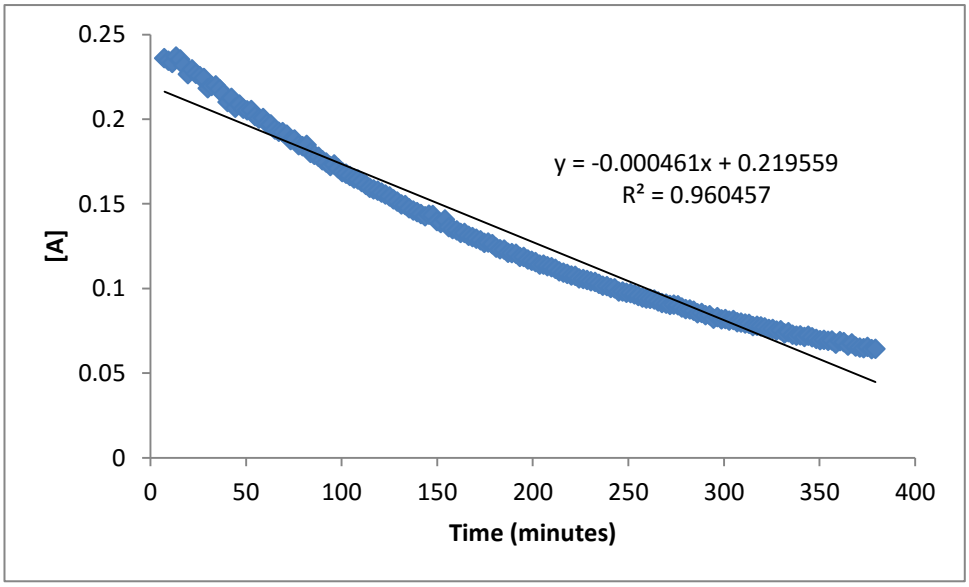

A2: Zeroth order plot for the uncatalysed DHA dimer dissociation in DMSO-*d6*: reaction # 3

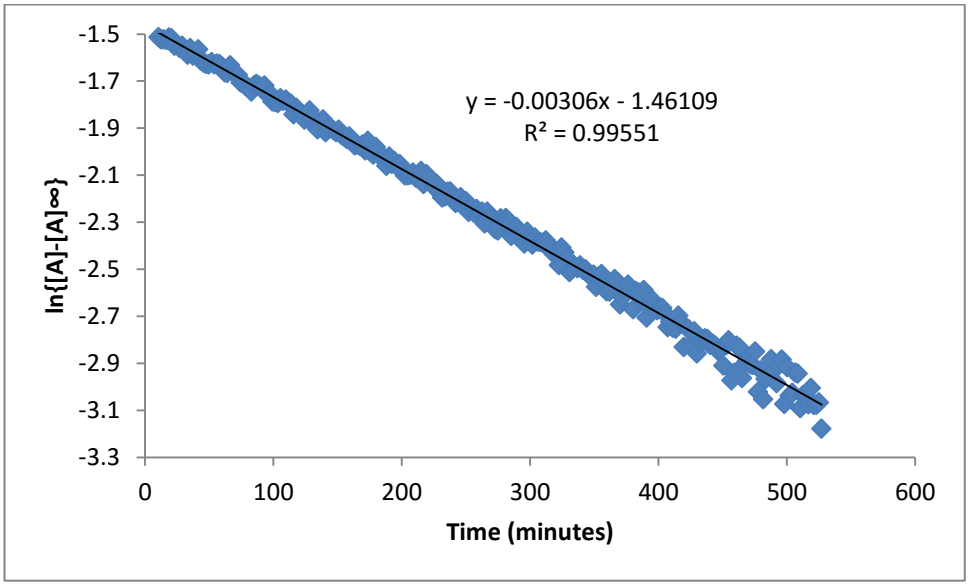

A3: First order plot for the uncatalysed DHA dimer dissociation in DMSO-*d6*: reaction # 2

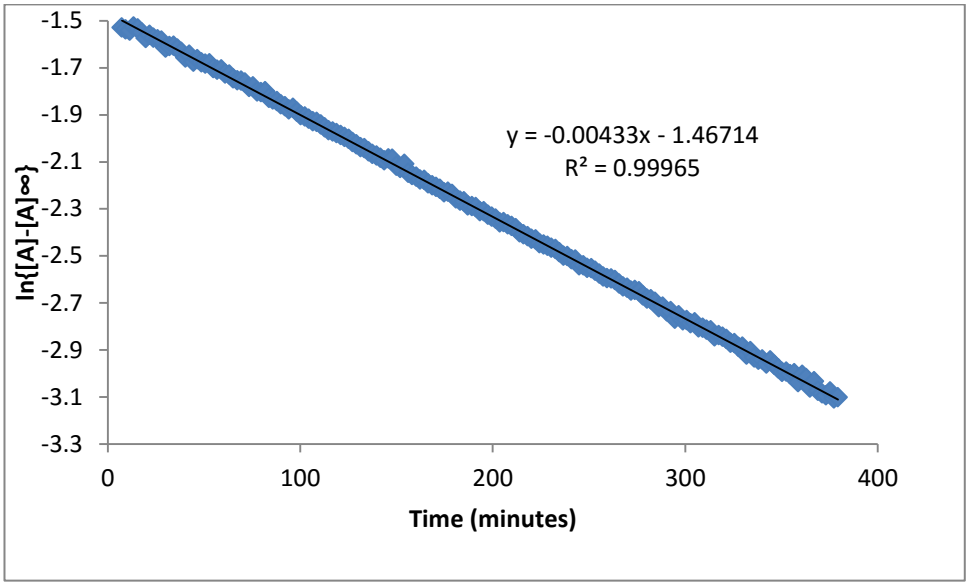

A4: First order plot for the uncatalysed DHA dimer dissociation in DMSO-*d6*: reaction # 3

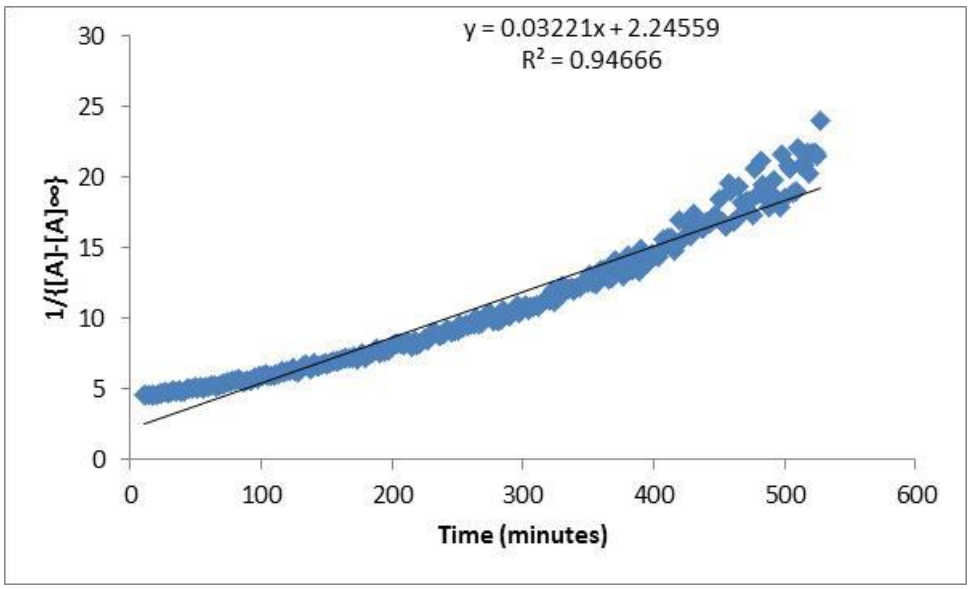

A5: Second order plot for the uncatalysed DHA dimer dissociation in DMSO-*d6*: reaction # 2

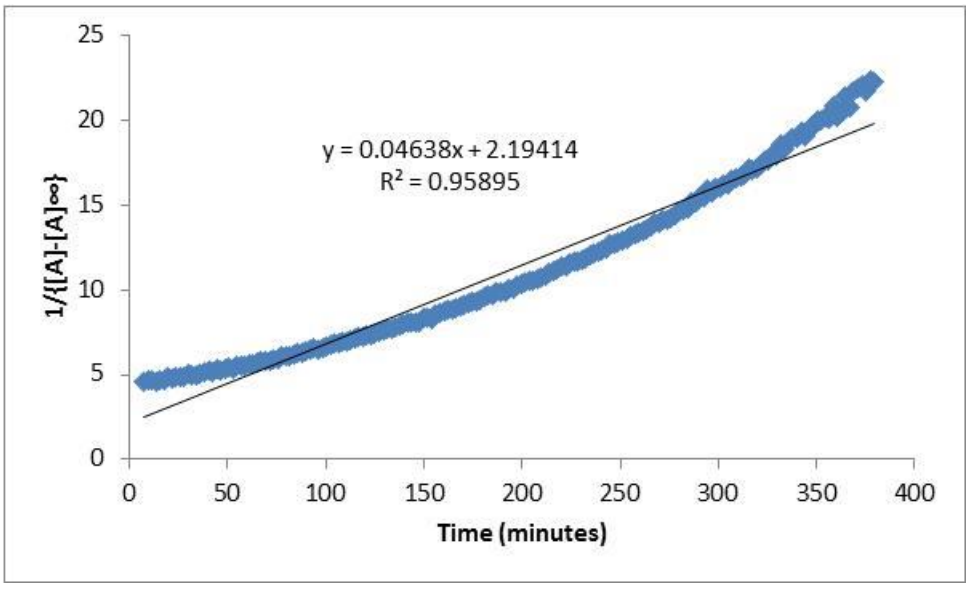

A6: Second order plot for the uncatalysed DHA dimer dissociation in DMSO-*d6*: reaction # 3

10.7.2 The graphs obtained using the second order reversible reaction rate expression

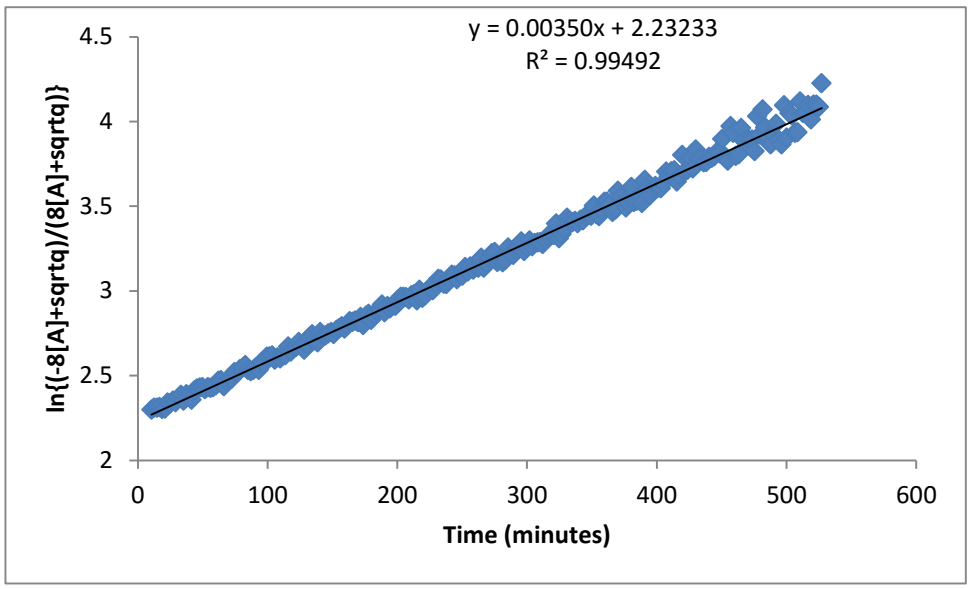

A7 : DHA dimer dissociation in DMSO-d6 processed using the second order rate expression: reaction #2

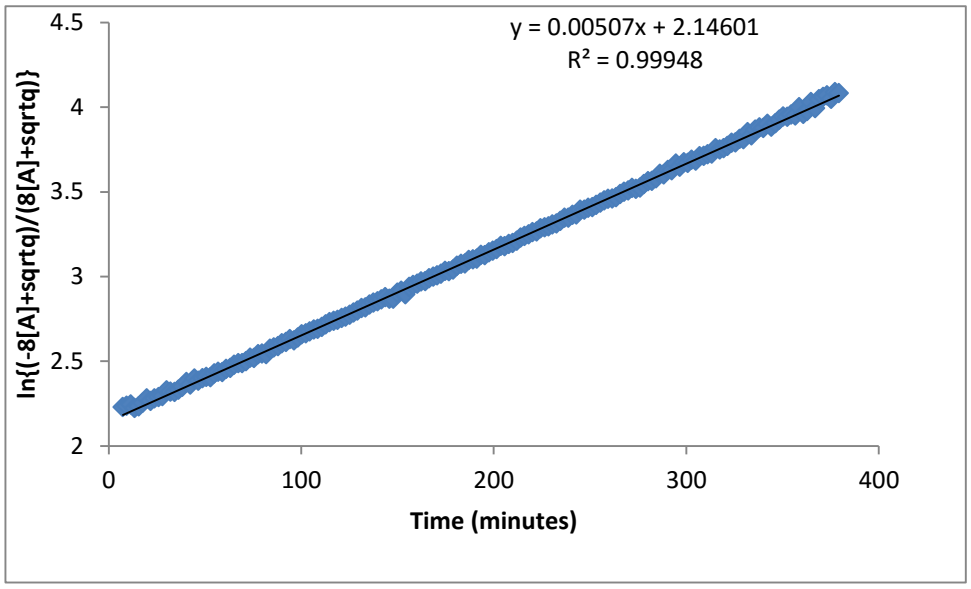

A8: DHA dimer dissociation in DMSO-d6 processed using the second order rate expression: reaction #3

10.8 The DHA dimer dissociation with D_2O catalysis

10.8.1 The first order graphs for the D_2O catalysed DHA dissociation in DMSO-*d6*

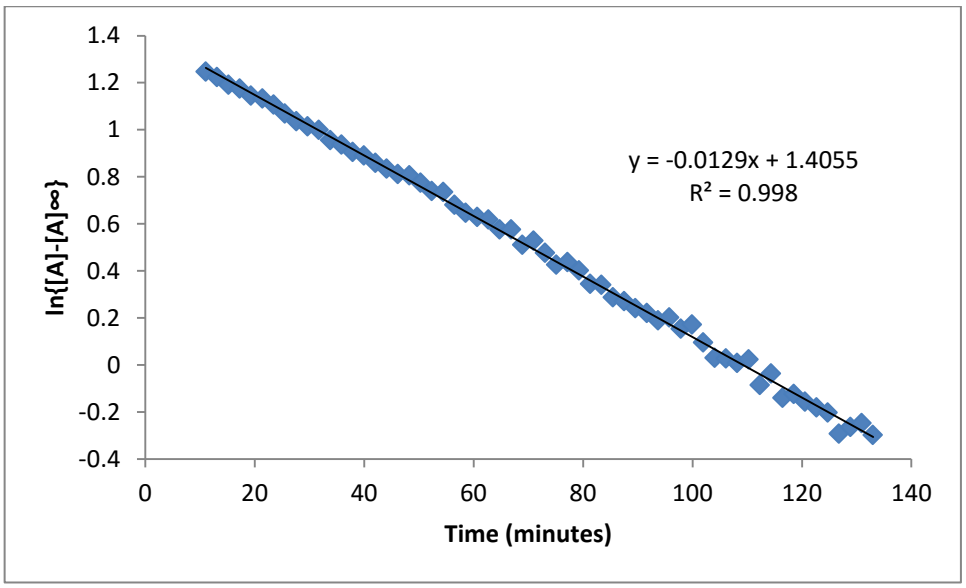

A9: The first order graph for ln concentration against time with a D_2O concentration of 2.00 mol%

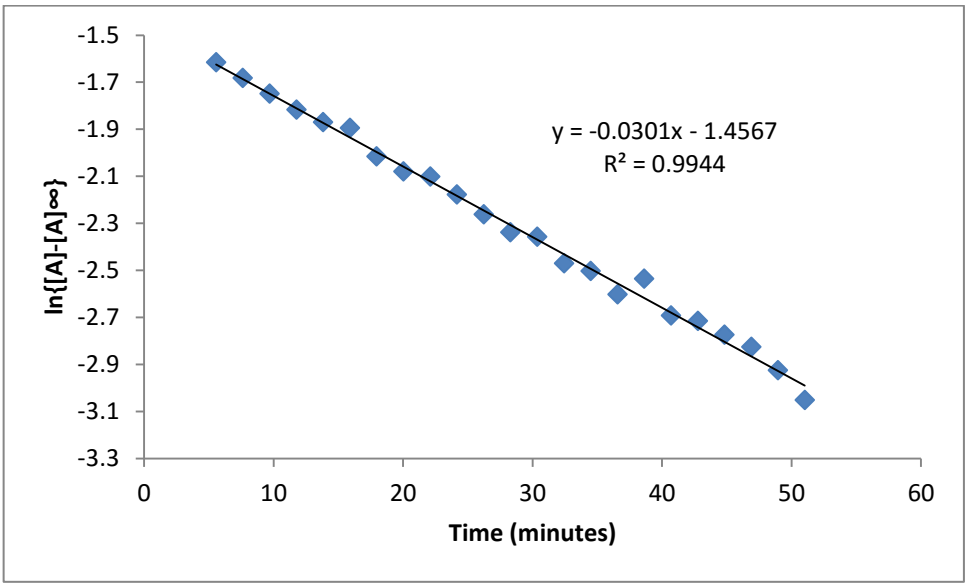

A10: The first order graph for ln concentration against time with a D_2O concentration of 5.00 mol%

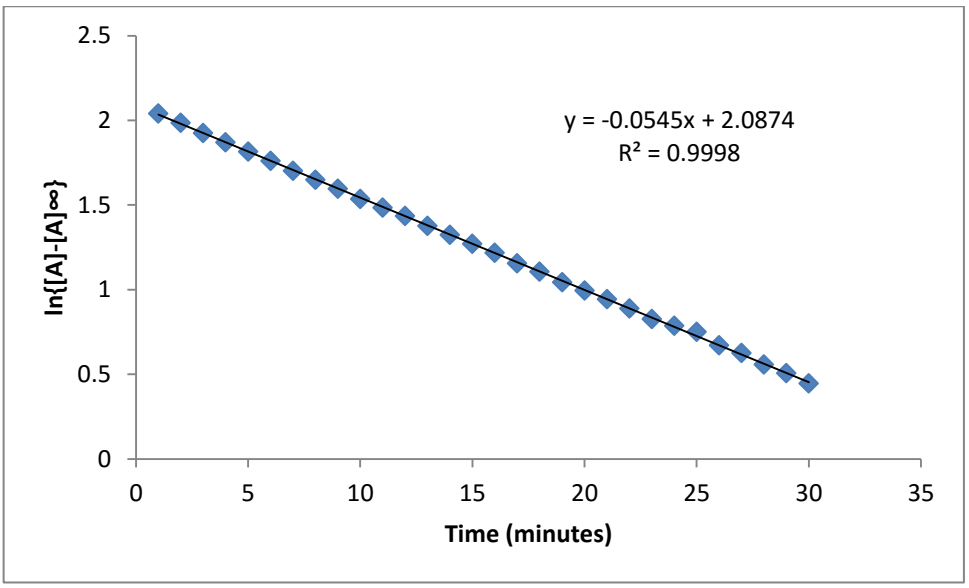

A11: The first order graph for ln concentration against time with a D_2O concentration of 5.58 mol%

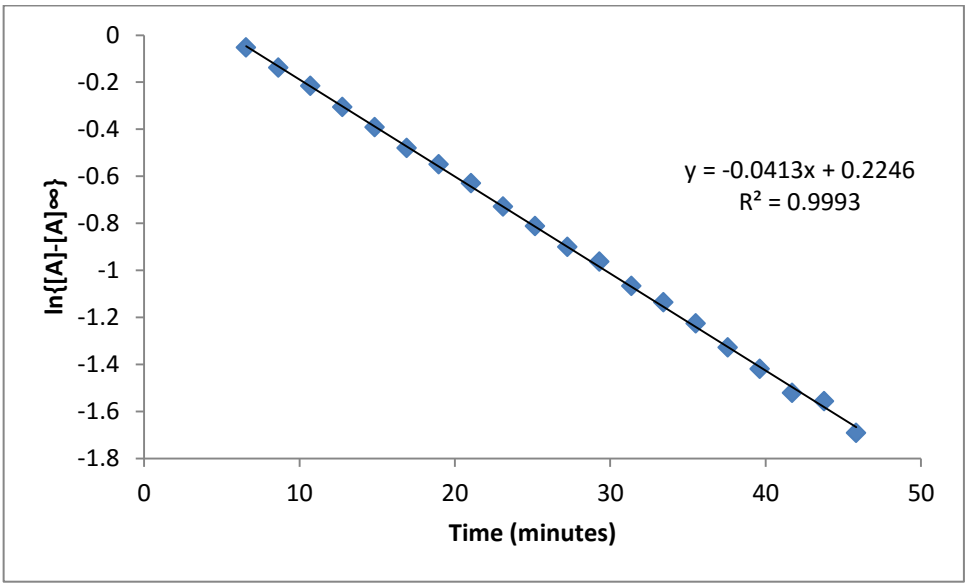

A12: The first order graph for ln concentration against time with a D_2O concentration of 9.90 mol%

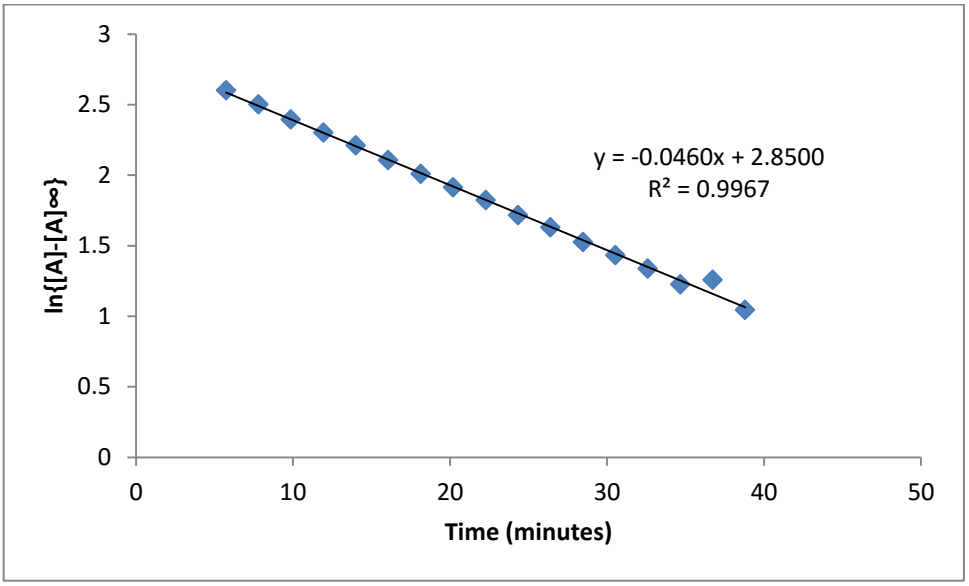

A13: The first order graph for ln concentration against time with a D_2O concentration of 9.90 mol%

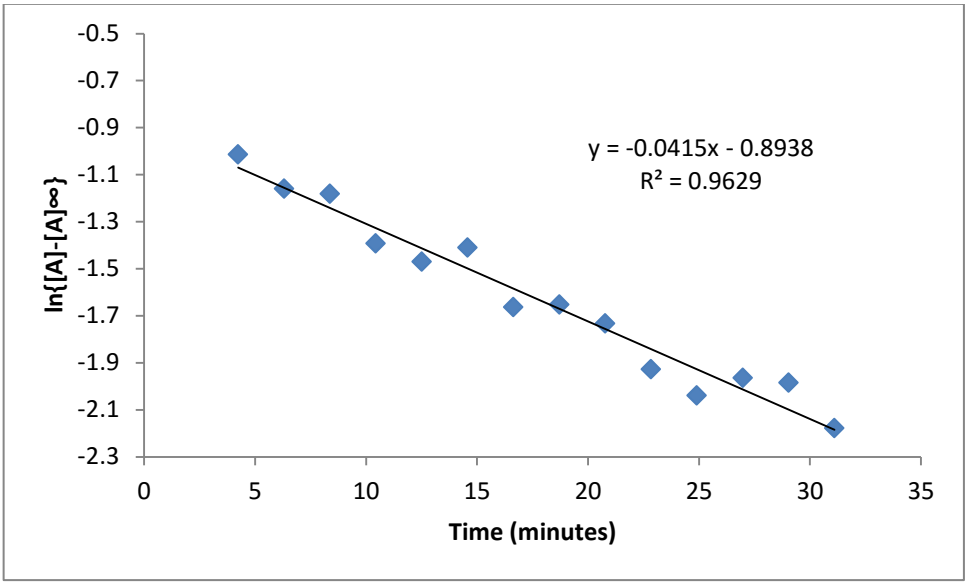

A14: The first order graph for ln concentration against time with a D_2O concentration of 14.9 mol%

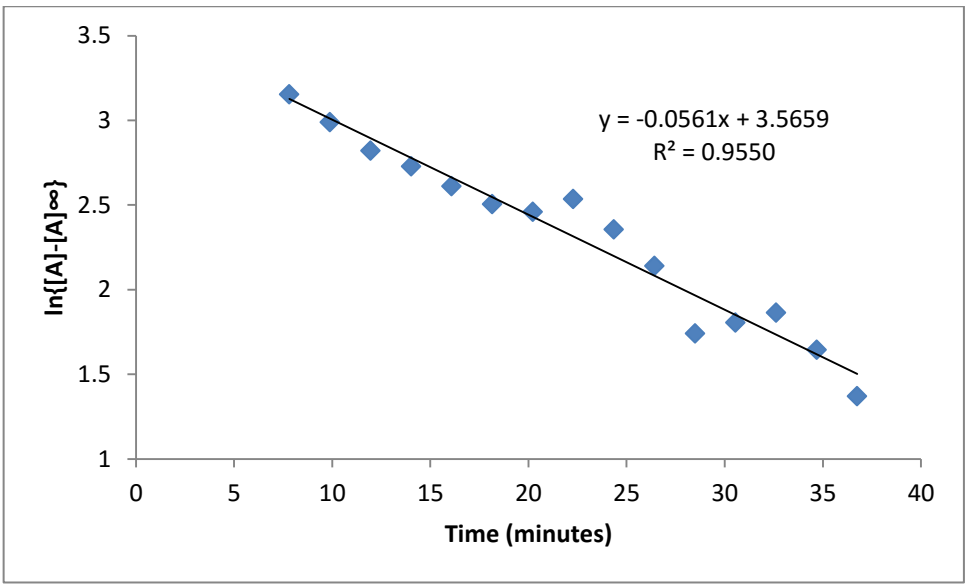

A15: The first order graph for ln concentration against time with a D_2O concentration of 14.9 mol%

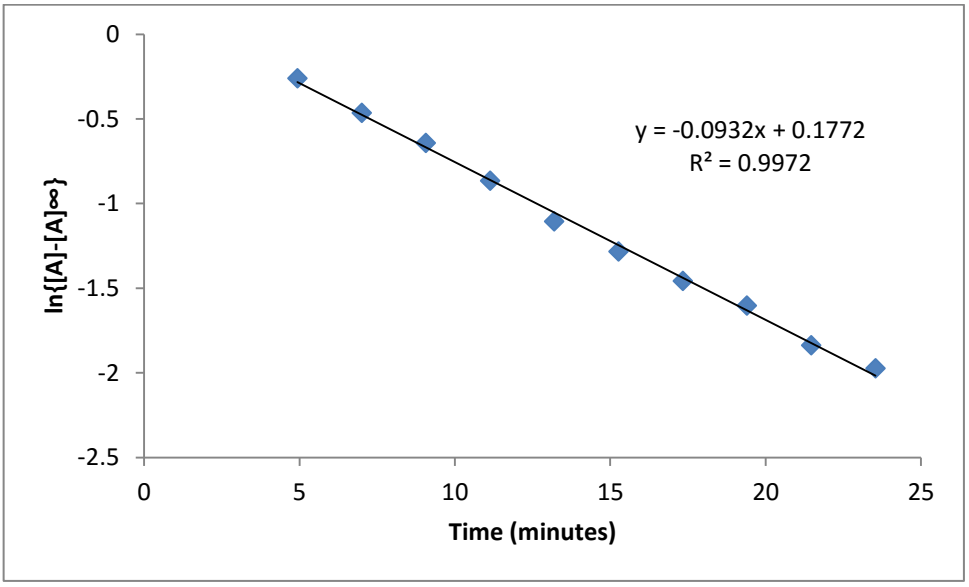

A16: The first order graph for ln concentration against time with a D_2O concentration of 19.8 mol%

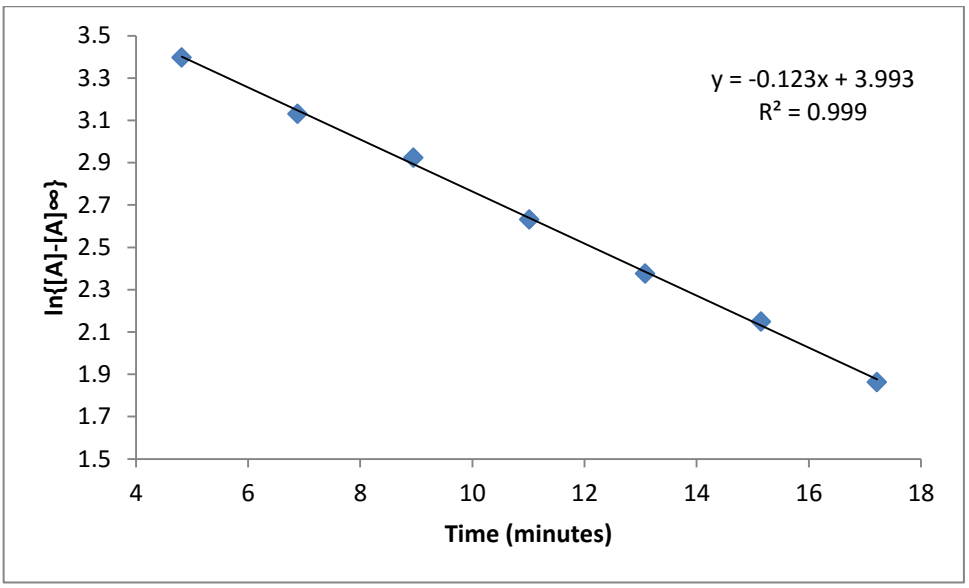

A17: The first order graph for ln concentration against time with a D_2O concentration of 19.9 mol%

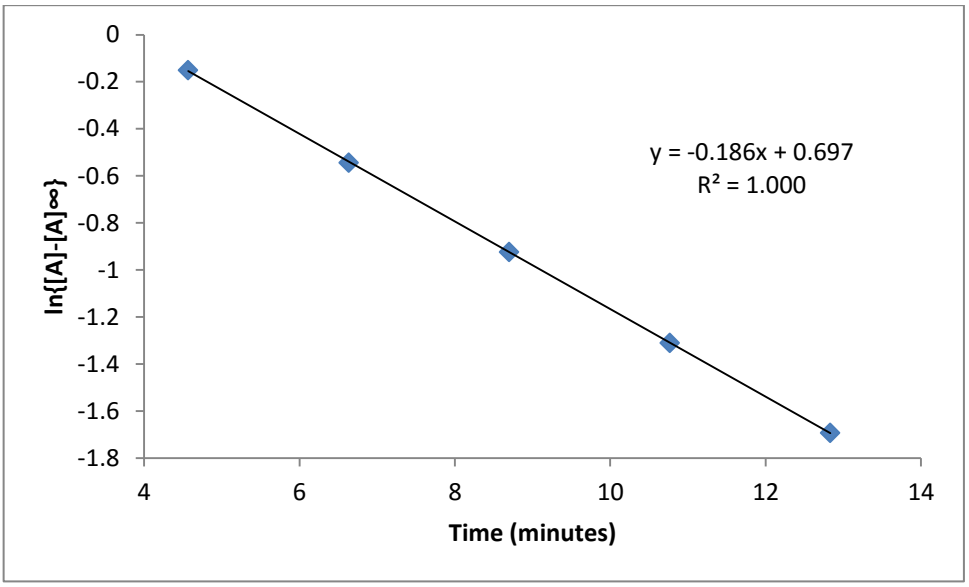

A18: The first order graph for ln concentration against time with a D_2O concentration of 24.9 mol%

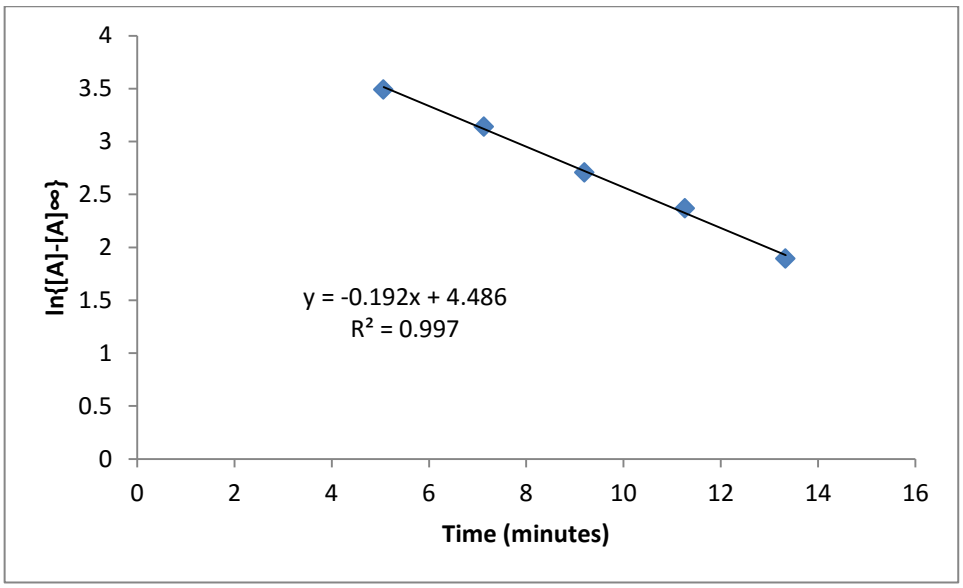

A19: The first order graph for ln concentration against time with a D_2O concentration of 25.0 mol%

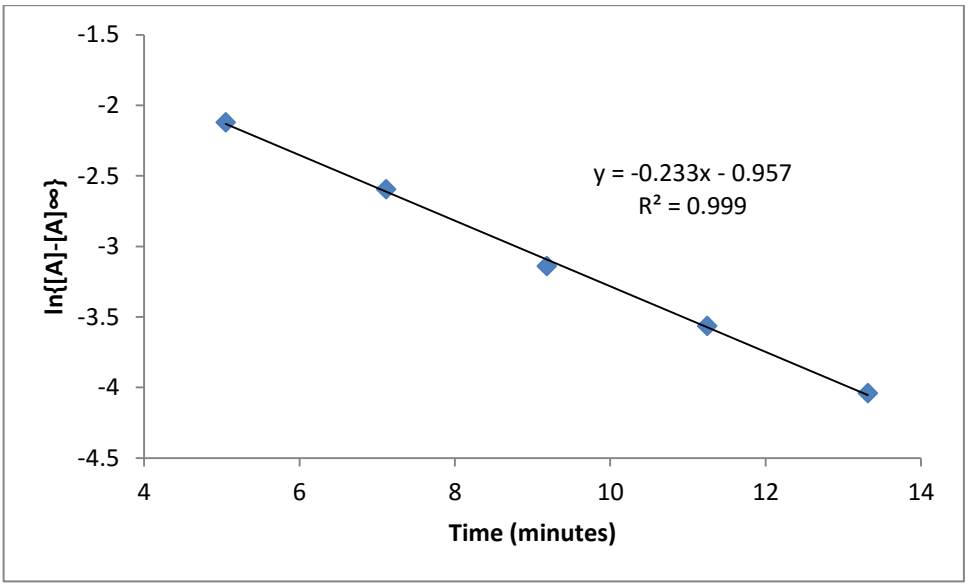

A20: The first order graph for ln concentration against time with a D_2O concentration of 29.6 mol%

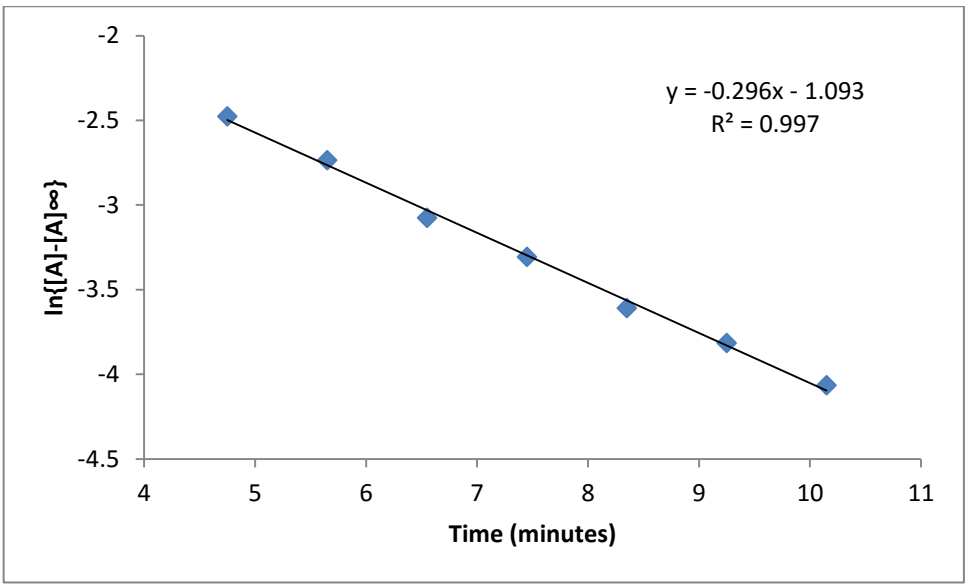

A21: The first order graph for ln concentration against time with a D_2O concentration of 29.9 mol%

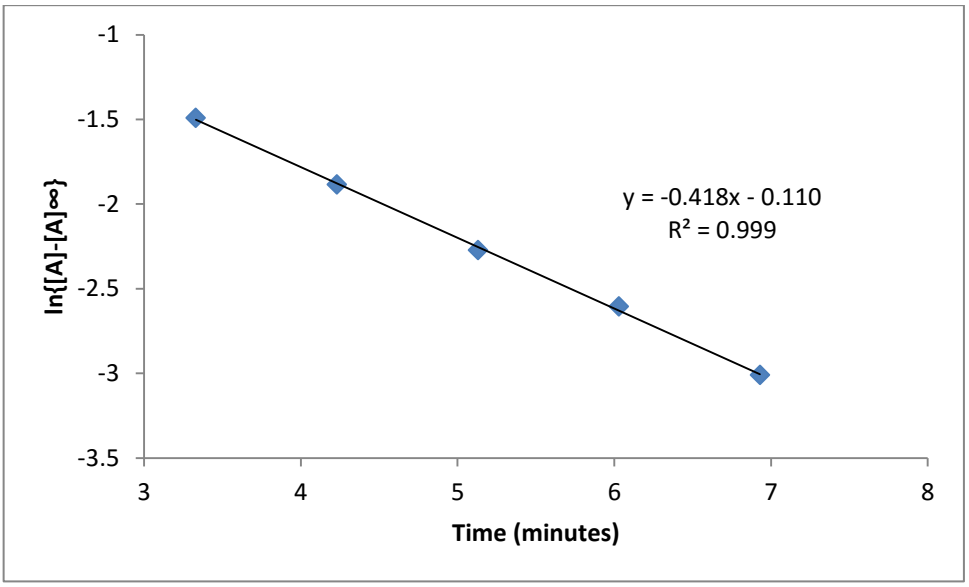

A22: The first order graph for ln concentration against time with a D_2O concentration of 34.3 mol%

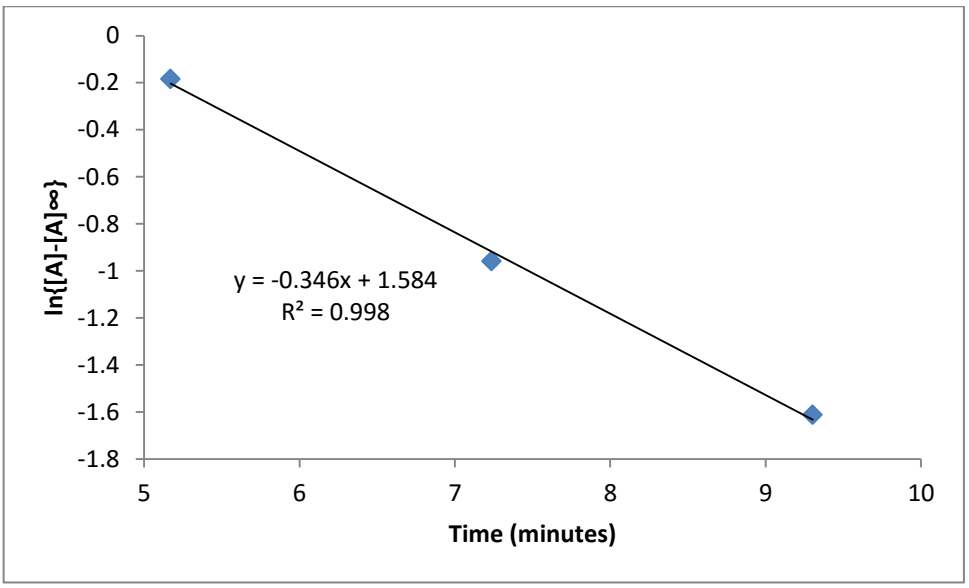

A23: The first order graph for ln concentration against time with a D_2O concentration of 34.6 mol%

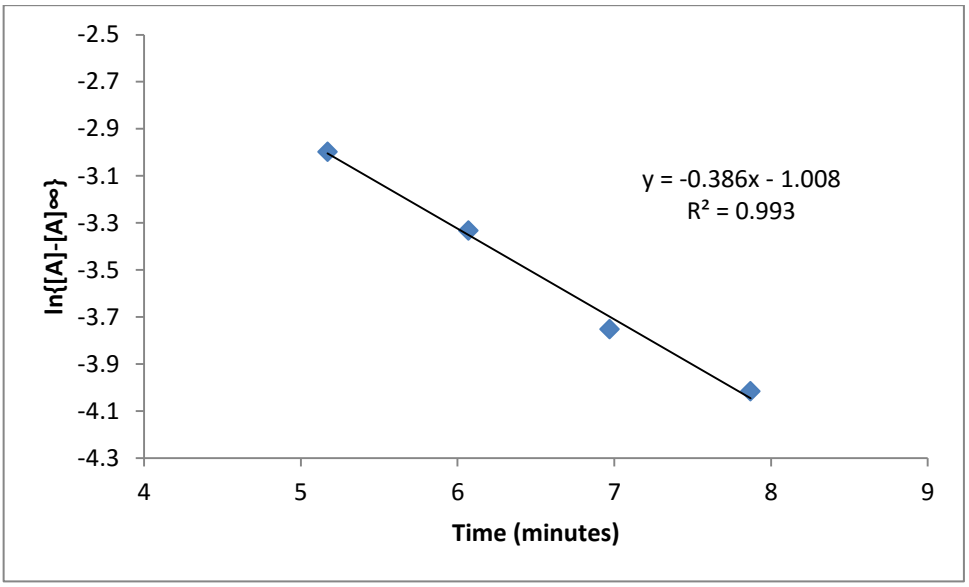

A24: The first order graph for ln concentration against time with a D_2O concentration of 39.0 mol%

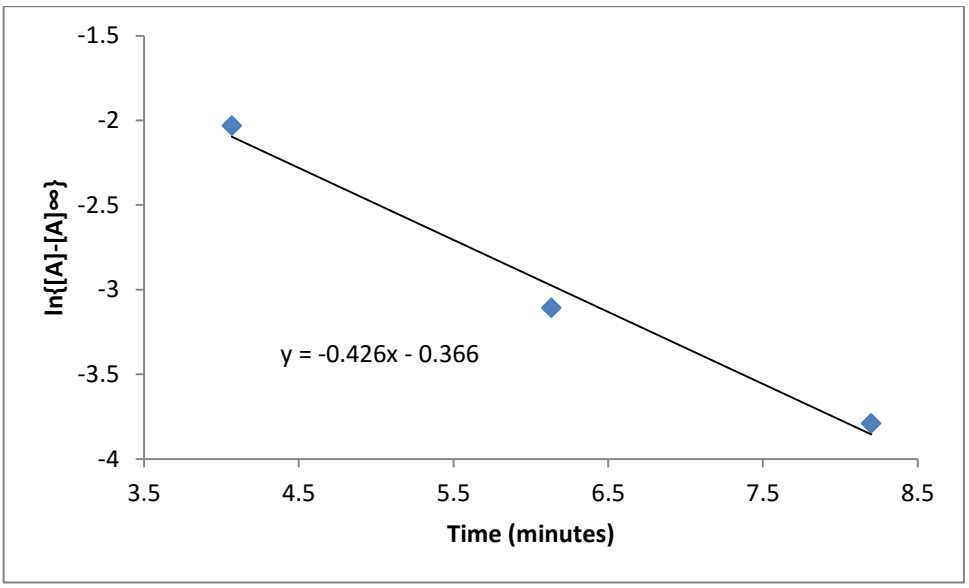

A25: The first order graph for ln concentration against time with a D_2O concentration of 39.1 mol%

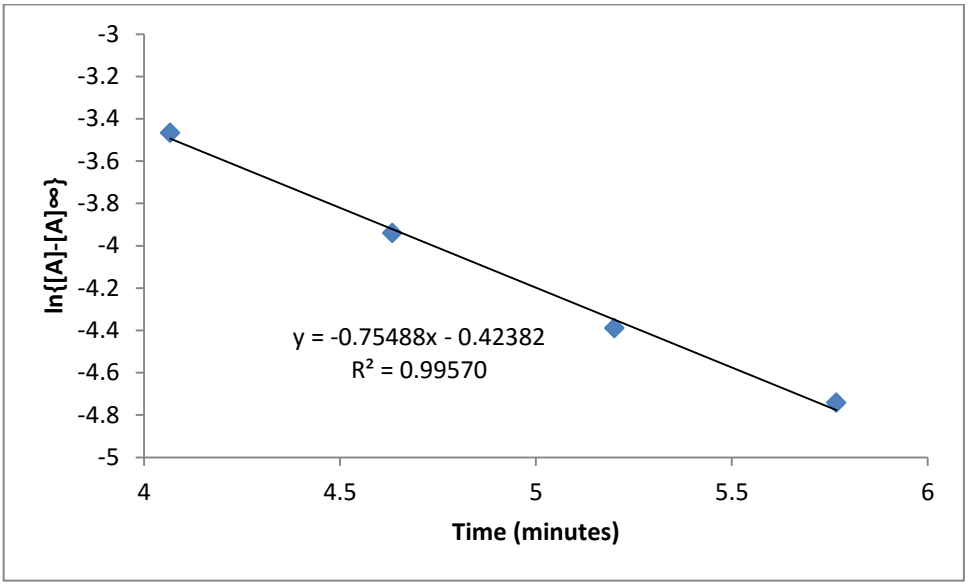

A26: The first order graph for ln concentration against time with a D_2O concentration of 44.5 mol%

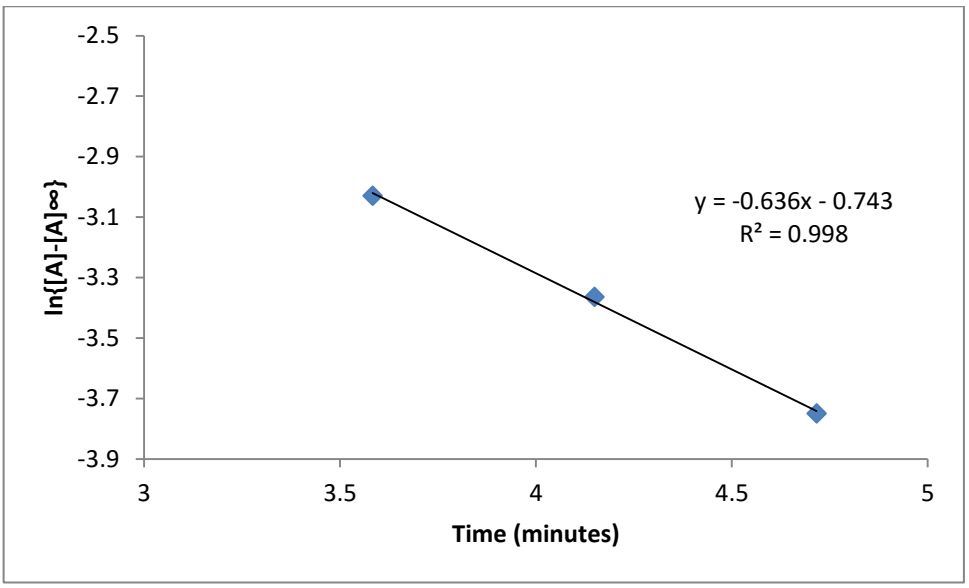

A27: The first order graph for ln concentration against time with a D_2O concentration of 44.6 mol%

10.9 The DHA dimer dissociation with CD_3COOD catalysis

10.9.1 The graphs for the DHA dimer dissociation in DMSO-*d6* catalysed with CD_3COOD

10.9.1.1 The first order graphs for the DHA dimer dissociation in DMSO-*d6* catalysed with CD_3COOD

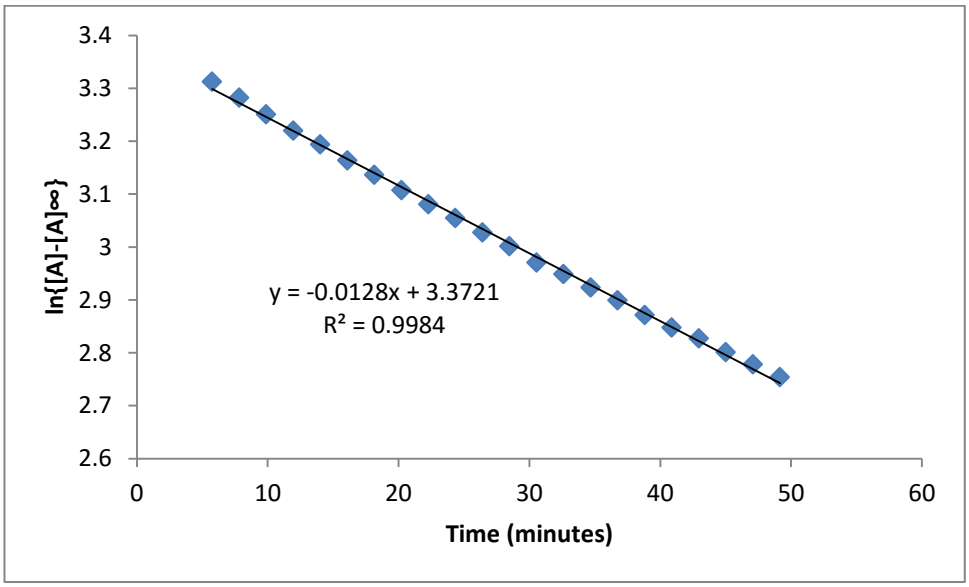

A28: First order graph for the DHA dimer dissociation in DMSO-d6 catalysed with 9.51 mol% CD_3COOD

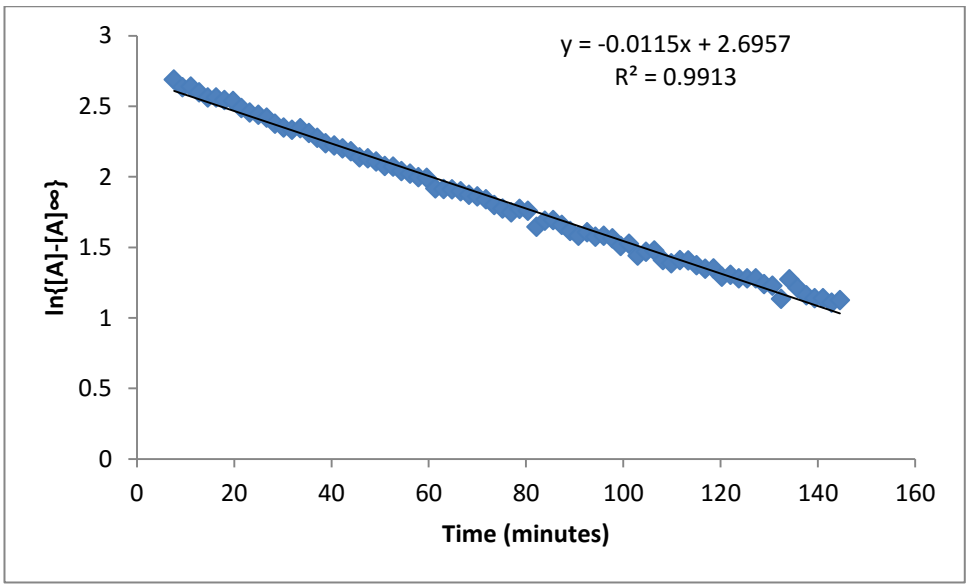

A29: First order graph for the DHA dimer dissociation in DMSO-d6 catalysed with 18.2 mol% CD_3COOD

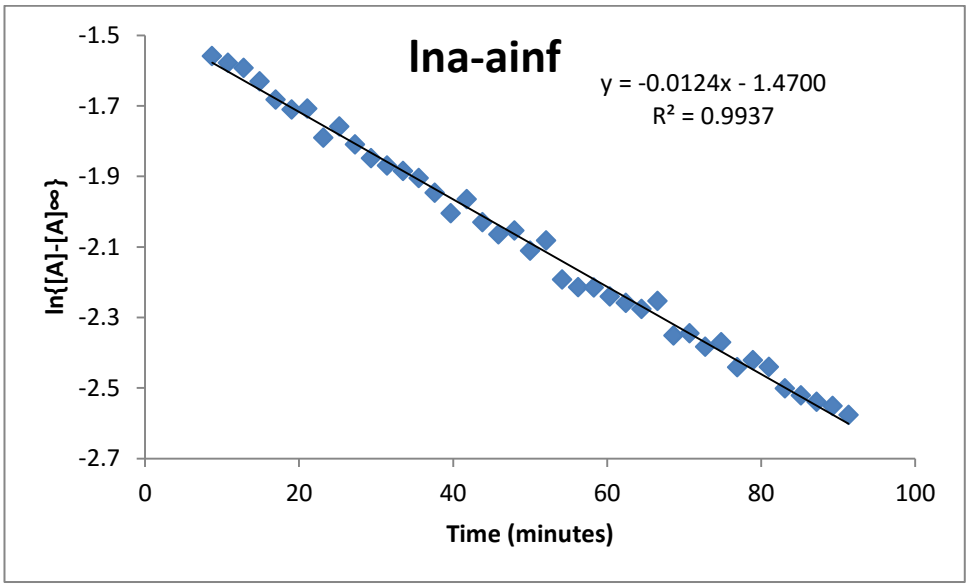

A30: First order graph for the DHA dimer dissociation in DMSO-d6 catalysed with 18.2 mol% CD3COOD

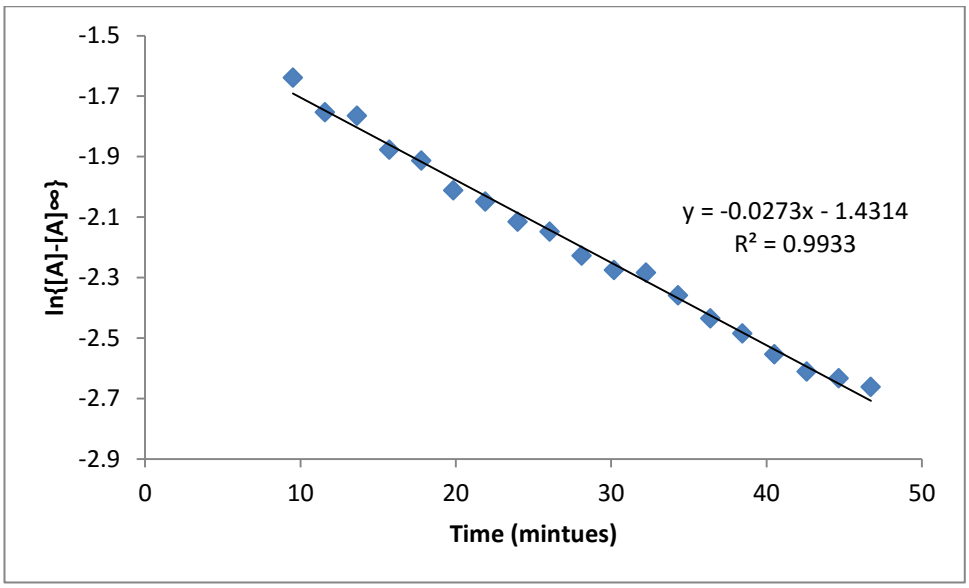

A31: First order graph for the DHA dimer dissociation in DMSO-d6 catalysed with 31.3 mol% CD3COOD

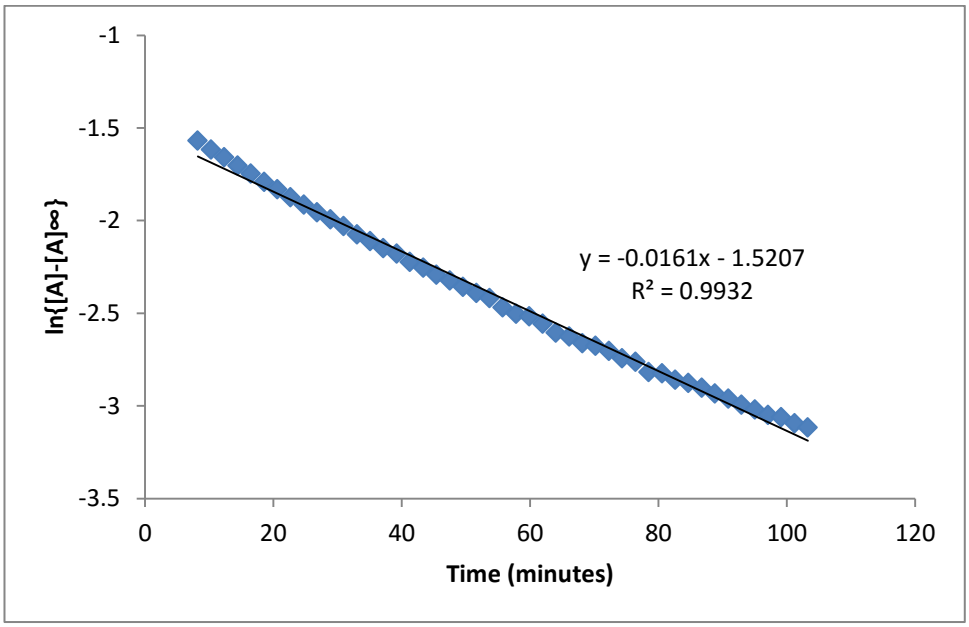

A32: First order graph for the DHA dimer dissociation in DMSO-d6 catalysed with 32.1 mol% CD3COOD

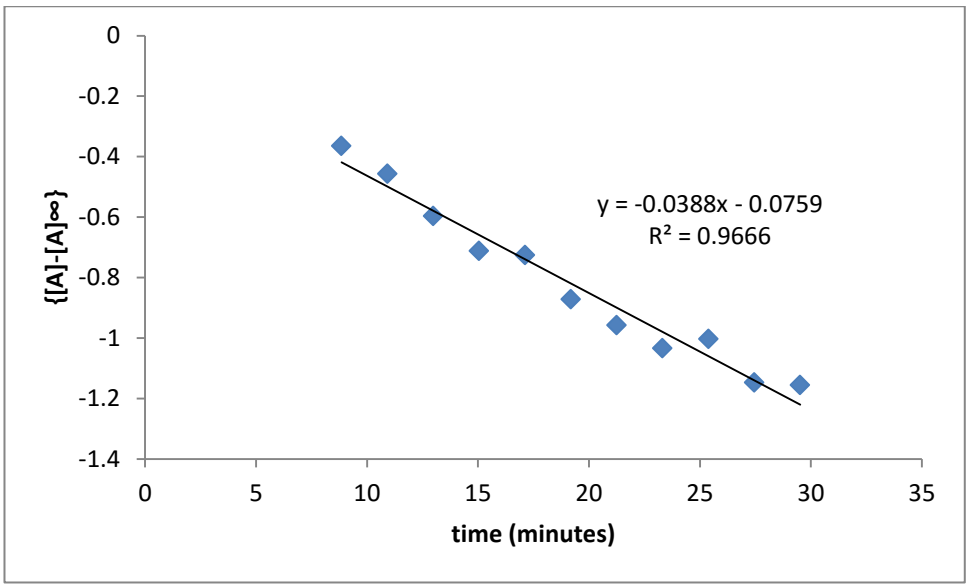

A33: First order graph for the DHA dimer dissociation in DMSO-d6 catalysed with 51.1 mol% CD3COOD

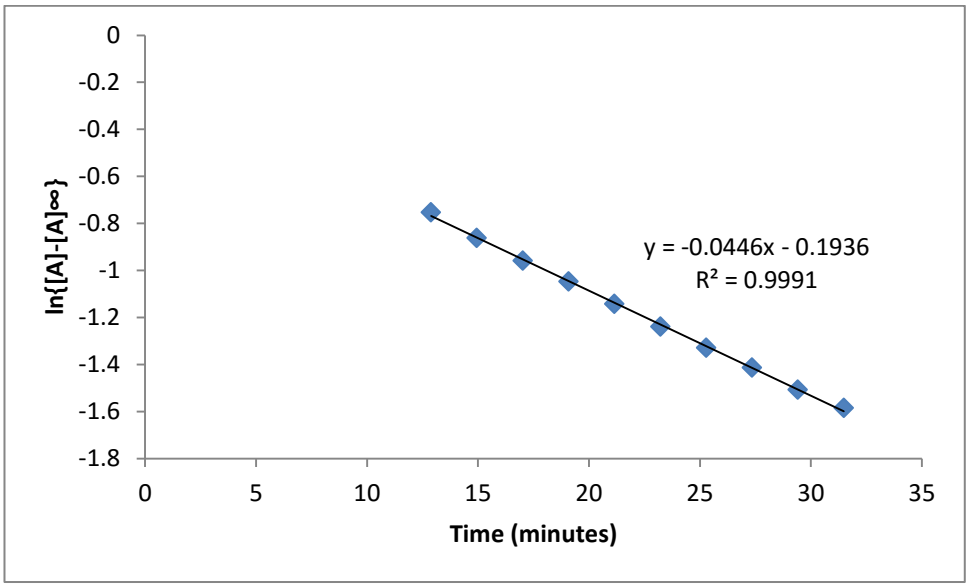

A34 First order graph for the DHA dimer dissociation in DMSO-d6 catalysed with 51.7 mol% CD3COOD

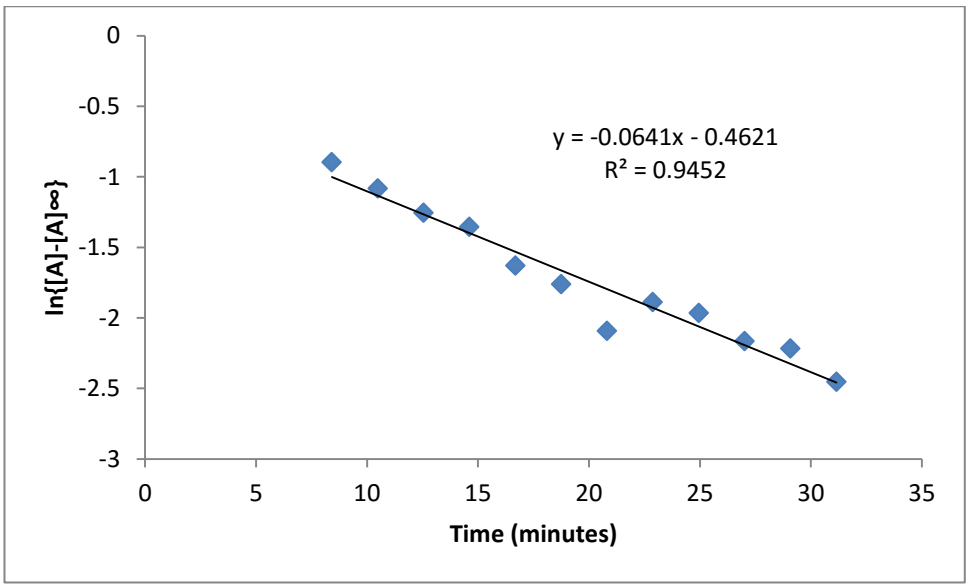

A35: First order graph for the DHA dimer dissociation in DMSO-d6 catalysed with 57.1 mol% CD3COOD

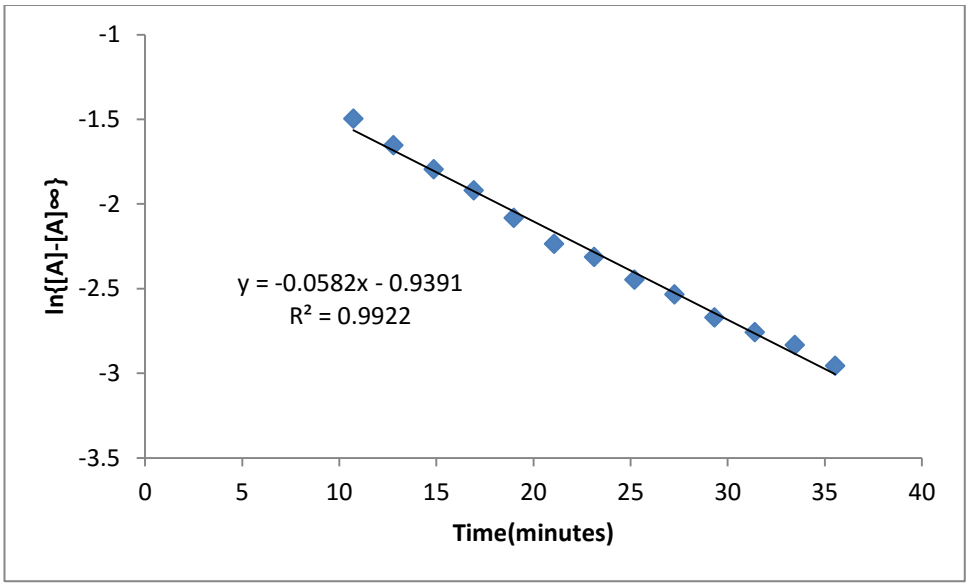

A36: First order graph for the DHA dimer dissociation in DMSO-d6 catalysed with 58.4 mol% CD3COOD

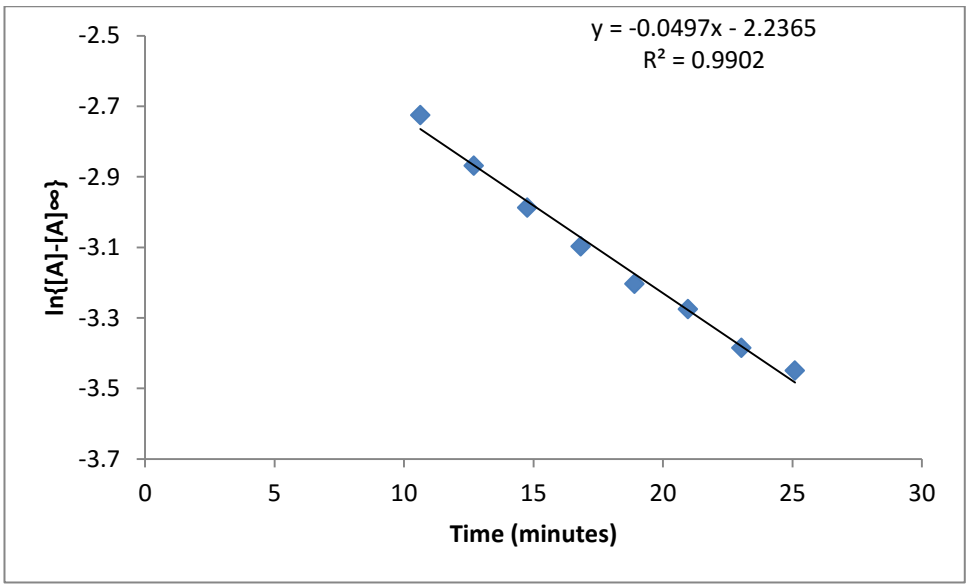

A37: First order graph for the DHA dimer dissociation in DMSO-d6 catalysed with 65.0 mol% CD3COOD

10.9.2 The graphs for the formation of Int#1 in DMSO-*d6* catalysed with CD_3COOD

10.9.2.1 The zeroth, first and second order graphs for the formation of Int#1 in DMSO-*d6* catalysed with CD_3COOD

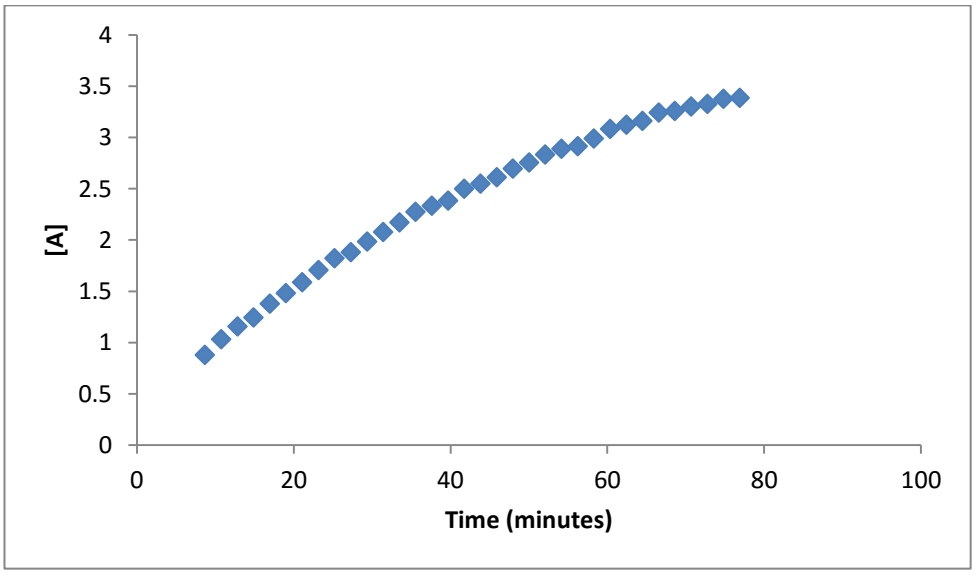

A38: The zeroth order graph for the formation of Int#1 in DMSO-d6 catalysed with CD3COOD

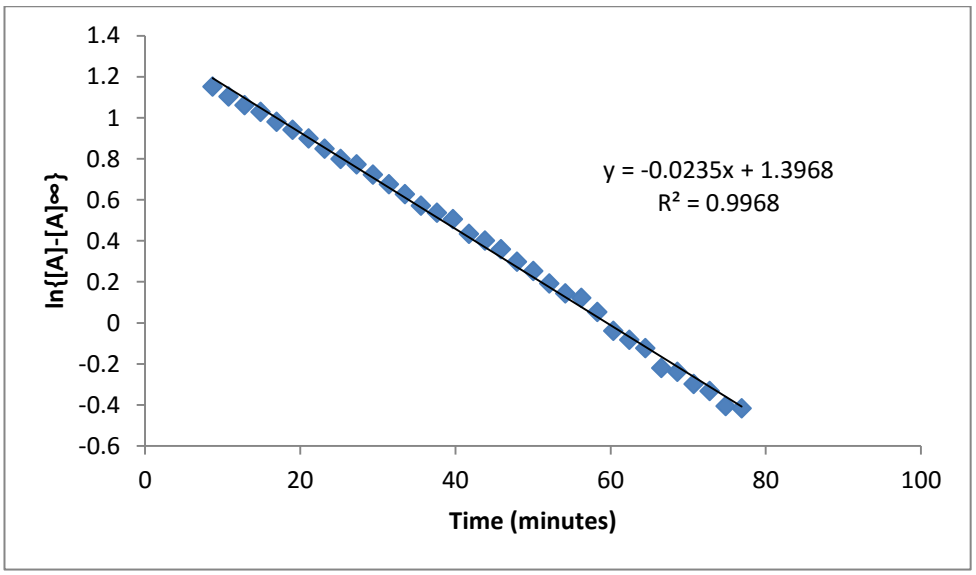

A39: The first order graph for the formation of Int#1 in DMSO-d6 catalysed with CD3COOD

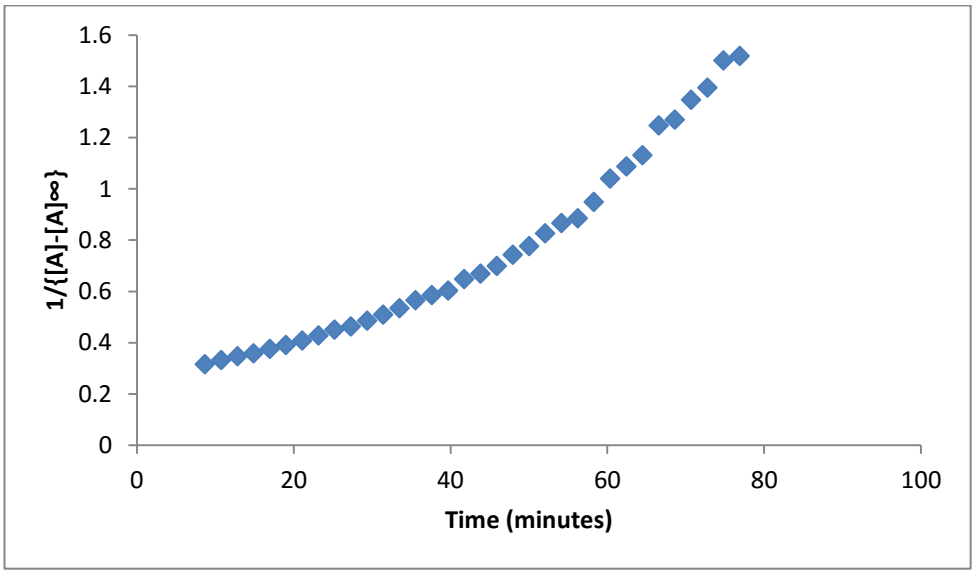

A40: The second order graph for the formation of Int#1 in DMSO-d6 catalysed with CD3COOD

10.9.2.2 The first order graphs for the formation of Int#1 in DMSO-*d6* catalysed with CD_3COOD

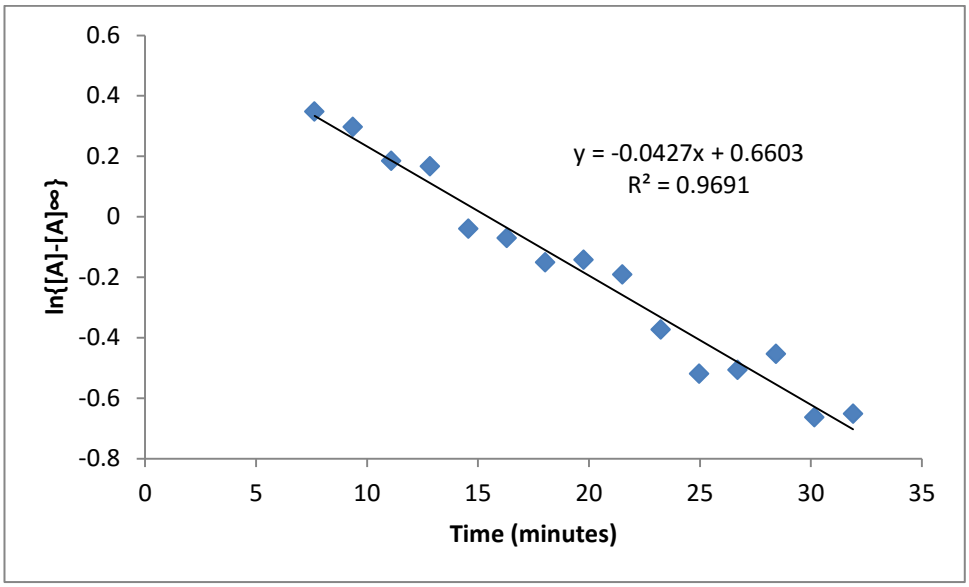

A41: The first order graph for the formation of Int#1 in DMSO-d6 catalysed with 18.2 mass% CD3COOD

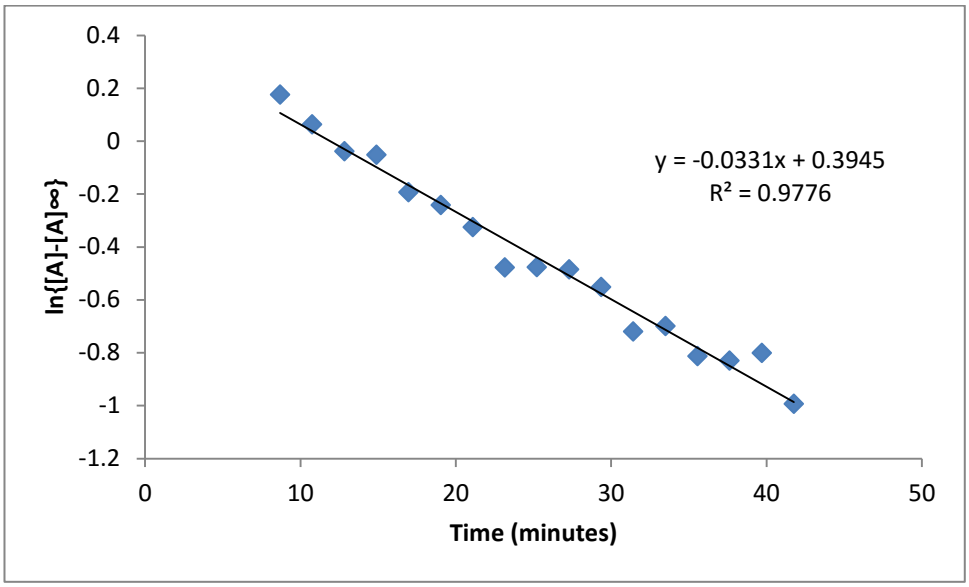

A42: The first order graph for the formation of Int#1 in DMSO-d6 catalysed with 18.2 mass% CD3COOD

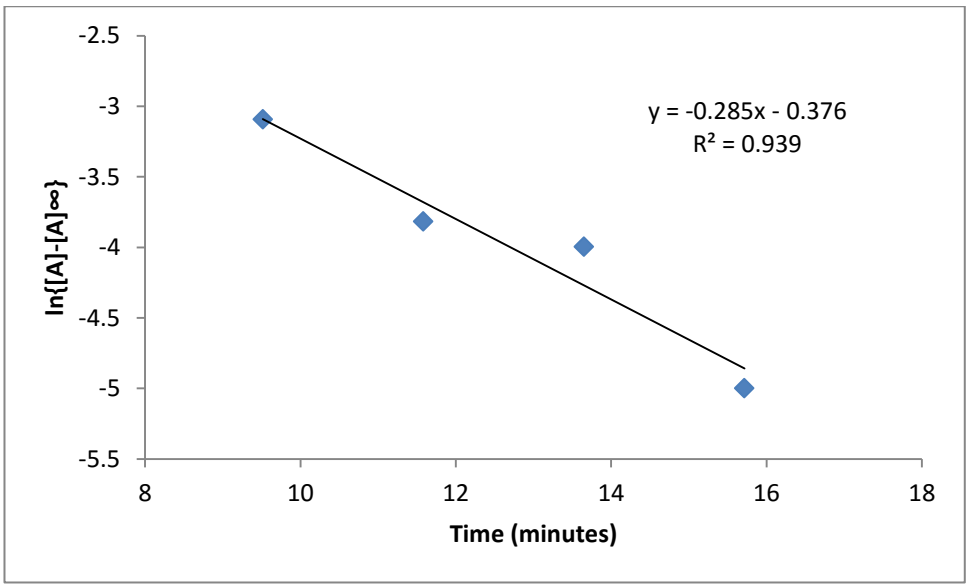

A43: The first order graph for the formation of Int#1 in DMSO-d6 catalysed with 31.3 mass% CD3COOD

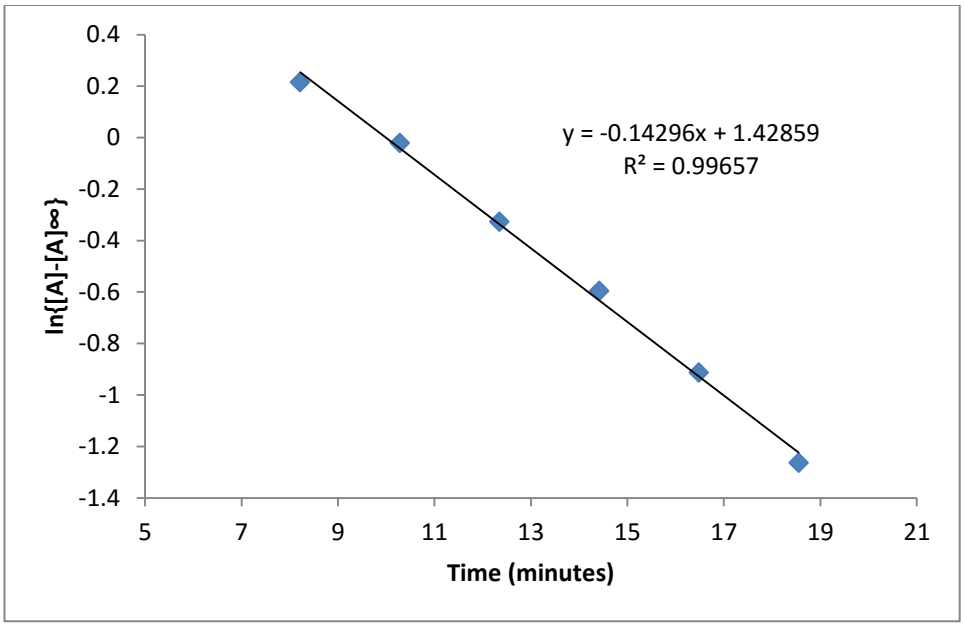

A44: The first order graph for the formation of Int#1 in DMSO-d6 catalysed with 32.1 mass% CD3COOD

10.9.3 The graphs for the formation of Int#2 in DMSO-*d6* catalysed with CD_3COOD

10.9.3.1 The zeroth, first and second order graphs for the formation of Int#2 in DMSO-*d6* catalysed with CD_3COOD

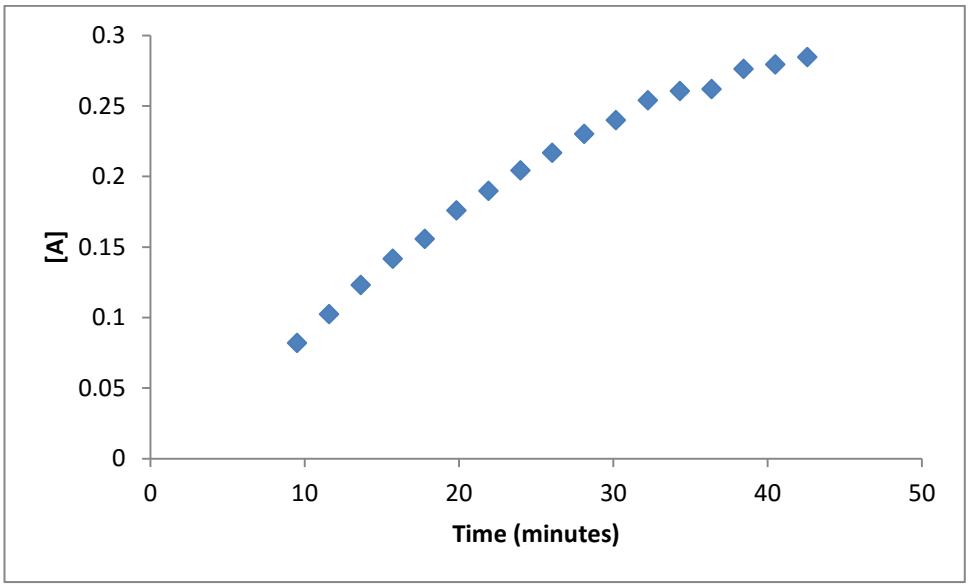

A45: The zeroth order graph for the formation of Int#2 in DMSO-d6 catalysed with CD3COOD

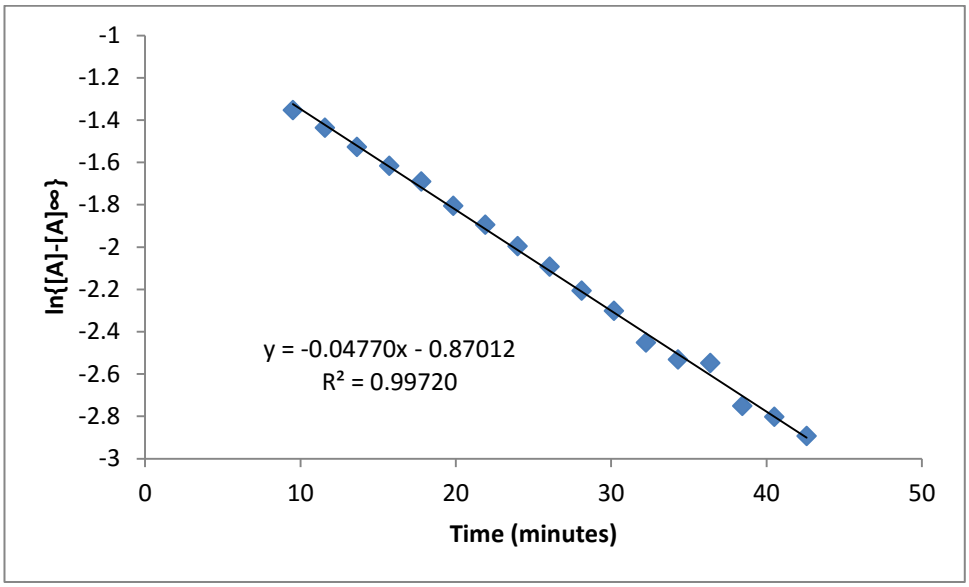

A46: The first order graph for the formation of Int#2 in DMSO-d6 catalysed with CD3COOD

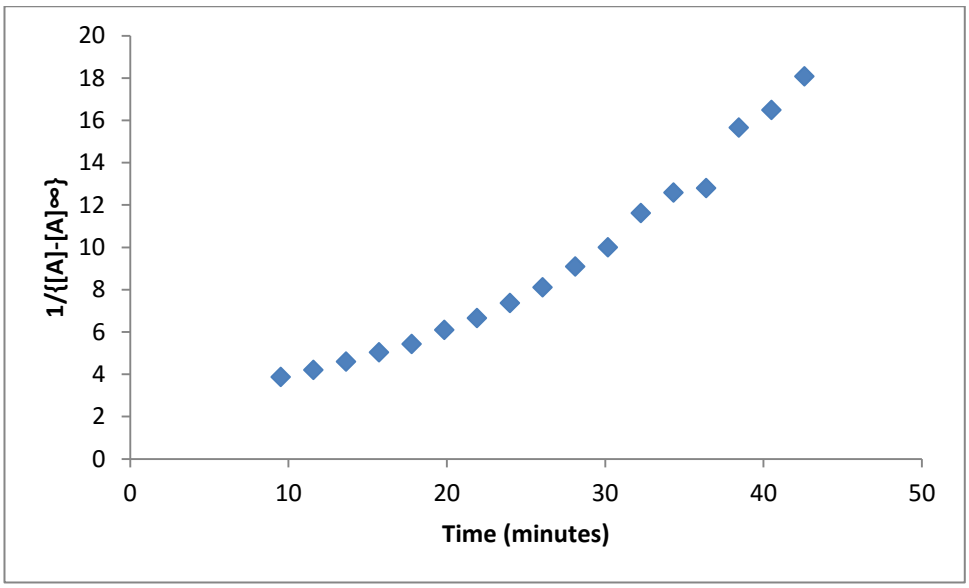

A47: The second order graph for the formation of Int#2 in DMSO-d6 catalysed with CD3COOD

10.9.3.2 The first order graphs for the formation of Int#2 in DMSO-*d6* catalysed with CD_3COOD

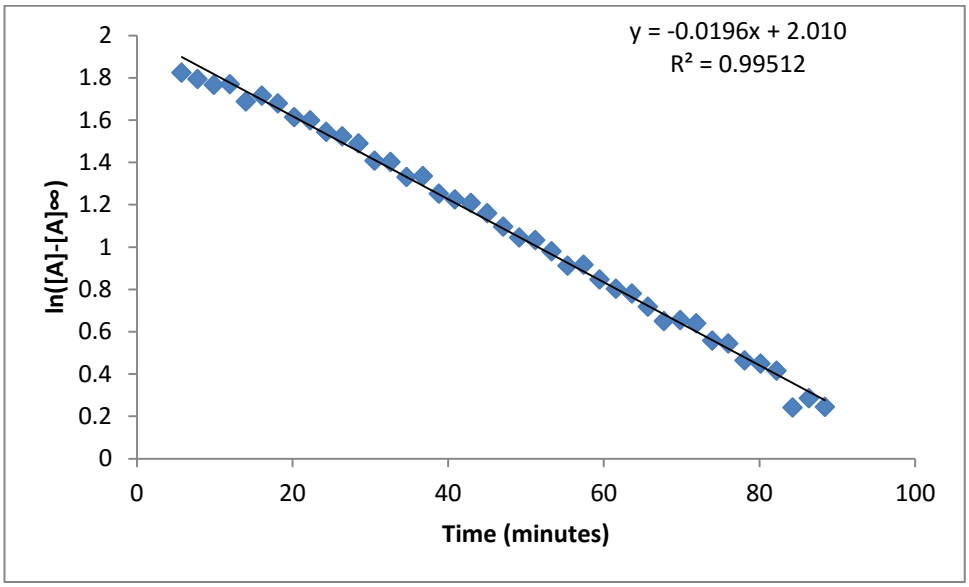

A48: First order graph for the formation of Int#2 in the dissociation reaction of DHA in DMSO-d6 catalysed with 9.51 mol% CD3COOD

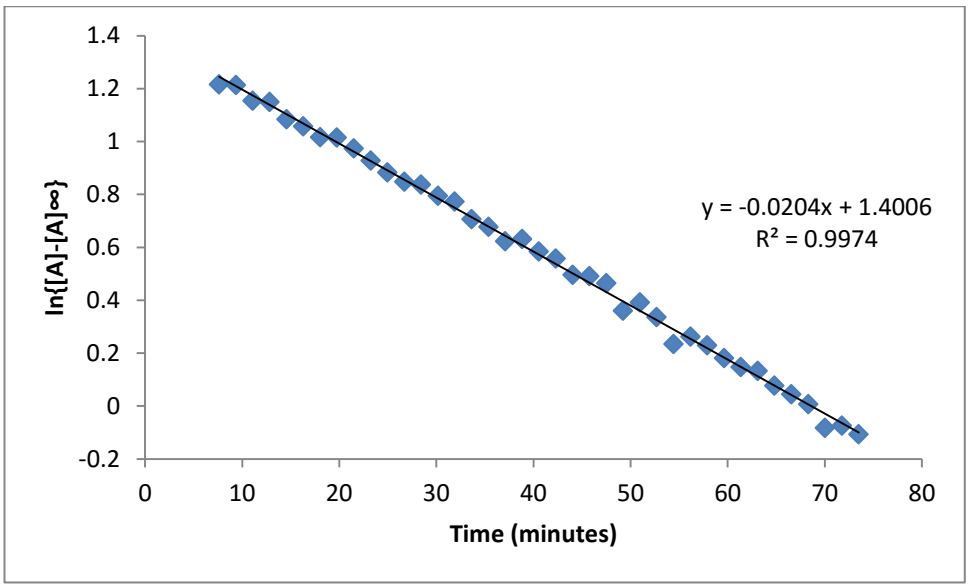

A49: First order graph for the formation of Int#2 in the dissociation reaction of DHA in DMSO-d6 catalysed with 18.2 mol% CD3COOD

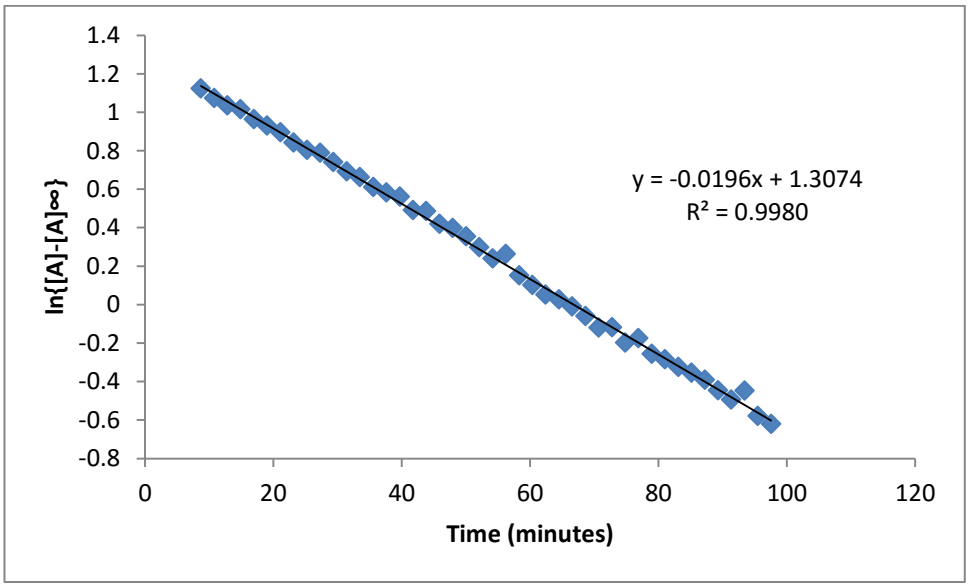

A50: First order graph for the formation of Int#2 in the dissociation reaction of DHA in DMSO-d6 catalysed with 18.2 mol% CD3COOD

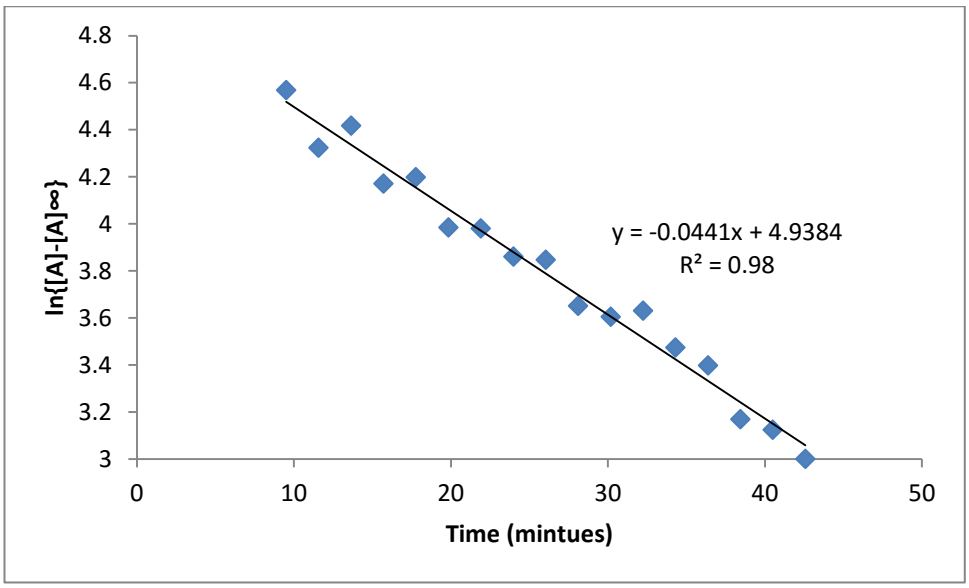

A51: First order graph for the formation of Int#2 in the dissociation reaction of DHA in DMSO-d6 catalysed with 31.3 mol% CD3COOD

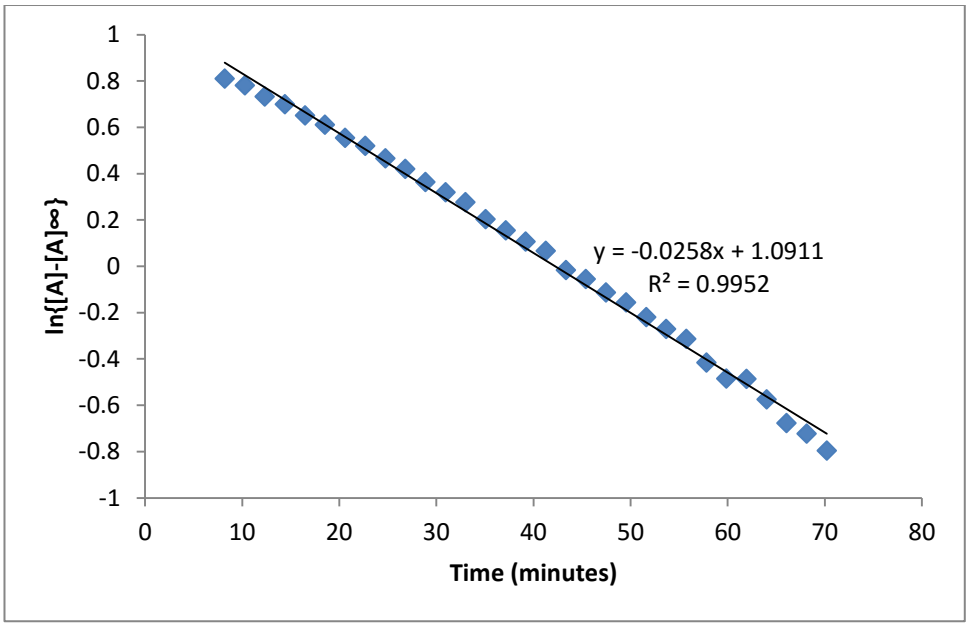

A52: First order graph for the formation of Int#2 in the dissociation reaction of DHA in DMSO-d6 catalysed with 32.1 mol% CD3COOD

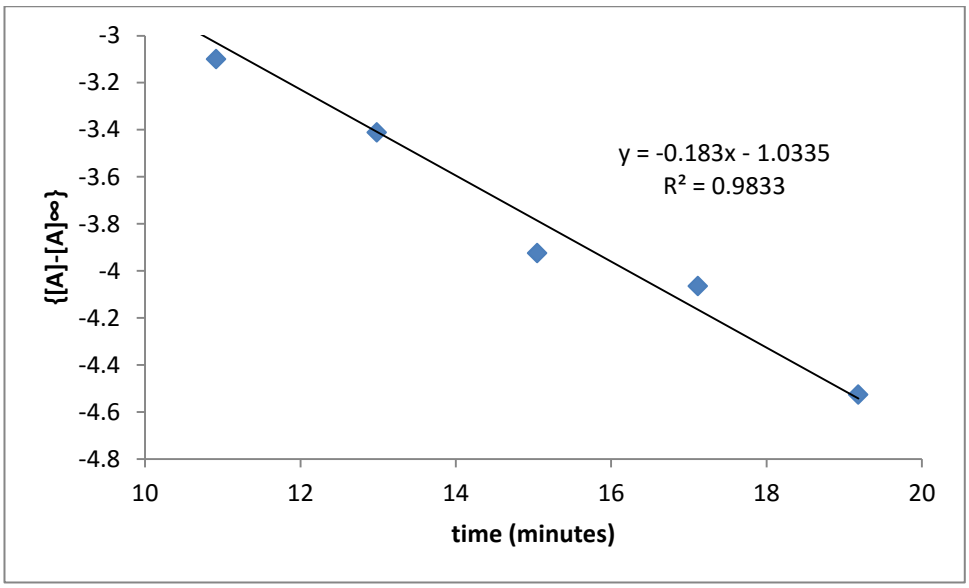

A53: First order graph for the formation of Int#2 in the dissociation reaction of DHA in DMSO-d6 catalysed with 51.1 mol% CD3COOD

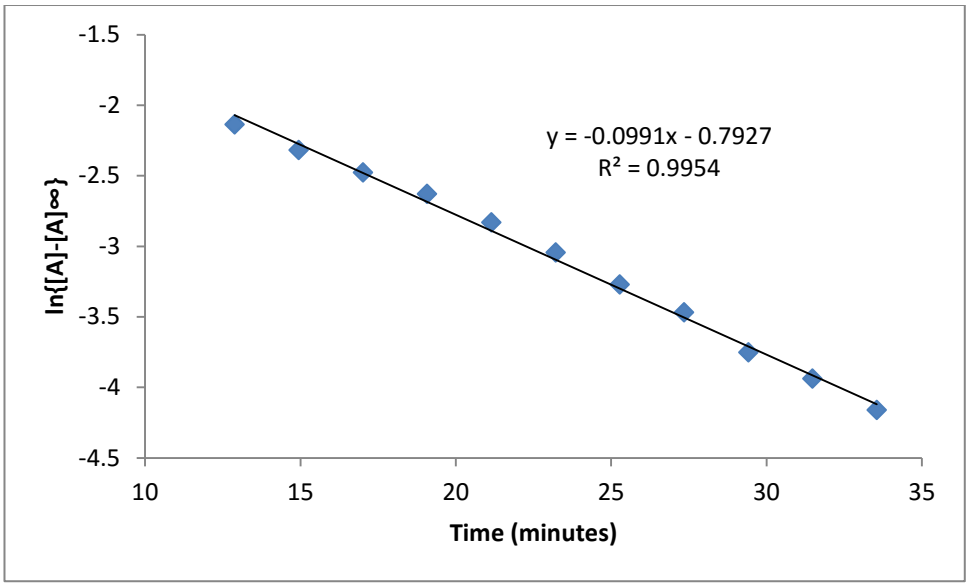

A54: First order graph for the formation of Int#2 in the dissociation reaction of DHA in DMSO-d6 catalysed with 51.7 mol% CD3COOD

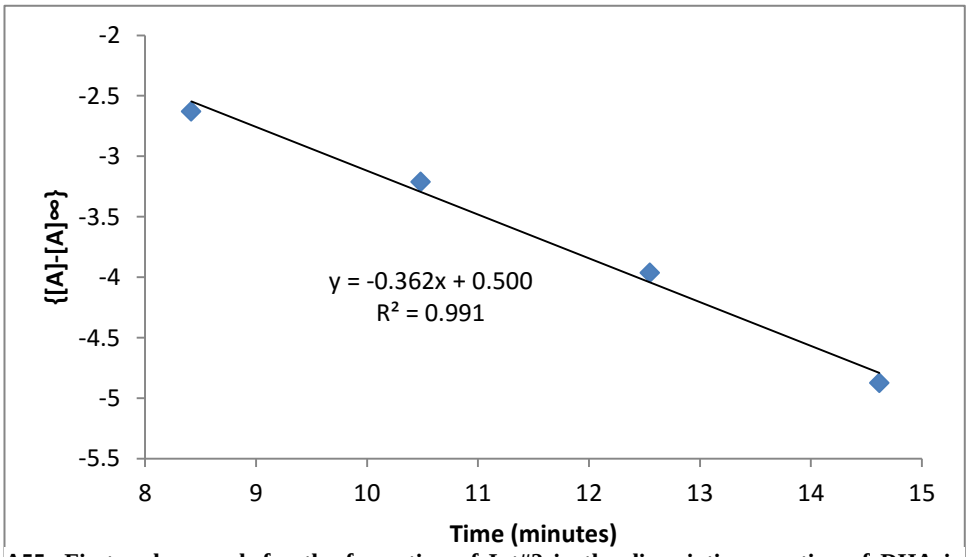

A55: First order graph for the formation of Int#2 in the dissociation reaction of DHA in DMSO-d6 catalysed with 57.1 mol% CD3COOD

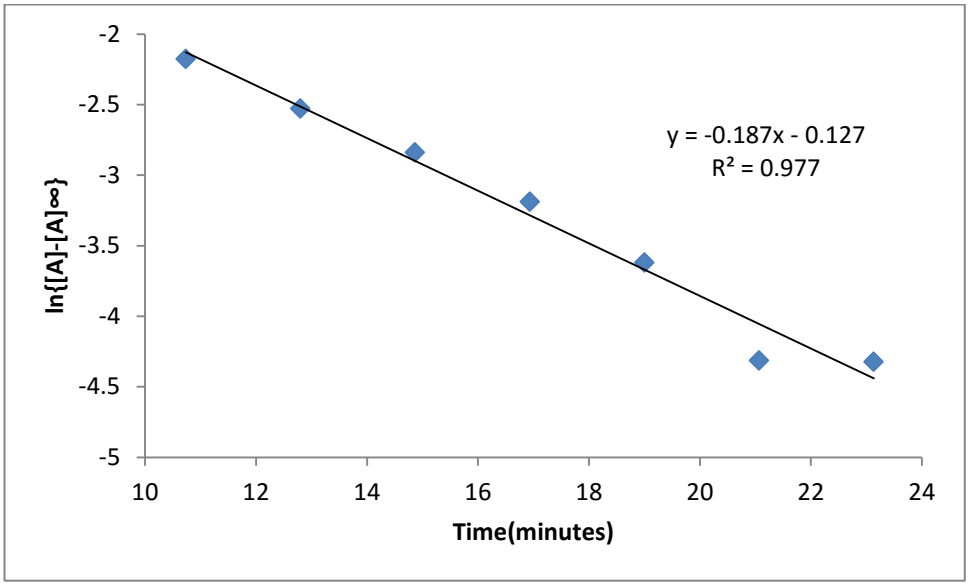

A56: First order graph for the formation of Int#2 in the dissociation reaction of DHA in DMSO-d6 catalysed with 58.4 mol% CD3COOD

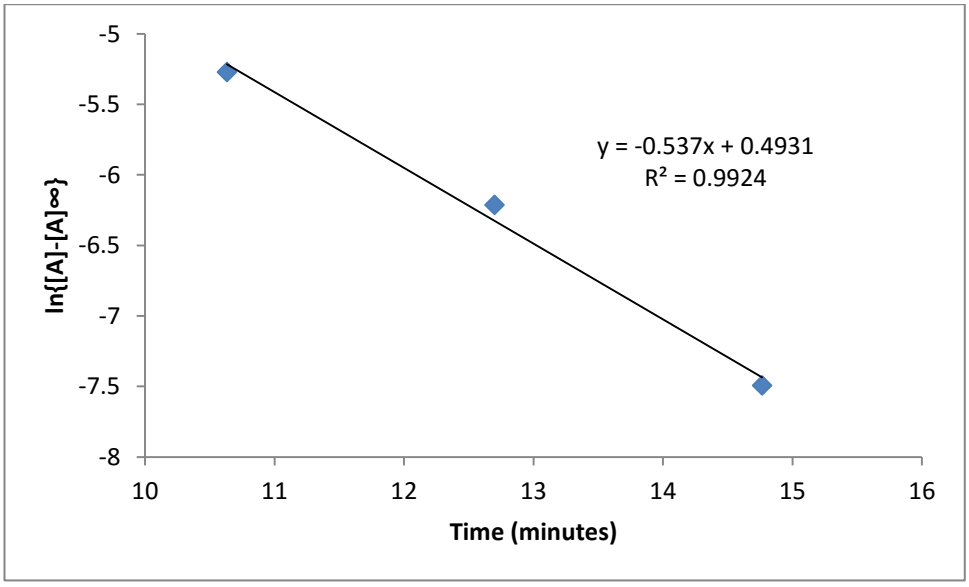

A57: First order graph for the formation of Int#2 in the dissociation reaction of DHA in DMSO-d6 catalysed with 65.0 mol% CD3COOD

10.9.4 The graphs for the DHA dimer dissociation in DMSO-*d6* catalysed with CD_3COOD/CD_3COO^-

10.9.4.1 The zeroth, first and second order graphs for the DHA dimer dissociation in DMSO-*d6* catalysed with CD_3COOD/CD_3COO^-

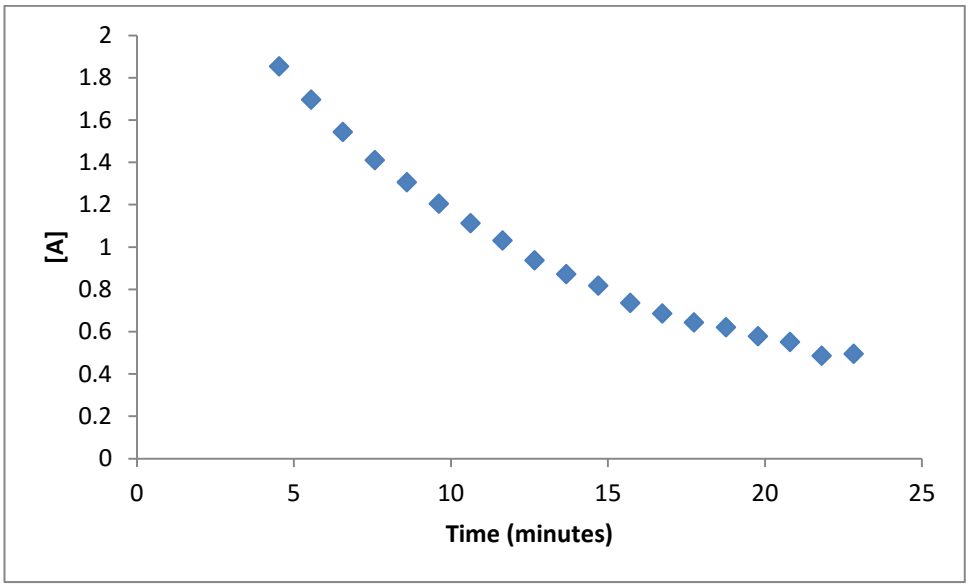

A58: The zeroth order graph for the DHA dimer dissociation in DMSO-d6 catalysed with 1.00 mol% CD_3COO^-

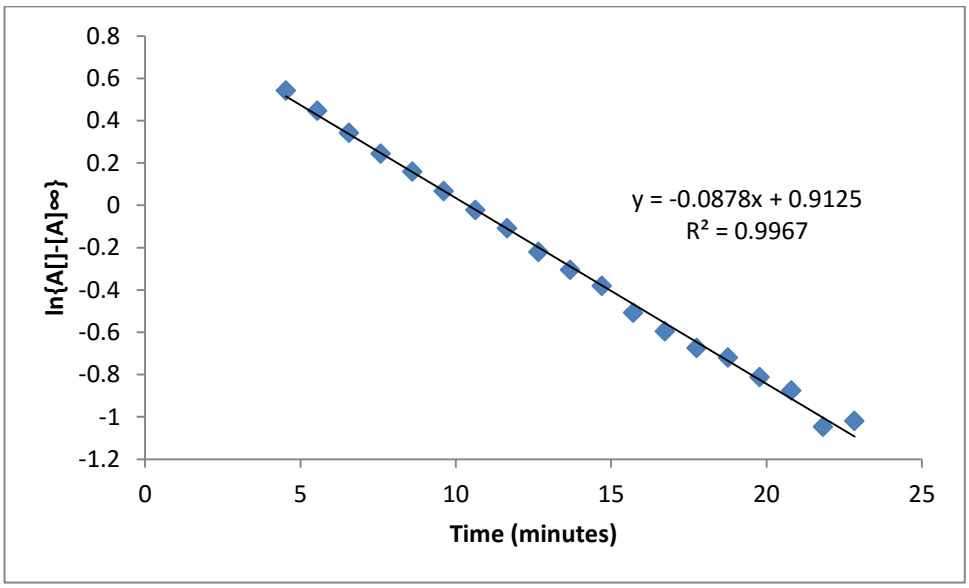

A59: The first order graph for the DHA dimer dissociation in DMSO-d6 catalysed with 1.00 mol% CD_3COO^-

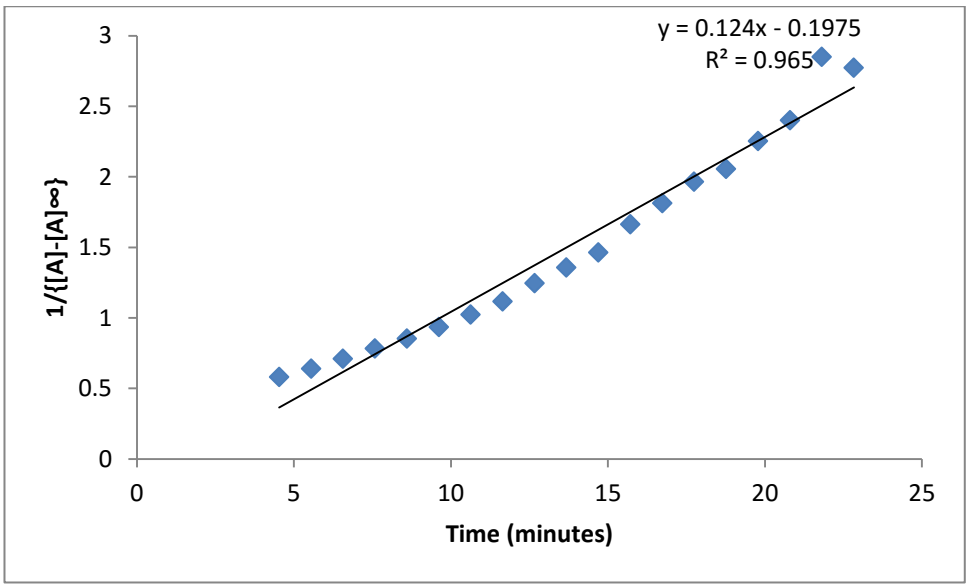

A60: The zeroth order graph for the DHA dimer dissociation in DMSO-d6 catalysed with 1.00 mol% CD_3COO^-

10.9.4.2 First order graphs for the DHA dimer dissociation in DMSO-*d6* catalysed with CD_3COOD/CD_3COO^-

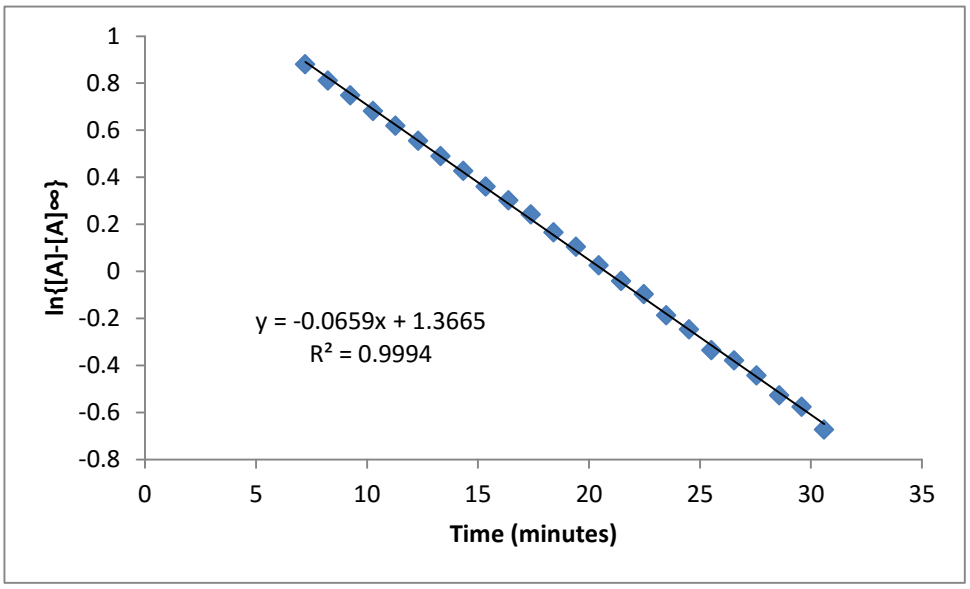

A61: The first order graph for the DHA dimer dissociation in DMSO-d6 catalysed with 0.500 mass% CD_3COO^-

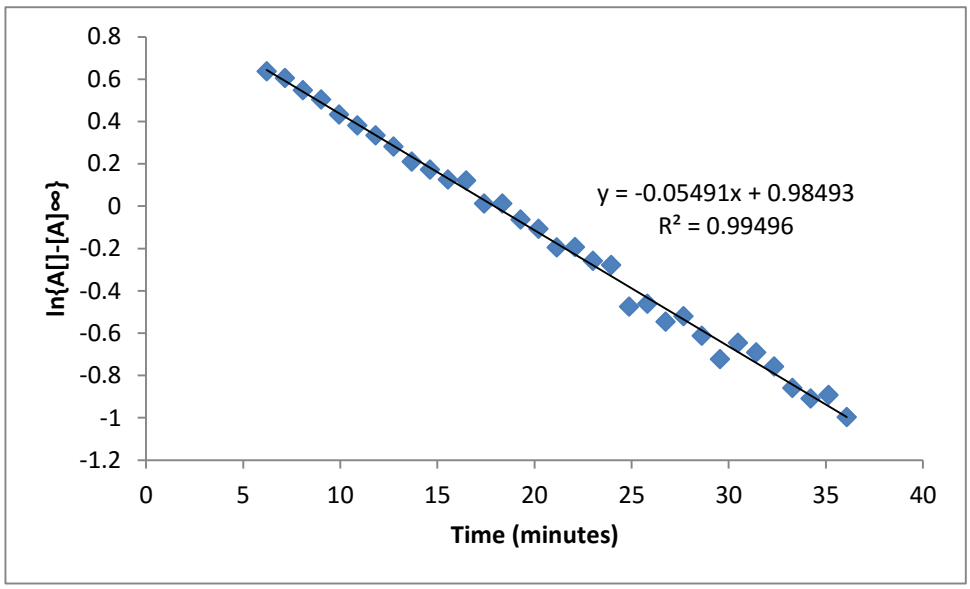

A62: The first order graph for the DHA dimer dissociation in DMSO-d6 catalysed with 0.500 mass% CD_3COO^-

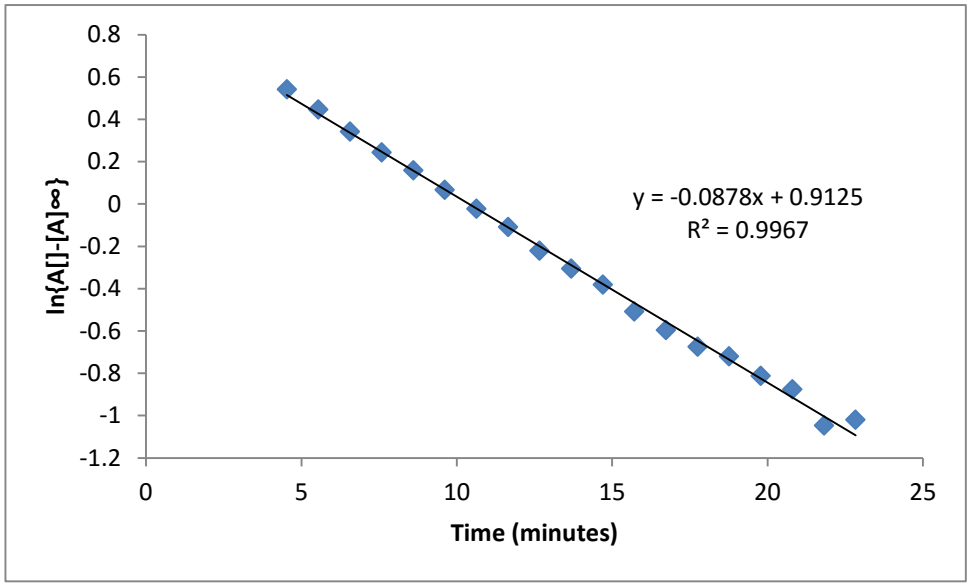

A63: The first order graph for the DHA dimer dissociation in DMSO-d6 catalysed with 1.00 mass% CD_3COO^-

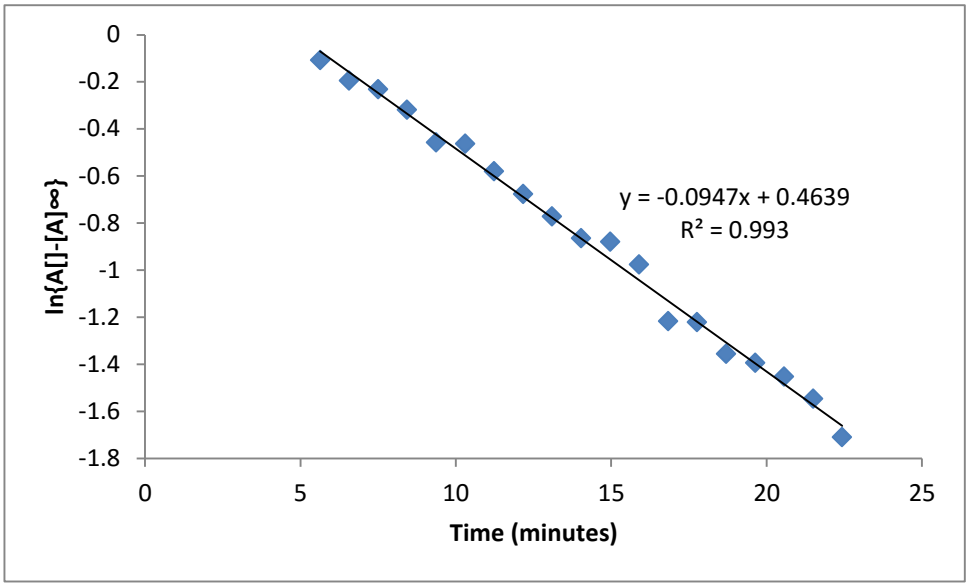

A64: The first order graph for the DHA dimer dissociation in DMSO-d6 catalysed with 1.00 mass% CD_3COO^-

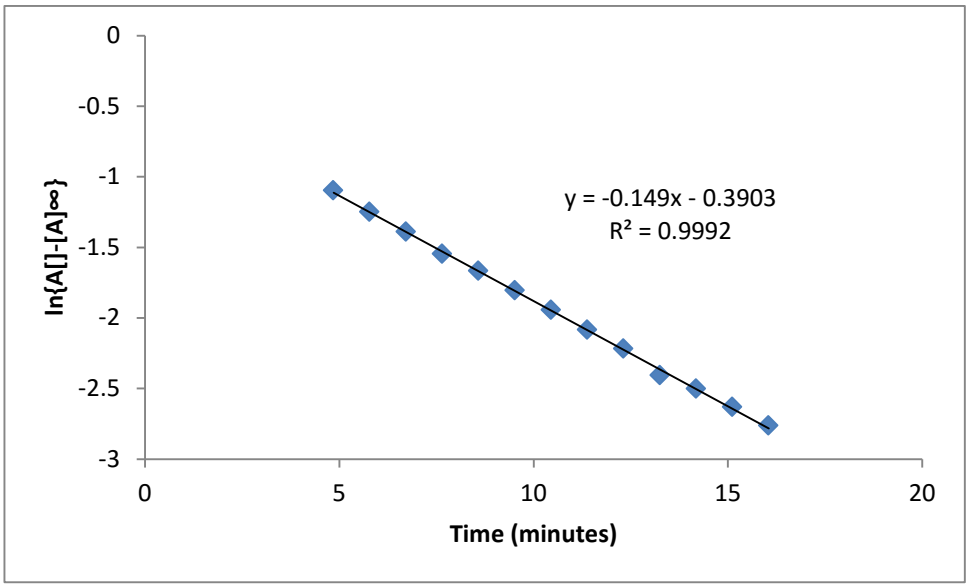

A65: The first order graph for the DHA dimer dissociation in DMSO-d6 catalysed with 2.00 mass% CD_3COO^-

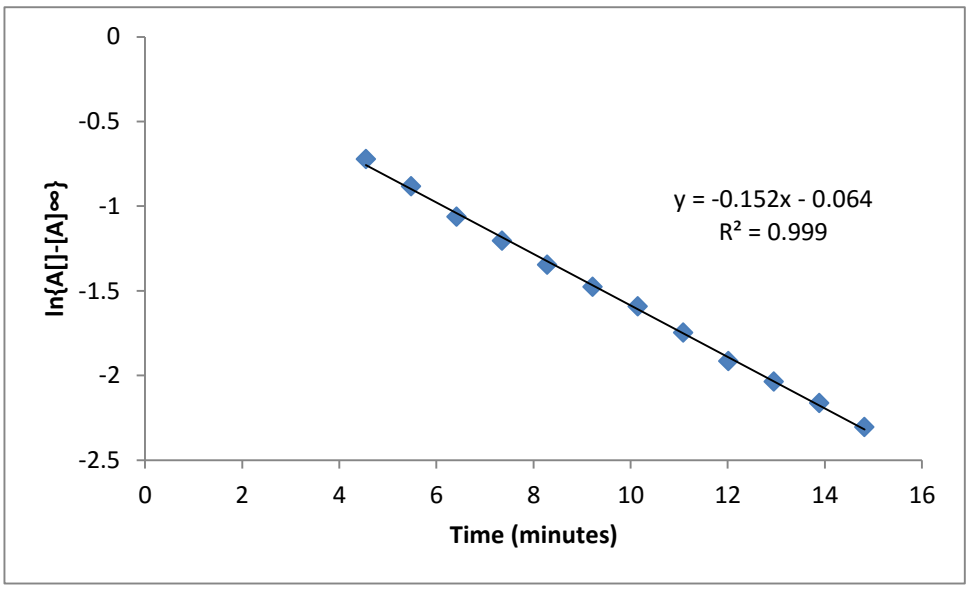

A66: The first order graph for the DHA dimer dissociation in DMSO-d6 catalysed with 2.00 mass% CD_3COO^-

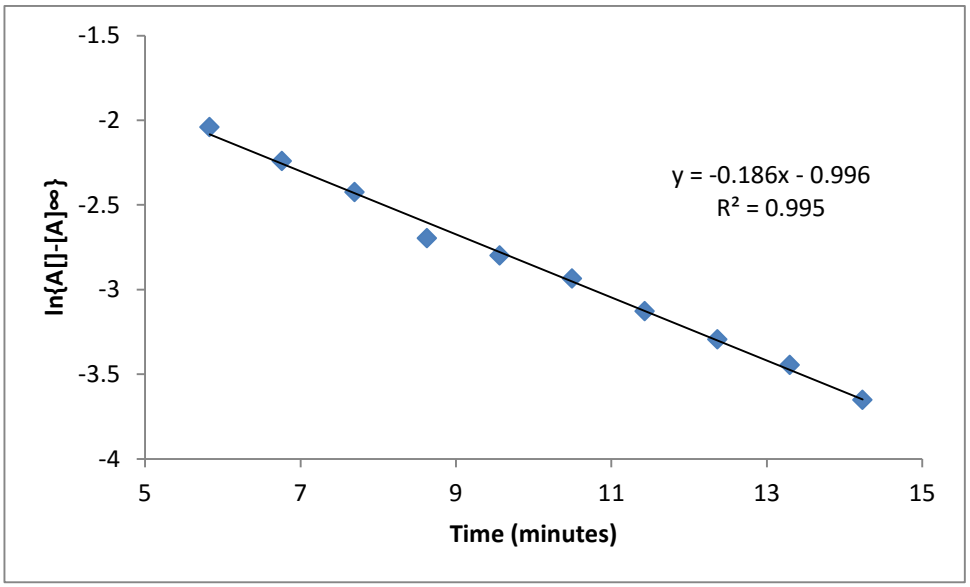

A67: The first order graph for the DHA dimer dissociation in DMSO-d6 catalysed with 3.00 mass% CD_3COO^-

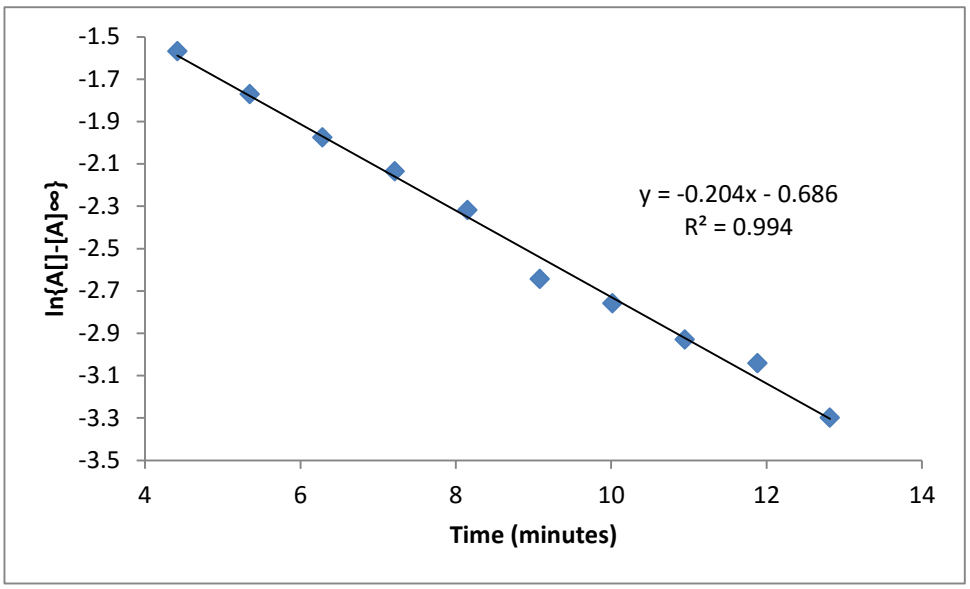

A68: The first order graph for the DHA dimer dissociation in DMSO-d6 catalysed with 3.00 mass% CD_3COO^-

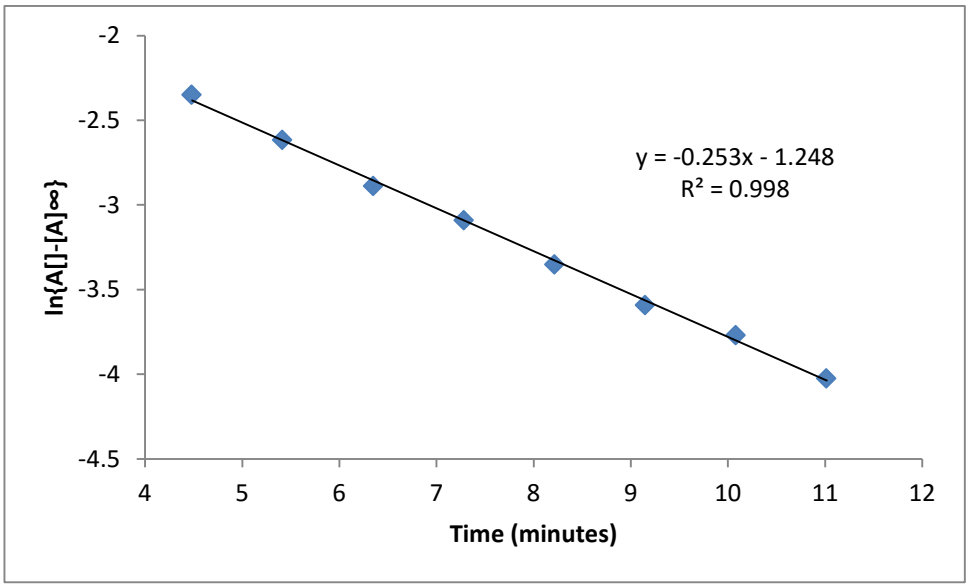

A69: The first order graph for the DHA dimer dissociation in DMSO-d6 catalysed with 4.00 mass% CD_3COO^-

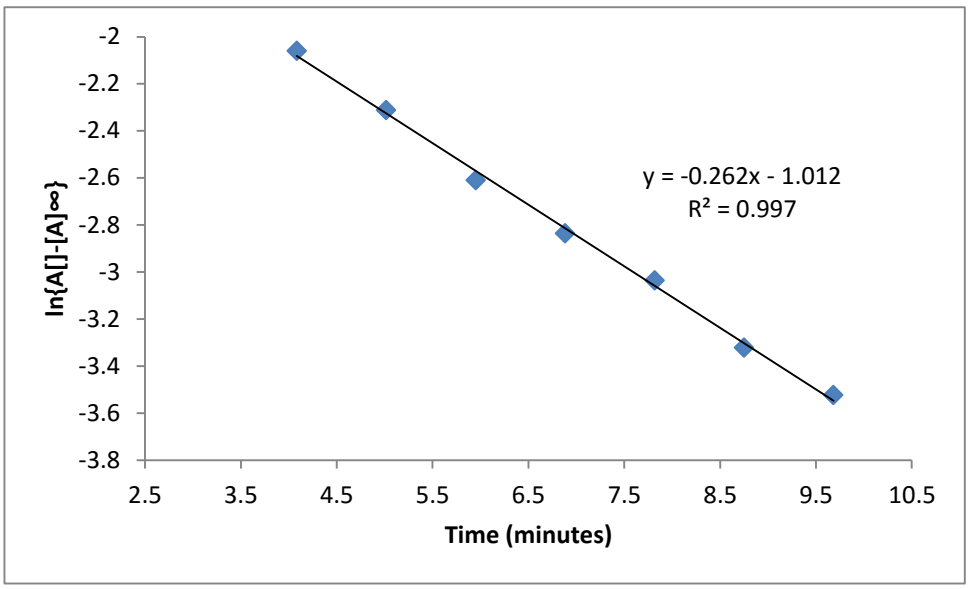

A70: The first order graph for the DHA dimer dissociation in DMSO-d6 catalysed with 4.00mass% CD_3COO^-

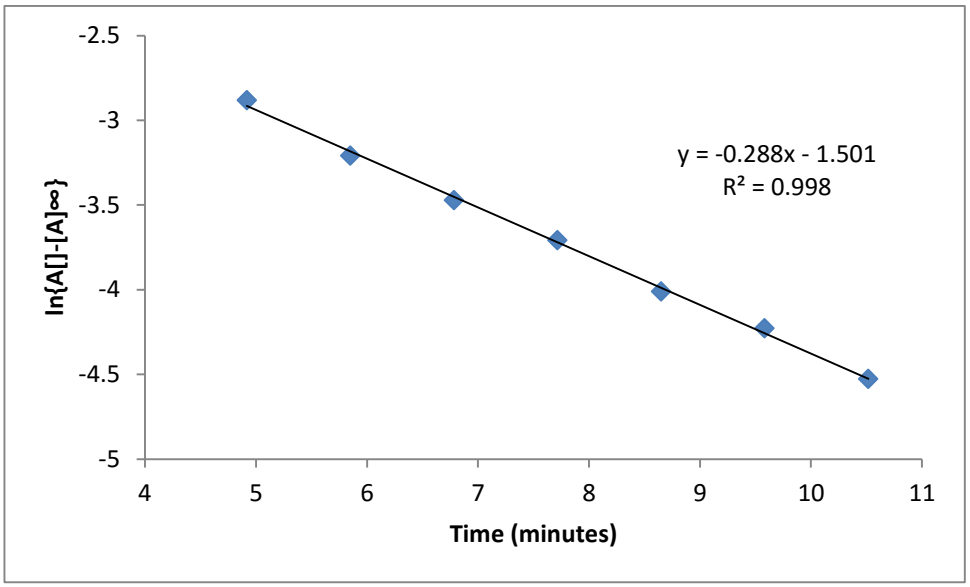

A71: The first order graph for the DHA dimer dissociation in DMSO-d6 catalysed with 5.00 mass% CD_3COO^-

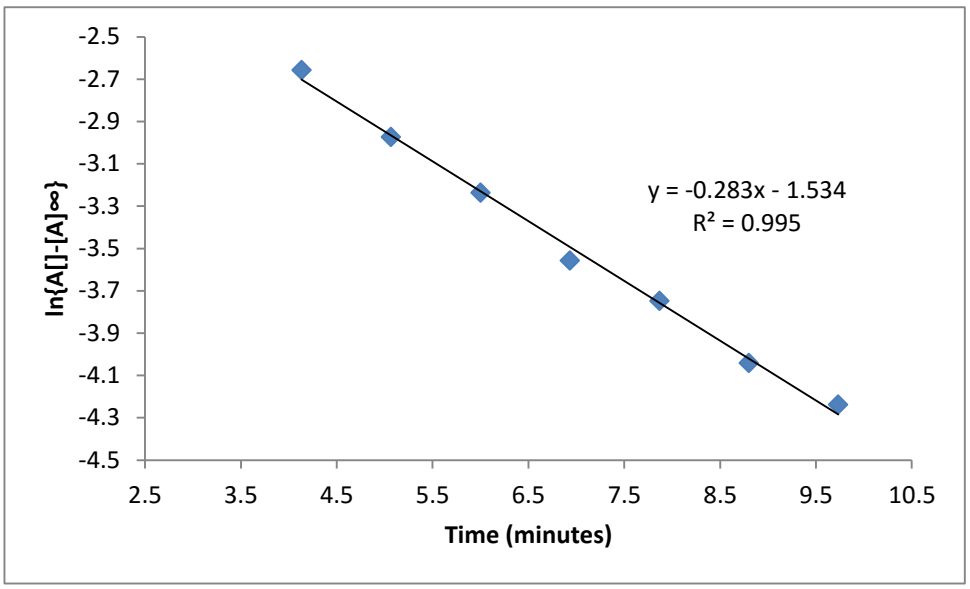

A72: The first order graph for the DHA dimer dissociation in DMSO-d6 catalysed with 5.00 mass% CD_3COO^-

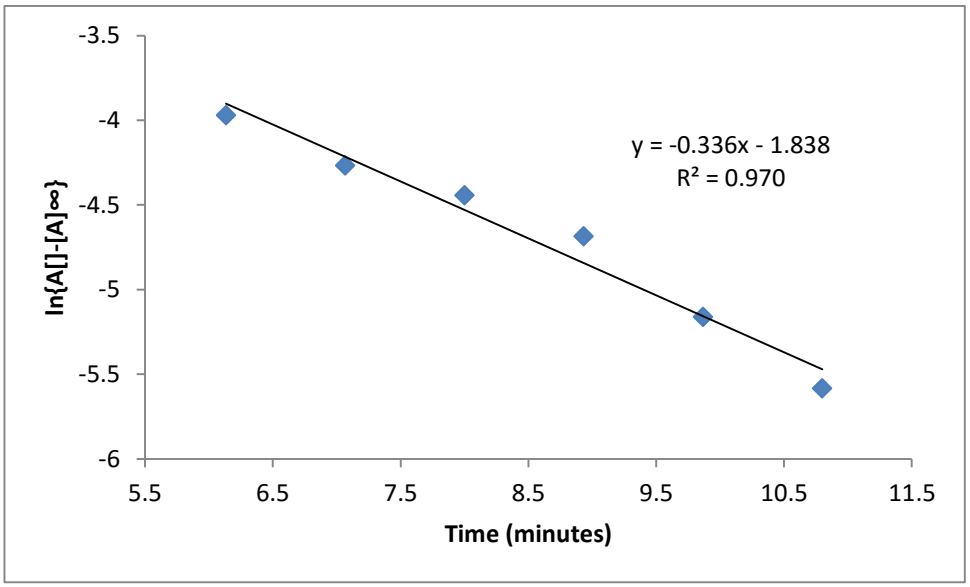

A73: The first order graph for the DHA dimer dissociation in DMSO-d6 catalysed with 6.00 mass% CD_3COO^-

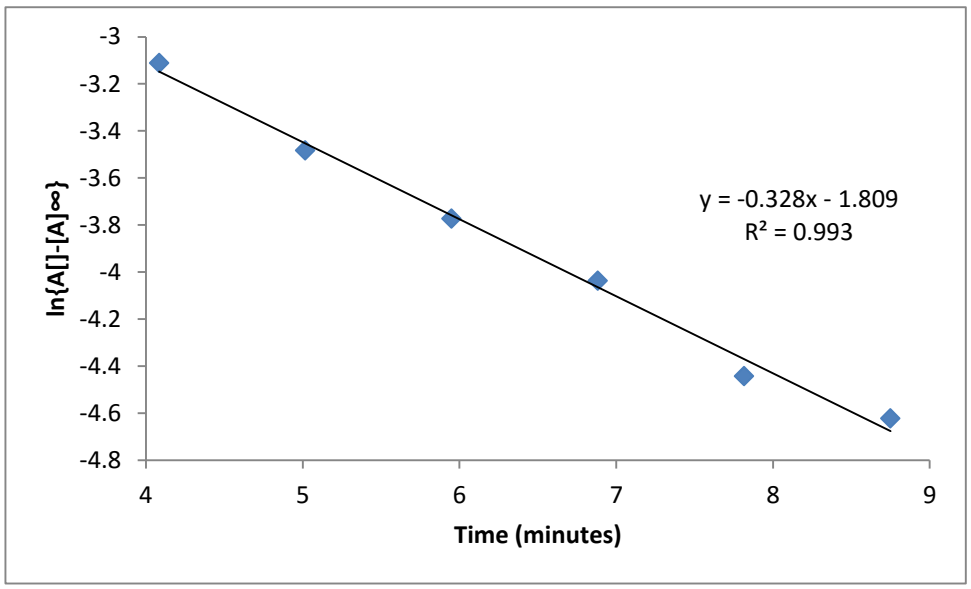

A74: The first order graph for the DHA dimer dissociation in DMSO-d6 catalysed with 6.00 mass% CD_3COO^-